Effective Models for the Single Impurity Anderson and Kondo Model from Continuous Unitary Transformations

Dissertation

zur Erlangung des Doktorgrades
der Naturwissenschaften
der Fakultät Physik
der Technischen Universität Dortmund

vorgelegt von
Jörn Krones
aus Witten

Oktober 2014

Contents

1 Introduction

Strongly correlated electron systems are of great importance in the field of condensed matter physics as a wide range of physical phenomena, e.g. certain properties of magnetism and conductivity, can only be understood in the framework of a quantum mechanical description of many-body systems in which interactions between electrons are important. However, even fairly simple models including interacting electrons can already be very challenging and exact solutions can only be derived in rare cases. An effective way to deal with such models is to reduce the complicated many-body problem to a simpler effective model with a focus on the physical aspects under consideration.

Two very important examples of strongly correlated electron systems [1] are the *Kondo* (or sd-exchange) *model* [2] and the *single impurity Anderson model* (SIAM) [3]. These are the most basic archetypes of models describing magnetic impurities in a host metal and most of the works in the field of magnetic impurities have been based on these two models [1].

The Kondo model describes the interaction of a local magnetic moment and the conduction electrons of a host metal via a spin-spin exchange interaction. This interaction leads to the *Kondo effect* [1, 2, 4] which results in the anomalous behavior of the susceptibility, specific heat and resistivity at small temperatures [5, 6].

The single impurity Anderson model is able to explain how such local moments arise in the first place. It describes a single impurity level which is hybridized with a non-interacting bath of electrons. The local magnetic moment arises from a repulsive Coulomb interaction which favors a singly occupied impurity level.

The main challenge of such impurity models lies, on the one hand, within the largely separated energy scales that reach from the bath electrons' bandwidth D down to the exponentially small Kondo temperature T_K. On the other hand, it is posed by the break-down of standard perturbation theory below the Kondo energy scale T_K. The search for a complete theory down to arbitrarily small temperatures is known as the *Kondo problem* [1] and was first solved by the *numerical renormalization group* (NRG) [7–10].

The Continuous Unitary Transformation (CUT) (or flow equation) **approach** [11–14] is a method of theoretical quantum mechanics which is able to systematically derive simpler effective models. The approach constructs a unitary transformation which continuously transforms a given Hamiltonian closer to diagonality. In realistic many-body problems the exact construction of a CUT is, in general, far too complex which necessitates the introduction of approximations, e.g., by truncating certain contributions. Fortunately, this is not necessarily a disadvantage because the resulting effective model can be much simpler while still containing the key features of the initial model. CUTs can be set up non-perturbatively and exhibit an intrinsic energy separation which are essential features when treating the Kondo problem.

The objective of this thesis is to apply the method of Continuous Unitary Transformations to the single impurity Anderson and the Kondo model in order to derive effective models avoiding infrared divergences which occur in perturbative treatments. CUTs have been applied successfully to a wide range of problems in many-body theory in which most commonly gapped systems are discussed. In this thesis, on the other hand, we face the problem of an impurity in

a gapless host material which gives rise to a system with largely separated energy scales and a non-trivial low-temperature strong-coupling behavior. Besides the research interest in the CUT approach itself, the method has also the potential to derive intuitively easily accessible effective models.

There are a few earlier approaches in which CUTs have been applied to the Kondo problem. A number of works have been published in the case of the Kondo model. Conventional "poor man's scaling" results [15] could be reproduced by CUT [16] in which, however, diverging differential equations arise and thus the approach fails to yield effective models. Another direct approach applying a CUT to the Kondo model [17] results in an effective model where the parameters still exhibit logarithmic infrared divergences very similar to those found by a standard perturbative treatment [2]. There are CUT approaches which are able to derive effective models for the Kondo model, but these approaches rely on a bosonized form of the Kondo model before applying the CUT [18–20].

In the case of the Anderson model, on the other hand, only a few approaches [21–23] were published while none of them reveal the exponential character of the Kondo temperature T_K. Nevertheless, an important previous work is able to reconstruct the Schrieffer-Wolff transformation using CUTs [22].

We investigate three different approaches to the Anderson and Kondo model – which are further outlined in Sec. 1.1 – and construct effective models using Continuous Unitary Transformations.

1.1 Thesis Overview

A short overview and a very brief summary of each chapter is given in the following.

Chapter 2 provides a general overview of the history and the basic physics of the Anderson and Kondo model as well as the representations used in this thesis. References to further literature on the subject are presented.

Chapter 3 introduces the basic ideas of conventional scaling theory which is able to reveal the exponential character of the Kondo temperature T_K but fails to solve the Kondo problem due to diverging couplings. The CUT approach exhibits parallels to the scaling approach from Chap. 3 and it is non-perturbative which motivates the usage of this method in the context of the Anderson and Kondo model.

Chap. 3 is supposed to give the reader not familiar with conventional scaling theory enough information to understand the similarity between the conventional scaling and the Continuous Unitary Transformation approach outlined in Chap. 4.

Chapter 4 introduces the concept of Continuous Unitary Transformations and provides a wide range of literature for further information on the method. Additionally, in the end of Chap. 4 the similarity between the scaling approach from Chap. 3 and the CUT approach is explicitly shown. Both methods exhibit an intrinsic energy separation as higher energetic processes are treated before lower ones. This is a very useful feature when treating the Kondo problem.

Chapter 5 describes our first approach applying the Continuous Unitary Transformation to the Anderson model. We use a chain representation of the Anderson Hamiltonian which is sim-

ilar to the starting point used for a numerical renormalization group calculation [8, 10]. We use a different parametrization, separating particle and hole states by constructing two chains (one for each of them) using two separate Lanczos tridiagonalizations. The Continuous Unitary Transformation is set up such that the ground state of the effective Hamiltonian becomes the vacuum, i.e., the state without particles and holes. We try to keep the chain local by focusing on nearest-neighbor interactions in most parts while we study the influence of interactions over longer ranges later in this chapter. We study the influence of the interaction U on the single-particle energies of the effective Hamiltonian and compare them to those calculated from simple effective Hamiltonians already known to describe the respective energy regimes. Additionally, we compare them to the flow of the lowest non-zero many-particle energy of states with total charge $Q = 1$ (with respect to half-filling) and total spin $S = 0$ obtained by NRG calculations (cf. Ref. [10]).

We find good agreement within the high and intermediate energy regimes for larger values of U and nearest-neighbor interactions. For smaller values of U, we have to include interactions over longer ranges in order to obtain comparatively good results.

The most interesting regime, the strong-coupling regime, is missed in this approach which brought us to analyze further approaches described in Chaps. 6 and 7.

Chapter 6 again deals with the Anderson model alone. We use a parametrization in which the non-interacting model is diagonal and thus the ground state is simply given by a Fermi sea. The interaction term in this approach is completely non-local. Our aim is to transform the Hamiltonian in a way that the Fermi sea becomes also the ground state of the interacting model. The parametrization in Chap. 6 enables us to derive the flow equations analytically if operators are truncated in orders of the interaction U.

We find converging differential equations yielding an effective model without any divergences, even for energies arbitrarily close to the Fermi level.

We study the low-energy interaction vertex $U_{n_\mathrm{F} n_\mathrm{F} n_\mathrm{F} n_\mathrm{F}}$ at the Fermi level which becomes attractive for a certain parameter regime of the initial interaction U.

In order to find out if the effective model captures the low-temperature strong-coupling behavior, we calculate the impurity contribution to the magnetic susceptibility χ_d. In the first part of Chap. 6 we derive χ_d numerically and find an exponential increase with respect to the Coulomb interaction U over some parameter regime which is in agreement with the correct behavior. We, however, miss a factor of two in the exponent. The second part of Chap. 6 examines a low-order *scaling expansion* to the flow equation which enables us to derive an analytical expression for the susceptibility χ_d. Again, we find an exponential increase in the interaction U but this time the exponent is too large by a factor $\frac{16}{\pi^2} \approx 1.62$.

Chapter 7 deals with both the Anderson as well as the Kondo model. We investigate a third parametrization, starting from the initial star-parametrization including the interaction U in the diagonal part of the Hamiltonian H_D and truncating terms in orders of the hybridization V.

An approach using a similar parametrization, which is able to reconstruct the Schrieffer-Wolff transformation, was already used in literature [22]. We revisit this procedure comparing different generators. We use deepCUT ideas in order to find the induced spin-spin interaction analytically in a way that simplifies the calculation significantly in contrast to the calculation already used in literature.

Reproducing ”poor man’s scaling” results by diagonalizing the spin-spin interaction has al-

ready been achieved for the Kondo model but has not been done for the Anderson model so far. Thus, we try to diagonalize the induced spin-spin interaction of the Anderson model which results in the same differential equations as already known for the Kondo model. These differential equations are able to reproduce results obtained from conventional scaling but fail to solve the Kondo problem due to diverging contributions on the Kondo energy scale.

The main goal of Chap. 7 is to modify this approach in a way that enables us, in contrast to earlier approaches, to construct effective models without infrared divergences. We will follow the increasing spin-spin interactions during the flow and determine a new reference state as soon as the diagonal spin-flip contributions become large enough in order to account for a new ground state.

Our adapted method prevents the divergences which occur in the previous approaches and results in an effective model that reveals the exponentially small Kondo energy scale as the binding energy of a singlet ground state in the diagonal part of the effective model.

Chapter 8 summarizes the applied methods and results and provides an outlook on open questions and possible further investigations.

2 Anderson Impurity Model

2.1 Historical Overview

In the mid 1930's an unexpected low-temperature dependence of the resistivity in metals hosting magnetic impurities was measured [4] and led to a quest for the understanding of the physical mechanism behind this phenomenon [1] that lasted more than three decades. This observation contradicted the expected low-temperature behavior of the resistivity of metals which had the form

$$R = R_0 + \alpha T^2 + \beta T^5. \tag{2.1}$$

The finite resistivity R_0 at $T = 0$ is induced by impurities while the T^2-behavior is attributed to electron-electron interactions [24, 25] which are described by Fermi-liquid theory. At higher temperatures the resistivity is dominated by electron-phonon scattering [25] which leads to "Bloch's T^5 law" [26].

When a non-magnetic metal, such as gold, contains magnetic impurities, such as a $3d$ transition metal (e.g. iron) or a $4f$ rare earth element, the resistivity shows a minimum at very low temperatures. When the temperature is lowered further, the resistivity increases first before it reaches a constant value R_0.

It was not before the mid 60's that significant advances in the understanding of this problem were made by J. Kondo [2, 27]. He used the so-called sd-exchange model [28–30] which describes a local moment associated with an impurity that couples to the bath electrons of the host metal via a spin-spin coupling J. The Hamiltonian is explicitly given in Eq. (2.3). He was able to calculate the resistivity of this model in third-order perturbation theory and found

$$R = R_0 + \alpha T^5 - \gamma \ln\left(\frac{k_\mathrm{B} T}{D}\right) \tag{2.2}$$

where k_B is the Boltzmann constant, D the bath electrons' bandwidth and R_0, α as well as γ are constants with respect to the temperature T with γ depending on the spin-spin interaction J [2]. The T^5-term stems from the phonon contribution while the $\ln(T)$ term is an effect of the impurity. A logarithmic increase of the resistivity fits the experimental data close to the resistivity minimum. Nevertheless, the theory has a serious problem as it breaks down for very small temperatures due to a diverging resistivity for $T \to 0$.

Anderson introduced a model based on earlier experimental [31] and theoretical [5] works on impurities. His model contains important insights on the nature of localized magnetic moments in dilute magnetic alloys and has played a crucial role in the understanding of the theory of magnetic impurities. Today it is called the Anderson impurity model [3] and is based on the idea of a virtual bound state just below the Fermi level which is almost localized and associated with the impurity. In order to explain the appearance of a local moment at low temperatures, he introduced a short-range Coulomb interaction U between electrons localized on the impurity. Once the local moment is present, the low-temperature physics can be understood in terms of an effective Kondo model. This was explicitly shown by Schrieffer and Wolff [32] who were able to map the Anderson model to an effective Kondo model.

In the late 60's Anderson and co-workers developed a method that was better suited to describe the physics of such models by reorganizing perturbation theory in a way that eliminates higher energetic excitations first [33–36]. With this method, called scaling, he was able to find an exponentially small energy scale, known as the Kondo temperature T_K, where the exchange coupling J becomes infinitely large [15]. This behavior could be associated with the appearance of a new bound state, the so-called Kondo singlet. Such a singlet ground state was already conjectured earlier [37–40].

The local moment of the impurity becomes completely screened by the formation of the singlet between the impurity spin and the spin of a bath electron. This leads to anomalous contributions to numerous material properties such as the resistivity, susceptibility and specific heat [1, 5, 6]. This effect is now called the *Kondo effect*. For an overview, see for example Ref. [41].

The search for a complete theory which describes the Kondo effect down to arbitrarily small temperatures is one of the fundamental problems of many-body theory as it appears in a lot of correlated electron systems, for example, in Heavy-Fermion physics [1, 42], the Mott-Hubbard metal-insulator [43, 44] or in ultra-small quantum dots [45]. It became famous by the name "*Kondo problem*".

As perturbation theory breaks down at $T \approx T_K$, non-perturbative methods had to be developed. The one that finally solved the Kondo problem was found in the mid 70's by Wilson [46] and was rewarded with the Nobel prize in 1982. It combines renormalization group ideas known from quantum field theory and the scaling approach mentioned earlier. The result was the *numerical renormalization group* (NRG) [7] which described for the first time the complete crossover from the high-energy physics of a free impurity orbital down to the low-energy physics of a screened impurity spin.

Krishna, Wilkins and Wilson applied this method extensively to the symmetric [8] and asymmetric Anderson model [9]. A recent review is given in Ref. [10]. In the 80's exact analytical results were obtained independently by Andrei [47] and Wiegmann [48] using the Bethe ansatz which confirmed the NRG calculations.

A series of works were published by Hewson and co-workers from the early 90's until recent times. In these works he developed a perturbative approach which is able to describe the low-energy physics of the Anderson impurity model, the so-called renormalized perturbation theory [49–52].

There were extensive investigations of the Anderson impurity model throughout the last decades and the model has been essential for the understanding of the theory of magnetic impurities. Of course, many-body theory has moved on since these days but, nevertheless, the single impurity Anderson as well as the Kondo model remain the most basic impurity models and are thus the perfect candidates for applying new methods to the Kondo problem.

2.2 Kondo Model

The Kondo model was introduced by J. Kondo [2] in order to explain the resistivity minimum found in metals hosting magnetic impurities. It describes the interaction of the bath electrons of a host metal with a dispersion $\varepsilon_{\mathbf{k}}$ and a localized spin $\vec{\tau}$ associated with the impurity. The interaction is exchanged by a spin-spin coupling J between the impurity spin and the spins of

the bath electrons $\vec{s}_\mathrm{b}$

$$H_\mathrm{K} = \sum_{\mathbf{k},\sigma} \varepsilon_\mathbf{k} c^\dagger_{\mathbf{k}\sigma} c_{\mathbf{k}\sigma} + J\vec{\tau}\cdot\vec{s}_\mathrm{b}. \tag{2.3}$$

The Hamiltonian is written down in second quantization, i.e., $c^\dagger_{\mathbf{k}\sigma}$ ($c_{\mathbf{k}\sigma}$) creates (annihilates) a bath electron with momentum $\mathbf{k}$ and spin σ while $\vec{s}_\mathrm{b}$ is the bath electrons' spin

$$\vec{s}_\mathrm{b} = \frac{1}{N}\sum_{\mathbf{k},\mathbf{k}'}\sum_{\alpha,\beta} c^\dagger_{\mathbf{k}\alpha}\vec{\sigma}_{\alpha\beta}c_{\mathbf{k}'\beta} \tag{2.4}$$

which interacts with the local impurity spin. The vector $\vec{\sigma}$ contains the Pauli matrices $\vec{\sigma} = \sum_{\mu\in x,y,z}\sigma^\mu\vec{e}_\mu$. In Eq. (2.3) the exchange coupling J is isotropic. A more general version is the anisotropic Kondo model

$$H_\mathrm{K} = \sum_{\mathbf{k},\sigma}\varepsilon_\mathbf{k}c^\dagger_{\mathbf{k}\sigma}c_{\mathbf{k}\sigma} + \sum_{\mu\in x,y,z}\frac{J^\mu}{N}\sum_{\mathbf{k},\mathbf{k}'}\sum_{\alpha,\beta}\sigma^\mu_{\alpha\beta}\tau^\mu c^\dagger_{\mathbf{k}\alpha}c_{\mathbf{k}'\beta} \tag{2.5}$$

where σ^μ describes the Pauli matrix with $\mu = x,y,z$ and is associated with the bath electrons' spin while τ^μ is the spin operator of the impurity.

In order to gain a better understanding, we can rewrite the Hamiltonian by introducing the well-known ladder operators

$$\tau^\pm = \tau^x \pm i\tau^y \tag{2.6}$$

and splitting the coupling into a polarization part J_z and a spin-flip contribution $J_x = J_y = J_\perp$

$$H_\mathrm{K} = \sum_{\mathbf{k},\sigma}\varepsilon_\mathbf{k}c^\dagger_{\mathbf{k}\sigma}c_{\mathbf{k}\sigma} + \frac{J_z}{N}\sum_{\mathbf{k},\mathbf{k}'}\left[\tau^z\left(c^\dagger_{\mathbf{k}\uparrow}c_{\mathbf{k}'\uparrow} - c^\dagger_{\mathbf{k}\downarrow}c_{\mathbf{k}'\downarrow}\right) + \lambda\left(\tau^+c^\dagger_{\mathbf{k}\downarrow}c_{\mathbf{k}'\uparrow} + \tau^-c^\dagger_{\mathbf{k}\uparrow}c_{\mathbf{k}'\downarrow}\right)\right] \tag{2.7}$$

with $\lambda = {}^{J_\perp}\!/_{J_z}$. A ferromagnetic coupling $J_z < 0$ polarizes the electrons close to the impurity and the electrons' spin is then parallel to the impurity spin. The spin-flip terms are irrelevant in this case as they only come into play if the electrons' spin and the impurity spin are antiparallel. Thus, in the ferromagnetic case the physics is dominated by J_z and spin-flips do not play a significant role.

This changes drastically as soon as an antiferromagnetic coupling $J_z > 0$ is introduced. As the spins of the electrons and the impurity are now antiparallel, spin-flip contributions become a dominant part. Standard second-order perturbation theory results in integrals of the form

$$E^{(2)} \propto J_\perp^2\int_\delta^D\frac{\mathrm{d}\varepsilon}{\varepsilon} \propto \ln(\delta) \tag{2.8}$$

where δ is a constant which is given by the difference of the smallest contributing energy level to the Fermi energy ε_F. The bath electrons form a quasi-continuum with energies arbitrarily close to the Fermi level which results in a logarithmic divergence for $\varepsilon \to \varepsilon_\mathrm{F}$. This is a typical infrared problem of quantum field theory. When calculating physical quantities, the only cut-off for δ is the temperature and consequently the results diverge when T tends to zero.

One can say that divergent spin-flip contributions are lying at the heart of the problem. These spin-flip contributions lead to the Kondo singlet mentioned in Sec. 2.1. The binding energy of this singlet is given by an exponentially small energy scale, the so-called Kondo temperature

$$T_\mathrm{K} \propto \mathrm{e}^{-\frac{1}{2\rho J}} \tag{2.9}$$

where ρ describes the density of states of the bath electrons at the Fermi level and J is the exchange coupling from Eq. (2.3).

The Kondo energy scale can already be seen in perturbation theory as the divergent contributions become of order $\mathcal{O}(1)$ at the Kondo temperature T_K. This marks the point were perturbation theory breaks down.

2.3 Single Impurity Anderson Model (SIAM)

The single impurity Anderson model was introduced by Anderson in 1963 [3] in order to explain the occurrence of localized moments in dilute magnetic alloys. The most straightforward idea to introduce an impurity would be to assume an effective potential $V_\mathrm{imp}(\mathbf{r})$ which is associated with the impurity. This would lead to a potential scattering model

$$H = \sum_{\mathbf{k},\sigma} \varepsilon_\mathbf{k} c^\dagger_{\mathbf{k}\sigma} c_{\mathbf{k}\sigma} + \sum_{\mathbf{k},\mathbf{k}',\sigma} V_{\mathbf{k}\mathbf{k}'} c^\dagger_{\mathbf{k}\sigma} c_{\mathbf{k}'\sigma} \tag{2.10}$$

with $V_{\mathbf{k}\mathbf{k}'} = \langle \mathbf{k}|V_\mathrm{imp}|\mathbf{k}'\rangle$. However, such a model is not sufficient to deliver a good description of transition metals or rare earth impurities [1].

Earlier works [5, 31] led to the idea of a virtual bound state close below the Fermi level ε_F which is associated with the impurity. A repulsive Coulomb interaction U favors the single occupation of the impurity and leads to a local moment at smaller temperatures. The interaction term renders the problem much more difficult and it cannot be understood in a single-particle picture anymore.

The bath electrons can be localized on the impurity due to an overlap of the conduction electron's wave function and the impurity's valence orbital. For $3d$ transition metals (such as iron), these are the d-orbitals. This is the reason why the impurity state is often denoted by $|d\rangle$ and operators creating (annihilating) a particle on the impurity by $d^\dagger$ (d). Sometimes the notation $|f\rangle$ and for the operators $f^\dagger$ (f) is used because the valence orbitals of rare earth impurities are the f-orbitals.

Mathematically, we can construct such hybridization matrix elements as the overlap integral between the bath electron's wave function described by Wannier functions

$$\Psi_{\mathbf{r}_n}(\mathbf{r}) = \frac{1}{\sqrt{N}} \sum_\mathbf{k} \mathrm{e}^{-\mathrm{i}\mathbf{k}\cdot\mathbf{r}_n} \phi_\mathbf{k}(\mathbf{r}) \tag{2.11}$$

– where $\phi_\mathbf{k}(\mathbf{r})$ are the Bloch states of the conduction electrons – and the valence orbital of the impurity $\phi_\mathrm{d}(\mathbf{r})$. The overlap matrix element, or hybridization function, is then given by

$$V_\mathbf{k} = \sum_n \mathrm{e}^{\mathrm{i}\mathbf{k}\cdot\mathbf{r}_n} \langle \phi_\mathrm{d}|H|\Psi_{\mathbf{r}_n}\rangle. \tag{2.12}$$

An additional Coulomb interaction between electrons on the impurity is introduced in order to obtain an energy regime where the impurity is singly occupied and contains a fixed local moment.

The Coulomb interaction is given by

$$U = \int\int \phi^*_\mathrm{d}(\mathbf{r})\, \phi^*_\mathrm{d}(\mathbf{r}')\, \frac{e^2}{|\mathbf{r}-\mathbf{r}'|}\, \phi_\mathrm{d}(\mathbf{r})\, \phi_\mathrm{d}(\mathbf{r}')\, \mathrm{d}^3 r \mathrm{d}^3 r'. \tag{2.13}$$

This interaction strength can be of the order of several eV, even after taking effects of delocalization and screening into account [1, 53].

Now we are ready to write down a Hamiltonian based on the idea of a virtual bound state with an energy level ε_d close below the Fermi level on which conduction electrons can be localized as a result of the hybridization function $V_{\mathbf{k}}$. The single impurity Anderson model can be written in the form

$$H = \sum_{\mathbf{k},\sigma} \varepsilon_{\mathbf{k}} c^\dagger_{\mathbf{k}\sigma} c_{\mathbf{k}\sigma} + \sum_{\mathbf{k},\sigma} \left(V_{\mathbf{k}}\, d^\dagger_\sigma c_{\mathbf{k}\sigma} + V^*_{\mathbf{k}} c^\dagger_{\mathbf{k}\sigma} d_\sigma \right) + \sum_\sigma \varepsilon_d d^\dagger_\sigma d_\sigma + U d^\dagger_\uparrow d^\dagger_\downarrow d_\downarrow d_\uparrow . \tag{2.14}$$

We use the simplest form of a non-degenerate d-orbital. In this case, there are only three different configurations of the impurity level

1) empty: $|0\rangle$: $E = 0$
2) singly occupied: $|\sigma\rangle$: $E = \varepsilon_d$
3) doubly occupied: $|\uparrow\downarrow\rangle$: $E = 2\varepsilon_d + U$.

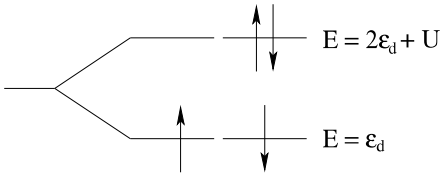

Figure 2.1: Configurations of the impurity level. For $\varepsilon_d < 0$ and $U > -\varepsilon_d$, the singly occupied state has the lowest energy. For $\varepsilon_d = -\frac{U}{2}$, the empty and doubly occupied state are degenerate.

From this simple picture we can understand why the Coulomb interaction will lead to a local moment. If $\varepsilon_d < 0$ and $U > -\varepsilon_d$, the singly occupied state is the lowest-lying so that at low temperatures the impurity level is occupied by one spin. This leads to the presence of a fixed local moment on the impurity.

2.3.1 Particle-Hole Symmetry

The Hamiltonian (2.14) obviously conserves spin symmetry

$$c^\dagger_{\mathbf{k}\sigma} \longleftrightarrow c^\dagger_{\mathbf{k}\bar{\sigma}} \tag{2.15}$$

as long as the coefficients are spin-independent. This is not necessarily the case as, for example, spin-orbit interactions or an external magnetic field can lead to spin dependent coefficients and thus to a spin-symmetry broken case.

Besides the spin symmetry, there is a certain set of parameters for which the model additionally exhibits particle-hole symmetry in the sense that

$$\begin{aligned} c^\dagger_{\mathbf{k}\sigma} &\longleftrightarrow c_{-\mathbf{k}\sigma} \\ d^\dagger_\sigma &\longleftrightarrow -d_\sigma . \end{aligned} \tag{2.16}$$

One can verify that the Hamiltonian is invariant under the substitution (2.16) if

$$\varepsilon_{-\mathbf{k}\sigma} = -\varepsilon_{\mathbf{k}\sigma} , \quad V_{-\mathbf{k}} = V^*_{\mathbf{k}} , \quad \varepsilon_d = -\frac{U}{2}. \tag{2.17}$$

Under these conditions, the interacting Hamiltonian conserves particle-hole symmetry (2.16) which leads to a symmetric density of states around the Fermi level ε_F. This gives the model with the special parameters (2.17) the name *symmetric Anderson model*.

2.4 Schrieffer-Wolff Transformation

The Schrieffer-Wolff transformation [32] reveals a relation between the Anderson impurity and the Kondo model. We will reproduce this transformation using Continuous Unitary Transformations and so we want to discuss the Schrieffer-Wolff transformation in more detail.

The idea is to eliminate charge fluctuations on the impurity induced by the hybridization $V_{\mathbf{k}}$ and to construct an effective Hamiltonian by applying a unitary transformation

$$H_{\text{eff}} = \mathrm{e}^{\lambda \hat{S}} H \mathrm{e}^{-\lambda \hat{S}} \tag{2.18}$$

where $\hat{S}$ is the generator of the transformation. In order to conserve the hermiticity of the Hamiltonian, the generator has to be anti-hermitian

$$\hat{S}^\dagger = -\hat{S} \ . \tag{2.19}$$

It is convenient to expand the effective Hamiltonian in a power series of λ as long as λ is sufficiently small

$$H_{\text{eff}} = H + \sum_{n=1}^{N} \frac{\lambda^n}{n!} \left[\hat{S}, H\right]_n \tag{2.20}$$

where the recursive definition

$$\begin{aligned} \left[\hat{S}, H\right]_1 &= \left[\hat{S}, H\right] \\ \left[\hat{S}, H\right]_n &= \left[\hat{S}, \left[\hat{S}, H\right]\right]_{n-1} , \quad n > 1 \end{aligned} \tag{2.21}$$

was introduced. We write the initial Hamiltonian in the form

$$H = H_{\text{D}} + \lambda \hat{V} \tag{2.22}$$

with

$$\hat{V} = \sum_{\mathbf{k},\sigma} \left(\overline{V}_{\mathbf{k}} d_\sigma^\dagger c_{\mathbf{k}\sigma} + \overline{V}_{\mathbf{k}}^* c_{\mathbf{k}\sigma}^\dagger d_\sigma \right) \tag{2.23}$$

where $V_{\mathbf{k}} = \lambda \overline{V}_{\mathbf{k}}$. The Schrieffer-Wolff transformation eliminates the charge fluctuations induced by the hybridization in linear order. If we focus on orders up to λ^2, the effective Hamiltonian has the form

$$H_{\text{eff}} = H_{\text{D}} + \lambda \hat{V} + \lambda \left[\hat{S}, H_{\text{D}}\right] + \lambda^2 \left[\hat{S}, \hat{V}\right] + \frac{\lambda^2}{2} \left[\hat{S}, \left[\hat{S}, H_{\text{D}}\right]\right] + \mathcal{O}\left(\lambda^3\right) . \tag{2.24}$$

In order to eliminate the linear order, the generator must fulfill

$$\left[\hat{S}, H_{\text{D}}\right] = -\hat{V} \tag{2.25}$$

which is achieved by the choice of the generator

$$\hat{S} = \sum_{\mathbf{k},\sigma} \frac{\overline{V}_{\mathbf{k}}^*}{\varepsilon_{\mathbf{k}} - (\varepsilon_{\text{d}} + U)} n_{\text{d},\bar{\sigma}} c_{\mathbf{k}\sigma}^\dagger d_\sigma + \sum_{\mathbf{k},\sigma} \frac{\overline{V}_{\mathbf{k}}^*}{\varepsilon_{\mathbf{k}} - \varepsilon_{\text{d}}} \left(1 - n_{\text{d},\bar{\sigma}}\right) c_{\mathbf{k}\sigma}^\dagger d_\sigma - \text{h.c.} \ . \tag{2.26}$$

By using Eq. (2.25) in Eq. (2.24) we derive

$$H_{\text{eff}} = H_{\text{D}} + \frac{\lambda^2}{2} \left[\hat{S}, \hat{V}\right] + \mathcal{O}\left(\lambda^3\right) . \tag{2.27}$$

The commutator between the generator from Eq. (2.26) and $\hat{V}$ from Eq. (2.23) yields

$$\frac{\lambda^2}{2}\left[\hat{S},\hat{V}\right] = H_{\mathrm{ex}} + H_{\mathrm{dir}} + H_0^{'} + H_{\mathrm{ch}}. \tag{2.28}$$

All four emerging terms can be expressed in a compact way using the notation

$$\vec{\psi}_{\mathbf{k}} = \begin{pmatrix} c_{\mathbf{k}\uparrow} \\ c_{\mathbf{k}\downarrow} \end{pmatrix} \qquad \vec{\psi}_{\mathrm{d}} = \begin{pmatrix} d_{\uparrow} \\ d_{\downarrow} \end{pmatrix}. \tag{2.29}$$

The four terms are given by

a) a spin-spin exchange interaction

$$H_{\mathrm{ex}} = -\frac{1}{2}\sum_{\mathbf{k},\mathbf{k}'} J_{\mathbf{k}\mathbf{k}'}\left(\vec{\psi}_{\mathbf{k}}^{\dagger}\vec{\sigma}\vec{\psi}_{\mathbf{k}'}\right)\cdot\left(\vec{\psi}_{\mathrm{d}}^{\dagger}\vec{\sigma}\vec{\psi}_{\mathrm{d}}\right), \tag{2.30}$$

b) a direct spin-spin interaction

$$H_{\mathrm{dir}} = \sum_{\mathbf{k},\mathbf{k}'}\left[W_{\mathbf{k}\mathbf{k}'}\vec{\psi}_{\mathbf{k}}^{\dagger}\vec{\psi}_{\mathbf{k}'} + \frac{1}{2}J_{\mathbf{k}\mathbf{k}'}\left(\vec{\psi}_{\mathrm{d}}^{\dagger}\vec{\psi}_{\mathrm{d}}\right)\left(\vec{\psi}_{\mathbf{k}}^{\dagger}\vec{\psi}_{\mathbf{k}'}\right)\right], \tag{2.31}$$

c) an additional term to the impurity contributions

$$H_0^{'} = -\sum_{\mathbf{k}}\left[\sum_{\sigma} W_{\mathbf{k}\mathbf{k}}\, d_{\sigma}^{\dagger}d_{\sigma} + 2J_{\mathbf{k}\mathbf{k}}\, d_{\uparrow}^{\dagger}d_{\downarrow}^{\dagger}d_{\downarrow}d_{\uparrow}\right], \tag{2.32}$$

d) a term that couples the empty impurity level to the doubly occupied impurity level

$$H_{\mathrm{ch}} = \frac{1}{2}\sum_{\mathbf{k},\mathbf{k}'}\left(J_{\mathbf{k}\mathbf{k}'} + J_{\mathbf{k}'\mathbf{k}}\right)\left(d_{\uparrow}^{\dagger}d_{\downarrow}^{\dagger}c_{\mathbf{k}\downarrow}c_{\mathbf{k}'\uparrow} + \mathrm{h.c.}\right). \tag{2.33}$$

The coupling constants are given by

$$\begin{aligned} J_{\mathbf{k}\mathbf{k}'} &= \frac{1}{2}V_{\mathbf{k}}^{*}V_{\mathbf{k}'}\left[\frac{1}{\varepsilon_{\mathbf{k}} - (\varepsilon_{\mathrm{d}}+U)} + \frac{1}{\varepsilon_{\mathbf{k}'} - (\varepsilon_{\mathrm{d}}+U)} - \frac{1}{\varepsilon_{\mathbf{k}} - \varepsilon_{\mathrm{d}}} - \frac{1}{\varepsilon_{\mathbf{k}'} - \varepsilon_{\mathrm{d}}}\right] \\ W_{\mathbf{k}\mathbf{k}'} &= \frac{1}{2}V_{\mathbf{k}}^{*}V_{\mathbf{k}'}\left[\frac{1}{\varepsilon_{\mathbf{k}} - \varepsilon_{\mathrm{d}}} + \frac{1}{\varepsilon_{\mathbf{k}'} - \varepsilon_{\mathrm{d}}}\right]. \end{aligned} \tag{2.34}$$

The spin-spin exchange interaction contains the same operator structure as the Kondo Hamiltonian with an effective exchange coupling $J_{\mathbf{k}\mathbf{k}'}$. Thus, we have mapped the Anderson Hamiltonian to an effective Kondo model.

If we consider the spin-symmetric case $\varepsilon_{\mathrm{d}} = -\frac{U}{2}$, the diagonal elements of the spin-spin exchange coupling become

$$J_{\mathbf{k}\mathbf{k}} = |V_{\mathbf{k}}|^2\left[\frac{1}{\varepsilon_{\mathbf{k}} - \frac{U}{2}} - \frac{1}{\varepsilon_{\mathbf{k}} + \frac{U}{2}}\right]. \tag{2.35}$$

At the Fermi level we find

$$J_{\mathbf{k}_\mathrm{F}\mathbf{k}_\mathrm{F}} = -\frac{4\,|V_{\mathbf{k}_\mathrm{F}}|^2}{U}. \tag{2.36}$$

This is an antiferromagnetic coupling as an additional minus sign was introduced in Eq. (2.30). The antiferromagnetic coupling of the spin-spin exchange interaction leads to the Kondo singlet just as explained in Sec. 2.2. The Kondo temperature for the symmetric Anderson model is given by

$$T_\mathrm{K} \propto \mathrm{e}^{-\frac{1}{2\rho J}} = \mathrm{e}^{-\frac{U}{8\rho V^2}}. \tag{2.37}$$

The bath electrons' density of states ρ is evaluated at the Fermi level. The exponential behavior in the Coulomb interaction U is a good benchmark to check if a method describes the Kondo effect or not.

2.5 Energy Representation

It is very useful to express the SIAM in terms of new operators labeling energies instead of momenta. Explicit results are given for the diagonal dispersion

$$H_\mathrm{D} = \sum_{\mathbf{k},\sigma} \varepsilon_\mathbf{k} c^\dagger_{\mathbf{k}\sigma} c_{\mathbf{k}\sigma}, \tag{2.38}$$

the hybridization

$$H_\mathrm{V} = \sum_{\mathbf{k},\sigma} \left(V_\mathbf{k}\, d^\dagger_\sigma c_{\mathbf{k}\sigma} + V^*_\mathbf{k} c^\dagger_{\mathbf{k}\sigma} d_\sigma \right) \tag{2.39}$$

and for a very general structured operator

$$H_\mathrm{J} = \sum_{\{\mathbf{k}_i,\sigma_i\}} J^{\sigma_1\cdots\sigma_N}_{\mathbf{k}_1\cdots\mathbf{k}_N} \hat{O}^{\sigma_1\cdots\sigma_N}_{\mathbf{k}_1\cdots\mathbf{k}_N} + \mathrm{h.c.} \tag{2.40}$$

where the operator $\hat{O}^{\sigma_1\cdots\sigma_N}_{\mathbf{k}_1\cdots\mathbf{k}_N}$ is of the form

$$\hat{O}^{\sigma_1\cdots\sigma_N}_{\mathbf{k}_1\cdots\mathbf{k}_N} = \hat{O} : \prod_{i=1}^{N} c^{(\dagger)}_{\mathbf{k}_i\sigma_i} : . \tag{2.41}$$

The operator $\hat{O}$ denotes an arbitrary operator acting only on the impurity. Note that, for example, the spin-spin interaction from Eq. (2.30) is governed by such an operator of this general structure. The first step is to introduce a continuum approximation for the quasi-continuum of the bath electrons. Because of the isotropic coefficients $\varepsilon_{|\mathbf{k}|}$ and $V_{|\mathbf{k}|}$, it is convenient to introduce spherical coordinates. Finally, a substitution $k \to \varepsilon(k)$ is used. Carrying out these steps leads to the continuum energy representation. The reader is referred to Ref. [8] or App. 9.6 for the explicit execution of these steps.

The continuum energy representation for the operators from Eqs. (2.38) - (2.40) is given by

$$\begin{aligned} H_{\mathrm{D}} &\rightarrow \sum_{\sigma} \int_{-D}^{D} \mathrm{d}\varepsilon \; \varepsilon \, c_{\varepsilon\sigma}^{\dagger} c_{\varepsilon\sigma} \\ H_{\mathrm{V}} &\rightarrow \sum_{\sigma} \int_{-D}^{D} \mathrm{d}\varepsilon \; \sqrt{\rho(\varepsilon)} \; \left(V(\varepsilon) \, d_{\sigma}^{\dagger} c_{\varepsilon\sigma} + V^{*}(\varepsilon) \, c_{\varepsilon\sigma}^{\dagger} d_{\sigma} \right) \\ H_{\mathrm{J}} &\rightarrow \sum_{\{\sigma_i\}} \int_{-D}^{D} \mathrm{d}\varepsilon_1 \cdots \int_{-D}^{D} \mathrm{d}\varepsilon_N \, J_{\varepsilon_1 \cdots \varepsilon_N}^{\sigma_1 \cdots \sigma_N} \left(\prod_{i=1}^{N} \sqrt{\rho(\varepsilon_i)} \right) \hat{O}_{\varepsilon_1 \cdots \varepsilon_N}^{\sigma_1 \cdots \sigma_N} + \mathrm{h.c.} \end{aligned} \tag{2.42}$$

where $\rho(\varepsilon)$ is the density of states of the bath electrons. We see that the structure of the general operator only depends on the number of bath operators.

The Anderson model in energy representation is of the form

$$\begin{aligned} H &= \sum_{\sigma} \int_{-D}^{D} \mathrm{d}\varepsilon \; \varepsilon \, c_{\varepsilon\sigma}^{\dagger} c_{\varepsilon\sigma} + \sum_{\sigma} \int_{-D}^{D} \mathrm{d}\varepsilon \; \sqrt{\rho(\varepsilon)} \; \left(V_{\varepsilon} \, d_{\sigma}^{\dagger} c_{\varepsilon\sigma} + V_{\varepsilon}^{*} c_{\varepsilon\sigma}^{\dagger} d_{\sigma} \right) \\ &+ \varepsilon_{\mathrm{d}} \sum_{\sigma} d_{\sigma}^{\dagger} d_{\sigma} + U d_{\uparrow}^{\dagger} d_{\downarrow}^{\dagger} d_{\downarrow} d_{\uparrow}. \end{aligned} \tag{2.43}$$

The continuum representation is not very well suited for a numerical treatment. Consequently, we need to discretize this representation again. At first sight, it might seem a bit like running in circles but note that during the transformation a lot of information is shifted to the density of states ρ of the bath electrons. Additionally, the energy representation is better suited to develop a discretization scheme that fits the challenges of the exponentially varying energy scales of the Kondo problem.

2.6 Logarithmic Discretization

The important energy scales of the Kondo problem reach from energies of the order of the bandwidth D down to exponentially small energies below the Kondo temperature T_{K}. A linear discretization is not a suitable approach for such a problem. A discretization scheme that is better suited for the challenges of the Kondo problem is the logarithmic discretization sketched in Fig. 2.2. For a detailed discussion, see Ref. [10].

The continuum of the bath electron states is discretized in exponentially decreasing intervals

$$\frac{I_n^{+}}{D} = \left[\Lambda^{-n-1}, \Lambda^{-n} \right] \qquad \frac{I_n^{-}}{D} = \left[-\Lambda^{-n}, -\Lambda^{-n-1} \right] \tag{2.44}$$

where $\Lambda > 1$ is a discretization parameter and $n \in \mathbb{N}$. The length of such an interval is given by

$$\frac{d_n}{D} = \left(1 - \Lambda^{-1} \right) \Lambda^{-n}. \tag{2.45}$$

The higher energy scales are only covered with a low precision while small energy scales have a very high resolution. This discretization scheme easily reaches down to exponentially small energy scales. In the following, the two different discretization schemes used in this thesis are discussed.

2.6.1 Discretization of a Flat Density Of States

The discretization of the model (2.43) is achieved by discretizing the bath electrons' density of states [10]. We replace the continuum by one energy level in each interval $I_n^{\pm}$.

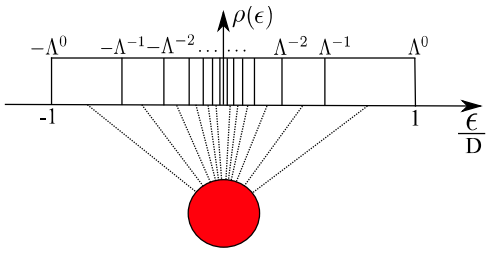

Figure 2.2: Logarithmic discretization of a continuum of bath-electron states sketched for a flat density of states $\rho(\varepsilon) = \rho_0 \Theta(D-|\omega|)$ with $\rho_0 = \frac{1}{2D}$ and a bandwidth $2D$ coupled to an impurity.

The energy levels are given as the energy average over the corresponding interval where the averaging function is the bath electrons' density of states ρ.

The real information about the density of states is contained within the discretization of the hybridization function.

If we take a constant hybridization function into account, then each level should carry the same weight as the undiscretized interval. Hence, we collect all the weight in each interval by integrating the bath electrons' density of states. The formal representation is given by

$$\varepsilon_n^{\pm} = \frac{1}{\left|\gamma_n^{\pm}\right|^2} \int_{n,\pm} \varepsilon\, \rho(\varepsilon)\, \mathrm{d}\varepsilon\,, \quad \left|\gamma_n^{\pm}\right|^2 = \int_{n,\pm} \rho(\varepsilon)\, \mathrm{d}\varepsilon \tag{2.46}$$

where we integrate over the intervals $I_n^{\pm}$

$$\int_{n,+} = \int_{D\Lambda^{-n-1}}^{D\Lambda^{-n}}, \qquad \int_{n,-} = \int_{-D\Lambda^{-n}}^{-D\Lambda^{-n-1}}. \tag{2.47}$$

Then the discretized Hamiltonian is of the form

$$H = \sum_{s=\pm} \sum_{n,\sigma} \varepsilon_n^s c_{n\sigma,s}^{\dagger} c_{n\sigma,s} + \sum_{s=\pm} \sum_{n,\sigma} V \gamma_n^s \left(c_{n\sigma,s}^{\dagger} d_\sigma + d_\sigma^{\dagger} c_{n\sigma,s} \right). \tag{2.48}$$

For a flat density of states

$$\rho(\omega) = \rho_0 \Theta(D-|\omega|)\,, \quad \rho_0 = \frac{1}{2D}, \tag{2.49}$$

we can easily calculate the parameters (2.46) as

$$\frac{\varepsilon_n^{\pm}}{D} = \pm \frac{1}{2} \left(1+\Lambda^{-1}\right) \Lambda^{-n}, \quad \left|\gamma_n^{\pm}\right|^2 = \frac{1}{2} \left(1-\Lambda^{-1}\right) \Lambda^{-n}. \tag{2.50}$$

As this procedure does not affect the d-operators at all, we can simply use the initial interaction part of the undiscretized Hamiltonian

$$\begin{aligned} H &= \sum_{s=\pm} \sum_{n,\sigma} \varepsilon_n^s c_{n\sigma,s}^{\dagger} c_{n\sigma,s} + \sum_{s=\pm} \sum_{n,\sigma} V \gamma_n^s \left(c_{n\sigma,s}^{\dagger} d_\sigma + d_\sigma^{\dagger} c_{n\sigma,s} \right) \\ &+ \varepsilon_{\mathrm{d}} \sum_{\sigma} d_\sigma^{\dagger} d_\sigma + U d_\uparrow^{\dagger} d_\downarrow^{\dagger} d_\downarrow d_\uparrow. \end{aligned} \tag{2.51}$$

This discretization scheme is very well established and was extensively used throughout the last decades. For further information, the reader is referred to Refs. [8, 10].

2.6.2 Discretization of the Lorentzian Density Of States

We can also construct a different discretized approximation for the continuum Hamiltonian (2.43). The approach in the last section focused on the flat density of states of the bath electrons. The resulting Hamiltonian still contains a hybridization term and is thus not diagonal for $U = 0$. Now we want to construct a discretized approximation so that the Hamiltonian is diagonal for $U = 0$. The influence of the hybridization is then shifted to the dispersion and the d-operators. The density of states of the Anderson model without interaction is given by the Lorentzian DOS [1]

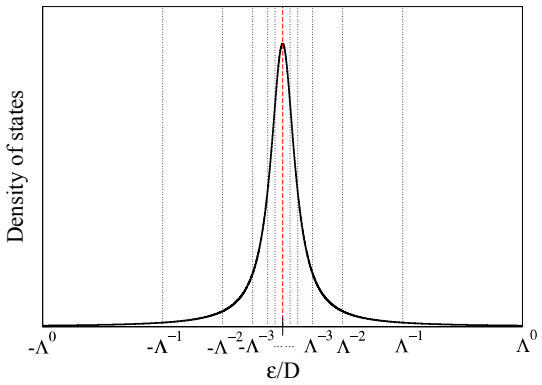

Figure 2.3: Logarithmic discretization of the Lorentzian DOS.

$$\rho^0_{\mathrm{dd}} = \frac{1}{\pi}\frac{\Delta}{\Delta^2+\omega^2} \tag{2.52}$$

where $\Delta = \pi\rho_0 V^2$. In contrast to the previous approach, the d-operators must be transformed so that the Hamiltonian is diagonal. The transformation will be chosen in a way that the discretized model reproduces the density of states (2.52). We denote the transformation of the impurity operator by

$$d^\dagger_\sigma = \sum_{\alpha=\pm}\sum_n \gamma^\alpha_n c^\dagger_{n\sigma,\alpha}. \tag{2.53}$$

The $\gamma^\pm_n$ are chosen so that the density of states of the free Hamiltonian ρ^0_{dd} can be reconstructed from the discretized model. The dd-Green's function of the discretized model

$$G^\pm_{\mathrm{dd}} = \langle \mathrm{gs}|d_\sigma \frac{1}{\omega-\left(H-E_{\mathrm{gs}}\right)\pm is} d^\dagger_\sigma|\mathrm{gs}\rangle + \langle \mathrm{gs}|d^\dagger_\sigma \frac{1}{\omega+\left(H-E_{\mathrm{gs}}\right)\pm is} d_\sigma|\mathrm{gs}\rangle \tag{2.54}$$

can be calculated by exploiting Eq. (2.53) and using the Fermi sea as the ground state. The density of states can then be calculated by using the Sokhatsky-Weierstrass theorem and focusing on the imaginary part

$$\rho^0_{\mathrm{dd}}(\omega) = -\lim_{s\to 0^+}\frac{1}{\pi}\mathrm{Im}G^+_{\mathrm{dd}} = \sum_{s=\pm}\sum_n |\gamma^s_n|^2\delta\left(\omega-\varepsilon^s_n\right). \tag{2.55}$$

In the spirit of the last section, we choose for the on-site energies $\varepsilon^\pm_n$ the energy average with respect to the Lorentzian density of states over an interval $I^\pm_n$. From Eq. (2.55) we see that the $|\gamma^\pm_n|^2$ must be the collected weight of the Lorentzian density of states of an interval $I^\pm_n$

$$\varepsilon^\pm_n = \frac{1}{\left|\gamma^\pm_n\right|^2}\int_{n,\pm}\varepsilon\,\rho^0_{\mathrm{dd}}(\varepsilon)\,\mathrm{d}\varepsilon\,, \quad \left|\gamma^\pm_n\right|^2 = \int_{n,\pm}\rho^0_{\mathrm{dd}}(\varepsilon)\mathrm{d}\varepsilon. \tag{2.56}$$

For the Lorentzian density of states, these parameters can still be calculated analytically as

$$\begin{aligned}\left|\gamma^\pm_n\right|^2 &= \frac{1}{\pi}\tan^{-1}\left(\frac{D}{\Delta}\Lambda^{-n}\right) - \frac{1}{\pi}\tan^{-1}\left(\frac{D}{\Delta}\Lambda^{-n-1}\right) \\ \frac{\varepsilon^\pm_n}{D} &= \pm\frac{1}{2\pi\left|\gamma^\pm_n\right|^2}\frac{\Delta}{D}\ln\left(\frac{\Lambda^{-2n}+\left(\frac{\Delta}{D}\right)^2}{\Lambda^{-2n-2}+\left(\frac{\Delta}{D}\right)^2}\right).\end{aligned} \tag{2.57}$$

The major difference to the approach of the last section is the transformation of the d-operator which leads to a completely non-local Hamiltonian. The discretized effective Hamiltonian is of the form

$$\begin{aligned} H &= \sum_{s=\pm}\sum_{n,\sigma} \varepsilon_n^s c_{n\sigma,s}^\dagger c_{n\sigma,s} + \varepsilon_\mathrm{d} \sum_{s_1,s_2=\pm} \sum_{n_1,n_2,\sigma} \gamma_{n_1}^{s_1}\gamma_{n_2}^{s_2} c_{n_1\sigma,s_1}^\dagger c_{n_2\sigma,s_2} \\ &+ U \sum_{\{n_i,s_i=\pm\}} \gamma_{n_1}^{s_1}\gamma_{n_2}^{s_2}\gamma_{n_3}^{s_3}\gamma_{n_4}^{s_4} c_{n_1\uparrow,s_1}^\dagger c_{n_2\downarrow,s_2}^\dagger c_{n_3\downarrow,s_3} c_{n_4\uparrow,s_4}. \end{aligned} \tag{2.58}$$

This representation is well suited for an expansion in the interaction parameter U. Additionally, the ground state of the non-interacting Hamiltonian is a Fermi sea. On the other hand, the resulting Hamiltonian exhibits a strong non-locality as all combinations of the sites appear in the interaction part.

We will use both approaches in this thesis and try to construct an effective Hamiltonian using Continuous Unitary Transformations. The representation (2.58) can be mapped to a local problem using a Lanczos tridiagonalization which is described in Chap. 5.

2.7 Energy Regimes of the SIAM

The physics of the Anderson model strongly depends on the considered energy scales. In the symmetric Anderson model ($\varepsilon_\mathrm{d} = -\frac{U}{2}$) there are three different energy regimes with distinct features which will be explained briefly in the following. For an extensive discussion, see Ref. [8].

A. **Free-orbital (FO) regime** ($E \gg U, \Delta$)
On high energy scales (larger than the U-energy scale) the interaction does not play a significant role. Excitations on these energy scales are not affected by the small interaction on the impurity. This leads to an impurity that behaves effectively as if it were non-interacting. Hence, in this regime we look at free bath electrons and an effectively free impurity orbital which gives rise to the name of this regime. The energy levels of the Hamiltonian in this regime can be constructed from the non-interacting Hamiltonian for $U, V = 0$. Of course, one can use the interaction term U and the hybridization V as small perturbations which only provides satisfying results for large temperatures well above the U- and Δ-energy scale. When the temperature is lowered, perturbation theory breaks down. The effect of U lifts the quadruple degeneracy of the possible impurity configurations while the hybridization shifts the energies by a factor proportional to V^2. As mentioned earlier, these effects are very small on the considered energy scales.

B. **Local-moment (LM) regime** ($U \gg E \gg T_\mathrm{K}$)
As energies are reduced below the U-energy scale, it becomes important that the quadruple degeneracy of the possible impurity configurations is lifted by the interaction. Well below the U-energy scale, charge fluctuations are frozen out by the interaction U as the empty or doubly occupied states lie with an energy $\frac{U}{2}$ above the singly occupied state. Consequently, in the local-moment regime the impurity is singly occupied and a localized spin-carrying state is present at the impurity. As we already know from the Schrieffer-Wolff transformation, this energy regime can be described by an effective Kondo Hamiltonian where the singly occupied impurity is coupled to the bath with an effective coupling $J = \frac{4V^2}{U}$ close to the Fermi level. As the effective coupling J is small while the

Coulomb interaction U is large compared to the considered energies, one can also use the limit $J = 0$ and $U \to \infty$. Again, one can include the influence of the coupling J perturbatively as long as one stays well inside the local-moment regime. The perturbative treatment is identical to the one for the Kondo model from which we know that it breaks down on the Kondo energy scale.

C. **Strong-coupling (SC) regime** ($E \ll T_K$)
When energies are decreased even further below the exponentially small Kondo temperature T_K, the spin-spin interaction J, induced by the hybridization V and interaction U, leads to the formation of a singlet state of the local moment on the impurity and a bath electron's spin. Well below the Kondo energy scale T_K, where excitation energies are smaller than the binding energy of the singlet, one can use the effective Kondo model in the strong-coupling limit $J \to \infty$. In this limit the excitation energies are too small to break up the singlet state. This additionally freezes out spin-fluctuations on the impurity and results in the complete screening of the impurity.

There are two more energy regimes in the case of the asymmetric Anderson model ($\varepsilon_d \neq -\frac{U}{2}$) [9]. Because the asymmetric Anderson model is not discussed in this thesis, the additional energy regimes are only mentioned very briefly.

D. **Valence-fluctuation regime**
The valence-fluctuation regime corresponds to the case where the doubly occupied state is thermally depopulated while the remaining empty and singly occupied levels are degenerate and decoupled from the bath electrons. When energies are lowered, the free-orbital regime crosses to the valence-fluctuation regime which itself crosses to the local-moment regime when energies are decreased further. The basic physics well inside this regime can be understood by using the limit $\Delta, \varepsilon_d = 0$ and $U \to \infty$.

E. **Frozen-impurity regime**
In the asymmetric case, there is also the stable frozen-impurity regime in which additionally the doubly occupied state becomes thermally depopulated while only the empty impurity level remains. Well inside this regime, one can use an effective Hamiltonian which is given by the free-electron Hamiltonian and an empty impurity state which corresponds to the limit $\Delta, U = 0$ and $\varepsilon_d \to \infty$.

2.8 Density Of States (DOS)

The above mentioned energy scales for the symmetric Anderson model are also manifest in the density of states (DOS). For $U = 0$, the DOS can be calculated analytically. The interested reader is referred to Ref. [1]. For the bath electrons, a flat density of states

$$\rho_0(\omega) = \rho_0 \Theta(D - |\omega|), \quad \rho_0 = \frac{1}{2D} \tag{2.59}$$

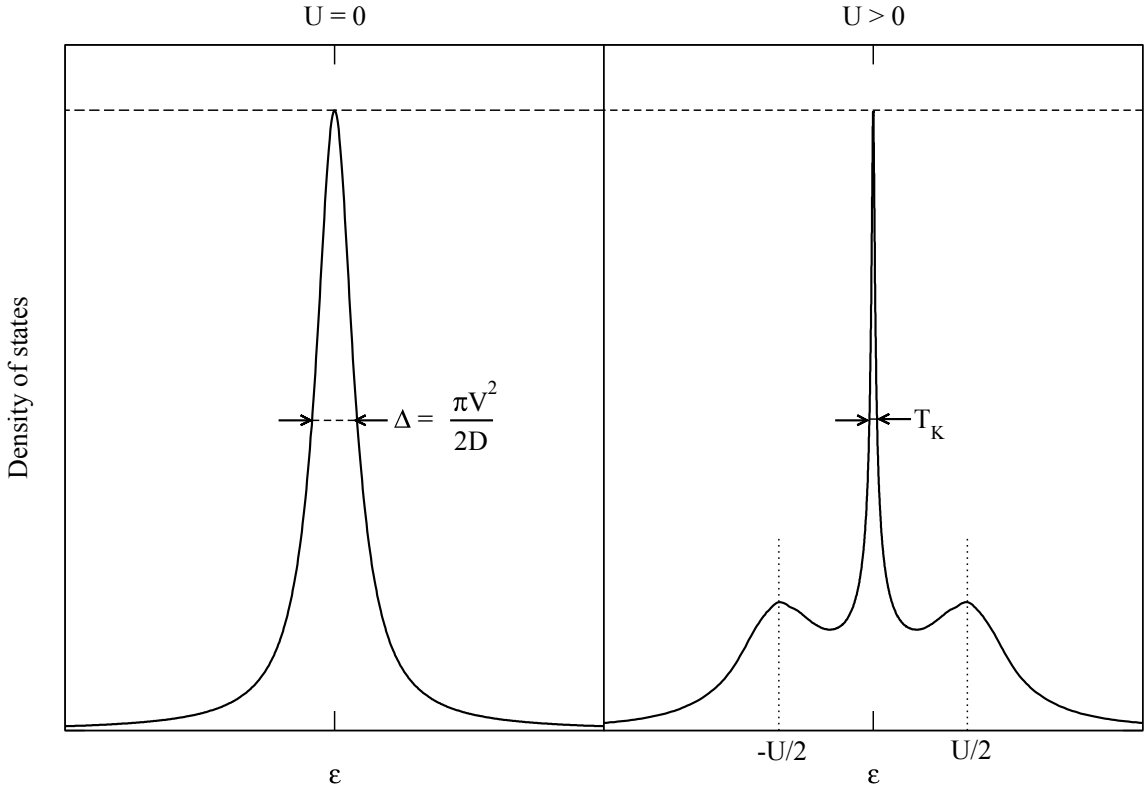

Figure 2.4: Density of states for the non-interacting (left) and the interacting symmetric Anderson model (right). For $U = 0$, the density of states is a Lorentzian with width $\Delta = \pi\rho_0 V^2$ where $\rho_0 = \frac{1}{2D}$. For $U > 0$, the width of the Kondo peak around the Fermi level becomes exponentially small and is given by the Kondo temperature T_K. Additionally, the so-called Hubbard satellites occur on the U-energy scale.

with a bandwidth $2D$ is used. In this case, the hybridization leads to a Lorentzian density of states

$$\rho(\omega) = \frac{1}{\pi}\frac{\Delta}{\Delta^2 + \omega^2} \tag{2.60}$$

with the width $\Delta = \pi\rho_0 V^2$ where $\rho_0 = \frac{1}{2D}$. Introducing the interaction changes the appearance of the DOS. The width of the Kondo peak around the Fermi level becomes exponentially small and is given by the Kondo temperature T_K. This many-body resonance is induced by magnetic scattering at the Fermi level and can be understood in a Fermi liquid quasi-particle picture [1] which is appropriate in the strong-coupling regime below the exponentially small Kondo temperature T_K. The interactions of the quasi-particles can be absorbed into renormalizations of the resonance width of the non-interacting model by replacing Δ from Eq. (2.60) by $\tilde{\Delta} \sim T_K$. The height of the Kondo peak of the interacting Anderson model at the Fermi level remains constant, although the peak's width is reduced. There is additionally a new feature, the so-called Hubbard satellites which arise symmetrically around the Kondo peak. For the atomic limit $\Delta = 0$, it can be shown that the Hubbard satellites occur at the positions $\varepsilon = \pm\frac{U}{2}$ [1].

3 Scaling Theory

In the following sections we refer to scaling theory as the construction of a series of effective Hamiltonians, each of the same form but with a reduced bandwidth and renormalized parameters. Anderson termed this method in the context of the Kondo model a "poor man's scaling approach" [15]. This method is able to reveal the exponential character of the Kondo temperature but fails to solve the Kondo problem due to diverging couplings.

This chapter is supposed to give the reader that is not familiar with conventional scaling enough information in order to understand the similarity between scaling and the CUT approach explained in Chap. 4.

The forerunners of this scaling approach came from a series of papers in which Anderson *et. al.* showed the equivalence between the Kondo model and a one-dimensional statistical problem [33–36] for which they derived scaling laws. Anderson reproduced these results with the new version of scaling [15]. Further information on the history of scaling and renormalization can be found in the literature given in Sec. 3.3.

The idea of scaling theory is to construct an effective Hamiltonian with an effective bandwidth $D_{\text{eff}} < D$ which contains the same low-energy physics as the initial model. In order to construct this effective model, all couplings to energies larger than the effective bandwidth are eliminated first. In the "poor man's version" the couplings to higher energies are eliminated in second-order perturbation theory. For further information on the scaling approach, see Refs. [16, 54]. The first example of a very similar procedure was used in the context of the construction of an effective potential in superconductivity theory [55]. This work inspired Anderson to develop the "poor man's scaling" for the Kondo model [15, 35, 36]. The method was also applied to the Anderson model [56, 57]. We will revisit the examples discussed in this chapter later in the context of Continuous Unitary Transformations in Sec. 4.6.

In the scaling approach the Hilbert space is separated in a subspace of low and a subspace of high energies

$$\begin{aligned} H_{\mathrm{D}}|\mathrm{p}\rangle &= E_{\mathrm{p}}|p\rangle \quad \text{where } |p\rangle \in \text{subspace of low energies } \left|E_{\mathrm{p}}\right| < \frac{D}{s} \\ H_{\mathrm{D}}|\mathrm{q}\rangle &= E_{\mathrm{q}}|q\rangle \quad \text{where } |q\rangle \in \text{subspace of high energies } \left|E_{\mathrm{q}}\right| > \frac{D}{s} \end{aligned} \tag{3.1}$$

with $s > 1$ and where H_{D} describes the diagonal part of the Hamiltonian. We introduce projectors P and $Q = 1 - P$, where P projects on the low-energy subspace H_{P} while Q projects on the high-energy subspace H_{Q}. By using these projectors the Hamiltonian can be written in the form

$$H = PHP + QHQ + PHQ + QHP. \tag{3.2}$$

The most crude approximation would be to neglect all parts but that projected to small energies

$$\bar{H} = PHP. \tag{3.3}$$

In most cases, the successive application of H leads to hopping processes from small to high energies and back. Those terms already occur in second order and therefore the approximation

(3.3) would neglect physically important contributions to the low-energy physics even in second order.

A much better approximation is to eliminate the couplings between low- and high-energy states in second-order perturbation theory first, before projecting on the low-energy subspace. A single-step transformation was already introduced for the Schrieffer-Wolff transformation in Sec. 2.4. We can again use the expansion (2.20) for the Hamiltonian

$$H_{\text{eff}} = \mathrm{e}^{\lambda \hat{S}} H \mathrm{e}^{-\lambda \hat{S}}. \tag{3.4}$$

The Hamiltonian is split into a diagonal part and a non-diagonal part

$$H = H_{\text{D}} + \lambda H_{\text{V}} \tag{3.5}$$

while the generator is determined by

$$\left[\hat{S}, H_{\text{D}}\right] = -\tilde{H}_{\text{V}} \tag{3.6}$$

where $\tilde{H}_{\text{V}}$ contains all parts of H_{V} that couple the high- and the low-energy part of the Hamiltonian. This choice leads to the effective Hamiltonian

$$H_{\text{eff}} = H_{\text{D}} + \lambda \left(H_{\text{V}} - \tilde{H}_{\text{V}}\right) + \mathcal{O}\left(\lambda^2\right). \tag{3.7}$$

The Hamiltonian H_{eff} (before projecting on the low-energy subspace) does not couple the low- and high-energy subspaces in linear order anymore and thus hopping processes from small to high energies and back do not occur in second order.

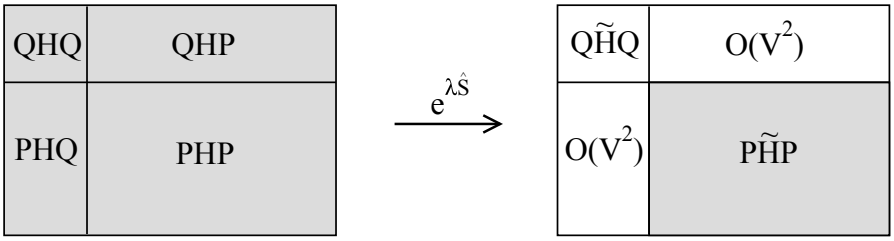

Figure 3.1: Sketch of the separation of the high and small energy subspaces in the scaling approach. The part $H_{\text{V}} = PHQ + QHP$ is eliminated by a second-order one-step transformation before neglecting the parts $Q\tilde{H}Q$, $P\tilde{H}Q$ and $Q\tilde{H}P$.

Projecting the effective Hamiltonian (3.7) on small energies

$$PH_{\text{eff}}P = P\left(H_{\text{D}} + \lambda H_{\text{V}}\right)P + \frac{\lambda^2}{2} P\left[\hat{S}, H_{\text{V}}\right]P + \mathcal{O}\left(\lambda^3\right) \tag{3.8}$$

yields a much better approximation than the one from Eq. (3.3). If the effective Hamiltonian is of the same form as the initial Hamiltonian, we can take the limit $s \to 1$ and derive the change of the couplings induced by an infinitesimally small step $\delta D = \left(1 - \frac{1}{s}\right) D$. From this we can derive a scaling equation which describes the flow of the parameters to smaller energies.

In the next sections some examples for the scaling approach are discussed. We will revisit these examples in the context of Continuous Unitary Transformations in Sec. 4.6.

3.1 Potential Scattering Model

In order to introduce the scaling approach, one might start with an elementary but very instructive example [16] which also provides insights on the interpretation of the results obtained from the scaling of the Kondo model.

We turn to a simple bilinear, non-interacting Hamiltonian in the form

$$H = \sum_{\mathbf{k}} \varepsilon_{\mathbf{k}} c_{\mathbf{k}}^{\dagger} c_{\mathbf{k}} + g \sum_{\mathbf{k},\mathbf{k}'} c_{\mathbf{k}}^{\dagger} c_{\mathbf{k}'} \tag{3.9}$$

which is also known as the potential scattering model. We further assume a constant density of states for $g = 0$

$$\rho = \begin{cases} \frac{1}{D} & \text{if } 0 < \varepsilon < D \\ 0 & \text{otherwise} \end{cases} . \tag{3.10}$$

Before solving the scaling equation we want to look at some characteristics we already know of the potential scattering model.

Analytical results

The exact solution (cf. Ref. [16]) can be found by using a $N \times N$ representation of the Hamiltonian (3.9) and applying it to a not yet determined eigenvector $\mathbf{v}$. Determining the components v_i and the eigenvalues E_i from the resulting equations has been achieved in Ref. [16]. For a repulsive potential $g > 0$, the exact one-particle energies $E_{\mathbf{k}} = \varepsilon_{\mathbf{k}} + \Delta\varepsilon_{\mathbf{k}}$ are given by

$$\Delta\varepsilon_{\mathbf{k}} = \frac{g}{1 + \rho g \ln\left(D/\varepsilon_{\mathbf{k}}\right)}. \tag{3.11}$$

For an attractive potential $g < 0$, a bound state with an energy

$$E = -D\mathrm{e}^{-\frac{1}{|\rho g|}} \tag{3.12}$$

forms close below the band edge [16]. The binding energy of this bound state is very small for $|\rho g| \ll 1$.

Perturbation theory

If we want to tackle the potential scattering model with standard second-order perturbation theory, we have to calculate

$$E_{\mathbf{k}} = \varepsilon_{\mathbf{k}} + \langle \mathbf{k}|H_{\mathrm{int}}|\mathbf{k}\rangle + \sum_{\mathbf{q}\neq\mathbf{k}} \frac{|\langle \mathbf{k}|H_{\mathrm{int}}|\mathbf{q}\rangle|^2}{\varepsilon_{\mathbf{k}} - \varepsilon_{\mathbf{q}}}. \tag{3.13}$$

Applying $H_{\mathrm{int}} = g\sum_{\mathbf{k},\mathbf{k}'} c_{\mathbf{k}}^{\dagger} c_{\mathbf{k}'}$ in Eq. (3.13) yields

$$E_{\mathbf{k}} = \varepsilon_{\mathbf{k}} + g + g^2 \sum_{\mathbf{q}\neq\mathbf{k}} \frac{1}{\varepsilon_{\mathbf{k}} - \varepsilon_{\mathbf{q}}} = \varepsilon_{\mathbf{k}} + g - \rho g^2 \ln\left(\frac{D - \varepsilon_{\mathbf{k}}}{\varepsilon_{\mathbf{k}}}\right) \tag{3.14}$$

where the sum was calculated in the continuum limit. For energies much smaller than the bandwidth $\varepsilon \ll D$, this is simply the second-order expansion of the exact result (3.11)

$$\Delta\varepsilon_{\mathbf{k}} = g - \rho g^2 \ln\left(\frac{D}{\varepsilon_{\mathbf{k}}}\right). \tag{3.15}$$

As we are in a quasi-continuum, we can always find an energy scale for which perturbation theory breaks down, even for an arbitrarily small coupling g. A negative energy shift is predicted which disagrees completely with the exact result. Thus, one is unable to describe the low-energy physics in second-order perturbation theory, even for very small couplings g where one would naively expect reliable results.

This is interesting because problems of the same kind occur in the Kondo model where standard perturbation theory also breaks down on the exponentially small Kondo energy scale T_K. This requires the development of new ways for using perturbation theory which better meet the challenges of such problems.

Scaling theory

We want to eliminate the terms that couple the low- and high-energy subspaces. We will focus on a continuum limit of the model

$$H = \int_0^D \varepsilon\, c_\varepsilon^\dagger c_\varepsilon \,\mathrm{d}\varepsilon + \rho g \int\int_0^D c_\varepsilon^\dagger\, c_{\varepsilon'} \,\mathrm{d}\varepsilon\,\mathrm{d}\varepsilon'. \tag{3.16}$$

The generator

$$\hat{S} = \rho \int\int_0^D S_{\varepsilon\varepsilon'}\, c_\varepsilon^\dagger\, c_{\varepsilon'} \,\mathrm{d}\varepsilon\,\mathrm{d}\varepsilon' \tag{3.17}$$

with

$$S_{\varepsilon\varepsilon'} = \begin{cases} \frac{g}{\varepsilon-\varepsilon'} & \text{if either } \varepsilon \text{ or } \varepsilon' > \frac{D}{s} \\ 0 & \text{otherwise} \end{cases} \tag{3.18}$$

fulfills Eq. (3.6) where H_D is the Hamiltonian for $g = 0$ and H_V the residual part. By calculating the commutator in Eq. (3.8), already projecting to low energies $\in H_\mathrm{P}$ via the projector P from Eq. (3.2) and focusing on small energies, we can determine the effective Hamiltonian (3.8)

$$PH_\mathrm{eff}P = \int_0^{D/s} \varepsilon\, c_\varepsilon^\dagger c_\varepsilon \,\mathrm{d}\varepsilon + \left[\rho g - \rho^2 g^2 \int_{D/s}^D \frac{1}{z}\,\mathrm{d}z\right] \int\int_0^{D/s} c_\varepsilon^\dagger\, c_{\varepsilon'} \,\mathrm{d}\varepsilon\,\mathrm{d}\varepsilon'. \tag{3.19}$$

The effective Hamiltonian is of the same form as the initial Hamiltonian but with a reduced bandwidth $\frac{D}{s}$ and an effective renormalized coupling

$$\rho g_\mathrm{eff} = \rho g - \frac{\rho^2 g^2}{D}\delta D \tag{3.20}$$

where the limit $s \to 1$ was used. δD describes the reduction of the bandwidth $D_\mathrm{eff} = D - \delta D$ or

$$\delta D = \left(1 - \frac{1}{s}\right) D. \tag{3.21}$$

We can now repeat this procedure, each time reducing the bandwidth by δD and rescaling the parameters of the Hamiltonian. From Eq. (3.20) we can deduce a *scaling equation* for $s \to 1$ which describes the change of the renormalized coupling during the flow to smaller effective bandwidths via

$$\frac{\mathrm{d}g}{\mathrm{d}D} = \frac{\rho g^2}{D}. \tag{3.22}$$

Such scaling equations are often written in the form

$$\frac{\mathrm{d}g}{\mathrm{d}\ln D} = \rho g^2. \tag{3.23}$$

This differential equation can be solved by separation of variables

$$g_{\mathrm{eff}} = \frac{g}{1+\rho g \ln\left(\frac{D}{D_{\mathrm{eff}}}\right)}. \tag{3.24}$$

For a repulsive coupling $g > 0$, the effective coupling becomes weaker when decreasing the effective bandwidth. The coupling g_{eff} is the energy shift $\Delta\varepsilon$ on the energy scale D_{eff}. Surprisingly enough, this result agrees perfectly with the exact result (3.11), although we only used second-order perturbation theory. This is a property of this special model and certainly not true in general. Nevertheless, the scaling approach rearranges perturbation theory in a way that enables us to derive correct results up to a certain order, even when standard perturbation theory breaks down.

If we take a closer look at the result (3.24), we see that the scaling equation does not always lead to a satisfying effective Hamiltonian. If we consider an attractive coupling constant $g < 0$, the effective coupling will increase and eventually diverge on an energy scale

$$D_{\mathrm{eff}} = D\mathrm{e}^{-\frac{1}{|\rho g|}} \tag{3.25}$$

which we recognize from Eq. (3.12). Thus, we can link the break-down of the scaling approach to the appearance of a bound state. The break-down occurs on the energy scale which corresponds to the binding energy of the bound state. This is a very interesting result and gives significant insights into the physics of the Kondo model as will be described in the following section.

3.2 Scaling for the Kondo Model

The scaling approach for the Kondo model is discussed in Refs. [15, 35, 36] and summarized in Refs. [1, 16]. We start from the Kondo Hamiltonian (2.5) in integral representation

$$H = \sum_{\sigma}\int_{-D}^{D} x : c^{\dagger}_{x\sigma}c_{x\sigma} : \mathrm{d}x + \rho_0 \sum_{\mu\in x,y,z}\sum_{\alpha,\beta}\int\int_{-D}^{D} J^{\mu}\sigma^{\mu}_{\alpha\beta}\tau^{\mu} : c^{\dagger}_{x_1\alpha}c_{x_2\beta} : \mathrm{d}x_1\mathrm{d}x_2 \tag{3.26}$$

where we use a flat density of states $\rho_0 = \frac{1}{2D}$ for the bath electrons. The colons denote normal-ordering with respect to the Fermi sea (cf. Sec. 4.5). The generator of the transformation is chosen to be of the form

$$\hat{S} = \rho_0 \sum_{\mu\in x,y,z}\sum_{\alpha,\beta}\int\int_{-D}^{D} S^{\mu}_{x_1x_2}\sigma^{\mu}_{\alpha\beta}\tau^{\mu} : c^{\dagger}_{x_1\alpha}c_{x_2\beta} : \mathrm{d}x_1\,\mathrm{d}x_2 \tag{3.27}$$

where

$$S^{\mu}_{x_1x_2} = \begin{cases} \frac{J^{\mu}}{x_1-x_2} & \text{if either } |x_1| \text{ or } |x_2| > \frac{D}{s} \\ 0 & \text{otherwise} \end{cases}. \tag{3.28}$$

Calculating the commutator between $\hat{S}$ and H_J

$$\begin{aligned}&\frac{1}{2}P\left[\hat{S},H_\mathrm{J}\right]P\\ =\;&\rho_0\sum_{\mu\in x,y,z}\sum_{\alpha,\beta}\int\int_{-D/s}^{D/s}\mathrm{d}x_1\mathrm{d}x_2\left[\rho_0\sum_{i,j}\left|\varepsilon_{ij\mu}\right|\left[\int_{D/s}^{D}\frac{n(-z)-n(z)}{z}\mathrm{d}z\right]J^iJ^j\right]\sigma^\mu_{\alpha\beta}\tau^\mu:c^\dagger_{x_1\alpha}c_{x_2\beta}:\end{aligned}$$

with the occupation number

$$n(z)=\langle\mathrm{FS}|c^\dagger_{z\sigma}c_{z\sigma}|\mathrm{FS}\rangle \tag{3.29}$$

yields the effective Hamiltonian (3.7) projected to small energies. The effective Hamiltonian is of the same form as the initial Hamiltonian but with a renormalized coupling

$$\tilde{J^\mu} \;=\; J^\mu-\rho_0\sum_{i,j}\left|\varepsilon_{ij\mu}\right|\left(\frac{n(D)-n(-D)}{D}\right)J^iJ^j\delta D. \tag{3.30}$$

The x-dependence of the expression in the integral over z is neglected which is justified when focusing on the renormalization at very small energies around the Fermi level. Additionally, the couplings J^i would exhibit an energy dependence at higher energies when applying the scaling step. Focusing only on the couplings at the Fermi level is an essential approximation of the scaling approach as analytical solutions could not be derived otherwise. This approximation is systematically justified in Sec. 6.8.2.

For zero temperature the occupation number is given by the Heaviside function $n(\varepsilon)=\Theta(-\varepsilon)$ and thus the scaling equations for the Kondo model become

$$\begin{aligned}\frac{\mathrm{d}J^x}{\mathrm{d}D} &= -\frac{2\rho_0}{D}J^yJ^z\\ \frac{\mathrm{d}J^y}{\mathrm{d}D} &= -\frac{2\rho_0}{D}J^xJ^z\\ \frac{\mathrm{d}J^z}{\mathrm{d}D} &= -\frac{2\rho_0}{D}J^xJ^y.\end{aligned} \tag{3.31}$$

In order to gain some insights into the behavior of these scaling equations, we consider the case

$$J^x=J^y=J_\perp \tag{3.32}$$

for which the scaling equations simplify to

$$\frac{\mathrm{d}J_\perp}{\mathrm{d}\ln D}=-2\rho_0J_\perp J_z\,,\quad \frac{\mathrm{d}J_z}{\mathrm{d}\ln D}=-2\rho_0J_\perp^2. \tag{3.33}$$

The hyperbolic scaling trajectory

$$J_\perp^2-J_z^2=\text{const.} \tag{3.34}$$

is constant during the flow to a smaller effective bandwidth D_eff. The flow trajectories are sketched in Fig. 3.2.

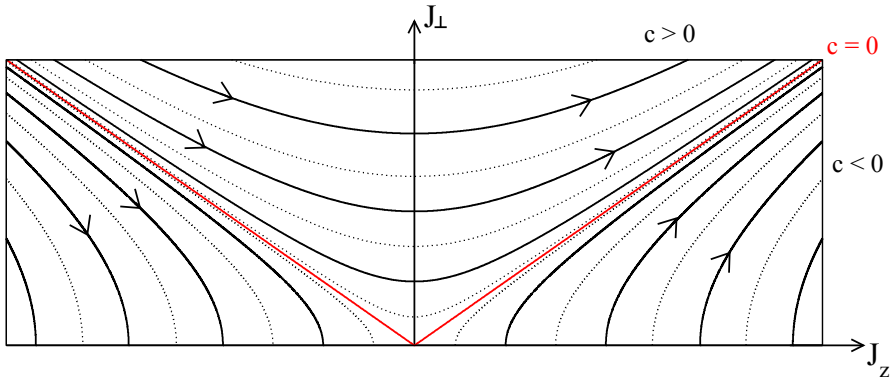

Figure 3.2: Scaling trajectories $J_\perp^2 - J_z^2 = c$ of the Kondo model with $J^x = J^y = J_\perp$. A fixed point of the equation (3.33) is $J_\perp = 0$. As we see from Eq. (3.33), J_z is always increasing for decreasing bandwidths. If initially $J_\perp = |J_z|$, we find the special trajectory $J_\perp = |J_z|$. This trajectory separates the regions where $J_\perp < |J_z|$ and $J_\perp > |J_z|$. In the first region in which $J_\perp < |J_z|$, the coupling $J_\perp$ scales to zero for a ferromagnetic coupling $J_z < 0$ and to ever stronger couplings for an antiferromagnetic coupling $J_z > 0$. The region where $J_\perp > |J_z|$ leads to a decreasing $J_\perp$ for $J_z < 0$ but flows towards a constant value $J_\perp > 0$ for $J_z \to 0^-$ and increases for $J_z > 0$ as the bandwidth decreases.

Finally, we want to study an isotropic coupling $J_\perp = J_z = J$. The scaling equation for the coupling is

$$\frac{\mathrm{d}J_{\mathrm{eff}}}{\mathrm{d}\ln D_{\mathrm{eff}}} = -2\rho_0 J_{\mathrm{eff}}^2. \tag{3.35}$$

Integrating this differential equation by separation of variables leads to

$$J_{\mathrm{eff}}(D_{\mathrm{eff}}) = \frac{J}{1 + 2\rho_0 J \ln(\frac{D_{\mathrm{eff}}}{D})}. \tag{3.36}$$

For a ferromagnetic coupling $J < 0$, the scaling equation converges and scales to zero for $D_{\mathrm{eff}} \to 0$. An antiferromagnetic coupling $J > 0$, on the other hand, leads to a divergence on the Kondo energy scale

$$T_{\mathrm{K}} = D\mathrm{e}^{-\frac{1}{2\rho_0 J}}. \tag{3.37}$$

We already encountered such a behavior in Eq. (3.24). We know from the potential scattering model that a bound state induces such a behavior so that we can suppose that a very similar mechanism leads to the divergence in the case of the Kondo model, i.e., in the case of an antiferromagnetic coupling we find a bound state with a binding energy that is given by the Kondo temperature T_{K}. We also know that the coupling is growing stronger during the flow to smaller energy scales, i.e., spin-flip contributions will dominate at small energies which results in the occurrence of a singlet ground state [58], the so-called Kondo singlet.

In conclusion, the ”poor man’s scaling” fails to solve the Kondo problem as it only leads to satisfying solutions as long as no bound state is present. In the case of the potential scattering model, we find the exact low-lying single-particle energies for $g > 0$ while the scaling approach fails for an attractive coupling $g < 0$. In the Kondo model the scaling equations converge for a ferromagnetic coupling $J < 0$ but lead to a divergent coupling J_{eff} for an antiferromagnetic coupling $J > 0$. Nevertheless, the method is able to reveal the exponential character of the Kondo temperature T_{K}.

A method that is able to solve the Kondo problem is the *numerical renormalization group* (NRG) where, in contrast to earlier methods, the renormalization step is performed numerically.

3.3 Numerical Renormalization Group (NRG)

The *numerical renormalization group* (NRG) is a very powerful tool that is able to deal with the challenges of the Kondo problem. We will compare some results obtained by CUT with NRG calculations in Chap. 5. For this reason, the main ideas of the NRG approach are briefly outlined in the following. For a detailed discussion of the method, the reader is referred to the literature given in this section, especially to the recent review [10].

Renormalization group (RG) ideas were first developed in high energy physics in order to deal with UV-divergences occurring in perturbative treatments. For a historical overview, see for example Ref. [59]. The first applications in statistical physics were in the context of phase transitions and critical exponents and were first introduced by Wilson [60, 61]. For an overview, see for example Refs. [7, 62–65]. A *RG transformation* (RGT) R is of the form

$$H_{N+1} = R(H_N) \tag{3.38}$$

where R transforms the Hamiltonian H_N, which describes the physics on a characteristic energy scale, onto another Hamiltonian H_{N+1} describing the physics on another (usually smaller) energy scale. Applying R successively leads to a RG flow which starts at high energies while it approaches ever smaller energies in the subsequent flow.

In the "poor man's version" of the earlier sections the RGT transforms the initial Hamiltonian into a Hamiltonian of the same form with the sole difference that the high-energy excitations of the bath electrons are absorbed in the renormalizations of the parameters.

The difference of Wilson's NRG approach [8–10, 46] to most other RG approaches is that the RG step is performed numerically. The general strategy in NRG is to use the logarithmic discretization from Sec. 2.6.1 and to transform the Hamiltonian to a semi-infinite chain by a Lanczos tridiagonalization which is discussed in Sec. 5.1. The RG transformation for the chain can be defined as the extension of the chain by one further site (and rescaling all energies by a factor $\sqrt{\Lambda}$) which corresponds to the inclusion of a smaller energy scale (and rescaling the current energy scale to be of the order $\mathcal{O}(1)$). Starting from a finite chain length, which can be diagonalized exactly, the Hilbert space increases by a constant factor in each RG step. In order for the NRG approach to remain numerically tractable, one has to truncate a certain fraction of the highest-lying eigenstates which are obtained after each diagonalization. This truncation relies on the separation of energy scales and the exponentially decreasing hopping elements t_n (5.11) of the chain representation.

A very important subject connected to the RG flow is the notion of fixed points

$$H^* = R(H^*)\,. \tag{3.39}$$

The fixed points of the Anderson model are related to the energy regimes discussed in Sec. 2.7. Note that only R^2 (applying R twice) has fixed points as the results differ for even and odd chain lengths N. As a result, applying R once – which extends the chain length by one – does not fulfill Eq. (3.39). During the RG flow the Hamiltonian comes close to different fixed point Hamiltonians H^* which can be described by fairly simple effective Hamiltonians. For the symmetric Anderson model, these fixed points are the unstable *free-orbital* and *local-moment fixed points* as well as the stable *strong-coupling fixed point* to which the flow finally converges. The physics of these fixed points is described in Sec. 2.7 and the simple effective Hamiltonians describing them are further explained in Sec. 5.4.4.

4 Continuous Unitary Transformations

4.1 Flow Equation

The method of Continuous Unitary Transformations provides a theoretical tool that transforms a Hamiltonian closer (or even completely) to diagonal form. Continuous Unitary Transformations were first introduced by Wilson and Głazek [66, 67] under the title *similarity renormalization scheme* in the context of high energy physics and independently by Wegner [11] under the name *flow equation method* in the context of condensed matter theory. Around the same time a similar approach was investigated by mathematicians under the name *Double Bracket Flow* [68] and *Isospectral Flow* [69, 70]. We will focus on the branch laid by Wegner. For more information about the *similarity renormalization scheme*, see Refs. [71, 72].

For easy problems, as for example Hamiltonians in the form of small finite matrices or non-interacting fermionic systems, the method of Continuous Unitary Transformations can be carried out without any approximations providing exact results. In terms of numerical accuracy and calculation effort, however, it is less efficient than most conventional methods such as the various numerical procedures for exact diagonalization. But with increasing complexity most methods, especially exact ones, start to become impractical while Continuous Unitary Transformations can still be a very powerful tool for constructing effective models describing the physical aspects under consideration.

The CUT approach was used for a wide range of problems in many-body theory including electron-phonon couplings [73, 74], dissipative quantum systems and the spin-boson model [75–78], the Hubbard model [79–82], the Anderson impurity model [21–23], spin-systems [13, 83–87], one-dimensional spinless fermions [88], the sine-Gordon model [89, 90], interacting bosonic systems [91], heavy fermions [92], Fermi and Luttinger liquids [93], and the Kondo model [18–20, 94, 95]. A very broad overview on further applications of CUT is given in Ref. [96]. The quartic oscillator [97] can be used as a pedagogical introduction to CUT. Further details on the method are outlined in Ref. [16].

The aim of CUT is to construct a Hamiltonian closer to diagonality which is connected to the initial Hamiltonian by a unitary transformation. In principle, a self-adjoint operator can always be brought to diagonality by a unitary transformation. Finding this transformation, however, is a major problem of theoretical quantum mechanics and, in general, a challenging task. The idea of CUT is to introduce a unitary transformation that changes continuously as a function of a flow parameter l. One might picture this procedure thinking of a piecewise transformation of a finite set of unitary transformations

$$H_{N+1} = U_N H_N U_N^\dagger \tag{4.1}$$

where the transformation U_N is constructed from H_N so that $\lim_{N\to\infty} H_N$ is closer to diagonality. The unitary transformation that connects the initial Hamiltonian H_0 with the Hamiltonian H_N is given by

$$U_N^{\text{full}} = U_{N-1} U_{N-2} \ldots U_1 U_0. \tag{4.2}$$

Approaching problems with a finite set of unitary transformations is used in the *projector-based renormalization method* (PRM) [98, 99]. Instead of performing a finite set of single unitary transformations, Wegner introduced a continuous parameter l which describes the change of the Hamiltonian induced by a sequence of infinitesimal unitary transformations. This procedure can still be expressed as one single unitary transformation connecting the initial Hamiltonian at $l = 0$ and the Hamiltonian at the current point of the flow

$$H(l) = U(l) H(0) U^{\dagger}(l). \tag{4.3}$$

From Eq. (4.3) one finds $U(0) = \mathbb{1}$. Taking the derivative of Eq. (4.3) leads to

$$\partial_l H(l) = [\eta(l), H(l)] \tag{4.4}$$

with the anti-hermitian generator

$$\eta(l) = \frac{\partial U(l)}{\partial l} U^{\dagger}(l). \tag{4.5}$$

The anti-hermiticity can be shown using the unitarity of U by calculating the derivative of $U^{\dagger}U = \mathbb{1}$. Equation (4.4) is called *flow equation* and is the heart of the Continuous Unitary Transformation approach. The transformation $U(l)$ from Eq. (4.3) can be constructed from the flow of the generator. Multiplying Eq. (4.5) with U from the right yields

$$\frac{\partial U(l)}{\partial l} = \eta(l) U(l). \tag{4.6}$$

The formal solution of the resulting equation (4.6) is given by

$$U(l) = \mathcal{L} \mathrm{e}^{\int_0^l \eta(l') \mathrm{d}l'} \tag{4.7}$$

where $\mathcal{L}$ is an l-ordering super-operator which orders products of operators depending on l from left to right in descending order in l. The l-ordering is important because, in general,

$$\left[\eta(l), \eta\left(l'\right)\right] \neq 0. \tag{4.8}$$

Constructing U from Eq. (4.7) for further calculations of an observable $\hat{O}$

$$\hat{O}(l) = U(l) \hat{O} U^{\dagger}(l) \tag{4.9}$$

is not efficient. Instead, we can solve the flow equation for observables

$$\partial_l \hat{O}(l) = \left[\eta(l), \hat{O}(l)\right] \tag{4.10}$$

with the initial condition $\hat{O}(0) = \hat{O}$. The flow equation for observables (4.10) can be deduced by taking the derivative of Eq. (4.9) and by identifying the generator (4.5) in the resulting expression. In order to set up the flow equation, we need to know how to choose the generator (4.5). There are a number of different possibilities and in the following sections the most common ones are discussed.

4.2 Generators

4.2.1 Wegner's Generator

The first suggestion for the choice of a generator was given by Wegner [11]. He separated the Hamiltonian into a diagonal part H_d and a non-diagonal part H_r. The generator is then chosen as

$$\eta_\mathrm{W}(l) = [H_\mathrm{d}(l), H_\mathrm{r}(l)]. \tag{4.11}$$

Note that we do not need more information than we already have at the current state of the flow. If we write the Hamiltonian in matrix representation with the matrix elements

$$h_{nm} = \langle n|H|m\rangle, \quad \varepsilon_n = \langle n|H|n\rangle, \tag{4.12}$$

then the matrix elements of Wegner's generator are of the form

$$\eta_{\mathrm{W},nm} = (\varepsilon_n - \varepsilon_m) h_{nm}. \tag{4.13}$$

The flow equation (4.4) becomes

$$\partial_l h_{nm} = -(\varepsilon_n - \varepsilon_m)^2 h_{nm} + \sum_{s\neq n,m} (\varepsilon_n + \varepsilon_m - 2\varepsilon_s) h_{ns} h_{sm}. \tag{4.14}$$

From this simple calculation we can draw very insightful conclusions. If we calculate the derivative of the square sum of the non-diagonal elements, we find

$$\partial_l \sum_{\substack{n,m \\ n\neq m}} |h_{nm}|^2 = -2 \sum_{\substack{n,m \\ n\neq m}} (\varepsilon_n - \varepsilon_m)^2 |h_{nm}|^2 \leq 0. \tag{4.15}$$

The norm of the off-diagonal elements is monotonically decreasing and finally even vanishing for the limit $l \to \infty$ as long as no degeneracies[1] occur. Terms that couple degenerate states are not eliminated by Wegner's generator while all terms that couple non-degenerate states will eventually vanish for $l \to \infty$. Thus, Wegner's generator fulfills all the required properties. We can already identify the energy separation of the CUT approach as matrix elements with large energy differences converge faster than those with small energy differences.

Since a matrix representation is, in general, not very well suited to describe realistic problems in many-body theory because of the exponentially large size of the considered Hilbert space, a representation in second quantization is often used. One can then still construct Wegner's generator from Eq. (4.11).

4.2.2 Mielke's Generator

Mielke used another generator [12] that has the special advantage that matrices which are initially band diagonal, i.e.,

$$h_{nm} = 0 \quad \forall\ |n-m| > N_c \tag{4.16}$$

maintain this property during the flow. The generator he proposed is based on a sign function and its matrix elements are given by

$$\eta_{\mathrm{M},nm} = \mathrm{sgn}(n-m)\, h_{nm}. \tag{4.17}$$

[1] By degeneracies we refer to $\varepsilon_n(l) = \varepsilon_m(l)$.

The flow equation induced by this choice of the generator is of the form

$$\partial_l h_{nm} = -\mathrm{sgn}\,(n-m)\,(\varepsilon_n - \varepsilon_m)\,h_{nm} + \sum_{s\neq n,m} \left[\mathrm{sgn}\,(n-s) - \mathrm{sgn}\,(s-m)\right] h_{ns} h_{sm}. \tag{4.18}$$

By setting $m = n + N_c + r$ with $r > 0$ and using Eq. (4.16) for $l = 0$ we find

$$\partial_l h_{n,n+N_c+r} = 0 \quad \forall\, r > 0, \tag{4.19}$$

i.e., the band structure (4.16) is indeed conserved during the whole flow. From the flow equation (4.18) we can construct

$$\partial_l \sum_{n=0}^{r} \varepsilon_n = -2 \sum_{n=0}^{r} \sum_{s=r+1}^{N} |h_{ns}|^2 \leq 0 \tag{4.20}$$

where all elements for $s < r+1$ cancel because of the sign function and the hermiticity of H. If the Hamiltonian is bounded from below, which is always true for finite matrices, Eq. (4.20) implies that the differential equation (DEQ) must converge. In this case, the non-diagonal matrix elements h_{nm} must tend to zero for $l \to \infty$ for all n and m as r is arbitrary.

In contrast to the flow induced by Wegner's generator, the derivative of the square sum over the non-diagonal elements is not necessarily negative, i.e., the norm of the off-diagonal elements h_{nm} is not a monotonically decreasing function of l and thus the Hamiltonian can be less diagonal at finite l than it is for $l = 0$. In the limit $l \to \infty$, however, the Hamiltonian will become diagonal as the non-diagonal elements tend to zero.

We can analyze the asymptotic behavior of the flow. If the non-diagonal elements vanish for large l, the quadratic term in Eq. (4.18) becomes negligible at some point during the flow. For large values of l, we can then write

$$\partial_l h_{nm} = -\mathrm{sgn}\,(n-m)\,(\varepsilon_n - \varepsilon_m)\,h_{nm}. \tag{4.21}$$

We already know that the h_{nm} must tend to zero and thus we conclude

$$\mathrm{sgn}\,(n-m)\,(\varepsilon_n - \varepsilon_m) > 0 \tag{4.22}$$

for large l. As we did not require this ordering of the diagonal elements for $l = 0$, Mielke's generator must order the diagonal elements in ascending order during the flow so that $n < m \Rightarrow \varepsilon_n < \varepsilon_m$.

4.2.3 Knetter and Uhrig's Generator

Particle Conserving Generator

Knetter and Uhrig suggested a generator suited for Hamiltonians in second quantization [13, 14]. Their choice leads to a particle conserving effective Hamiltonian for $l \to \infty$. This generator can be considered a generalization of Mielke's generator for Hamiltonians in second quantization and is thus often referred to as MKU- (Mielke-Knetter-Uhrig) or pc- (particle-conserving) generator. A detailed discussion of the MKU- and further generators described in this section can be found in Refs. [81, 100]. A Hamiltonian in second quantization can always be written in the form

$$H = \sum_{i,j} H_i^j \tag{4.23}$$

where H_i^j contains all contributions that annihilate i and create j particles. Then the pc-generator is defined as

$$\eta_{\mathrm{pc}} = \sum_{i,j} \mathrm{sgn}\,(j-i)\, H_i^j \tag{4.24}$$

or in the eigenbasis $\{|n\rangle\}$ of the particle-counting operator Q with $Q|n\rangle = q_n|n\rangle$

$$\eta_{\mathrm{pc},ij} = \mathrm{sgn}\left(q_i - q_j\right) h_{ij} \tag{4.25}$$

where $h_{ij} = \langle i|H|j\rangle$ is the coefficient of the operator that changes from the state $|j\rangle$ to the state $|i\rangle$. Without loss of generality, the eigenstates shall be ordered as follows

$$i > j \quad \Rightarrow \quad q_i \geq q_j. \tag{4.26}$$

One can again construct the flow equation (4.4) which is of a very similar formal structure as for the generators before

$$\partial_l h_{ij} = -\mathrm{sgn}\left(q_i - q_j\right)\left(h_{ii} - h_{jj}\right) h_{ij} + \sum_{s\neq i,j} \left[\mathrm{sgn}\left(q_i - q_s\right) - \mathrm{sgn}\left(q_s - q_j\right)\right] h_{is} h_{sj}. \tag{4.27}$$

In order to analyze properties of the pc-generator, we investigate the derivative of the first $r+1$ diagonal elements

$$\partial_l \sum_{i=0}^{r} h_{ii} = 2 \sum_{i=0}^{r} \sum_{s=r+1}^{N} \mathrm{sgn}\left(q_i - q_s\right) |h_{is}|^2 \tag{4.28}$$

where again all terms with $s < r+1$ cancel because of the anti-hermiticity of the generator. From the ordering (4.26) we find

$$\partial_l \sum_{i=0}^{r} h_{ii} < 0. \tag{4.29}$$

From Eq. (4.29) we can deduce that the DEQ must converge if the Hamiltonian is bounded from below and thus

$$\lim_{l\to\infty} \mathrm{sgn}\left(q_i - q_j\right) \left|h_{ij}\right|^2 = 0 \quad \forall\, i,j. \tag{4.30}$$

The limit holds true for all i and j because r is arbitrary. Equation (4.30) implies that the effective model will contain no terms that switch from one subspace with a fixed number of particles to another one. Only terms that conserve the number of particles survive the flow, i.e.,

$$[Q, H_{\mathrm{eff}}] = 0. \tag{4.31}$$

This is a major simplification as one can treat all subspaces with a fixed number of particles separately.

We can again analyze the asymptotic behavior and look at i and j with $q_i \neq q_j$. Then the elements h_{ij} tend to zero for large l and the quadratic term in Eq. (4.27) can be neglected which yields

$$\partial_l h_{ij} = -\mathrm{sgn}\left(q_i - q_j\right)\left(h_{ii} - h_{jj}\right) h_{ij}. \tag{4.32}$$

From Eq. (4.30) we know that these elements have to vanish for $l \to \infty$ and thus

$$\mathrm{sgn}\left(q_i - q_j\right)\left(h_{ii} - h_{jj}\right) > 0 \tag{4.33}$$

for large l. As we do not rely on the ordering (4.26) (we just introduced it to verify that the generator converges), we know from Eq. (4.33) that the pc-generator orders the diagonal elements in ascending order of the particle number of the eigenstates [12, 88, 100].

Sign-Generator

If the considered Hamiltonian is already particle conserving, the pc-generator is obviously not very well suited for the problem. One can use the sign-generator in such a case.

We split the Hamiltonian in a part H_d (which we know how to treat) and the residual part H_r. We switch to the eigenbasis of H_d

$$H_\mathrm{d}|n\rangle = \varepsilon_n|n\rangle. \tag{4.34}$$

Without loss of generality, the basis states shall be ordered such that

$$m > n \quad \Rightarrow \quad \varepsilon_m \geq \varepsilon_n. \tag{4.35}$$

Then the matrix elements of the sign-generator have the form

$$\eta_{\mathrm{sign},nm} = \mathrm{sgn}\,(\varepsilon_n - \varepsilon_m)\, h_{nm} \tag{4.36}$$

where h_{nm} are the coefficients of the operators connecting the states $|n\rangle$ and $|m\rangle$. The flow equation is of the well-known structure

$$\partial_l h_{nm} = -\,|\varepsilon_n - \varepsilon_m|\, h_{nm} + \sum_{s\neq n,m} \left[\mathrm{sgn}\,(\varepsilon_n - \varepsilon_s) - \mathrm{sgn}\,(\varepsilon_s - \varepsilon_m)\right] h_{ns} h_{sm} \tag{4.37}$$

and again we find

$$\partial_l \sum_{n=0}^{r} \varepsilon_n = 2 \sum_{n=0}^{r} \sum_{s=r+1}^{N} \mathrm{sgn}\,(\varepsilon_n - \varepsilon_s)\, |h_{ns}|^2 < 0 \tag{4.38}$$

where the inequality holds true because of the ordering (4.35). If the Hamiltonian is bounded from below, it follows from Eq. (4.38) that the DEQ must converge and that

$$\lim_{l\to\infty} \mathrm{sgn}\,(\varepsilon_n - \varepsilon_m)\, |h_{nm}|^2 = 0 \quad \forall\, n,m \tag{4.39}$$

as r is arbitrary. Consequently, operators that couple two non-degenerate states must vanish in the limit $l \to \infty$.

Next, we take a closer look at the asymptotic behavior. Again, terms which couple two non-degenerate states must vanish for large l. When these elements become small, the quadratic term in Eq. (4.37) is negligible and leads to the asymptotic behavior

$$\partial_l h_{nm} = -\,|\varepsilon_n - \varepsilon_m|\, h_{nm} \tag{4.40}$$

where ε_n and ε_m have already converged, i.e., their l-dependence can be neglected in leading order. Thus, the matrix elements exhibit an exponential behavior for large l

$$h_{nm} = \tilde{h}_{nm} \mathrm{e}^{-|\varepsilon_n - \varepsilon_m| l} \tag{4.41}$$

where $\tilde{h}_{nm}$ is a constant with respect to the flow parameter l. As ε_n is an energy, we now find a physical interpretation of the flow parameter which is an inverse energy in the case of the sign-generator. Thus, while l increases during the flow, we proceed to smaller energy differences of the range l^{-1}. When the flow has proceeded to an energy scale l^{-1}, coefficients of operators contributing to the generator and connecting two states with higher energy difference than l^{-1} have commonly already approached their asymptotic behavior and vanish exponentially. On the other hand, coefficients of operators which are not present in the generator and which correspond to higher energy differences than l^{-1} have already converged, i.e., their l-dependence is negligible in the subsequent flow. This again is a property of the flow equation method which is similar to the energy separation of RG approaches and which is demonstrated in Chap. 5 explicitly.

4.2.4 Ground-State Generator

There are further variants of the generator. One of the most important ones is the ground-state (gs-) generator (see e.g. Refs. [81, 100–102]). If the transformation eliminates all terms that couple the reference state, which is chosen as the ground state of H_d, to higher excited states, the generator features gs-generator properties. In this case, the reference state becomes the ground state of the effective Hamiltonian for $l \to \infty$. If the minimal requirements for a gs-generator are fulfilled, the generator can be referred to as the gs-generator. All generators introduced so far fulfill gs-generator properties (and more).

In general, the gs-generator can be expressed as

$$\eta_\mathrm{gs} = \sum_{i>0} (H_{0i} - H_{i0}) \tag{4.42}$$

where H_{0i} denotes all terms that couple the ground state of H_d (denoted by the index 0) to an excitation above it (denoted by the index $i > 0$).

If all creation operators from the chosen operator basis in which H_d is diagonal create excitations, the reference state is the vacuum with respect to the respective operator basis[2]. In this case, all terms that contain only creation or only annihilation operators have to be included in the generator as far as the operators are normal-ordered with respect to the vacuum state. This generator is used explicitly in Chap. 5.

If, on the other hand, the chosen operator basis in which H_d is diagonal contains creation operators which create particles on a level with negative energy, all negative levels in the reference state are occupied. In this case, all terms that result in an excitation above the Fermi sea must be eliminated for $l \to \infty$. As far as the operators are normal-ordered with respect to the Fermi sea, a term is included into the generator if all energy differences occurring in this term are of the same sign. This generator is explicitly used in Chap. 6.

The gs-generator converges if the energy spectrum is bounded from below. A detailed discussion and a proof of convergence of the gs-generator can be found in Ref. [101] and an overview is given in Ref. [81].

The ground-state generator in the context of a zero-particle state suggests other variants of generators. One could, for example, include all terms that couple the zero-particle vacuum state and all states including one particle to states with more particles. This generator is often referred to as $\eta_\mathrm{gs,1p}$ or simply η_1p. These kind of generators are also discussed in the references given above.

4.3 Variants of Continuous Unitary Transformations

So far we presented a general theoretical framework for the method of Continuous Unitary Transformations. We know how to set up the flow equation and how to construct the generator. When we commute the generator and the Hamiltonian in order to derive the flow equation (4.4), in general, new terms arise which are not present in the initial Hamiltonian. These new terms arise during the flow and must be commuted with the generator as well which leads to further terms and so on. For an infinitely large system, the number of arising terms is often arbitrarily

[2] An example is the separation of particle and hole states. In this case, the Fermi sea corresponds to a vacuum with respect to particles and holes.

large while in finite systems the number of arising terms is growing exponentially. This leads to practical problems and the necessity to introduce approximations at some point.

Different more or less systematic ways of determining how to find sensible approximations have been developed. Famous examples are the self-similar CUT (sCUT) that was used in the original work by Wegner [11] and which was extensively used in Refs. [81, 100–107], the perturbative CUT (pCUT) [13, 108, 109] and the enhanced perturbative CUT (epCUT) with its non-perturbative extrapolation: the directly evaluated enhanced perturbative CUT (deepCUT) [110, 111]. A further branch is a graph-theory based version called gCUT [112].

In this thesis the sCUT approach is used in Chap. 5, and in Chaps. 6 and 7 the employed truncation schemes are justified by deepCUT. A brief overview of the different approaches is given in the following (except gCUT).

4.3.1 Self-Similar CUT (sCUT)

A self-similar approach to CUT can be applied by choosing a fixed class of basis operators $\hat{O}_n$ beforehand (most commonly by a truncation scheme that determines the classes of terms which are discarded) and then performing all commutations between the generator and the Hamiltonian as long as new terms emerge.

Determining which terms to keep and which to neglect is one of the main problems within this CUT approach. Common criteria are, for example, the distance between two operators (e.g. in real space or energy) or the number of operators that a term includes. Of course, a physical understanding of the problem helps to decide which terms are important and which ones are not, but such rules vary from model to model and cannot be deduced generally.

Another common and more systematic way of deciding if a term is important or not is to count how many commutations it takes until the term emerges first. This procedure is justified if the coefficients of the commuted terms are small. In this case, every commutation increases the order of the small parameter in which the new term emerges. This procedure sounds perturbative but it is not. Self-similar CUTs are non-perturbative in nature, even when truncated in orders of a small parameter. Because of the truncation, one can find a closed system of differential equations. The Hamiltonian during the flow is expressed as

$$H(l) = \sum_n h_n(l)\,\hat{O}_n \tag{4.43}$$

where only the coefficients h_n depend on l while the operator basis $\hat{O}_n$ is fixed. Although the construction of the flow equation is, in general, a hard task, it is easy to write down the general structure of the resulting differential equation which is bilinear

$$\partial_l h_n(l) = \sum_{i,j} D^n_{ij}\, h_i(l)\, h_j(l)\,. \tag{4.44}$$

The main task is to calculate the explicit form of the D^n_{ij} which depend on the choice of the generator and stem from the commutations of the basis operators $\hat{O}_n$. In most problems the D^n_{ij} must be calculated numerically by a program which is able to calculate the needed commutators and add newly arising terms to the Hamiltonian. Such a program was originally developed by S. Duffe [102] (see Sec. 5.4.1).

The non-perturbative character of the sCUT approach is explicitly required when encountering the Kondo problem as perturbative approaches result in IR-divergences and are not able to describe the crossover from one energy regime (described in Sec. 2.7) to another.

4.3.2 Perturbative CUT (pCUT)

In contrast to the non-perturbative sCUT approach, Continuous Unitary Transformations can also be performed perturbatively [13, 108, 109]. As the Kondo problem needs non-perturbative tools, a pCUT approach is not suitable for the challenges faced in this thesis. Nevertheless, the pCUT approach shall be mentioned because deepCUT ideas stemming from perturbative ideas are used in this thesis. A pCUT can be applied to systems which can be written in the form

$$H = H_0 + \lambda \sum_{m=-N}^{N} T_m \quad \text{with} \quad [H_0, T_m] = mT_m \tag{4.45}$$

where λ is a small parameter and T_m contains all terms that create m particles (annihilate m particles if $n < 0$). The pCUT approach relies on two prerequisites which the Hamiltonian must fulfill

1. The unperturbed energy spectrum of H_0 must be equidistant with a lower boundary. The eigenenergies of H_0 are proportional to the particle number.
2. The perturbation is of the form $V = \lambda \sum_{m=-N}^{N} T_m$ (cf. Eq. (4.45)).

The initial generator is chosen to be

$$\eta = \lambda \sum_{m=-N}^{N} \operatorname{sgn}(m)\, T_m. \tag{4.46}$$

Calculating the commutator between η and H yields products of the T_m which are denoted by

$$T(\mathbf{m}) = T_{m_1} T_{m_2} ... T_{m_k} \tag{4.47}$$

where $\mathbf{m}$ is an index vector

$$\mathbf{m} = (m_1, m_2, ..., m_k) \tag{4.48}$$

with dimension $|\mathbf{m}| = k$ and where the $m_i \in \{0, \pm 1, \pm 2, ..., \pm N\}$. One can define the netto particle number that is created (annihilated) by $T(\mathbf{m})$ as

$$M(\mathbf{m}) = \sum_{i=1}^{k} m_i. \tag{4.49}$$

Then the complete Hamiltonian during the flow can be written in the form

$$H = H_0 + \sum_{k=1}^{\infty} \lambda^k \sum_{|\mathbf{m}|=k} F(l, \mathbf{m})\, T(\mathbf{m}) \tag{4.50}$$

while the full generator is given by

$$\eta = \sum_{k=1}^{\infty} \lambda^k \sum_{|\mathbf{m}|=k} \operatorname{sgn}(M(\mathbf{m}))\, F(l, \mathbf{m})\, T(\mathbf{m}) \tag{4.51}$$

where $|\mathbf{m}|$ denotes the dimension of $\mathbf{m}$. The perturbative character lies within the ansatz in which, in contrast to the sCUT approach, the coefficients are compared with respect to the

order of λ. Calculating the commutator of the generator and the Hamiltonian and comparing the coefficients leads to a differential equation for the coefficients

$$\begin{aligned} \partial_l F(l,\mathbf{m}) &= -|M(\mathbf{m})|\,F(l,\mathbf{m}) \\ &+ \sum_{\mathbf{m}=(\mathbf{m}_1,\mathbf{m}_2)} [\operatorname{sgn}(M(\mathbf{m}_1)) - \operatorname{sgn}(M(\mathbf{m}_2))]\,F(l,\mathbf{m}_1)\,F(l,\mathbf{m}_2) \end{aligned} \tag{4.52}$$

which does not depend on the specific model at hand. The structure of the differential equation is recursive with respect to the order in which the coefficients appear. Consequently, if the orders are not too large, one finds closed systems of differential equations.

4.3.3 Enhanced Perturbative CUT (epCUT)

The enhanced perturbative CUT [110, 111] is again constructed for Hamiltonians of the form

$$H = H_0 + \lambda H_{\mathrm{V}}. \tag{4.53}$$

The Hamiltonian and the generator are represented in second quantization

$$\begin{aligned} H(l) &= \sum_i h_i(l)\,\hat{O}_i \\ \eta(l) &= \sum_i \eta_i(l)\,\hat{O}_i \end{aligned} \tag{4.54}$$

and the DEQ is given by

$$\partial_l h_n(l) = \sum_{i,j} D^n_{ij}\,h_i(l)\,h_j(l) \tag{4.55}$$

which is so far non-perturbative. As the D^n_{ij} have to be calculated just as in the sCUT approach, one could ask for the advantage of the enhanced perturbative CUT compared to the sCUT. The answer is that epCUT intrinsically delivers a truncation scheme so that the calculated coefficients are exact up to a certain order (as long as not combined with an additional truncation scheme). The coefficients are expanded in a small parameter λ

$$h_n(l) = \sum_k \lambda^k h_n^{(k)}(l) \tag{4.56}$$

through which the perturbative character becomes obvious. Inserting Eq. (4.56) in Eq. (4.55) and comparing the coefficients in orders of λ yields

$$\partial_l h_n^{(m)}(l) = \sum_{i,j} \sum_{p+q=m} D^n_{ij}\,h_i^{(p)}(l)\,h_j^{(q)}(l). \tag{4.57}$$

We can see from Eq. (4.57) that only coefficients up to order m act on the m-th order. Thus, we know that we can truncate all terms that emerge in higher orders and still be correct up to order m. For a systematic analysis, one defines the minimal order $O_{\min}(n)$ in which a term emerges. From Eq. (4.55) one finds

$$O_{\min}(n) = \min_{\{i,j|D^n_{ij}\neq 0\}} [O_{\min}(i) + O_{\min}(j)]. \tag{4.58}$$

A useful truncation scheme can then be used by choosing an order O_c up to which one wants to calculate the targeted quantities and truncate all terms for which

$$O_{\min}(n) > O_c. \tag{4.59}$$

One can even optimize the truncation scheme further if one is interested in a special quantity of the flow, e.g., the ground-state energy or the dispersion. It may very well be that terms are included so far which only act in a higher order than O_c on the targeted quantities. Such terms can be neglected while still being correct up to order O_c for the targeted quantities.

The maximal order $O_{\max}(n)$ [110], which is the order up to which one needs to know h_n so that the targeted quantity is still correct up to order O_c, can be calculated from

$$O_{\max}(i) = \max_{\{n,j|D^n_{ij}\neq 0\}} \left[O_{\max}(n) - O_{\min}(j)\right]. \tag{4.60}$$

Terms for which

$$O_{\min}(n) > O_{\max}(n) \tag{4.61}$$

can additionally be truncated. Furthermore, contributions to the right-hand side of the DEQ can be neglected. The contribution on the right-hand side with a coefficient D^n_{ij} can be neglected if

$$O_{\max}(n) < O_{\min}(i) + O_{\min}(j). \tag{4.62}$$

This process leads to a differential equation with less entries than before and which is still exact in the chosen order O_c, at least for the quantities in question. The coefficients of the thus truncated minimal system of differential equations are denoted by $\tilde{D}^n_{ij}$ (cf. Eqs. (4.55) and (4.63)).

A clear advantage of the epCUT in contrast to the pCUT approach is that it also works for an unperturbed Hamiltonian H_0 with a non-equidistant spectrum. On the other hand, one has to calculate the D^n_{ij} which is not necessary within the pCUT approach.

4.3.4 Directly Evaluated Enhanced Perturbative CUT (deepCUT)

The directly evaluated enhanced perturbative CUT [110, 111] follows the epCUT idea. After determining the minimal system of differential equations $\tilde{D}^n_{ij}$ based on epCUT ideas (cf. Sec. 4.3.3), one can simply use it in the full differential equation (4.55)

$$\partial_l h_n(l) = \sum_{i,j} \tilde{D}^n_{ij} h_i(l) h_j(l). \tag{4.63}$$

This approach is not perturbative anymore and the resulting coefficients can be of a much more complicated structure than a polynomial in the chosen order. Roughly, the deepCUT method is a version of sCUT with a clever and systematic way of truncating the system of differential equations.

In this thesis the deepCUT idea is used in Chap. 7 in order to optimize the reproduction of the Schrieffer-Wolff transformation and also to justify truncation schemes at various points in Chaps. 6 and 7.

4.4 Residual Off-Diagonality

The residual off-diagonality (ROD) [101–103, 113, 114] is defined as the square root of the sum of the squared absolute values of all coefficients contributing to the generator

$$\mathrm{ROD} = \left(\sum_{n:h_n \in \eta} |h_n|^2 \right)^{\frac{1}{2}} \tag{4.64}$$

where the h_n are the coefficients of the Hamiltonian in second quantization. For a matrix representation the definition is analogous and corresponds to the sum running over all matrix elements h_{nm} that contribute to the generator. The square root in Eq. (4.64) is introduced so that the ROD is an energy.

The residual-off diagonality tracks the convergence of the flow. From the flow equation (4.4) we know that there is no further change of the Hamiltonian as soon as the residual off-diagonality is zero. Consequently, if the ROD tends to zero for $l \to \infty$, the differential equations converge. For the proposed generators from Sec. 4.2, this is always the case as long as the system can be written in the form of finite matrices and no truncation is incorporated.

For infinite matrices or when a truncation scheme is introduced, the situation is not that clear anymore. In such a case, one might encounter diverging differential equations and thus a divergent residual off-diagonality. These divergences can be an intrinsic feature of the truncated flow equations but can also stem from numerical instabilities.

4.5 Reference State and Normal-Ordering

In order to set up the CUT approach for realistic many-body problems, we need to introduce normal-ordering with respect to an adequate reference state. The need for a normal-ordering scheme can be understood when looking at the example of the commutator of two quartic fermionic operators

$$\begin{aligned}\left[c_1^\dagger c_2 c_3^\dagger c_4, c_{1'}^\dagger c_{2'} c_{3'}^\dagger c_{4'}\right] &= c_1^\dagger c_2 c_{1'}^\dagger c_{2'} c_3^\dagger c_{4'} \delta_{4,3'} - c_1^\dagger c_2 c_{1'}^\dagger c_{2'} c_{3'}^\dagger c_4 \delta_{3,4'} \\ &- c_1^\dagger c_2 c_{1'}^\dagger c_4 c_{3'}^\dagger c_{4'} \delta_{3,2'} + c_1^\dagger c_2 c_3^\dagger c_{2'} c_{3'}^\dagger c_{4'} \delta_{4,1'} \\ &- c_{1'}^\dagger c_{2'} c_{3'}^\dagger c_2 c_3^\dagger c_4 \delta_{1,4'} + c_{1'}^\dagger c_{2'} c_1^\dagger c_{4'} c_3^\dagger c_4 \delta_{2,3'} \\ &- c_{1'}^\dagger c_2 c_{3'}^\dagger c_{4'} c_3^\dagger c_4 \delta_{1,2'} + c_1^\dagger c_{2'} c_{3'}^\dagger c_{4'} c_3^\dagger c_4 \delta_{2,1'}.\end{aligned} \tag{4.65}$$

At first sight, only terms with six operators occur but this depends on the ordering of the operators, e.g., ordering all creation operators to the left would also produce terms with four operators or less. Thus, truncating terms with six operators is problematic as there is still a feedback to terms with less operators.

In order to organize the operators in a way that we can truncate higher-order interaction terms in a well-behaved manner, we introduce normal-ordering of the operators which is chosen with respect to a reference state $|\mathrm{ref}\rangle$ so that

$$\langle \mathrm{ref}| : \hat{A} : |\mathrm{ref}\rangle = 0. \tag{4.66}$$

For the choice of the reference state during the flow, the Hamiltonian is split in two parts

$$H = H_\mathrm{d} + H_\mathrm{r} \tag{4.67}$$

where the ground state of H_d is known. The reference state is chosen to be the ground state of H_d. If the generator fulfills at least gs-generator properties, the reference state will become the ground state of the effective Hamiltonian for $l \to \infty$ (convergence assumed).

Normal-ordering is based on Wick's theorem [115, 116] and is explained in App. 9.7. If the operator basis is chosen such that all creation operators create excitations (cf. Sec. 4.2.4), the reference state is a vacuum with respect to these operators. In this case, normal-ordering coincides with the rule to shift all creation operators to the left. If there are creation operators in the chosen operator basis which create particles on a level with negative energy, the reference state is a Fermi sea with respect to these operators. In this case, the normal-ordering prescription is more complicated[3] and is explained in the following.

The normal-ordering of a bilinear operator is defined by subtracting the expectation value with respect to the reference state

$$: c_1^\dagger c_2 : = c_1^\dagger c_2 - \langle c_1^\dagger c_2 \rangle \tag{4.68}$$

with

$$\langle c_1^\dagger c_2 \rangle = \langle \mathrm{ref} | c_1^\dagger c_2 | \mathrm{ref} \rangle. \tag{4.69}$$

The definition (4.68) obviously fulfills Eq. (4.66). For terms containing more operators, all contractions have to be calculated (where a contraction denotes the expectation value with respect to the reference state). Normal-ordering for operators consisting of four operators takes the form

$$\begin{aligned} c_1^\dagger c_2^\dagger c_3 c_4 &= : c_1^\dagger c_2^\dagger c_3 c_4 : + : c_3 c_4 : \langle c_1^\dagger c_2^\dagger \rangle - : c_2^\dagger c_4 : \langle c_1^\dagger c_3 \rangle + : c_2^\dagger c_3 : \langle c_1^\dagger c_4 \rangle \\ &+ : c_1^\dagger c_4 : \langle c_2^\dagger c_3 \rangle - : c_1^\dagger c_3 : \langle c_2^\dagger c_4 \rangle + : c_1^\dagger c_2^\dagger : \langle c_3 c_4 \rangle + \langle c_1^\dagger c_2^\dagger \rangle \langle c_3 c_4 \rangle \\ &- \langle c_1^\dagger c_3 \rangle \langle c_2^\dagger c_4 \rangle + \langle c_1^\dagger c_4 \rangle \langle c_2^\dagger c_3 \rangle \end{aligned} \tag{4.70}$$

where all normal-ordered operators on the right-hand side also fulfill Eq. (4.66). The signs in Eq. (4.70) stem from the fermionic character of the operators. Every time a fermionic operator that is part of a contraction must be swapped with another fermionic operator in order to bring the contracted operators side by side, a minus sign is introduced.

One important feature of normal-ordered operators is that the order of the operators can be changed and only a sign appears every time two fermionic operators are swapped, e.g.,

$$: c_1^\dagger c_2^\dagger c_3^\dagger c_4 c_5 c_6 : = - : c_1^\dagger c_2^\dagger c_4 c_3^\dagger c_5 c_6 : = : c_1^\dagger c_2^\dagger c_4 c_5 c_3^\dagger c_6 : . \tag{4.71}$$

This means that there is no further direct feedback of such terms on terms including less operators. Hence, the truncation of such terms is controlled.

If the ground state of H_d is degenerate, as for example for the $V = 0$ Anderson model where the impurity level has a spin degree of freedom in the ground state, we can use a reference ensemble

$$\langle \uparrow | : \hat{A} : | \uparrow \rangle + \langle \downarrow | : \hat{A} : | \downarrow \rangle = 0. \tag{4.72}$$

A local impurity operator basis that fulfills Eq. (4.72) is introduced in Chap. 7.

Note that Wick's theorem only works for Slater determinants. A singlet state, for instance, cannot be normal-ordered using Wick's theorem.

[3] The normal-ordering prescription for the vacuum state, i.e. shifting all creation operators to the left, is a special case of the more general normal-ordering scheme outlined in Sec. 4.5.

4.6 Renormalization with CUT

The last part of this chapter outlines some similarities between conventional scaling discussed in Chap. 3 and the CUT approach. As mentioned earlier, it is a well-known fact that there is an intrinsic energy separation in the flow equation approach. In fact, we can obtain almost identical results as we did for the conventional scaling in Chap. 3.

Before we discuss how to reach beyond "poor man's scaling" with CUT in Chaps. 5-7, we reexamine the models from Chap. 3 in the light of Continuous Unitary Transformations.

4.6.1 Potential Scattering Model

A CUT of the potential scattering model (3.16) is given in Ref. [16]. We start from a continuum limit of the potential scattering model (3.16)

$$H = \int_0^D \varepsilon\, c_\varepsilon^\dagger c_\varepsilon \,\mathrm{d}\varepsilon + \rho \int\int_0^D g\left(\varepsilon,\varepsilon'\right) c_\varepsilon^\dagger c_{\varepsilon'} \,\mathrm{d}\varepsilon\,\mathrm{d}\varepsilon'. \tag{4.73}$$

The initial coupling for $l = 0$ is given by $g(\varepsilon,\varepsilon',l=0) = g$. Introducing the sign-generator

$$\eta = \rho \int\int_0^D \mathrm{sgn}\left(\varepsilon-\varepsilon'\right) g\left(\varepsilon,\varepsilon'\right) c_\varepsilon^\dagger c_{\varepsilon'} \,\mathrm{d}\varepsilon\,\mathrm{d}\varepsilon', \tag{4.74}$$

calculating the commutator between η and H and comparing the coefficients in Eq. (4.4) leads to the differential equation

$$\partial_l g\left(\varepsilon,\varepsilon'\right) = -\left|\varepsilon-\varepsilon'\right| g\left(\varepsilon,\varepsilon'\right) + \rho \int_0^D \left[\mathrm{sgn}\left(\varepsilon-z\right) - \mathrm{sgn}\left(z-\varepsilon'\right)\right] g\left(\varepsilon,z\right) g\left(z,\varepsilon'\right) \mathrm{d}z. \tag{4.75}$$

We can write the coefficient in the form

$$g\left(\varepsilon,\varepsilon'\right) = \bar{g}\left(\varepsilon,\varepsilon'\right) \mathrm{e}^{-|\varepsilon-\varepsilon'|l} \tag{4.76}$$

in order to absorb the linear term on the right-hand side of Eq. (4.75) into the coefficient. We introduce the so-called infrared (IR-) approximation

$$g\left(\varepsilon,\varepsilon'\right) = \tilde{g}\,\mathrm{e}^{-|\varepsilon-\varepsilon'|l} \tag{4.77}$$

where $\tilde{g} = \bar{g}\left(\varepsilon_\mathrm{F},\varepsilon_\mathrm{F}\right)$ is evaluated at the Fermi level ε_F. By using Eq. (4.77) in Eq. (4.75) for $\varepsilon = \varepsilon' = 0$ we find the differential equation for the coupling $\tilde{g}$ that will be renormalized during the flow to smaller energies

$$\partial_l \tilde{g} = -2\rho \int_0^D \mathrm{sgn}\left(z\right) \mathrm{e}^{-2|z|l} \mathrm{d}z\, \tilde{g}^2. \tag{4.78}$$

The integral can be calculated and the resulting differential equation for the renormalized coupling becomes

$$\partial_l \tilde{g} = -\frac{\rho\tilde{g}^2}{l}\left[1-\mathrm{e}^{-2Dl}\right]. \tag{4.79}$$

The exponential function will quickly tend to zero because D is the largest energy scale in the system and can be neglected as long as the integration starts from $l_0 > 0$. Note that the

exponential function is important for convergence for $l \to 0$. Nevertheless, taking the early flow into account only changes the prefactor in the result and not the exponent of the exponential function which is the object of interest. The different sign in Eq. (4.79) compared to Eq. (3.22) is due to the fact that l is an inverse energy and is thus increasing when energies are lowered. In order to compare the result (4.79) to the scaling equation (3.22), we have to substitute

$$l = \frac{1}{D_{\text{eff}}} \tag{4.80}$$

which leads to the flow equation for the renormalized coupling

$$\partial_{D_{\text{eff}}} \tilde{g} = \frac{\rho \tilde{g}^2}{D_{\text{eff}}}. \tag{4.81}$$

This is of the same form as the scaling equation for the potential scattering model (3.22). The IR-approximation is very similar to the procedure in the scaling approach and it is used later in this thesis in order to analyze the low-energy behavior of different systems.

Note that it is the IR-approximation that leads to the divergence in this example and not the CUT approach itself. Solving Eq. (4.75) numerically would lead to perfect agreement with exact results. This is due to the simplicity of the model and will change in the Kondo problem where the CUT approach itself will lead to a divergence just as the scaling approach does.

4.6.2 Kondo Model

A CUT approach reproducing the "poor man's scaling" results for an *isotropic coupling* using the IR-approximation has been accomplished in Ref. [16]. We will, however, reproduce the scaling equations for a general *anisotropic coupling*.

In order to use the IR-approximation in the CUT approach for the Kondo model, the flow equation has to be derived first. When commuting the generator (4.83) and the Hamiltonian (4.82), new terms emerge. On the one hand, we find terms with a quartic bath-operator structure while, on the other hand, bilinear terms emerge. Terms that are quartic in the bath operators are dismissed while hopping terms are included for the derivation of the flow equation as quartic terms scale faster to zero than bilinear ones (cf. Sec. 6.8.1). We also dismiss the hopping terms in the scaling approach of this chapter as their action on the spin-spin interaction is of order J^3 while we only include terms up to order J^2. We will revisit the differential equation including the hopping terms in Chap. 7.

Flow Equation

We start from the Kondo Hamiltonian in which the non-diagonal bilinear terms t_{nm} that emerge during the flow for $l > 0$ are already included

$$H = \sum_{n,m,\sigma} t_{nm} : c^\dagger_{n\sigma} c_{m\sigma} : + \sum_{\mu \in x,y,z} \sum_{n,m} \sum_{\alpha,\beta} J^\mu_{nm} \sigma^\mu_{\alpha\beta} \tau^\mu : c^\dagger_{n\alpha} c_{m\beta} : . \tag{4.82}$$

The generator is chosen to be

$$\eta = \sum_{n,m,\sigma} \eta^t_{nm} : c^\dagger_{n\sigma} c_{m\sigma} : + \sum_{\mu \in x,y,z} \sum_{n,m} \sum_{\alpha,\beta} \eta^\mu_{nm} \sigma^\mu_{\alpha\beta} \tau^\mu : c^\dagger_{n\alpha} c_{m\beta} : \tag{4.83}$$

with the coefficients

$$\eta^t_{nm} = \operatorname{sgn}(\varepsilon_n - \varepsilon_m)\, t_{nm}\,, \quad \eta^\mu_{nm} = \operatorname{sgn}(\varepsilon_n - \varepsilon_m)\, J^\mu_{nm}. \tag{4.84}$$

Commuting the generator η with the Hamiltonian and comparing the coefficients in order to derive the flow equation (4.4) while neglecting all terms with quartic bath operators leads to the flow equation (for a more detailed calculation see App. 9.5)

$$\begin{aligned}
\partial_l J^\mu_{nm} &= \sum_x \left(\eta^\mu_{nx} t_{xm} - \eta^\mu_{xm} t_{nx} + \eta^t_{nx} J^\mu_{xm} - \eta^t_{xm} J^\mu_{nx}\right) \\
&- \sum_x \sum_{k,q\in x,y,z} \left[\frac{1}{2}\left|\varepsilon_{kq\mu}\right|^2\right] \left(\eta^k_{nx} J^q_{xm} - \eta^q_{xm} J^k_{nx}\right)(1-2\theta_x) \\
\partial_l t_{nm} &= \sum_x \left(\eta^t_{nx} t_{xm} - \eta^t_{xm} t_{nx}\right) + \frac{1}{4} \sum_{\mu\in x,y,z} \sum_x \left[\eta^\mu_{nx} J^\mu_{xm} - \eta^\mu_{xm} J^\mu_{nx}\right]
\end{aligned} \tag{4.85}$$

where the occupation number

$$\theta_x = \langle c^\dagger_{x\sigma} c_{x\sigma}\rangle \tag{4.86}$$

stems from the normal-ordering with respect to the Fermi sea. In the case of an isotropic coupling $J^\mu_{nm} = J_{nm}$, the flow equation becomes

$$\begin{aligned}
\partial_l J_{nm} &= \sum_x \left(\eta^J_{nx} t_{xm} - \eta^J_{xm} t_{nx} + \eta^t_{nx} J_{xm} - \eta^t_{xm} J_{nx}\right) \\
&- \sum_x \left(\eta^J_{nx} J_{xm} - \eta^J_{xm} J_{nx}\right)(1-2\theta_x) \\
\partial_l t_{nm} &= \sum_x \left(\eta^t_{nx} t_{xm} - \eta^t_{xm} t_{nx}\right) + \frac{3}{4} \sum_x \left[\eta^J_{nx} J_{xm} - \eta^J_{xm} J_{nx}\right].
\end{aligned} \tag{4.87}$$

The starting values for Eqs. (4.85) and (4.87) are both given by

$$J^\mu_{nm} = J^\mu \gamma_n \gamma_m\,, \quad t_{nm} = \varepsilon_n \delta_{nm} \tag{4.88}$$

where in Eq. (4.87) $J^\mu = J$ while ε_n and γ_n are given by Eq. (2.50). Truncating the hopping elements as well leads to the DEQ

$$\partial_l J_{nm} = (\varepsilon_m - \varepsilon_n)\, \eta^J_{nm} - \sum_x \left(\eta^J_{nx} J_{xm} - \eta^J_{xm} J_{nx}\right)(1-2\theta_x)\,. \tag{4.89}$$

In the next section we will apply an IR-approximation to the DEQ (4.89).

Continuum Limit and IR-Approximation

For the IR-approximation, we will also dismiss the bilinear terms in Eq. (4.85) and thus use Eq. (4.89). We use the continuum limit (cf. Sec. 2.6 and Sec. 6.8.4)

$$\varepsilon_x \to \varepsilon\,, \quad \gamma_x \to \rho_0 \mathrm{d}\varepsilon\,, \quad \frac{J^\mu_{x_1 x_2}}{\gamma_{x_1}\gamma_{x_2}} \to J^\mu\left(\varepsilon, \varepsilon'\right) \tag{4.90}$$

which leads to the differential equation

$$\begin{aligned} \partial_l J^{\mu}_{\varepsilon\varepsilon'} &= -\left|\varepsilon-\varepsilon'\right| J^{\mu}_{\varepsilon\varepsilon'} \\ &- \frac{\rho_0}{2}\sum_{k,q}\left|\varepsilon_{kq\mu}\right|^2 \int_{-D}^{D}\left[\operatorname{sgn}(\varepsilon-z)-\operatorname{sgn}\left(z-\varepsilon'\right)\right] J^{k}_{\varepsilon z} J^{q}_{z\varepsilon'}\left(1-2\theta(z)\right)\mathrm{d}z \end{aligned} \tag{4.91}$$

for a constant DOS $\rho_0 = \frac{1}{2D}$ of the bath electrons. The starting values are given by

$$J^{\mu}\left(\varepsilon,\varepsilon'\right) = J^{\mu}. \tag{4.92}$$

Introducing the IR-approximation

$$J^{\mu}_{\varepsilon\varepsilon'} = \tilde{J}^{\mu}\mathrm{e}^{-|\varepsilon-\varepsilon'|l}, \tag{4.93}$$

where the renormalized coupling $\tilde{J}^{\mu}$ is calculated using $\varepsilon = \varepsilon' = \varepsilon_{\mathrm{F}} = 0$ in Eq. (4.91), leads to the flow equation for the coupling at the Fermi level

$$\partial_l \tilde{J}^{\mu} = \rho_0 \sum_{k,q}\left|\varepsilon_{kq\mu}\right|^2 \int_{-D}^{D}\operatorname{sgn}(z)\left(1-2\theta(z)\right)\mathrm{e}^{-2|z|l}\mathrm{d}z\,\tilde{J}^{k}\tilde{J}^{q}. \tag{4.94}$$

The integral can be solved analytically which finally yields the flow equation for the couplings at small energies

$$\partial_l \tilde{J}^{\mu} = \frac{\rho_0}{l}\sum_{k,q}\left|\varepsilon_{kq\mu}\right|^2 \tilde{J}^{k}\tilde{J}^{q}\left[1-\mathrm{e}^{-2Dl}\right] \tag{4.95}$$

or for an isotropic coupling

$$\partial_l \tilde{J} = \frac{2\rho_0\tilde{J}^2}{l}\left[1-\mathrm{e}^{-2Dl}\right]. \tag{4.96}$$

We can neglect the exponential function and substitute the flow parameter by an inverse energy $l = D_{\mathrm{eff}}^{-1}$. Following the argument which leads from Eq. (4.79) to Eq. (4.81) results in the flow equation for the anisotropic couplings from Eq. (4.95)

$$\begin{aligned} \partial_{D_{\mathrm{eff}}}\tilde{J}^{x} &= -\frac{2\rho_0}{D_{\mathrm{eff}}}\tilde{J}^{y}\tilde{J}^{z} \\ \partial_{D_{\mathrm{eff}}}\tilde{J}^{y} &= -\frac{2\rho_0}{D_{\mathrm{eff}}}\tilde{J}^{x}\tilde{J}^{z} \\ \partial_{D_{\mathrm{eff}}}\tilde{J}^{z} &= -\frac{2\rho_0}{D_{\mathrm{eff}}}\tilde{J}^{x}\tilde{J}^{y}. \end{aligned} \tag{4.97}$$

This is exactly the scaling behavior (3.31) that we found with the conventional scaling approach.

We will revisit the DEQ (4.87) in Chap. 7 and analyze the full DEQ without the IR-approximation. In contrast to the potential scattering model, the differential equation (4.87) leads to a divergence on the Kondo energy scale even for the full numerical solution without the IR-approximation. In Chap. 7 we will modify this approach in order to find an effective model with small finite coefficients arbitrarily close to the Fermi level.

5 Chain Representation

5.1 Tridiagonalization

The NRG approach (cf. Sec. 3.3) relies on a semi-infinite chain representation of the Anderson Hamiltonian [10]. This representation is obtained by a Lanczos tridiagonalization [117]. We use a similar starting point and study how far the CUT approach is able to describe the crossover between the energy regimes mentioned in Sec. 2.7. The standard way of deriving the chain representation is to use the discretization (2.51) which leads to

$$H = \sum_{n,\sigma} \varepsilon_n c^\dagger_{n\sigma} c_{n\sigma} + V \sum_\sigma \left(c^\dagger_{0\sigma} d_\sigma + d^\dagger_\sigma c_{0\sigma} \right) + U d^\dagger_\uparrow d^\dagger_\downarrow d_\downarrow d_\uparrow + \varepsilon_\mathrm{d} \sum_\sigma d^\dagger_\sigma d_\sigma \tag{5.1}$$

where the new operator

$$c^\dagger_{0\sigma} = \frac{1}{V} \sum_n V_n \, c^\dagger_{n\sigma} \quad \text{with} \quad V^2 = \sum_n V_n^2 \tag{5.2}$$

was introduced. If we choose the starting vector

$$|n_0\rangle \;=\; \frac{1}{V} \sum_n V_n \, c^\dagger_{n\sigma} |0\rangle, \tag{5.3}$$

the operator (5.2) will act on the zeroth site of the chain. The notation $|n_i\rangle$ denotes that the i-th site of the chain is occupied. Through the choice (5.2) the hybridization is absorbed into the coupling V between the impurity and the zeroth site of the chain. Hence, we only need to transform the diagonal part

$$H_\mathrm{D} = \sum_{n,\sigma} \varepsilon_n \, c^\dagger_{n\sigma} c_{n\sigma} \tag{5.4}$$

in order to obtain a semi-infinite chain. We can successively construct a basis in which the Hamiltonian H_D is tridiagonal by using the Lanczos algorithm.

A chain representation can be a huge advantage when the interaction is taken into account. The NRG, for example, relies on this representation in order to successively add a new site to the chain before diagonalizing the Hamiltonian. Such a representation seems also promising for the Continuous Unitary Transformation approach as we can truncate the system in a way that the Hamiltonian remains local during the flow. This resembles RG-like ideas where a certain locality of the energy scales is also assumed.

The aim of the Lanczos tridiagonalization is to find the parameters t_n and ε_n for a tridiagonalized form of H_D from Eq. (5.4)

$$H_\mathrm{c} = \sum_{n,\sigma} \varepsilon_n c^\dagger_{n\sigma} c_{n\sigma} + \sum_{n,\sigma} t_n \left(c^\dagger_{n\sigma} c_{n+1\sigma} + c^\dagger_{n+1\sigma} c_{n\sigma} \right). \tag{5.5}$$

If the Hamiltonian (5.5) acts on a normalized state $|n_i\rangle$, one finds

$$\begin{aligned} H_\mathrm{c}|n_0\rangle &= \varepsilon_0 |n_0\rangle + t_0 |n_1\rangle, \quad i = 0 \\ H_\mathrm{c}|n_i\rangle &= \varepsilon_i |n_i\rangle + t_i |n_{i+1}\rangle + t_{i-1} |n_{i-1}\rangle, \quad i > 0. \end{aligned} \tag{5.6}$$

Thus, we can construct the basis states after choosing the starting vector $|n_0\rangle$ by calculating

$$\begin{aligned} \varepsilon_0 &= \langle n_0|H_\mathrm{c}|n_0\rangle \\ |\tilde{n}_1\rangle &= H_\mathrm{c}|n_0\rangle - \varepsilon_0|n_0\rangle = t_0|n_1\rangle \end{aligned} \tag{5.7}$$

and successively constructing all further basis states $|n_i\rangle$ and parameters ε_i and t_i for $i \geq 1$ by the iterative algorithm

$$\begin{aligned} t_{i-1}^2 &= \langle \tilde{n}_i|\tilde{n}_i\rangle \\ |n_i\rangle &= \frac{1}{t_{i-1}}|\tilde{n}_i\rangle \\ \varepsilon_i &= \langle n_i|H_\mathrm{c}|n_i\rangle \\ |\tilde{n}_{i+1}\rangle &= H_\mathrm{c}|n_i\rangle - \varepsilon_i|n_i\rangle - t_{i-1}|n_{i-1}\rangle. \end{aligned} \tag{5.8}$$

For a symmetric density of states the tridiagonalized Hamiltonian including the interaction is of the form

$$\begin{aligned} H &= V\sum_\sigma \left(d_\sigma^\dagger c_{0\sigma} + c_{0\sigma}^\dagger d_\sigma\right) + \sum_{n,\sigma} t_n \left(c_{n\sigma}^\dagger c_{n+1\sigma} + c_{n+1\sigma}^\dagger c_{n\sigma}\right) \\ &+ U d_\uparrow^\dagger d_\downarrow^\dagger d_\downarrow d_\uparrow + \varepsilon_\mathrm{d}\sum_\sigma d_\sigma^\dagger d_\sigma. \end{aligned} \tag{5.9}$$

In the following, we refer to this representation as *c-chain*. If the density of states is symmetric, all on-site energies are zero, i.e.,

$$\varepsilon_n = 0 \quad \forall\, n. \tag{5.10}$$

We choose a flat density of states for the bath electrons with a bandwidth $2D$ which is symmetric around the Fermi level, i.e., on-site energies vanish. In the case of a flat DOS (2.59), analytical results [46] for the hopping elements are known

$$\frac{t_n}{D} = \frac{\left(1+\Lambda^{-1}\right)\left(1-\Lambda^{-n-1}\right)}{2\sqrt{1-\Lambda^{-2n-1}}\sqrt{1-\Lambda^{-2n-3}}}\Lambda^{-\frac{n}{2}}. \tag{5.11}$$

The Hamiltonian (5.9) describes a semi-infinite chain where the sites are coupled by the hopping elements t_n while the first site of the chain is coupled to the impurity via the hybridization V. Fig. 5.1 depicts the Hamiltonian (5.9).

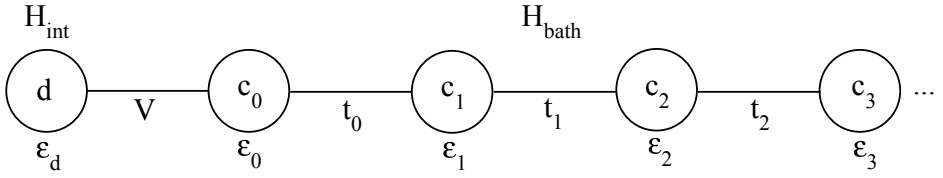

Figure 5.1: Chain representation of the Anderson Hamiltonian (5.9). The bath Hamiltonian H_D from Eq. (5.4) is mapped on a semi-infinite chain (5.5) with hopping elements t_n from Eq. (5.11) and on-site energies $\varepsilon_n = 0$ due to the symmetric DOS. The chain for the bath electrons is coupled to the impurity via the hybridization element $V = \sqrt{\sum_n |V_n|^2}$. In the following, we refer to this representation as *c-chain*.

This representation is widely used but not very well suited for a CUT as all on-site energies are zero. Thus, we have no criterion to determine the sign in the generator.

In the next section we modify the chain representation by separating particle and hole states which will result in a Hamiltonian (referred to as *ph-chain*) that is appropriate for a CUT.

5.2 Separation of Particle and Hole States

We will separate particle and hole states by applying two separate Lanczos tridiagonalizations in order to find a chain representation that is better suited for a CUT. In this case, all creation operators – $p^\dagger_{n\sigma}$ for particles as well as $h^\dagger_{n\sigma}$ for holes – create excitations and the vacuum[4] is the ground state of H_D. Instead of using the Hamiltonian (2.51), which is discretized with respect to the flat DOS, we will use the Hamiltonian (2.58) which is discretized with respect to the Lorentzian DOS. The coefficients $\tilde{\varepsilon}_n$ and γ_n are given by Eq. (2.57). The non-interacting Hamiltonian is diagonal for this discretization, i.e.,

$$H_\mathrm{D} = H_\mathrm{D}^+ + H_\mathrm{D}^- \tag{5.12}$$

with

$$H_\mathrm{D}^\pm = \sum_{n,\sigma} \tilde{\varepsilon}_n^\pm c^\dagger_{n\sigma,\pm} c_{n\sigma,\pm} \tag{5.13}$$

while the d-operator is given by

$$d^\dagger_\sigma = \sum_{s=\pm} \sum_n \gamma_n^s c^\dagger_{n\sigma,s}. \tag{5.14}$$

In the next step we separate particle and hole states by using two separate Lanczos tridiagonalizations for the part with positive $\tilde{\varepsilon}_n^+$ and the one with negative $\tilde{\varepsilon}_n^-$, respectively. We introduce

$$c^\dagger_{n\sigma,+} = \tilde{p}^\dagger_{n\sigma}, \quad c^\dagger_{n\sigma,-} = \tilde{h}_{n\sigma} \tag{5.15}$$

and choose the starting vectors

$$\begin{aligned} |p_{0,\sigma}\rangle &= \sqrt{2}\sum_n \gamma_n^+ \tilde{p}^\dagger_{n\sigma}|0\rangle \\ |h_{0,\sigma}\rangle &= \sqrt{2}\sum_n \gamma_n^- \tilde{h}_{n\sigma}|h_{1\sigma},\cdots,h_{N\sigma}\rangle \end{aligned} \tag{5.16}$$

for the separate tridiagonalizations. Note that the factor $\sqrt{2}$ is needed in order to normalize the states as each part for positive and negative energy carries only half the spectral weight. We can identify the d-operator from Eq. (5.14) as

$$d^\dagger_\sigma = \sum_n \gamma_n^+ \tilde{p}^\dagger_{n\sigma} + \sum_n \gamma_n^- \tilde{h}_{n\sigma} = \frac{1}{\sqrt{2}}\left(p^\dagger_{0\sigma} + h_{0\sigma}\right) \tag{5.17}$$

where the operators $p^\dagger_{0\sigma}$ and $h_{0\sigma}$ denote the operators acting on the zeroth site of the chain. The second equality in Eq. (5.17) holds true because of the choice of the starting vectors (5.16) through which the tridiagonalized Hamiltonian (5.18) is kept local.

Tridiagonalizing the Hamiltonians from Eq. (5.12) separately using the Lanczos algorithm (5.7) and (5.8) with the starting vectors (5.16) yields the non-interacting part of the Hamiltonian as two separated linear chains

$$H_\mathrm{c} = \sum_{n,\sigma} \varepsilon_n \left(p^\dagger_{n\sigma} p_{n\sigma} + h^\dagger_{n\sigma} h_{n\sigma}\right) + \sum_{n,\sigma} t_n \left(p^\dagger_{n\sigma} p_{n+1\sigma} + h^\dagger_{n\sigma} h_{n+1\sigma} + \mathrm{h.c.}\right), \tag{5.18}$$

[4] Referring to the state without particles and holes.

one for the particles and one for the holes. In the following, we refer to this representation as *ph-chain*. Fig. 5.2 depicts the Hamiltonian (5.18) where the two chains are coupled by the interaction term (5.21). The sites are each coupled by the hopping elements t_n.

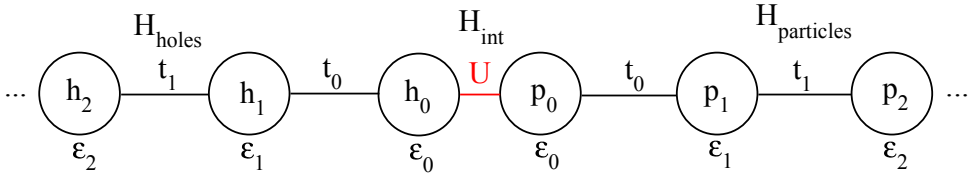

Figure 5.2: Chain representation of the Anderson Hamiltonian (5.18) with separated particle and hole states. The hybridization is already absorbed into the hopping elements t_n and the on-site energies ε_n. The interaction from Eq. (5.21) connects the two chains. In the following, we refer to this representation as *ph-chain*.

The remaining interaction term can be determined by replacing the d-operators in

$$H_{\mathrm{imp}} = \varepsilon_{\mathrm{d}} \sum_{\sigma} d_{\sigma}^{\dagger} d_{\sigma} + U d_{\uparrow}^{\dagger} d_{\downarrow}^{\dagger} d_{\downarrow} d_{\uparrow} \tag{5.19}$$

by Eq. (5.17) as the starting vector (5.16) remains unchanged by the Lanczos tridiagonalization. The full Anderson Hamiltonian in chain representation with separated particle and hole states is of the form

$$H = H_{\mathrm{c}} + H_{\mathrm{imp}} \tag{5.20}$$

with H_{c} from Eq. (5.18) and the impurity contribution

$$\begin{aligned} H_{\mathrm{imp}} \;=\; & \frac{1}{2} \sum_{\sigma} \left(\varepsilon_{\mathrm{d}} + \frac{U}{2} \right) \left(p_{0\sigma}^{\dagger} p_{0\sigma} - h_{0\sigma}^{\dagger} h_{0\sigma} + p_{0\sigma}^{\dagger} h_{0\sigma}^{\dagger} + h_{0\sigma} p_{0\sigma} \right) \\ - \; & \frac{U}{4} \Big(p_{0\uparrow}^{\dagger} p_{0\downarrow}^{\dagger} h_{0\uparrow}^{\dagger} h_{0\downarrow}^{\dagger} + p_{0\uparrow}^{\dagger} h_{0\uparrow}^{\dagger} h_{0\downarrow}^{\dagger} h_{0\downarrow} - p_{0\downarrow}^{\dagger} h_{0\uparrow}^{\dagger} h_{0\downarrow}^{\dagger} h_{0\uparrow} - p_{0\uparrow}^{\dagger} p_{0\downarrow}^{\dagger} h_{0\downarrow}^{\dagger} p_{0\uparrow} \\ & + p_{0\uparrow}^{\dagger} p_{0\downarrow}^{\dagger} h_{0\uparrow}^{\dagger} p_{0\downarrow} + p_{0\uparrow}^{\dagger} p_{0\downarrow}^{\dagger} p_{0\uparrow} p_{0\downarrow} + p_{0\uparrow}^{\dagger} h_{0\uparrow}^{\dagger} p_{0\downarrow} h_{0\downarrow} - p_{0\downarrow}^{\dagger} h_{0\uparrow}^{\dagger} p_{0\downarrow} h_{0\uparrow} \\ & - p_{0\uparrow}^{\dagger} h_{0\downarrow}^{\dagger} p_{0\uparrow} h_{0\downarrow} + p_{0\downarrow}^{\dagger} h_{0\downarrow}^{\dagger} p_{0\uparrow} h_{0\uparrow} + h_{0\uparrow}^{\dagger} h_{0\downarrow}^{\dagger} h_{0\uparrow} h_{0\downarrow} - p_{0\downarrow}^{\dagger} p_{0\uparrow} p_{0\downarrow} h_{0\uparrow} \\ & + p_{0\uparrow}^{\dagger} p_{0\uparrow} p_{0\downarrow} h_{0\downarrow} + h_{0\uparrow}^{\dagger} p_{0\downarrow} h_{0\uparrow} h_{0\downarrow} - h_{0\downarrow}^{\dagger} p_{0\uparrow} h_{0\uparrow} h_{0\downarrow} + p_{0\uparrow} p_{0\downarrow} h_{0\uparrow} h_{0\downarrow} \Big) . \end{aligned} \tag{5.21}$$

An additional constant due to the normal-ordering of the operators was dismissed.

5.2.1 Normal-Ordering and Reference State

When particles and holes are separated, the ground state for $U = 0$ is given by the vacuum $|0\rangle$, i.e., the state without particles and holes. Thus, we choose the vacuum as the reference state. The basic ideas of normal-ordering operators with respect to the vacuum state were already given in Sec. 4.5. We need a normal-ordering scheme for several reasons. An obvious one is that we need a unique operator representation in order to treat the problem numerically.

The main reason, however, is that we need to organize the operators in a way that we can truncate higher interaction terms which emerge during the flow in a well-behaved manner (see Sec.

4.5). Normal-ordering with respect to the vacuum coincides with the rule to order all creation operators to the left. A term stemming from Eq. (5.19), for instance, could be of the form

$$p^\dagger_{0\uparrow} h_{0\downarrow} h^\dagger_{0\downarrow} p_{0\uparrow} = p^\dagger_{0\uparrow} h^\dagger_{0\downarrow} p_{0\uparrow} h_{0\downarrow} + p^\dagger_{0\uparrow} p_{0\uparrow} \tag{5.22}$$

where the right-hand side is normal-ordered. With this rule the general definition of normal-ordering

$$\langle 0| : \hat{O} : |0\rangle = 0 \tag{5.23}$$

holds true. The only terms that couple the vacuum state to states with more particles are operators that only contain annihilation or only creation operators, e.g.,

$$p^\dagger_{0\sigma} h^\dagger_{0\sigma}, \quad p^\dagger_{0\uparrow} p^\dagger_{0\downarrow} h^\dagger_{0\uparrow} h^\dagger_{0\downarrow}, \quad p_{0\sigma} h_{0\sigma}, \quad p_{0\uparrow} p_{0\downarrow} h_{0\uparrow} h_{0\downarrow}. \tag{5.24}$$

The gs-generator eliminates these terms and the vacuum will become the ground state of the effective model.

5.2.2 Starting Values

We have to calculate the starting values of the ε_n and t_n from Eq. (5.18) numerically by a Lanczos tridiagonalization as outlined in Sec. 5.2.

Fig. 5.3 compares the starting values for the conventional c-chain (5.5) (given by Eq. (5.11)) and the starting values for the ph-chain (5.18) which are derived numerically.

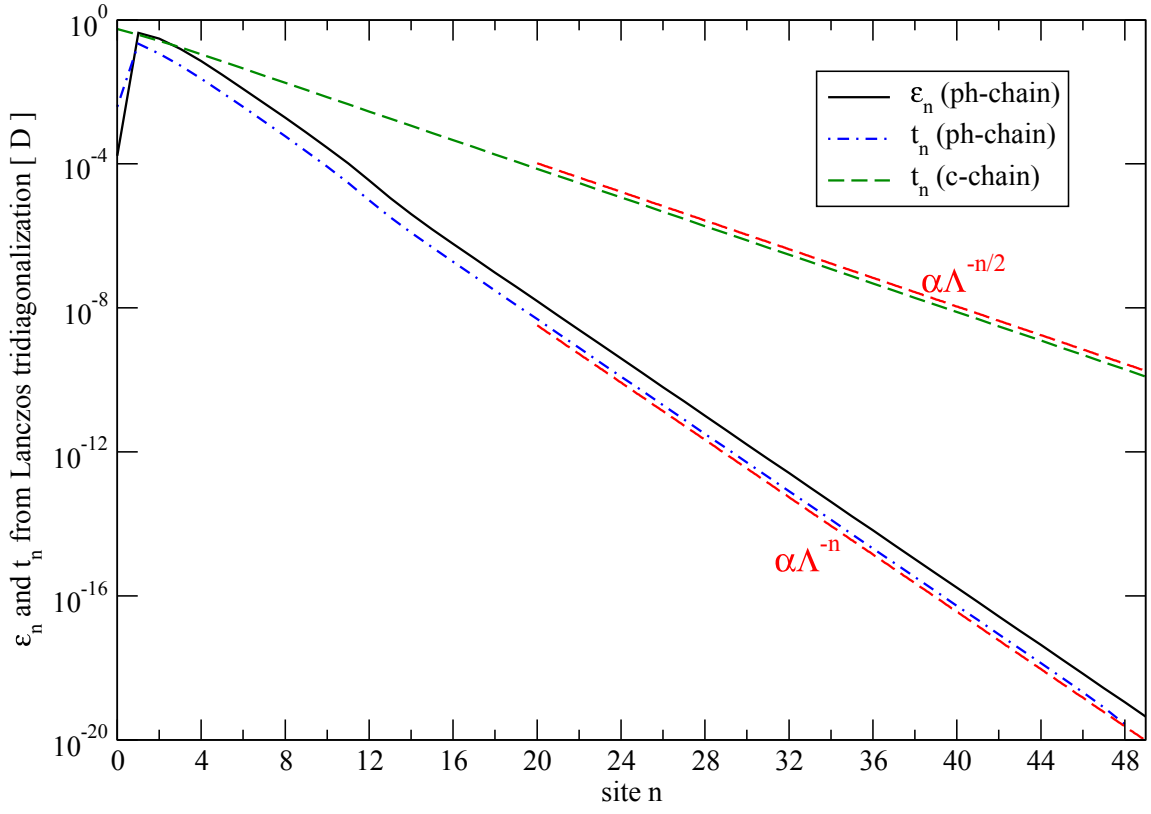

Figure 5.3: Starting values ε_n and t_n for the tridiagonalized Hamiltonian (5.18) with $N = 50$, $\Lambda = 2.5$ and $\frac{V}{D} = 4 \cdot 10^{-3}$ constructed from a Lanczos tridiagonalization with separated particle and hole states (ph-chain) compared to the hopping elements t_n of a tridiagonalization where particles and holes are not separated (c-chain) (5.9). In the case of the c-chain, all ε_n are zero and the hopping elements t_n decrease proportional to $t_n \propto \Lambda^{-\frac{n}{2}}$ for large n (cf. Eq. (5.11)). For the ph-chain (particles and holes separated) both the ε_n as well as the t_n decrease according to Λ^{-n} for large n.

The hopping elements t_n for the ph-chain (5.18) decrease proportional to $t_n \propto \Lambda^{-n}$ for large n in contrast to the hopping elements of the c-chain (5.9) which decrease according to $t_n \propto \Lambda^{-\frac{n}{2}}$ for large n (cf. Eq. (5.11)). This is due to the fact that twice as much hopping elements are needed for the c-chain compared to the ph-chain in order to reach the same energy scale.

In the case of the c-chain, two hopping elements are needed (describing two energy levels - the positive and the corresponding negative one -) to step forward to the next discretized interval (2.44) corresponding to the next lower energy scale $E_N \propto \Lambda^{-n}$. For the ph-chain, every hopping element links directly to the next lower energy scale. In exchange, the Hilbert space increases twice as fast in the exponent when increasing the length N of the ph-chain (factor 2^{4N}) compared to the c-chain (factor 2^{2N}).

5.3 Flow Equation for the Non-Interacting Model

We want to analyze the behavior of the non-interacting model as we can already find some characteristics that still hold true for $U > 0$. Additionally, we can see the intrinsic energy separation of the CUT approach.

We start from the Hamiltonian

$$H = \sum_{n=0,\sigma}^{N} \varepsilon_n p_{n\sigma}^\dagger p_{n\sigma} + \sum_{n=0,\sigma}^{N-1} t_n \left(p_{n\sigma}^\dagger p_{n+1\sigma} + p_{n+1\sigma}^\dagger p_{n\sigma} \right) \tag{5.25}$$

and choose the generator as

$$\eta = \sum_{n=0,\sigma}^{N-1} \eta_n \left(p_{n\sigma}^\dagger p_{n+1\sigma} - p_{n+1\sigma}^\dagger p_{n\sigma} \right) \tag{5.26}$$

with the coefficients

$$\eta_n = \operatorname{sgn}(\varepsilon_n - \varepsilon_{n+1}) t_n \tag{5.27}$$

in order to eliminate the hopping elements for $l \to \infty$. Because of the exponentially decreasing character of the ε_n, we find

$$\operatorname{sgn}(\varepsilon_n - \varepsilon_{n+1}) = 1. \tag{5.28}$$

Calculating the commutator between η from Eq. (5.26) and H from Eq. (5.25) we can find the flow equation (4.4)

$$\begin{aligned} \partial_l t_n &= -|\varepsilon_n - \varepsilon_{n+1}| t_n \\ \partial_l \varepsilon_n &= 2t_n^2 - 2t_{n-1}^2, \quad 0 < n < N \\ \partial_l \varepsilon_0 &= 2t_0^2 \\ \partial_l \varepsilon_N &= -2t_{N-1}^2 \\ \partial_l t_{n,n+2} &= t_n t_{n+1} - t_{n+1} t_n = 0 \end{aligned} \tag{5.29}$$

where $t_{n,n+2}$ are the coefficients of the newly emerging terms $p_{n\sigma}^\dagger p_{n+2\sigma}$. We would need to commute these terms again and even include them into the generator but as long as Eq. (5.28) is fulfilled they will not occur, i.e., the differential equation (5.29) is already exact.

5.3.1 Exponential Flow Parameter

The flow parameter l represents an inverse energy (cf. Sec. 4.2.3). It is useful to adjust the flow parameter to the exponentially decreasing energy scales $\varepsilon_n \propto \Lambda^{-n}$. This can be achieved by introducing a new flow parameter b that leads to an exponentially decreasing energy scale when increased linearly

$$l = \left(\Lambda^b - 1\right) D^{-1}. \tag{5.30}$$

The flow equation (4.4) can be rewritten using Eq. (5.30)

$$\partial_l H(l) = [\eta(l), H(l)] \quad \longrightarrow \quad \partial_b \tilde{H}(b) = \frac{\partial l}{\partial b} \left[\tilde{\eta}(b), \tilde{H}(b)\right] \tag{5.31}$$

where $\tilde{H}(b) = H(l(b))$. As $l(b=0) = 0$, the starting Hamiltonians for H and $\tilde{H}$ coincide and the only change that has to be taken into account in contrast to the flow equation of the old parameter l is the newly emerging term $\frac{\partial l}{\partial b} = \ln(\Lambda)\Lambda^b D^{-1}$. By using Eq. (5.31) we find

$$\partial_b H(b) = \ln(\Lambda)\Lambda^b [\eta(b), H(b)] D^{-1}. \tag{5.32}$$

When the new exponential flow parameter b increases linearly, the energy scale $l^{-1} \propto \Lambda^{-b}$ decreases exponentially. As the energy scale connected to the site n decreases as $\varepsilon_n \propto \Lambda^{-n}$, we can link b linearly to the sites n of the chain. This can also be seen in the numerical data shown in the following sections.

5.3.2 Residual Off-Diagonality of the Non-Interacting Model

A 4th-order Runge-Kutta algorithm was implemented in order to solve Eq. (5.29) numerically. In the case of $U = 0$, we have a closed system of differential equations without any approximations or truncations and thus expect to find exact results (apart from numerical errors).

At first, we can look at the residual off-diagonality (ROD) (cf. Sec. 4.4) which, for $U = 0$, is of the simple form

$$\mathrm{ROD} = \sqrt{\sum_n |t_n|^2}. \tag{5.33}$$

Fig. 5.4 depicts a typical example of the ROD which shows some oscillations for small b while it exhibits an exponential decrease

$$\mathrm{ROD} \propto \Lambda^{-b}, \quad b < N \tag{5.34}$$

as long as $b < N$ and finally results in a double exponential asymptotic behavior

$$\mathrm{ROD} \propto \mathrm{e}^{-\alpha\Lambda^b}, \quad b > N \tag{5.35}$$

for $b > N$. The double exponential behavior corresponds to the asymptotic behavior $\mathrm{ROD} \propto \mathrm{e}^{-\alpha l}$ for large flow parameters $l = \Lambda^b$ (cf. Eq. (4.41)) where the exponential flow parameter (5.30) is used.

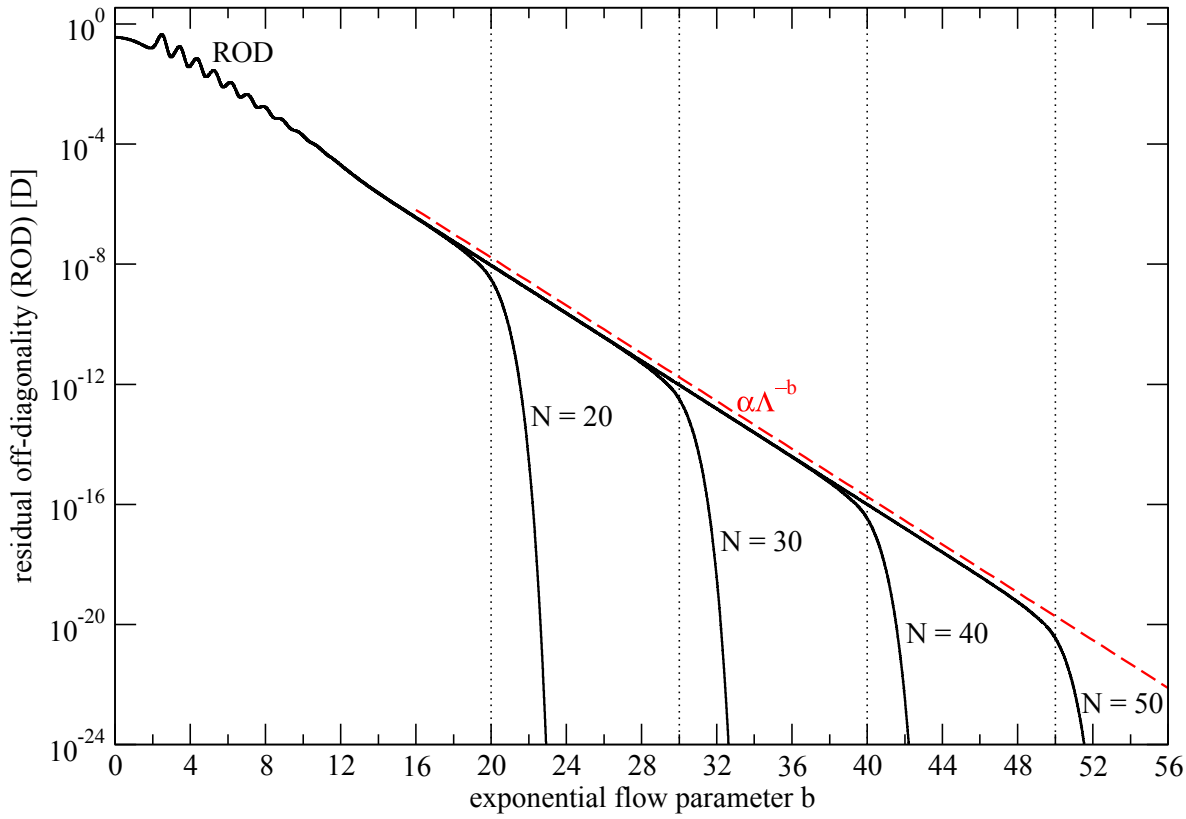

Figure 5.4: Residual off-diagonality ROD $= \sqrt{\sum_n |t_n|^2}$ for $\Lambda = 2.5$, $\frac{V}{D} = 4 \cdot 10^{-3}$, $U = 0$ and varying chain lengths N (from left to right: $N = 20$, 30, 40 and 50). We see an exponential decrease ROD $\propto \Lambda^{-b}$ for $b < N$ and a decrease of the form ROD $\propto \mathrm{e}^{-\alpha\Lambda^{-b}}$ for $b > N$. The exponential decrease corresponds to a power law ROD $\propto l^{-1}$ for the flow parameter l while the asymptotic behavior for large b corresponds to the well-known exponential decrease for large flow parameters ROD $\propto \mathrm{e}^{-\alpha l}$.

From Eq. (5.30) we find that the exponential behavior ROD $\propto \Lambda^{-b}$ corresponds to a power law[5] in the conventional flow parameter

$$\mathrm{ROD} \propto l^{-1}. \tag{5.36}$$

The power law is independent of the chosen discretization parameter Λ as can be seen from the results shown in Fig. 5.5 and occurs until the lowest energy scale in the system is reached which is linked to the chain length by $E_N \propto \Lambda^{-N}$. The exponential flow parameter is connected to an energy scale by $l^{-1} = \Lambda^{-b}$ for large b. Thus, the lowest energy scale is reached when $b \approx N$. On smaller energy scales the asymptotic behavior for large $b > N$ occurs and manifests as a double exponential behavior ROD $\propto \mathrm{e}^{-\alpha\Lambda^{-b}}$. If we identify $l \propto \Lambda^b$ for large b, we see that this behavior corresponds to the well-known exponential behavior

$$\mathrm{ROD} \propto \mathrm{e}^{-\alpha l} \tag{5.37}$$

which is a general behavior of differential equations generated by Continuous Unitary Transformations for large values of l (cf. Eq. (4.41)).

[5] For an analytical derivation of this power law, see App. 9.4.

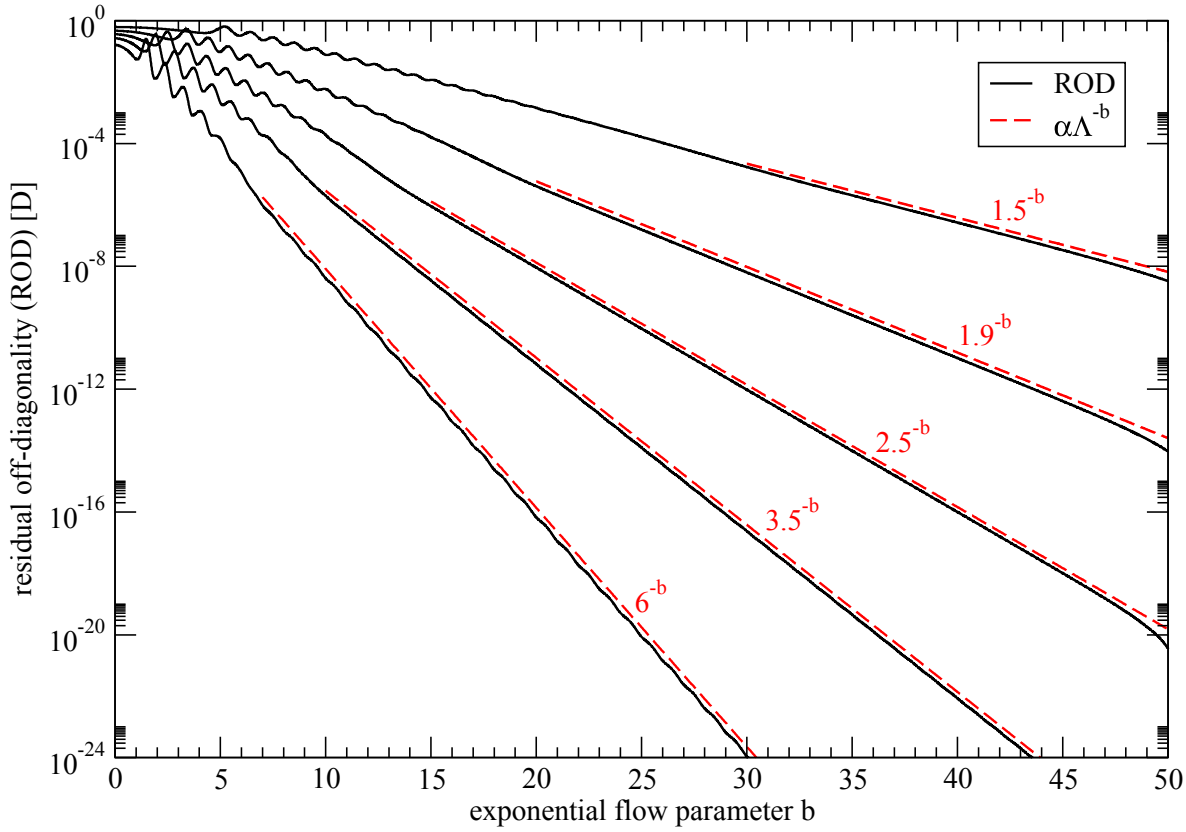

Figure 5.5: Residual off-diagonality ROD $= \sqrt{\sum_n |t_n|^2}$ for $N = 50$, $\frac{V}{D} = 4 \cdot 10^{-3}$ and $U = 0$ for different values of Λ. From top to bottom: $\Lambda = 1.5$, 1.9, 2.5, 3.5 and 6. For $b < N$, we see an exponential decrease Λ^{-b} which corresponds to a power law l^{-1} independent of the discretization parameter Λ.

Fig. 5.5 verifies that the prefactor in the exponent of the exponential behavior ROD $\propto \Lambda^{-b}$ is equal to one for various values of Λ which corresponds to a power law ROD $\propto l^{-1}$ independent of the discretization parameter Λ.

For small values of b, the residual off-diagonality exhibits some oscillations. Each oscillation stems from a hopping element t_n which initially increases when the site n on which it acts is of the order of the flow parameter b, i.e., the energy scale corresponding to the flow parameter lies in the region of the energy scale ε_n. If b increases further, the hopping element t_n decreases quickly and tends to zero. We see this effect as one oscillation because the next hopping element t_{n+1} already starts to increase.

This reflects an energy separation of the flow equation as processes on higher energy scales are affected first and have already converged when lower energy scales are reached. This behavior is a feature of the CUT approach that is very similar to RG approaches as it also exhibits an intrinsic energy separation.

Fig. 5.6 shows the above described occurrence of the oscillations. All qualitative observations mentioned in this section still hold true when an interaction $U > 0$ is introduced.

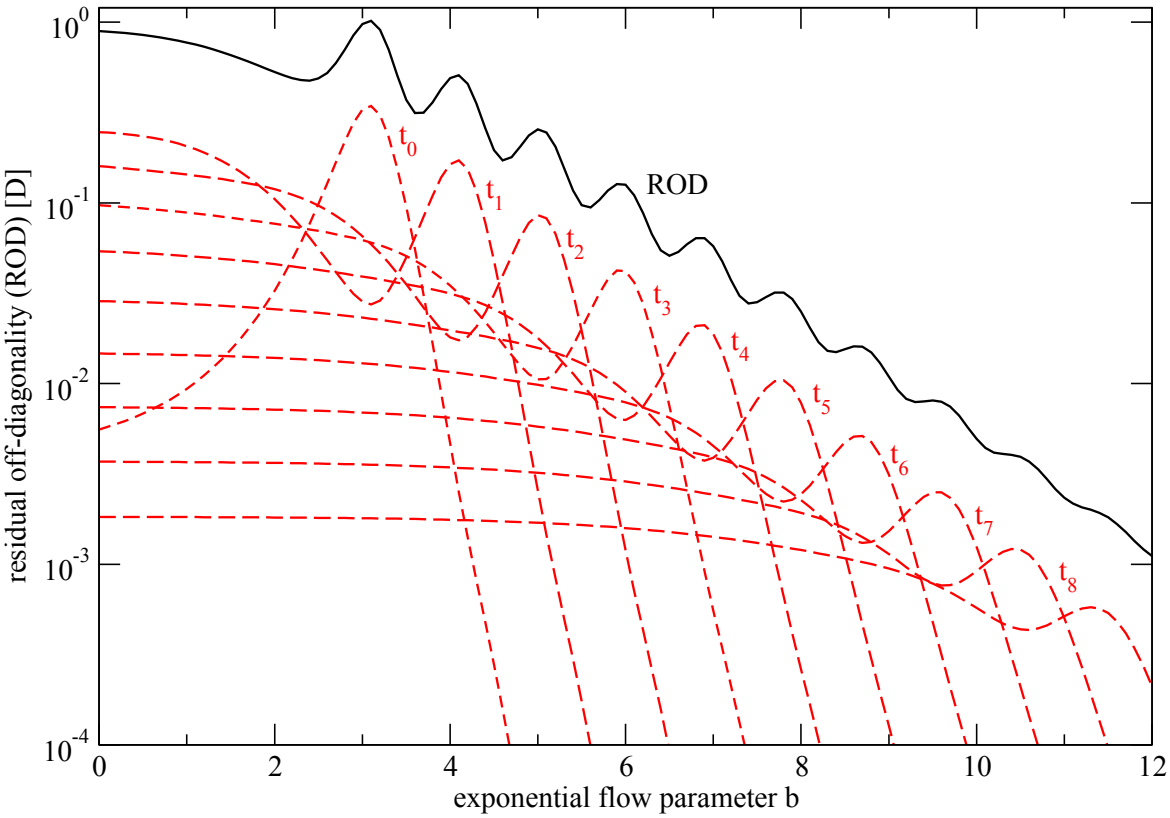

Figure 5.6: Residual off-diagonality ROD $= \sqrt{\sum_n |t_n|^2}$ for $\Lambda = 2.5$, $\frac{V}{D} = 4 \cdot 10^{-3}$, $U = 0$ and $N = 50$. The dashed red lines show the hopping elements t_n. The square sum of the t_n results in the square of the residual off-diagonality. The hopping elements t_n acting on larger energy scales converge before the ones acting on lower energy scales. This behavior is a feature of the CUT approach that is very similar to RG approaches as it also exhibits an intrinsic energy separation.

5.3.3 Flow of the Single-Particle Energies

In the non-interacting case, the only remaining coefficients are the single-particle energies ε_n. As the ROD tends to zero, the effective Hamiltonian becomes diagonal and we expect the on-site energies ε_n to converge to the single-particle energies d_n of the diagonalized Hamiltonian. The d_n can easily be derived from an exact diagonalization (e.g. Ref. [118]). Note that the starting values of the ε_n before the tridiagonalization also coincide with the d_n.

Fig. 5.7 depicts the flow of one exemplary energy level, here ε_{10}, which exemplifies that the ε_n indeed converge to the expected single-particle energies d_n of the diagonalized Hamiltonian. The single-particle energies flow from their starting values $\varepsilon_n(0)$ to their expected value d_n. The main crossover takes place when $b \approx n$, i.e., when the energy scale connected to the flow parameter b is in the region of ε_n. Beyond this value of the flow parameter, ε_n converges quickly to d_n.

Fig. 5.8 depicts the flow of the difference between the ε_n and the single-particle energies d_n of the diagonalized Hamiltonian. The flow parameter b at which the ε_n quickly converge to d_n increases linearly with n. This corresponds to the fact that the convergence for the respective energy level ε_n takes place when the energy scale connected to the flow parameter b is of the order of the energy scale ε_n. This represents the RG-like character of the flow equation approach as higher energetic processes are treated before lower ones.

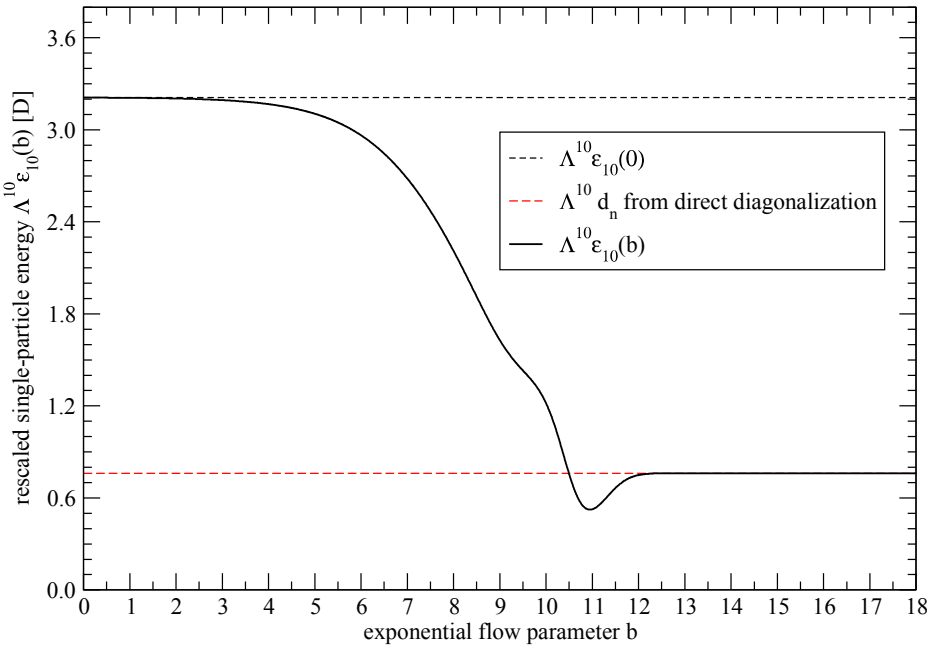

Figure 5.7: Flow of an exemplary rescaled single-particle energy $\Lambda^{10}\varepsilon_{10}$ for $N = 20$, $\Lambda = 2.5$, $\frac{V}{D} = 4 \cdot 10^{-3}$ and $U = 0$. The single-particle energy flows from its starting value $\varepsilon_{10}(0)$ to the expected single-particle energy d_{10} of the diagonalized Hamiltonian which is obtained from an exact diagonalization [118].

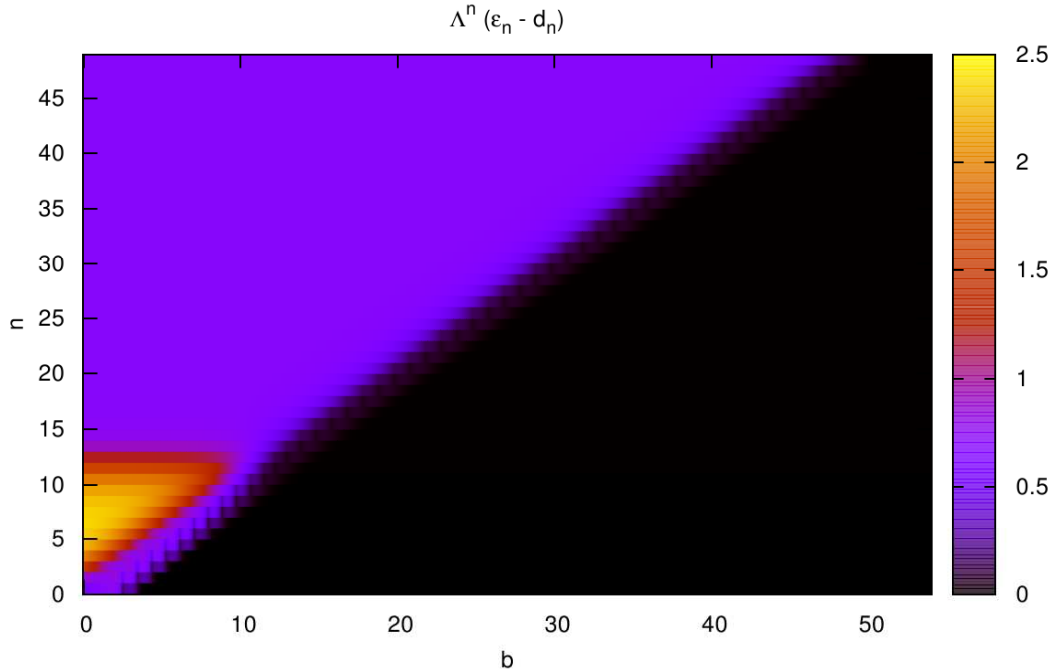

Figure 5.8: Flow of the difference $\Delta_n(b) = \Lambda^n(\varepsilon_n(b) - d_n)$ vs. the exponential flow parameter b for $N = 50$, $\Lambda = 2.5$, $\frac{V}{D} = 4 \cdot 10^{-3}$ and $U = 0$. The d_n denote the expected single-particle energies obtained from an exact diagonalization. $\Delta_n(b)$ is rescaled with a factor Λ^n in order to bring all quantities to order $\mathcal{O}(1)$. The exponential flow parameter b, at which the ε_n quickly converge to the single-particle energies d_n of the diagonalized Hamiltonian, increases linearly with n. Thus, the convergence for the respective energy levels takes place where the energy scale connected to the flow parameter b is of the order of ε_n. This represents the RG-like character of the flow equation approach as higher energetic processes are treated before lower ones.

5.4 Influence of the Interaction

5.4.1 Derivation of the Flow Equation

The next step is to introduce the interaction $U > 0$. In this case, it becomes impossible to derive a closed system of differential equations without approximations. It was necessary to write a program that is able to commute the Hamiltonian with the generator and to identify newly emerging operators which are added to the Hamiltonian and the generator while constructing the flow equation. Such a program was originally developed by S. Duffe [102] and was further modified by T. Fischer [101, 104], S.A. Hamerla [103] and N.A. Drescher [105].

For the program used in this thesis, numerous adaptations have been incorporated to account for the fermionic algebra and the operator basis with separated particle and hole states. The main ideas, however, remain the same:

1. Set up the initial Hamiltonian $H(0)$ in the basis $\hat{O}_n$.
2. Determine if a term belongs to the generator. If it does, the commutator between the generator contribution and the Hamiltonian is carried out and the resulting operators are calculated.
3. Check which of the operators generated in step 2 are truncated.
4. Compare the remaining operators to those in the initial Hamiltonian by a hashing algorithm. If the operator is found in the initial Hamiltonian, the term $D^n_{ij} h_i(l) h_j(l)$ is added to the right-hand side of the derivative of the coefficient $h_n(l)$ belonging to the operator $\hat{O}_n$. If the operator is not found, it is added to the Hamiltonian with a new coefficient $g_n(l)$.
5. Calculate the commutators emerging from the new terms and repeat step 2 to 5 until no new terms emerge.

The resulting differential equations are solved numerically, e.g., by a 4th-order Runge-Kutta algorithm [118]. We use the exponential flow parameter b (5.30) in order to solve the DEQs and thus the resulting flow equations have to be modified by the factor $\ln(\Lambda)\Lambda^b$ from Eq. (5.32).

5.4.2 Generator

The generator of choice should at least fulfill gs-generator properties (cf. Sec. 4.2.4) so that the ground state of the effective Hamiltonian becomes the vacuum $|0\rangle$, i.e., the state without particles and holes. Additionally, we want to eliminate the hopping elements t_n in order to study the influence of the interaction U on the single-particle energies ε_n.

Terms that must be included into the generator are terms that consist only of creation or only of annihilation operators because a normal-ordered term yields zero acting on the vacuum as soon as there is at least one annihilation operator present. Examples of operators included into the generator are

$$\begin{aligned} &c^\dagger_{n_1\alpha_1} c^\dagger_{n_2\alpha_2}\,, \quad c^\dagger_{n_1\alpha_1} c^\dagger_{n_2\alpha_2} c^\dagger_{n_3\alpha_3} c^\dagger_{n_4\alpha_4}\,, \quad c^\dagger_{n_1\alpha_1} c^\dagger_{n_2\alpha_2} c^\dagger_{n_3\alpha_3} c^\dagger_{n_4\alpha_4} c^\dagger_{n_5\alpha_5} c^\dagger_{n_6\alpha_6}\,, \quad \dots \\ &c_{n_1\alpha_1} c_{n_2\alpha_2}\,, \quad c_{n_1\alpha_1} c_{n_2\alpha_2} c_{n_3\alpha_3} c_{n_4\alpha_4}\,, \quad c_{n_1\alpha_1} c_{n_2\alpha_2} c_{n_3\alpha_3} c_{n_4\alpha_4} c_{n_5\alpha_5} c_{n_6\alpha_6}\,, \quad \dots \end{aligned} \tag{5.38}$$

where the c-operators can be both, particle- or hole-operators (if $c^\dagger_{n\alpha}$ is a hole-operator, the notation also denotes $h^\dagger_{n\alpha}$ and not the hermitian conjugated!). The sign in the generator is chosen according to the change of the particle number induced by the respective operator. If the particle number is increased, a sign $+1$ is chosen and a sign -1 if the number of particles is decreased. So, if $\hat{O}^\dagger_{i,\mathrm{gs}}$ denotes an operator that only consists of creation operators and h_i is its coefficient in the Hamiltonian, then the gs-generator takes the form

$$\eta_{\mathrm{gs}} = \sum_i h_i \left(\hat{O}^\dagger_{i,\mathrm{gs}} - \hat{O}_{i,\mathrm{gs}} \right). \tag{5.39}$$

Additionally, we want to eliminate the hopping elements t_n in order to gain the single-particle energies ε_n under the influence of the interaction U. Thus, we additionally include

$$\eta_{\mathrm{hopping}} = \sum_{n,\sigma} t^{\mathrm{p}}_n \left(p^\dagger_{n\sigma} p_{n+1\sigma} - p^\dagger_{n+1\sigma} p_{n\sigma} \right) + \sum_{n,\sigma} t^{\mathrm{h}}_n \left(h^\dagger_{n\sigma} h_{n+1\sigma} - h^\dagger_{n+1\sigma} h_{n\sigma} \right) \tag{5.40}$$

in the full generator

$$\eta = \eta_{\mathrm{hopping}} + \eta_{\mathrm{gs}}. \tag{5.41}$$

The sign in Eq. (5.40) is given by Eq. (5.28). Commuting two quartic operators yields terms with up to six operators. Commuting these terms in turn produces terms with even eight operators and so on. Furthermore, the local character vanishes because commuting a term acting on the sites n and $n+1$ with a term acting on the sites $n+1$ and $n+2$ results in a term that acts on the sites n and $n+2$. The number of occurring terms becomes too large to handle very quickly. There are $16^2 = 256$ ($p^{(\dagger)}_\uparrow$, $p^{(\dagger)}_\downarrow$, $h^{(\dagger)}_\uparrow$, $h^{(\dagger)}_\downarrow$) local operators acting on one site n. Thus, the full number of terms increases with the chain length N according to $N_{\mathrm{terms}} = 256^N$ which necessitates an adequate truncation scheme.

5.4.3 Truncation Scheme

There are two major criteria by which we choose the truncation scheme. On the one hand, we look at the range d (defined in Eq. (5.43)) of an occurring operator. On the other hand, the number of operators N_{ops} of the terms is considered. Our aim is to keep the operators local during the whole flow and thus we will truncate all terms that act on non-neighboring sites and study the influence of the number of operators.

As we truncate all operators with a range $d > 1$, all remaining terms act either on a site n or on the sites n and $n+1$. We do not include any further truncations and track the norm of terms with a fixed number of operators N_{ops}. The norm is plotted against the smallest site n on which the term acts and is defined as

$$G_{N_{\mathrm{ops}},n} = \sqrt{\sum_i \left| h_i \left(N_{\mathrm{ops}}, n \right) \right|^2} \tag{5.42}$$

where $h_i \left(N_{\mathrm{ops}}, n \right)$ are the coefficients of terms containing N_{ops} operators and the smallest site the term acts on is n. We solve the resulting flow equation numerically by a 4th-order Runge-Kutta algorithm and consider the norm (5.42) at large b where the differential equation has already converged.

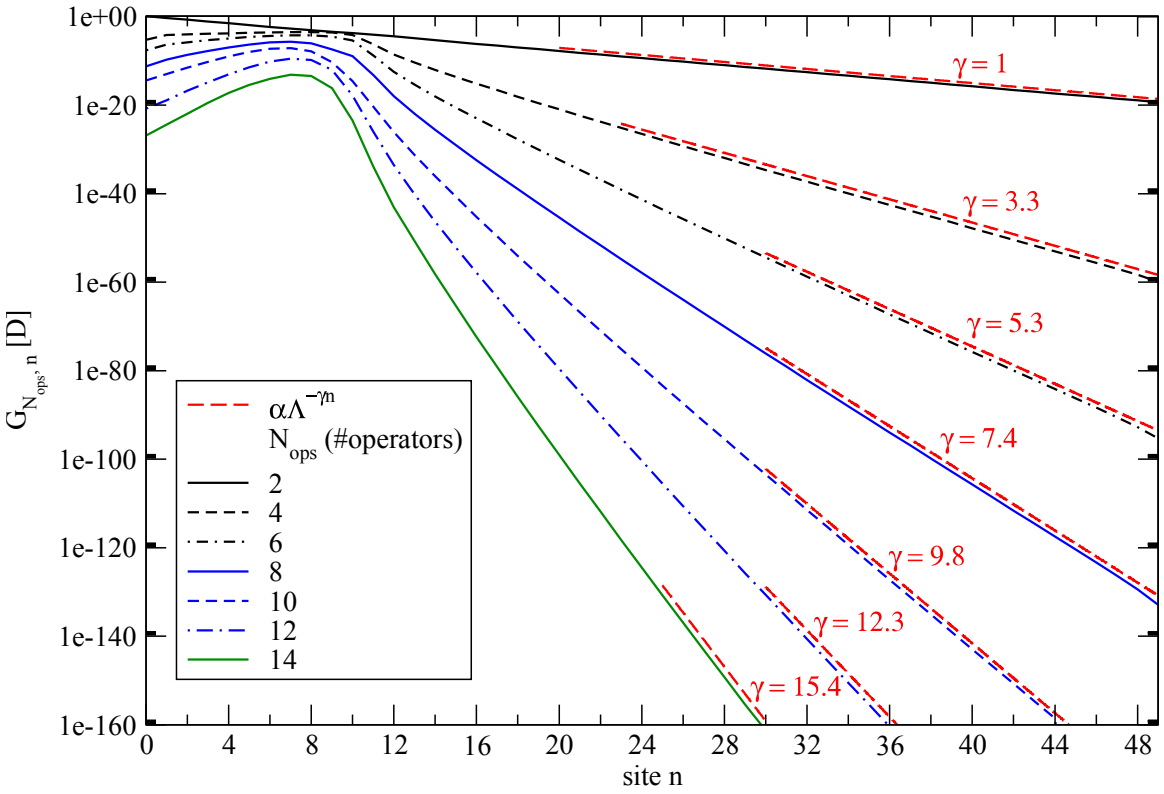

Figure 5.9: Norm $G_{N_{\text{ops}},n}$ from Eq. (5.42) of terms with a fixed number of operators N_{ops} and the smallest site n on which the term acts vs. site n. The parameters of the chain are $N = 50$, $\Lambda = 2.5$, $\frac{V}{D} = 4 \cdot 10^{-3}$, $\frac{U}{D} = 10^{-3}$ and from top to bottom the number of operators $N_{\text{ops}} = 2, 4, ..., 12, 14$. The larger the number of operators contained in the term, the faster the operators vanish for increasing n (linked to decreasing energies), i.e., operators with a large number of operators N_{ops} are irrelevant. Thus, truncating terms with a larger number of operators is a justified approximation.

Operators with a large number of operators N_{ops} decrease much faster for increasing n which corresponds to decreasing energy scales. This is a strong indication that terms containing a large number of operators are irrelevant and do not play a significant role in the flow of low-energy contributions. Therefore, we neglect all terms containing more than six operators. Comparing the results obtained for a truncation of terms containing more than six operators to the results obtained without a truncation with respect to the number of operators yields almost indistinguishable results.

A much harder question to answer is how far it is justified to truncate terms with higher ranges d. The range of a term is defined as

$$d = \sum_i (n_i - n_0) \tag{5.43}$$

where n_0 is the smallest site occurring in the term while n_i denotes the other sites on which the operators act. We will consider results for $d > 1$ in Sec. 5.4.8 and discuss the influence of the interaction-range.

5.4.4 Effective Fixed-Point Hamiltonians

In order to study how far the Continuous Unitary Transformation approach as outlined in this chapter is able to describe the crossover between the different energy regimes of the Anderson model, explained in Sec. 2.7, we have to find a good criterion by which we can decide if we see the crossover between the energy regimes. Well inside the different energy regimes, the Anderson model can be approximated by simple single-particle Hamiltonians which can be found from the chain representation (5.5) (c-chain representation). The energy regimes as well as the fixed-point Hamiltonians are discussed in Refs. [1, 8].

As the flow parameter l can be interpreted as an inverse energy, we will start the flow at high energies corresponding to the energy scales of the free-orbital regime. In this regime we can construct the single-particle energies from the $U = 0$ Anderson model

$$H_{\mathrm{FO}} = V \sum_{\sigma} \left(d_{\sigma}^{\dagger} c_{0\sigma} + c_{0\sigma}^{\dagger} d_{\sigma} \right) + \sum_{n=0,\sigma}^{N-1} t_n \left(c_{n\sigma}^{\dagger} c_{n+1\sigma} + c_{n+1\sigma}^{\dagger} c_{n\sigma} \right) \tag{5.44}$$

where the t_n are given by Eq. (5.11). In principle, one can also set $V = 0$ which will have no significant effect on high energy scales.

When the flow parameter l increases, i.e., energies are decreasing, we will cross the U-energy scale and a singly occupied impurity becomes energetically favored. Thus, in the vicinity of the impurity a spin-carrying state will be localized. This gives rise to the local-moment regime at intermediate energy scales. As the energies are still far above the binding energy of the Kondo singlet, only charge excitations are frozen out while spin fluctuations still occur. The effective Hamiltonian describing this energy regime can be constructed from

$$H_{\mathrm{LM}} = \sum_{n=0,\sigma}^{N-1} t_n \left(c_{n\sigma}^{\dagger} c_{n+1\sigma} + c_{n+1\sigma}^{\dagger} c_{n\sigma} \right) + J \sum_{\alpha,\beta} c_{0\alpha}^{\dagger} \vec{\sigma}_{\alpha\beta} c_{0\beta} \vec{\tau} \tag{5.45}$$

with $J = \frac{4V^2}{U}$. At first sight, it might seem as if the effective Hamiltonian of the local-moment regime (5.45) and the one of the free-orbital regime (5.44) coincide for $V = 0$. But there is a subtle difference as in the free-orbital regime the impurity is still present as a free level with zero energy while the impurity is already occupied and decoupled from the rest of the chain in the local-moment regime.

Finally, if the flow parameter becomes large enough so that the corresponding energy scale lies below the Kondo temperature T_{K}, the formation of the Kondo singlet additionally freezes out spin fluctuations on the impurity. The effective Hamiltonian describing the single-particle energies of this regime is given by

$$H_{\mathrm{SC}} = \sum_{n=1,\sigma}^{N-1} t_n \left(c_{n\sigma}^{\dagger} c_{n+1\sigma} + c_{n+1\sigma}^{\dagger} c_{n\sigma} \right) \tag{5.46}$$

and can be pictured as a screening of the impurity and the first site of the chain by the formation of a singlet between them.

We can gain the expected single-particle energies in the respective energy regimes by diagonalizing the fixed-point Hamiltonians (5.44) - (5.46) – where the fixed-point Hamiltonian (5.45) is diagonalized for $J = 0$.

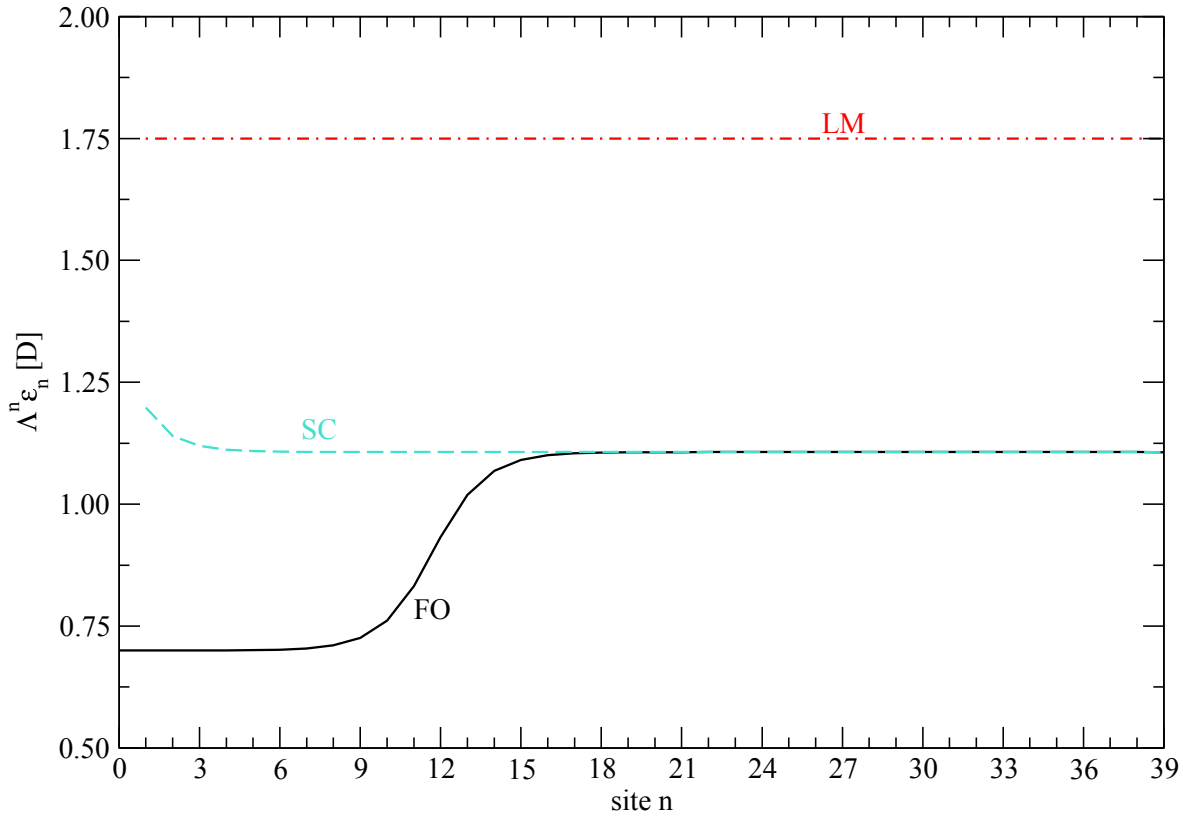

Figure 5.10: Rescaled single-particle energies $\Lambda^n\varepsilon_n$ from the diagonalization of the fixed-point Hamiltonians (5.44) - (5.46) for $N = 42$, $\frac{V}{D} = 4 \cdot 10^{-3}$ and $\Lambda = 2.5$. These energy levels represent the expected single-particle energies of the effective Hamiltonian from the CUT for $b \to \infty$ in the respective energy regimes.

Fig. 5.10 shows the single-particle energies from the diagonalized fixed-point Hamiltonians (5.44) - (5.46) after rescaling the single-particle energies with a factor Λ^n in order to bring all energy scales to the same order.

As in each fixed-point Hamiltonian one site less is present, the first site in the free-orbital regime is rescaled by a factor one while the first site in the local-moment regime is rescaled by a factor Λ and in the strong-coupling regime by a factor Λ^2.

If the CUT is able to describe the different energy regimes, we expect that the single-particle energies $\Lambda^n\varepsilon_n$ of the effective Hamiltonian for $b \to \infty$ coincide with the single-particle energies of the fixed-point Hamiltonians (5.44) - (5.46) (plotted in Fig. 5.10) in the respective energy regimes [8]. We expect the crossover between the energy levels of the free-orbital fixed-point Hamiltonian and the local-moment fixed-point Hamiltonian around the U-energy scale and the crossover from the local-moment fixed-point Hamiltonian H_{LM} to the strong-coupling fixed-point Hamiltonian H_{SC} in the region of the the Kondo energy scale T_{K}. This is our benchmark for determining if we are able to describe the crossover between the different energy regimes within the CUT approach which will be analyzed in the following sections.

5.4.5 Residual Off-Diagonality of the Interacting Model

If the interaction U is introduced, the residual off-diagonality is at first sight of the same form as in the case of $U = 0$ (cf. Fig. 5.4). The residual off-diagonality of the interaction terms has

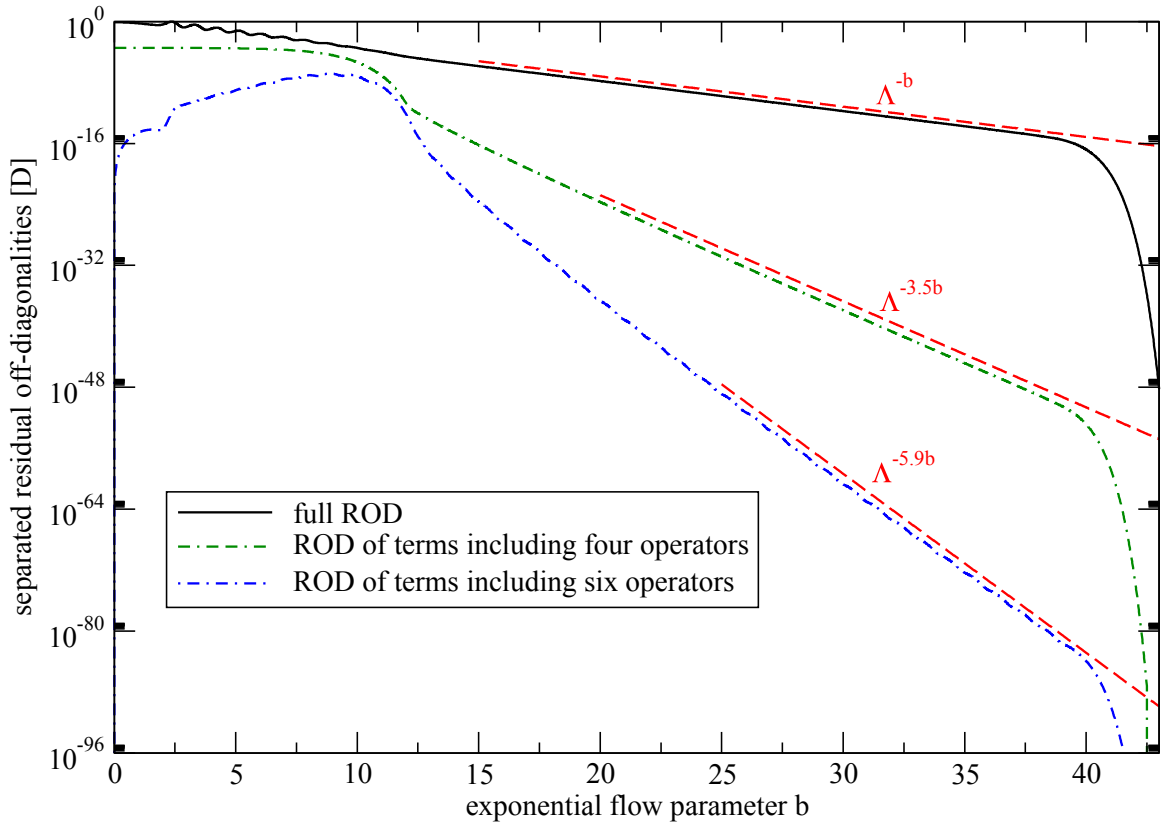

Figure 5.11: Separated residual off-diagonalities for $N = 40$, $\Lambda = 2.5$, $\frac{V}{D} = 4 \cdot 10^{-3}$ and $\frac{U}{D} = 10^{-3}$. The full ROD (dominated by bilinear terms), the ROD for terms with four and the ROD for terms with six operators are shown. The ROD of terms with a larger number of operators vanishes faster than ROD $\propto \Lambda^{-b}$ for large b which renders them irrelevant.

to be separated, e.g., by the number of operators in order to make their flow visible. Fig. 5.11 shows the full residual off-diagonality and the ones for four and six operators. Terms containing more than six operators are truncated.

The residual off-diagonalities for terms with four or six operators vanish much faster than ROD $\propto \Lambda^{-b}$ which renders them irrelevant and indicates that the interaction terms do not play a significant role for the flow of terms acting on small energies.

This might already indicate that the correct low-energy physics of the Anderson model is not covered within the CUT approach as used in this chapter because we expect that the crossover from the local-moment to the strong-coupling regime is again driven by interactions and that the single-particle picture breaks down during the crossover.

5.4.6 Single-Particle Energies of the Effective Hamiltonian

We now turn to the single-particle energies ε_n of the effective Hamiltonian for $b \to \infty$. The single-particle energies for $U = 0$ flow to the exact single-particle energies of the non-interacting model. As we now include the interaction U, the single-particle energies flow to a different value for $b \to \infty$ than in the non-interacting case.

The rescaled single-particle energies $\Lambda^n \varepsilon_n(\infty)$ are plotted in Fig. 5.12 for various values of U.

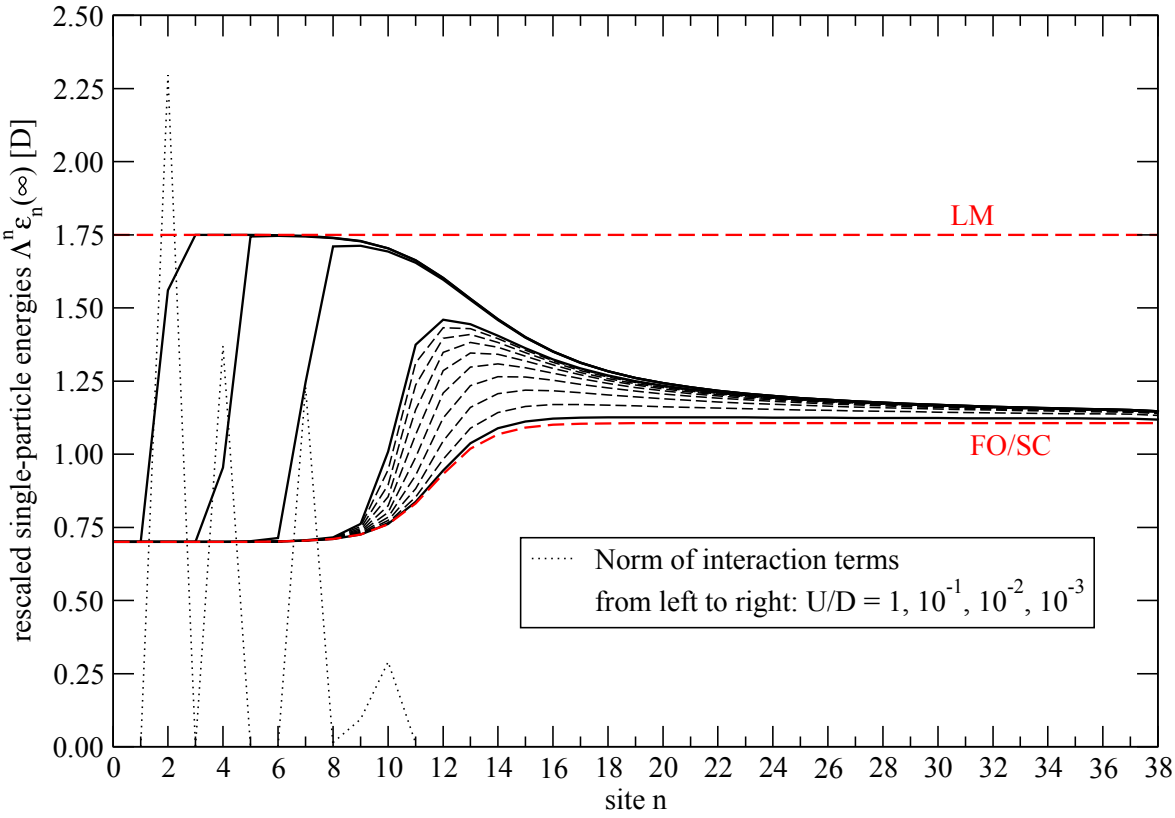

Figure 5.12: Rescaled single-particle energies $\Lambda^n \varepsilon_n$ of the effective Hamiltonian for $b \to \infty$ for $N = 40$, $\Lambda = 2.5$, $\frac{V}{D} = 4 \cdot 10^{-3}$ and from left to right: $\frac{U}{D} = 1$, 10^{-1}, 10^{-2}, 10^{-3}, $9 \cdot 10^{-4}$, $8 \cdot 10^{-4}$, ..., $2 \cdot 10^{-4}$, $1 \cdot 10^{-4}$. The single-particle energies of the fixed-point Hamiltonians are calculated from Eqs. (5.44) - (5.46) and are represented by the dashed red lines. We see a crossover from the single-particle energies for $U = 0$ (which coincides with the free-orbital fixed point) to the expected energy levels of the local-moment regime (cf. Sec. 5.4.4). In both regimes the norm of interaction terms calculated by Eq. (5.47) are negligible and become significantly large only in the region of the crossover. This is in agreement with the picture described in Sec. 5.4.4. The crossover to the strong-coupling regime cannot be retrieved as the single-particle energies are not reaching the reference energy levels of the strong-coupling regime (SC), although the lowest energy scale in the system is well below the Kondo temperature T_K.

In Fig. 5.12 we additionally plotted the norm of local interaction terms

$$G_n = \Lambda^{n-1} \sqrt{\sum_i |h_n^i|^2} \tag{5.47}$$

where the h_n^i denote the coefficients of local interaction terms acting on site n.

By a local interaction term we refer to a term that consists only of density operators acting on the site n, e.g.,

$$p_{n\uparrow}^\dagger p_{n\uparrow} p_{n\downarrow}^\dagger p_{n\downarrow}, \quad p_{n\uparrow}^\dagger p_{n\uparrow} h_{n\uparrow}^\dagger h_{n\uparrow}, \quad p_{n\uparrow}^\dagger p_{n\uparrow} p_{n\downarrow}^\dagger p_{n\downarrow} h_{n\uparrow}^\dagger h_{n\uparrow}. \tag{5.48}$$

The local interaction terms are also rescaled with a factor Λ^{n-1} in order to compare them to the single-particle energies. Even after rescaling the local interaction terms they are almost zero everywhere except for the crossover region on the U-energy scale where we see a shift of the single-particle energies due to the interaction. We see two distinct regions linked to

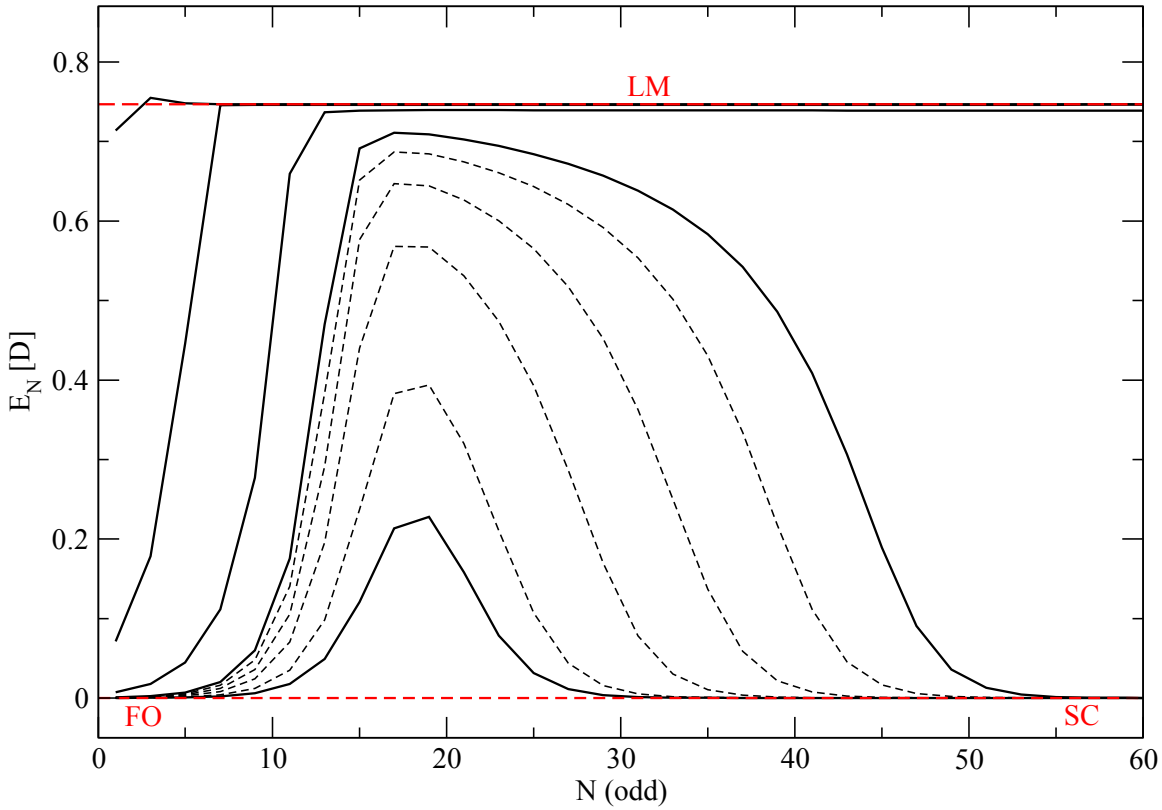

Figure 5.13: NRG results for the flow of the lowest non-zero many-particle energies with odd N and total charge $Q = 1$ (with respect to half-filling) and total spin $S = 0$ (cf. Ref. [8, 10]). The lowest-lying energy level from a state with one particle added to the ground state ($Q = 1$), where the ground-state energy is set to zero, is plotted for $\frac{V}{D} = 4 \cdot 10^{-3}$ and from left to right: $\frac{U}{D} = 1$, 10^{-1}, 10^{-2}, 10^{-3}, $8 \cdot 10^{-4}$, $6 \cdot 10^{-4}$, $4 \cdot 10^{-4}$, $2 \cdot 10^{-4}$ and $1 \cdot 10^{-4}$. The different expected many-particle energies represented by the red dashed lines can be understood by the fixed-point Hamiltonians (5.44) - (5.46). If the number of sites for the free-orbital regime $N+1$ is odd, then the additional particle is added to a zero energy level. The same is true for the strong-coupling regime as $N-1$ must be odd as well. In the local-moment regime N is even and by adding a particle to the ground state the energy is increased by the lowest positive single-particle energy.

the free-orbital and the local-moment regime where a single-particle picture holds well inside the respective regimes and the single-particle Hamiltonians are well described by the effective fixed-point Hamiltonians (5.44) and (5.45). The single-particle energies after diagonalizing the fixed-point Hamiltonians are shown in Fig. 5.12 as the red dashed lines. The single-particle picture breaks down in the crossover region between the free-orbital and the local-moment regime where local interaction terms are not negligible anymore.

The appearance of the single-particle energies of the effective Hamiltonian is very similar to NRG results (cf. Ref. [8, 10] or Fig. 5.13) when focusing on states where one particle is added to the ground state (denoted by the total charge $Q = 1$ with respect to half-filling). We derived the flow of the lowest non-zero many-particle energies from states with total charge $Q = 1$ and total spin $S = 0$ (cf. Ref. [10]) of the Anderson model with a NRG program originally developed by F.B. Anders which was kindly provided to us by S. Schmitt in order to compare our results to those obtained by NRG calculations.

Fig. 5.13 shows the flow of the lowest-lying many-particle levels of states with $Q = 1$ and $S = 0$. The reference energy levels of the different fixed-point Hamiltonians (5.44) - (5.46) can

be obtained by the following reasoning.

The chain lengths of the effective fixed-point Hamiltonians (5.44) and (5.46) are $N+1$ and $N-1$ which shall be odd. In this case, the chain length for the fixed-point Hamiltonian (5.45) is N and must be even. Because the spectrum is symmetric around the Fermi level, a zero energy level is present in the case of an odd number of sites and thus adding a particle results in the same energy as the ground-state energy – which is set to zero. For an even N (in the local-moment regime), the zero energy level is not present and thus adding a particle increases the energy by the lowest single-particle energy present in the effective Hamiltonian. The expected energy levels of the respective fixed-point Hamiltonians obtained from this reasoning are shown as the red dashed lines in Fig. 5.13. The general structure of the results obtained with NRG is very similar to the one gained with CUT.

For smaller interactions, below $\frac{U}{D} = 10^{-3}$, the local-moment regime is not as clearly distinct in the CUT data as it is in the NRG data. Additionally, the local interaction terms are decreasing very quickly with decreasing U and are already small for $\frac{U}{D} = 10^{-3}$ while they are almost zero for $\frac{U}{D} = 10^{-4}$. For such small $\frac{U}{D} \leq 10^{-4}$, we see almost no development of the local-moment regime within the CUT data while it is still clearly distinct in the NRG data. If we pass further to ever smaller energies, we expect to see the single-particle energies reaching the $U = 0$ energy levels again when crossing to the strong-coupling regime which is not observed in the data obtained with the CUT approach.

It seems that the rapid decrease of the interaction terms with decreasing energies results in an effective model that misses the correct low-energy physics of the Anderson model. This result is not completely satisfying but we can, nevertheless, clearly identify the crossover from the free-orbital to the local-moment regime.

5.4.7 Crossover from the Free-Orbital to the Local-Moment Regime

We want to study the crossover from the free-orbital to the local-moment regime further. On the one hand, we are interested in the question how far the crossover region coincides with already known results while, on the other hand, we want to study how far the interaction-range d from Eq. (5.43) influences the results.

From NRG calculations [8] we know that the crossover between the free-orbital and the local-moment regime occurs on an energy scale between $\frac{U}{20}$ and $\frac{U}{2}$. The site n of the chain is linked to the energy scale by

$$\varepsilon_n = \frac{1}{2}\left(1+\Lambda^{-1}\right)\Lambda^{-n}. \tag{5.49}$$

Thus, a given energy ε_n corresponds to the site

$$n = -\frac{\ln \frac{2\varepsilon_n}{1+\Lambda^{-1}}}{\ln \Lambda}. \tag{5.50}$$

In Fig. 5.14 we compare the crossover regions obtained with the CUT to the sites n connected to the energy scales $\frac{U}{20}$ and $\frac{U}{2}$. We find an almost perfect agreement of the crossover region for large values of U. In the energy interval in which we expect the crossover between the free-orbital and the local-moment regime to occur, the single-particle energies switch from the single-particle energies of the free-orbital fixed-point Hamiltonian (5.44) to the single-particle energies of the local-moment fixed-point Hamiltonian (5.45).

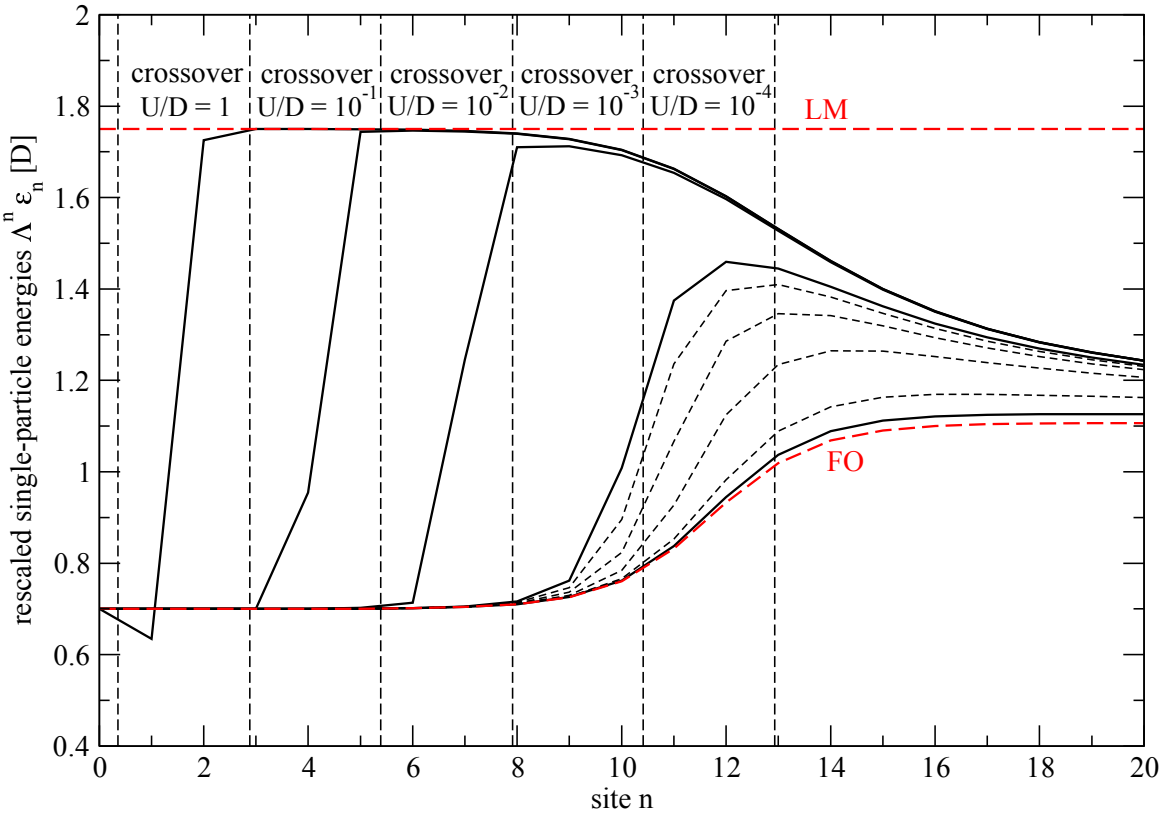

Figure 5.14: Rescaled single-particle energies $\Lambda^n \varepsilon_n$ of the effective Hamiltonian for $b \to \infty$ for $N = 30$, $\Lambda = 2.5$, $\frac{V}{D} = 4 \cdot 10^{-3}$ and from left to right: $\frac{U}{D} = 1$, 10^{-1}, 10^{-2}, 10^{-3}, $8 \cdot 10^{-4}$, $6 \cdot 10^{-4}$, $4 \cdot 10^{-4}$, $2 \cdot 10^{-4}$ and $1 \cdot 10^{-4}$. Terms with more than six operators or a range (5.43) $d > 1$ are truncated. The dashed red lines denote the single-particle energies of the free-orbital fixed-point Hamiltonian (FO) (5.44) and the local-moment fixed-point Hamiltonian (LM) (5.45). The dashed black vertical lines mark the energy intervals $\frac{U}{20} < E < \frac{U}{2}$ which denote the expected crossover region known from NRG calculations [8]. For large values of U, the crossover takes place exactly in the expected regions. For smaller values of $\frac{U}{D} \leq 10^{-3}$, the crossover takes place beyond the expected energy scale and is less distinct than in the NRG data.

For smaller values of U, we again observe that the crossover is less distinct than it is in the NRG data. Additionally, the crossover takes place beyond the expected energy scale which is an additional hint towards the fact that we might lose some important information during the flow due to the truncation.

5.4.8 Influence of the Interaction-Range

In Fig. 5.15 the single-particle energies with an interaction-range $d = 7$ are shown. Terms with more than six operators are truncated just as before but this time terms with an interaction-range up to $d = 7$ are also taken into account. The dotted lines show the single-particle energies from Fig. 5.14 with $d = 1$ in order to illustrate the improvement of the results for higher interaction ranges.

The results for larger values of U are already in good agreement with the NRG data and are thus not significantly affected by the interaction-range. When we consider smaller values of U, the results for $d = 7$ show a much more distinct crossover than for $d = 1$ which is in good agreement with NRG calculations. Furthermore, we see a shift of the energy scale of the

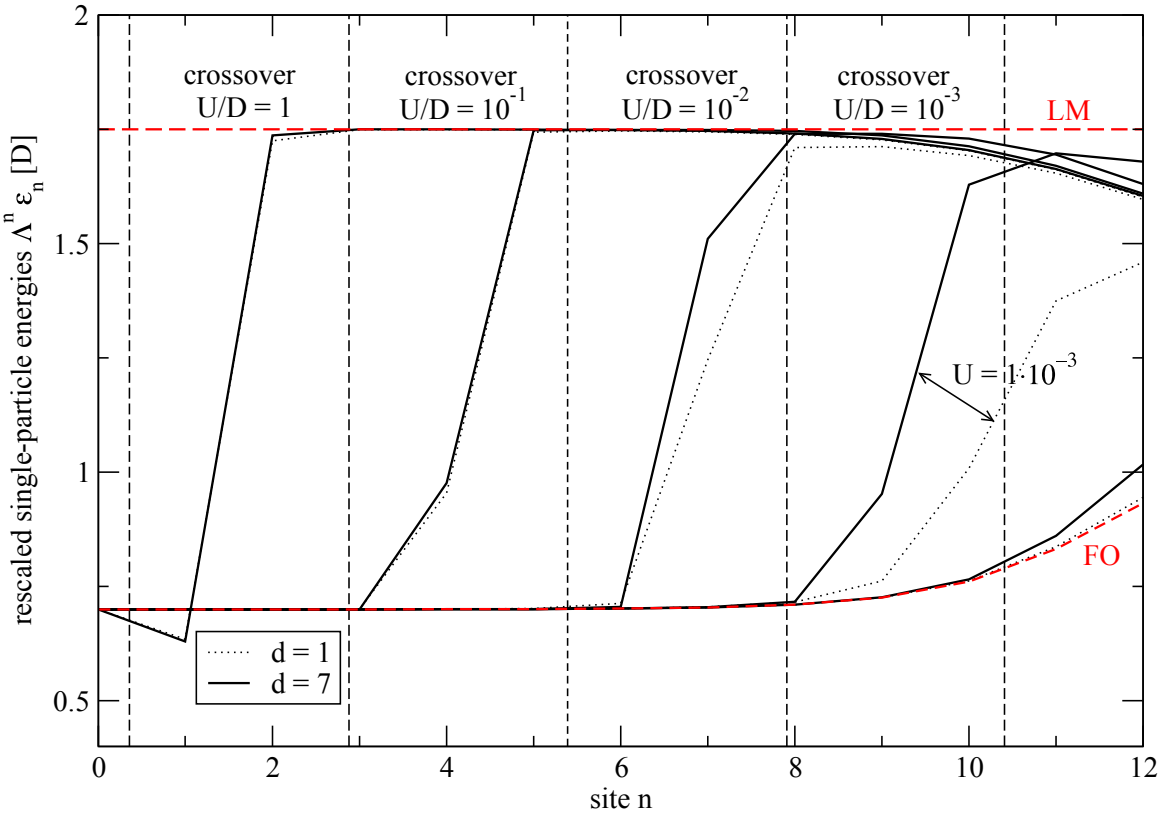

Figure 5.15: Rescaled single-particle energies $\Lambda^n \varepsilon_n$ of the effective Hamiltonian for $b \to \infty$ for $N = 13$, $\Lambda = 2.5$, $\frac{V}{D} = 4 \cdot 10^{-3}$ and from left to right: $\frac{U}{D} = 1$, 10^{-1}, 10^{-2}, 10^{-3}. Terms with more than six operators or a range (5.43) $d > 7$ are truncated. The dotted lines show the results from Fig. 5.14 where the interaction-range was $d = 1$. The dashed red lines denote the single-particle energies of the free-orbital fixed-point Hamiltonian (FO) (5.44) and the local-moment fixed-point Hamiltonian (LM) (5.45). The dashed black vertical lines show the energy intervals $\frac{U}{20} < E < \frac{U}{2}$ which denote the expected crossover region known from NRG calculations [8]. Compared to the results for $d = 1$ (cf. Fig. 5.14), we find a more distinct crossover in the correct energy region for smaller U. Thus, including larger interaction-ranges improves the results further.

crossover between the results for $d = 1$ and $d = 7$ towards the correct crossover region. Thus, we are able to improve the results by including larger interaction-ranges d.

In summary, we can state that the CUT approach as used in this chapter is able to describe the crossover from the free-orbital to the local-moment regime. The approach works very well for larger values of U on higher energy scales. The calculation effort for these parameters is decent and the results fit the NRG data. For smaller values of U, however, the numerical effort increases significantly as large interaction-ranges d are required. If we wanted to approach smaller values of U, we would need even larger values of d, i.e., we would have to include even more terms which would increase the calculation effort further.

We find no indication that the strong-coupling physics is captured within this approach. Thus, we limit our analysis to the crossover between the free-orbital and the local-moment regime. In the next chapters we investigate two different approaches with the aim of capturing the strong-coupling regime.

6 Truncation in Orders of the Coulomb Interaction U

6.1 Parametrization and Reference State

In this chapter we use the energy parametrization (2.58) and choose the ground state for $U = 0$ as the reference state which is given by the Fermi sea

$$|\mathrm{ref}\rangle = |\mathrm{FS}\rangle. \tag{6.1}$$

The single-particle energies ε_n and the weights γ_n are given by Eq. (2.57) where the hybridization is already absorbed into the parameters ε_n and γ_n. We normal-order the operators with respect to the Fermi sea which results in the Hamiltonian

$$H = \sum_{n_1,n_2,\sigma} t_{n_1 n_2} : c^\dagger_{n_1\sigma} c_{n_2\sigma} : + \sum_{\{n_i\}} U_{n_1 n_2 n_3 n_4} : c^\dagger_{n_1\uparrow} c^\dagger_{n_2\downarrow} c_{n_3\downarrow} c_{n_4\uparrow} : + E_0 \mathbb{1}, \tag{6.2}$$

cf. Eq. (2.58), where an additional energy constant due to the normal-ordering was dismissed so that $E_0 = 0$ and the coefficients for the starting Hamiltonian are given by

$$t_{n_1 n_2} = \varepsilon_{n_1} \delta_{n_1 n_2} + \left(\varepsilon_\mathrm{d} + \frac{U}{2}\right) \gamma_{n_1} \gamma_{n_2}\,, \quad U_{n_1 n_2 n_3 n_4} = U \gamma_{n_1} \gamma_{n_2} \gamma_{n_3} \gamma_{n_4}\,, \quad E_0 = 0. \tag{6.3}$$

The single-particle energies ε_n and the weights γ_n are given by Eq. (2.57). In order to derive the coefficients in the form (6.3), we use

$$\sum_n |\gamma_n|^2 \langle c^\dagger_{n\sigma} c_{n\sigma} \rangle = \frac{1}{2}. \tag{6.4}$$

Note that the hopping terms $t_{n_1 n_2}$ vanish in the particle-hole symmetric case $\varepsilon_\mathrm{d} = -\frac{U}{2}$.

In this chapter we will derive the impurity contribution to the susceptibility χ_d so that we need to apply a magnetic field to the impurity which can be achieved by the substitution

$$\varepsilon_\mathrm{d} \quad \longleftrightarrow \quad \varepsilon_\mathrm{d} - \sigma h \tag{6.5}$$

where $\sigma = \pm 1$ is the sign connected to the spin index of the operator $n_{\mathrm{d},\sigma}$. The energy h is connected to a magnetic field B via $h = \frac{1}{2} g_\mathrm{e} \mu_\mathrm{B} B$ where g_e is the Landé g-factor while μ_B denotes the Bohr magneton. In the following, we refer to the energy h as the magnetic field.

6.2 Flow Equation and Truncation

The flow equations in this chapter are derived analytically. Since we will apply a magnetic field to the impurity, we consider a spin-symmetry broken case and thus explicitly use spin-dependent

coefficients. The generator is chosen to be of the general structure

$$\begin{aligned}\eta &= \sum_{n_1,n_2,\sigma} \eta^t_{n_1n_2,\sigma} : c^\dagger_{n_1\sigma} c_{n_2\sigma} : + \sum_{\{n_i\}} \eta^U_{n_1n_2n_3n_4} : c^\dagger_{n_1\uparrow} c^\dagger_{n_2\downarrow} c_{n_3\downarrow} c_{n_4\uparrow} : \\ &+ \sum_{\substack{n_1,n_2,n_3,n_4 \\ n_2>n_1,n_4>n_3}} \eta^{R,\sigma}_{n_1n_2n_3n_4} : c^\dagger_{n_1\sigma} c^\dagger_{n_2\sigma} c_{n_3\sigma} c_{n_4\sigma} :\end{aligned} \tag{6.6}$$

with the coefficients

$$\eta^t_{n_1n_2,\sigma} = s^t_{n_1n_2,\sigma} t^\sigma_{n_1n_2}\,, \quad \eta^U_{n_1n_2n_3n_4} = s^U_{n_1n_2n_3n_4} U_{n_1n_2n_3n_4}\,, \quad \eta^{R,\sigma}_{n_1n_2n_3n_4} = s^{R,\sigma}_{n_1n_2n_3n_4} R^\sigma_{n_1n_2n_3n_4}. \tag{6.7}$$

The coefficients $s^t_{n_1n_2,\sigma}$, $s^U_{n_1n_2n_3n_4}$ and $s^{R,\sigma}_{n_1n_2n_3n_4}$ are arbitrary so far and will be specified later when calculating explicit results. The third interaction term, where all operators have the same spin, is not present in the initial Hamiltonian but will emerge during the flow. We will eliminate some of these terms and thus include them in the generator.

We calculate the commutator of η from Eq. (6.6) and H from Eq. (6.2) and derive the flow equation (4.4). New terms emerge during the flow which are discussed later (cf. Eq. (6.10)). The flow equation stemming from the initial Hamiltonian (6.2) is of the form

$$\begin{aligned}\partial_l E_0 &= 2 \sum_{x_1,x_2,x_3,,x_4} s^U_{x_1x_2x_3x_4} \theta^\uparrow_{x_1} \theta^\downarrow_{x_2} \left(1-\theta^\downarrow_{x_3}\right)\left(1-\theta^\uparrow_{x_4}\right) U^2_{x_1x_2x_3x_4} \\ &+ \sum_{x_1,x_2,\sigma} s^\sigma_{x_1x_2} \left(\theta^\sigma_{x_1}-\theta^\sigma_{x_2}\right)\left(t^\sigma_{x_1x_2}\right)^2\end{aligned} \tag{6.8a}$$

$$\begin{aligned}\partial_l t^\uparrow_{n_1n_2} &= \sum_{x_1} \left(s^\uparrow_{n_1x_1} - s^\uparrow_{x_1n_2}\right) t^\uparrow_{n_1x_1} t^\uparrow_{x_1n_2} + \sum_{x_1,x_2} \left(s^\downarrow_{x_1x_2} - s^U_{n_1x_2x_1n_2}\right)\left(\theta^\downarrow_{x_1}-\theta^\downarrow_{x_2}\right) t^\downarrow_{x_1x_2} U_{n_1x_2x_1n_2} \\ &+ \sum_{x_1,x_2,x_3} \left(s^U_{n_1x_1x_2x_3} - s^U_{x_3x_2x_1n_2}\right)\left(\theta^\downarrow_{x_1}\left(1-\theta^\downarrow_{x_2}-\theta^\uparrow_{x_3}\right)+\theta^\downarrow_{x_2}\theta^\uparrow_{x_3}\right) U_{n_1x_1x_2x_3} U_{x_3x_2x_1n_2}\end{aligned} \tag{6.8b}$$

$$\begin{aligned}\partial_l t^\downarrow_{n_1n_2} &= \sum_{x_1} \left(s^\downarrow_{n_1x_1} - s^\downarrow_{x_1n_2}\right) t^\downarrow_{n_1x_1} t^\downarrow_{x_1n_2} + \sum_{x_1,x_2} \left(s^\uparrow_{x_1x_2} - s^U_{x_2n_1n_2x_1}\right)\left(\theta^\uparrow_{x_1}-\theta^\uparrow_{x_2}\right) t^\uparrow_{x_1x_2} U_{x_2n_1n_2x_1} \\ &+ \sum_{x_1,x_2,x_3} \left(s^U_{x_1n_1x_3x_2} - s^U_{x_2x_3n_2x_1}\right)\left(\theta^\uparrow_{x_1}\left(1-\theta^\uparrow_{x_2}-\theta^\downarrow_{x_3}\right)+\theta^\uparrow_{x_2}\theta^\downarrow_{x_3}\right) U_{x_1n_1x_3x_2} U_{x_2x_3n_2x_1}\end{aligned} \tag{6.8c}$$

$$\begin{aligned}\partial_l U_{n_1n_2n_3n_4} &= \sum_{x_1}\left(s^\uparrow_{n_1x_1} - s^U_{x_1n_2n_3n_4}\right) t^\uparrow_{n_1x_1} U_{x_1n_2n_3n_4} + \sum_{x_1}\left(s^\downarrow_{n_2x_1} - s^U_{n_1x_1n_3n_4}\right) t^\downarrow_{n_2x_1} U_{n_1x_1n_3n_4} \\ &+ \sum_{x_1}\left(s^U_{n_1n_2x_1n_4} - s^\downarrow_{x_1n_3}\right) t^\downarrow_{x_1n_3} U_{n_1n_2x_1n_4} + \sum_{x_1}\left(s^U_{n_1n_2n_3x_1} - s^\uparrow_{x_1n_4}\right) t^\uparrow_{x_1n_4} U_{n_1n_2n_3x_1} \\ &+ \sum_{x_1,x_2}\left(s^U_{n_1n_2x_1x_2} - s^U_{x_2x_1n_3n_4}\right) U_{n_1n_2x_1x_2} U_{x_2x_1n_3n_4}\left(1-\theta^\downarrow_{x_1}-\theta^\uparrow_{x_2}\right) \\ &+ \sum_{x_1,x_2}\left(s^U_{n_1x_1n_3x_2} - s^U_{x_2n_2x_1n_4}\right) U_{n_1x_1n_3x_2} U_{x_2n_2x_1n_4}\left(\theta^\uparrow_{x_2}-\theta^\downarrow_{x_1}\right)\end{aligned} \tag{6.8d}$$

where the starting values are given by Eqs. (6.3) and (2.57) while

$$\theta_n^\sigma = \langle c_{n\sigma}^\dagger c_{n\sigma} \rangle \tag{6.9}$$

stems from the normal-ordering with respect to the Fermi sea. The starting value for E_0 is set to zero because we are only interested in the dependence on the magnetic field h which does not affect the dismissed constant as the magnetic field cancels due to the different signs for different spin. All emerging terms are normal-ordered with respect to the Fermi sea in order to capture all feedback of newly emerging terms. Useful calculation rules for products of normal-ordered operators are described in App. 9.7.

When calculating the commutator of two quartic terms with the coefficient $U_{n_1 n_2 n_3 n_4}$, new terms emerge which are of the form

$$\begin{aligned} H_{\text{new}} &= \sum_\sigma \sum_{\substack{n_1,n_2,n_3,n_4 \\ n_2>n_1,n_4>n_3}} R^\sigma_{n_1 n_2 n_3 n_4} : c^\dagger_{n_1\sigma} c^\dagger_{n_2\sigma} c_{n_3\sigma} c_{n_4\sigma} : \\ &+ \sum_\sigma \sum_{n_1,n_6} \sum_{\substack{n_2,n_3,n_4,n_5 \\ n_3>n_2,n_5>n_4}} \Gamma^\sigma_{n_1 n_2 n_3 n_4 n_5 n_6} : c^\dagger_{n_1\sigma} c^\dagger_{n_2\bar\sigma} c^\dagger_{n_3\bar\sigma} c_{n_4\bar\sigma} c_{n_5\bar\sigma} c_{n_6\sigma} : . \end{aligned} \tag{6.10}$$

The flow of the newly emerging R- and Γ-terms from Eq. (6.10) are given in Eqs. (6.11a) - (6.11d). The DEQ describing the generation of the R- and Γ-terms during the flow is given by

$$\begin{aligned} \partial_l R^\uparrow_{n_1 n_2 n_3 n_4} &= \frac{1}{2} \sum_{x_1,x_2} \left(\eta^U_{n_2 x_1 x_2 n_3} U_{n_1 x_2 x_1 n_4} - \eta^U_{n_1 x_2 x_1 n_4} U_{n_2 x_1 x_2 n_3}\right) \left(\theta^\downarrow_{x_1} - \theta^\downarrow_{x_2}\right) \\ &- \frac{1}{2} \sum_{x_1,x_2} \left(\eta^U_{n_2 x_1 x_2 n_4} U_{n_1 x_2 x_1 n_3} - \eta^U_{n_1 x_2 x_1 n_3} U_{n_2 x_1 x_2 n_4}\right) \left(\theta^\downarrow_{x_1} - \theta^\downarrow_{x_2}\right) \\ &- \frac{1}{2} \sum_{x_1,x_2} \left(\eta^U_{n_1 x_1 x_2 n_3} U_{n_2 x_2 x_1 n_4} - \eta^U_{n_2 x_2 x_1 n_4} U_{n_1 x_1 x_2 n_3}\right) \left(\theta^\downarrow_{x_1} - \theta^\downarrow_{x_2}\right) \\ &+ \frac{1}{2} \sum_{x_1,x_2} \left(\eta^U_{n_1 x_1 x_2 n_4} U_{n_2 x_2 x_1 n_3} - \eta^U_{n_2 x_2 x_1 n_3} U_{n_1 x_1 x_2 n_4}\right) \left(\theta^\downarrow_{x_1} - \theta^\downarrow_{x_2}\right) \end{aligned} \tag{6.11a}$$

$$\begin{aligned} \partial_l R^\downarrow_{n_1 n_2 n_3 n_4} &= \frac{1}{2} \sum_{x_1,x_2} \left(\eta^U_{x_1 n_2 n_3 x_2} U_{x_2 n_1 n_4 x_1} - \eta^U_{x_2 n_1 n_4 x_1} U_{x_1 n_2 n_3 x_2}\right) \left(\theta^\uparrow_{x_1} - \theta^\uparrow_{x_2}\right) \\ &- \frac{1}{2} \sum_{x_1,x_2} \left(\eta^U_{x_1 n_2 n_4 x_2} U_{x_2 n_1 n_3 x_1} - \eta^U_{x_2 n_1 n_3 x_1} U_{x_1 n_2 n_4 x_2}\right) \left(\theta^\uparrow_{x_1} - \theta^\uparrow_{x_2}\right) \\ &- \frac{1}{2} \sum_{x_1,x_2} \left(\eta^U_{x_1 n_1 n_3 x_2} U_{x_2 n_2 n_4 x_1} - \eta^U_{x_2 n_2 n_4 x_1} U_{x_1 n_1 n_3 x_2}\right) \left(\theta^\uparrow_{x_1} - \theta^\uparrow_{x_2}\right) \\ &+ \frac{1}{2} \sum_{x_1,x_2} \left(\eta^U_{x_1 n_1 n_4 x_2} U_{x_2 n_2 n_3 x_1} - \eta^U_{x_2 n_2 n_3 x_1} U_{x_1 n_1 n_4 x_2}\right) \left(\theta^\uparrow_{x_1} - \theta^\uparrow_{x_2}\right) \end{aligned} \tag{6.11b}$$

$$
\begin{aligned}
\partial_l \Gamma^{\uparrow}_{n_1 n_2 n_3 n_4 n_5 n_6} &= \sum_{x_1} \left(\eta^U_{x_1 n_3 n_5 n_6} U_{n_1 n_2 n_4 x_1} - \eta^U_{n_1 n_2 n_4 x_1} U_{x_1 n_3 n_5 n_6} \right) \\
&- \sum_{x_1} \left(\eta^U_{x_1 n_2 n_5 n_6} U_{n_1 n_3 n_4 x_1} - \eta^U_{n_1 n_3 n_4 x_1} U_{x_1 n_2 n_5 n_6} \right) \\
&- \sum_{x_1} \left(\eta^U_{x_1 n_3 n_4 n_6} U_{n_1 n_2 n_5 x_1} - \eta^U_{n_1 n_2 n_5 x_1} U_{x_1 n_3 n_4 n_6} \right) \\
&+ \sum_{x_1} \left(\eta^U_{x_1 n_2 n_4 n_6} U_{n_1 n_3 n_5 x_1} - \eta^U_{n_1 n_3 n_5 x_1} U_{x_1 n_2 n_4 n_6} \right)
\end{aligned} \tag{6.11c}
$$

$$
\begin{aligned}
\partial_l \Gamma^{\downarrow}_{n_1 n_2 n_3 n_4 n_5 n_6} &= \sum_{x_1} \left(\eta^U_{n_3 x_1 n_6 n_5} U_{n_2 n_1 x_1 n_4} - \eta^U_{n_2 n_1 x_1 n_4} U_{n_3 x_1 n_6 n_5} \right) \\
&- \sum_{x_1} \left(\eta^U_{n_2 x_1 n_6 n_5} U_{n_3 n_1 x_1 n_4} - \eta^U_{n_3 n_1 x_1 n_4} U_{n_2 x_1 n_6 n_5} \right) \\
&- \sum_{x_1} \left(\eta^U_{n_3 x_1 n_6 n_4} U_{n_2 n_1 x_1 n_5} - \eta^U_{n_2 n_1 x_1 n_5} U_{n_3 x_1 n_6 n_4} \right) \\
&+ \sum_{x_1} \left(\eta^U_{n_2 x_1 n_6 n_4} U_{n_3 n_1 x_1 n_5} - \eta^U_{n_3 n_1 x_1 n_5} U_{n_2 x_1 n_6 n_4} \right)
\end{aligned} \tag{6.11d}
$$

In order to justify a truncation scheme, we want to use deepCUT ideas (cf. Sec. 4.3.4) targeting the ground-state energy E_0. We are interested in the second derivative of E_0 with respect to the magnetic field h (cf. Sec. 6.6) and thus we want to be exact up to order h^2 for E_0. Additionally, we want the second derivative of E_0 to be correct up to order U^2 and thus E_0 must be correct for the orders $h^n U^m$ with $n,m \leq 2$. In the following, we mean by correct in order $h^x U^y$ that we are correct in all orders for which $h^n U^m$ with $n \leq x$ and $m \leq y$. For the order hU^2, for example, these are the orders U, U^2, h, hU and hU^2.

In this case, the Γ-terms can be neglected as they act in lowest order h^3U^2 or h^2U^3 on the ground-state energy E_0 while we only want to include terms up to order h^2U^2. Additionally, we can argue from a scaling perspective that terms with a higher number of operators will scale faster to zero than terms with less operators (cf. Sec. 6.8). The R-terms, on the other hand, are quartic operators and thus not negligible from a scaling perspective. Additionally, there is an action on the constant E_0 in order h^2U^2 from R-terms, i.e., there is no justification to neglect such terms. Nevertheless, from a deepCUT point of view we only need to take the commutation of R-terms with bilinear terms into account because the commutation between a R-term and another quartic term is at least of order U^3.

The commutation of an R-term and a bilinear term is at least of order hU^2 and the resulting terms will contribute to the right-hand side of the flow equation for the bilinear terms and the R-terms. Since we are using deepCUT ideas, we are only interested in the orders $h^n U^m$ with $n,m \leq 2$ for E_0. The action induced by the order hU^2 of the hopping terms on E_0 is at least of order h^2U^2 (one additional commutation with bilinear terms increases the order of h by one) while the order hU^2 from the R-terms acts at least in order h^3U^2 on E_0 (one commutation with a bilinear term affects the order h^2U^2 of the bilinear terms while one further commutation with a bilinear term affects the order h^3U^2 of E_0). A commutation with a quartic term would result in an expression which is of order U^3. Thus, we have to include the right-hand side of the

flow equation stemming from the commutation of bilinear terms with R-terms for the derivative of bilinear terms but we can neglect them for the derivative of the R-terms. The remaining commutations described above result in the additional differential equation

$$\partial_l R^{\sigma}_{n_1 n_2 n_3 n_4} = \left(t^{\sigma}_{n_4 n_4} + t^{\sigma}_{n_3 n_3} - t^{\sigma}_{n_2 n_2} - t^{\sigma}_{n_1 n_1}\right) \eta^{R}_{n_1 n_2 n_3 n_4, \sigma} \tag{6.12a}$$

$$\begin{aligned}
\partial t^{\sigma}_{n_1 n_2} = & \sum_{x_1<n_1} \sum_{x_2<n_2} \left(s^{\sigma}_{x_2 x_1} - s^{R}_{x_1 n_1 x_2 n_2, \sigma}\right) t^{\sigma}_{x_2 x_1} R^{\sigma}_{x_1 n_1 x_2 n_2} \left(\theta^{\sigma}_{x_1} - \theta^{\sigma}_{x_2}\right) \\
& - \sum_{x_1>n_1} \sum_{x_2<n_2} \left(s^{\sigma}_{x_2 x_1} - s^{R}_{n_1 x_1 x_2 n_2, \sigma}\right) t^{\sigma}_{x_2 x_1} R^{\sigma}_{n_1 x_1 x_2 n_2} \left(\theta^{\sigma}_{x_1} - \theta^{\sigma}_{x_2}\right) \\
& - \sum_{x_1<n_1} \sum_{x_2>n_2} \left(s^{\sigma}_{x_2 x_1} - s^{R}_{x_1 n_1 n_2 x_2, \sigma}\right) t^{\sigma}_{x_2 x_1} R^{\sigma}_{x_1 n_1 n_2 x_2} \left(\theta^{\sigma}_{x_1} - \theta^{\sigma}_{x_2}\right) \\
& + \sum_{x_1>n_1} \sum_{x_2>n_2} \left(s^{\sigma}_{x_2 x_1} - s^{R}_{n_1 x_1 n_2 x_2, \sigma}\right) t^{\sigma}_{x_2 x_1} R^{\sigma}_{n_1 x_1 n_2 x_2} \left(\theta^{\sigma}_{x_1} - \theta^{\sigma}_{x_2}\right)
\end{aligned} \tag{6.12b}$$

where the action on the hopping elements (6.12b) stems from the commutation of the R- and the hopping terms. In App. 9.8 the truncation scheme is outlined further. We use the DEQs (6.8a)-(6.8d), (6.11a), (6.11b), (6.12a) and (6.12b) and solve them by a 4th-order Runge-Kutta algorithm. With this system of differential equations the targeted quantity E_0 is exact for the orders $h^n U^m$ with $n, m \leq 2$.

6.3 Symmetries

There are two symmetries in the system which are conserved during the whole flow and can be used to increase the efficiency of the calculation. Without applying a magnetic field ($h = 0$) the system conserves spin symmetry

$$t^{\sigma}_{n_1 n_2} = t^{\bar{\sigma}}_{n_1 n_2}, \quad U_{n_1 n_2 n_3 n_4} = U_{n_2 n_1 n_4 n_3}, \quad R^{\sigma}_{n_1 n_2 n_3 n_4} = R^{\bar{\sigma}}_{n_1 n_2 n_3 n_4} \tag{6.13}$$

and in the particle-hole symmetric case ($\varepsilon_{\mathrm{d}} = -\frac{U}{2}$) without a magnetic field ($h = 0$) the coefficients additionally exhibit particle-hole symmetry

$$t^{\sigma}_{n_1 n_2} = -t^{\sigma}_{\bar{n}_2 \bar{n}_1}, \quad U_{n_1 n_2 n_3 n_4} = U_{\bar{n}_4 \bar{n}_3 \bar{n}_2 \bar{n}_1}, \quad R^{\sigma}_{n_1 n_2 n_3 n_4} = R^{\sigma}_{\bar{n}_4 \bar{n}_3 \bar{n}_2 \bar{n}_1} \tag{6.14}$$

where $\bar{n}_i$ denotes the site for which

$$\varepsilon^{\sigma}_{\bar{n}_i} = -\varepsilon^{\sigma}_{n_i}. \tag{6.15}$$

Of course, the fact that the Hamiltonian is self-adjoint[6] additionally implies

$$t^{\sigma}_{n_1 n_2} = t^{\sigma}_{n_2 n_1}, \quad U_{n_1 n_2 n_3 n_4} = U_{n_4 n_3 n_2 n_1}, \quad R^{\sigma}_{n_1 n_2 n_3 n_4} = R^{\sigma}_{n_3 n_4 n_1 n_2}. \tag{6.16}$$

If a magnetic field is introduced, the symmetries are reduced to Eq. (6.16) and the symmetry $c^{\dagger}_{n\sigma} \leftrightarrow c_{\bar{n}\bar{\sigma}}$ which implies

$$t^{\sigma}_{n_1 n_2} = -t^{\bar{\sigma}}_{\bar{n}_2 \bar{n}_1}, \quad U_{n_1 n_2 n_3 n_4} = U_{\bar{n}_3 \bar{n}_4 \bar{n}_1 \bar{n}_2}, \quad R^{\sigma}_{n_1 n_2 n_3 n_4} = R^{\bar{\sigma}}_{\bar{n}_4 \bar{n}_3 \bar{n}_2 \bar{n}_1}. \tag{6.17}$$

[6] The hermiticity of the Hamiltonian is not really a proper symmetry but manifests in the coefficients in a similar way.

6.4 Choice of the Generator

The generator should at least fulfill gs-generator properties (cf. Sec. 4.2.4). The bilinear part of the generator is chosen to be

$$\eta^t_{n_1 n_2,\sigma} = \operatorname{sgn}\left(\varepsilon^\sigma_{n_1} - \varepsilon^\sigma_{n_2}\right) t^\sigma_{n_1 n_2}. \tag{6.18}$$

The criteria for the sign of quartic terms are chosen by the signs of the energy differences

$$\varepsilon^\uparrow_{n_1} - \varepsilon^\uparrow_{n_4}, \quad \varepsilon^\downarrow_{n_2} - \varepsilon^\downarrow_{n_3}, \quad \varepsilon^\uparrow_{n_1} - \varepsilon^\downarrow_{n_3}, \quad \varepsilon^\downarrow_{n_2} - \varepsilon^\uparrow_{n_4}. \tag{6.19}$$

If all energy differences from Eq. (6.19) are positive, then we choose a positive sign $+1$. If, on the other hand, all energy differences (6.19) are negative, then a sign -1 is chosen. Through this choice the generator fulfills gs-generator properties. Thus, the sign in the generator is defined as

$$s^U_{n_1 n_2 n_3 n_4} = \begin{cases} +1 & \text{if } \varepsilon^\uparrow_{n_1} - \varepsilon^\uparrow_{n_4} > 0,\ \varepsilon^\downarrow_{n_2} - \varepsilon^\downarrow_{n_3} > 0,\ \varepsilon^\uparrow_{n_1} - \varepsilon^\downarrow_{n_3} > 0,\ \varepsilon^\downarrow_{n_2} - \varepsilon^\uparrow_{n_4} > 0 \\ -1 & \text{if } \varepsilon^\uparrow_{n_1} - \varepsilon^\uparrow_{n_4} < 0,\ \varepsilon^\downarrow_{n_2} - \varepsilon^\downarrow_{n_3} < 0,\ \varepsilon^\uparrow_{n_1} - \varepsilon^\downarrow_{n_3} < 0,\ \varepsilon^\downarrow_{n_2} - \varepsilon^\uparrow_{n_4} < 0 \\ 0 & \text{otherwise} \end{cases}. \tag{6.20}$$

We also need to eliminate some of the emerging R-terms from Eq. (6.10) as well in order to eliminate all terms that couple to the Fermi sea and thus

$$s^R_{n_1 n_2 n_3 n_4,\sigma} = \begin{cases} +1 & \text{if } \varepsilon^\sigma_{n_1} - \varepsilon^\sigma_{n_4} > 0,\ \varepsilon^\sigma_{n_2} - \varepsilon^\sigma_{n_3} > 0,\ \varepsilon^\sigma_{n_1} - \varepsilon^\sigma_{n_3} > 0,\ \varepsilon^\sigma_{n_2} - \varepsilon^\sigma_{n_4} > 0 \\ -1 & \text{if } \varepsilon^\sigma_{n_1} - \varepsilon^\sigma_{n_4} < 0,\ \varepsilon^\sigma_{n_2} - \varepsilon^\sigma_{n_3} < 0,\ \varepsilon^\sigma_{n_1} - \varepsilon^\sigma_{n_3} < 0,\ \varepsilon^\sigma_{n_2} - \varepsilon^\sigma_{n_4} < 0 \\ 0 & \text{otherwise} \end{cases}. \tag{6.21}$$

The generator (6.6) with the sign functions (6.18), (6.20) and (6.21) fulfills gs-generator properties because all remaining terms in the effective model yield zero acting on the Fermi sea. If the resulting DEQ converges, the ground state of the effective Hamiltonian will be the Fermi sea.

6.5 Numerical Results of the Flow without Magnetic Field

6.5.1 Residual Off-Diagonality

At first, we will focus on the particle-hole symmetric case ($\varepsilon_\mathrm{d} = -\frac{U}{2}$) without a magnetic field ($h = 0$). The coefficients $t_{n_1 n_2}$ for $n_1 \neq n_2$ are zero for $l = 0$ (cf. Eq. (6.3)) and thus emerge in lowest order U^2.

Fig. 6.1 shows the residual off-diagonalities for the different coefficients of the Hamiltonian (6.2) and (6.10). The residual off-diagonality converges and thus results in an effective model with the Fermi sea as its ground state. We separate the residual off-diagonality of the different contributions (bilinear, U- and R-terms), i.e., for the ROD of the bilinear terms only bilinear contributions are included into the generator while only U-terms are included in the ROD for U-terms and the same applies to the ROD of R-terms.

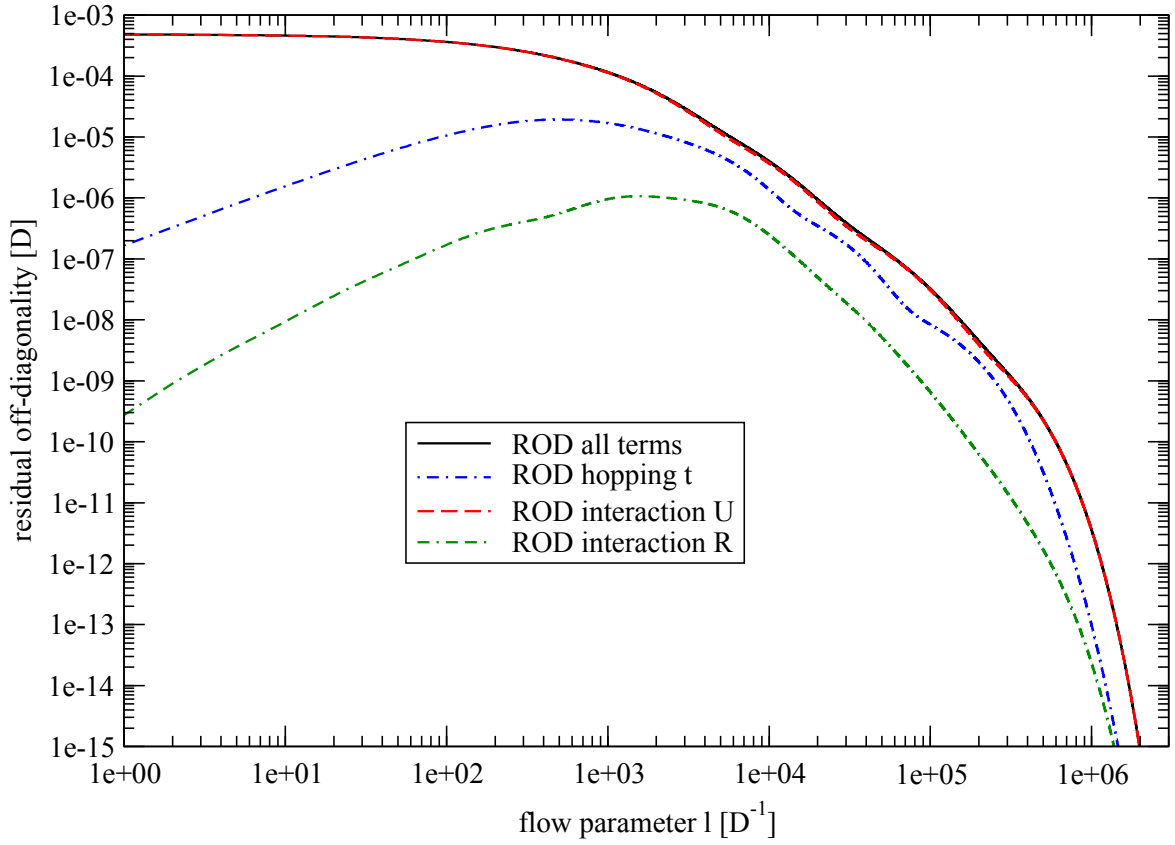

Figure 6.1: Residual off-diagonality for the Anderson model with $N = 16$, $\Lambda = 6$, $\frac{V}{D} = 0.01414$, $\frac{U}{D} = 10^{-3}$ and $h = 0$ for the different coefficients from Eqs. (6.2) and (6.10). The residual off-diagonality vanishes for $l \to \infty$ and thus the CUT constructs an effective Hamiltonian without any divergences with the Fermi sea as the ground state. The dominating part of the ROD for all l is the interaction part given by the coefficients $U_{n_1 n_2 n_3 n_4}$. The R-terms from Eq. (6.10) and the bilinear hopping terms are zero for $l = 0$ and emerge during the flow in order U^2. They remain smaller than the interaction terms during the whole flow.

The hopping terms as well as the R-terms are zero for $l = 0$ and remain smaller than the interaction contribution of the U-terms during the whole flow. The full ROD almost completely coincides with the ROD of the U-terms throughout the whole flow.

6.5.2 Interaction Vertex at the Fermi Level

Hewson developed a renormalized perturbation theory (cf. e.g. Ref. [50]) from which he constructs an effective low-energy Hamiltonian describing the correct strong-coupling physics. He finds a renormalized interaction strength $\tilde{U} = 4T_K$ for large enough values of $\frac{U}{\pi\Delta}$. Motivated by this finding, we investigate the behavior of the low-energy interaction vertex $U_{n_F n_F n_F n_F}$ as it describes the interaction of quasi-particles at the Fermi level. Note that there is no need for the two approaches to agree on this point. Nevertheless, similarities or differences between these two approaches are worthwhile to study.

Fig. 6.2 depicts the flow of the $U_{n_F n_F n_F n_F}$ for various initial interaction strengths U.

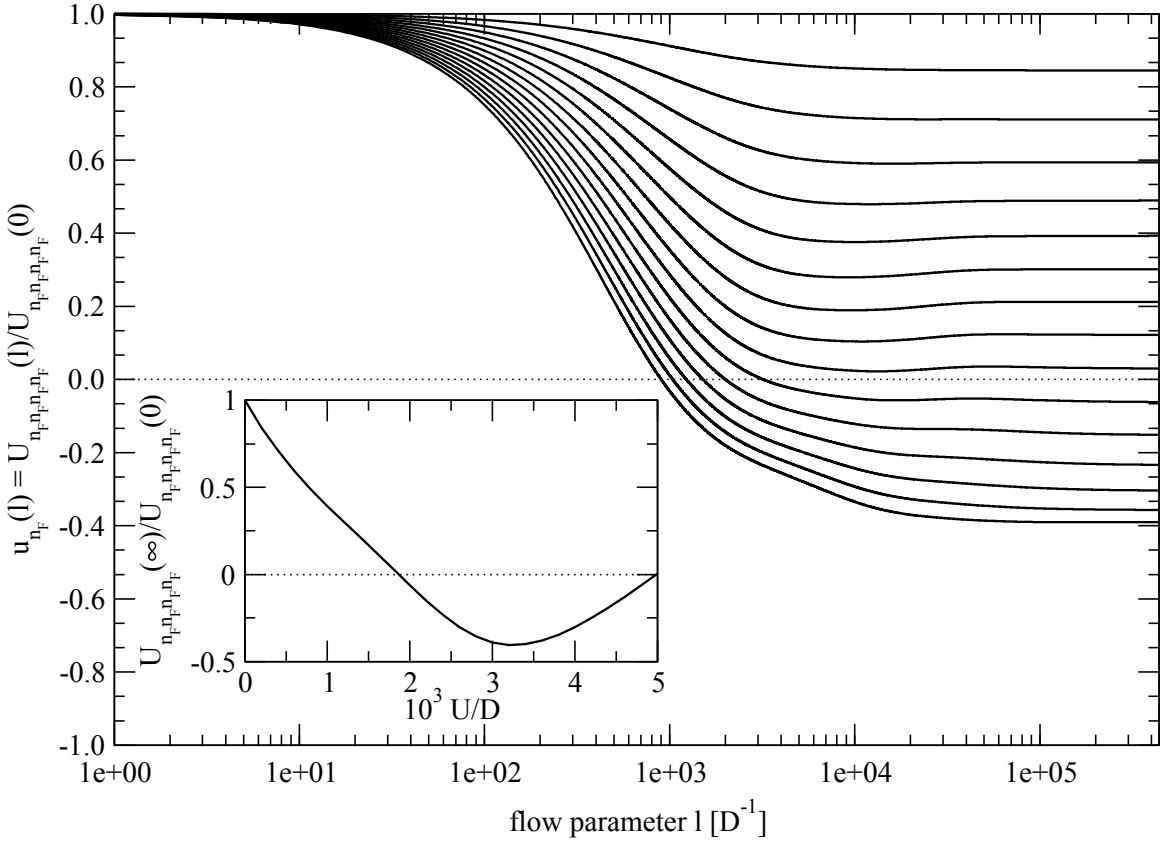

Figure 6.2: Renormalized interaction vertex u_{n_F} from Eq. (6.22) at the Fermi level $\varepsilon_F = 0$ for the Anderson model with $N = 16$, $\Lambda = 6$, $\frac{V}{D} = 0.01414$, from top to bottom $10^3 \frac{U}{D} = 0.2$, 0.4, ..., 2.8, 3 and $h = 0$. The inset shows the renormalized interaction vertex $u_{n_F}(\infty)$ of the effective Hamiltonian for $l \to \infty$. The renormalized interaction vertex $u_{n_F}(\infty)$ decreases linearly with U and even becomes attractive over some parameter regime before it increases again.

The interaction vertices U_{nnnn} are normalized to their initial value

$$u_n(l) = \frac{U_{nnnn}(l)}{U_{nnnn}(0)} \tag{6.22}$$

so that we can compare them for different U. Instead of an exponential behavior, we rather find a linear one and the interaction $u_{n_F}(\infty)$ becomes even attractive when U increases. At some point, the linear behavior ceases and $u_{n_F}(\infty)$ starts to increase again. This is an inconclusive result because, as stated earlier, it is unclear if the two approaches necessarily have to coincide in this point. Nevertheless, we can state that we do not find an exponential behavior for the low-energy vertex $u_{n_F}(\infty)$.

6.5.3 Interaction Vertex on Different Energy Scales

Fig. 6.3 shows the u_n defined in Eq. (6.22) for different n. The smaller the energy scales on which u_n acts, the larger the renormalization of u_n during the flow. At large energy scales the u_n show almost no renormalization which corresponds to the free-orbital regime. For small energies, the u_n exhibit the same flow.

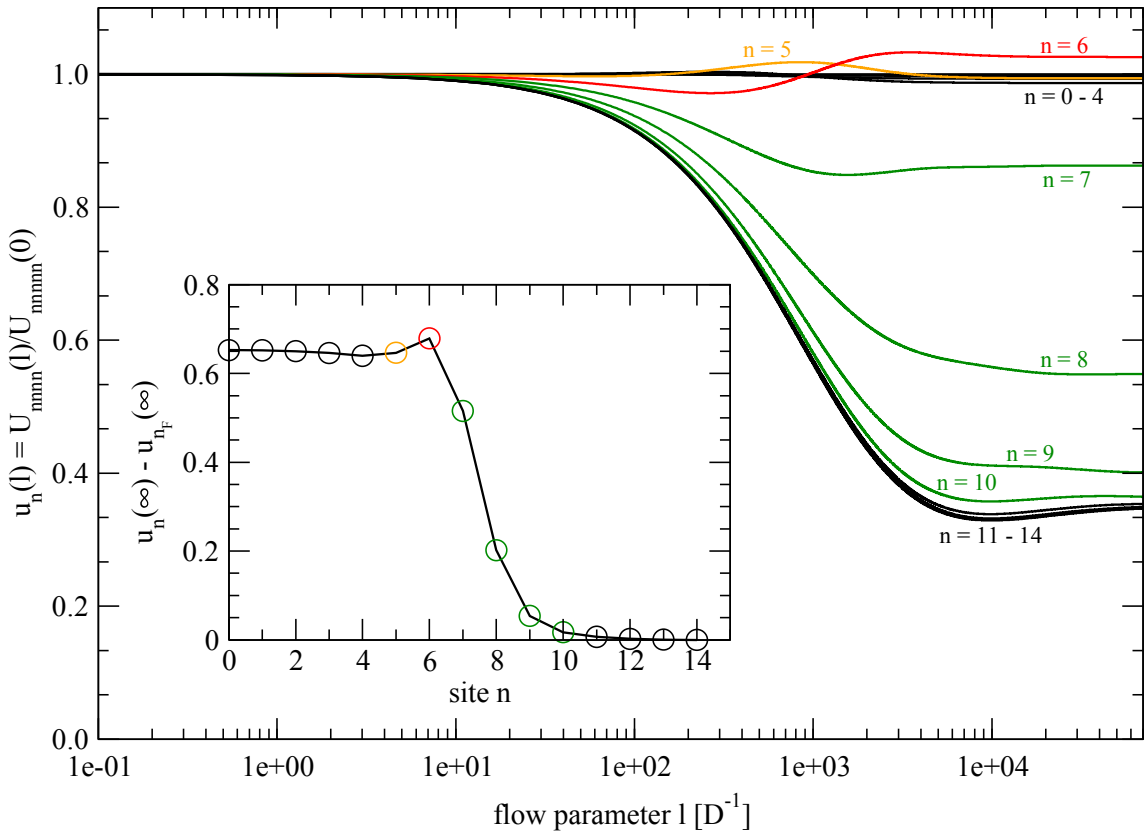

Figure 6.3: Renormalized interaction vertex u_n from Eq. (6.22) for the Anderson model with $N = 30$, $\Lambda = 3$, $\frac{V}{D} = 0.01414$, $\frac{U}{D} = 10^{-3}$ and $h = 0$. The local interaction terms on high-energy scales are not renormalized (free-orbital regime) while there is a strong renormalization at small energies. The inset shows the difference of the renormalized interaction vertex $u_n(\infty)$ to the interaction vertex $u_{n_\mathrm{F}}(\infty)$ at the Fermi level $\varepsilon_\mathrm{F} = 0$ for $l \to \infty$ vs. the site n. At small energies, the local interaction vertices $u_n(l)$ exhibit the same flow.

As the results are inconclusive so far, we need a better criterion to decide if we have taken the important contributions into account in order to describe the strong-coupling physics. In the next sections we will apply a magnetic field h in order to calculate the impurity contribution to the magnetic susceptibility χ_d for small h.

6.6 Magnetization and Susceptibility

The calculation of the impurity contribution to the susceptibility χ_d is a good criterion to decide if we are able to describe the Kondo effect. On the one hand, we are able to calculate this quantity without an observable transformation while, on the other hand, we know precisely what to expect if we capture the low-energy physics correctly [50, 119].

The impurity contribution to the susceptibility χ_d is given by

$$\chi_\mathrm{d} = \frac{g_\mathrm{e}^2 \mu_\mathrm{B}^2}{4 T_\mathrm{K}} \tag{6.23}$$

for large enough values of $\frac{U}{\pi\Delta}$. We can calculate this quantity within our approach by applying a magnetic field h to the impurity in order to capture the impurity contribution alone. The

magnetic field h is incorporated into the Hamiltonian (6.2) through the substitution

$$\varepsilon_\mathrm{d} \quad \longleftrightarrow \quad \varepsilon_\mathrm{d} - \sigma h. \tag{6.24}$$

Note that the substitution will lead to bilinear terms in order h in the initial Hamiltonian, even for the particle-hole symmetric case $\varepsilon_\mathrm{d} = -\frac{U}{2}$, cf. Eq. (6.3). Thus, not only the spin symmetry is broken by applying a magnetic field but the particle-hole symmetry as well. We determine the susceptibility by starting from the Anderson model in the form

$$H(h) = H(h=0) - \sum_\sigma \sigma h n_{\mathrm{d},\sigma} \tag{6.25}$$

where the substitution (6.24) was used. Calculating the ground-state energy E_0 results in

$$E_0 = \langle \mathrm{gs}|H|\mathrm{gs}\rangle = \langle \mathrm{gs}| \left(H(h=0) - \sum_\sigma \sigma h n_{\mathrm{d},\sigma} \right) |\mathrm{gs}\rangle. \tag{6.26}$$

Taking the derivative with respect to the magnetic field yields

$$\frac{\mathrm{d}E_0}{\mathrm{d}h} = E_0 \frac{\mathrm{d}\langle \mathrm{gs}|\mathrm{gs}\rangle}{\mathrm{d}h} - \langle \mathrm{gs}|n_{\mathrm{d},\uparrow} - n_{\mathrm{d},\downarrow}|\mathrm{gs}\rangle. \tag{6.27}$$

The norm of the ground state is independent of the magnetic field as it is normalized to one. Using additionally the definition of the magnetization of the impurity

$$m(h) = \frac{g_\mathrm{e}\mu_\mathrm{B}}{2} \langle \mathrm{gs}|n_{\mathrm{d},\uparrow} - n_{\mathrm{d},\downarrow}|\mathrm{gs}\rangle \tag{6.28}$$

we find

$$m(h) = -\frac{g_\mathrm{e}\mu_\mathrm{B}}{2} \frac{\mathrm{d}E_0}{\mathrm{d}h}. \tag{6.29}$$

As the generator outlined in Sec. 6.4 fulfills gs-generator properties and we normal-order the operators with respect to the Fermi sea (chosen as the ground state of the Hamiltonian (6.2) for ε_d, U and $h = 0$), the Fermi sea becomes the ground state of the effective Hamiltonian. Additionally, all remaining operators yield zero acting on the Fermi sea and thus the constant E_0 must converge to the ground-state energy of the effective model.

We can find the susceptibility for $h = 0$ by differentiating Eq. (6.29)

$$\chi_\mathrm{d} = -\frac{g_\mathrm{e}^2\mu_\mathrm{B}^2}{4} \frac{\mathrm{d}^2E_0}{\mathrm{d}h^2}\bigg|_{h=0}. \tag{6.30}$$

Thus, we expect to find

$$-\frac{\mathrm{d}^2E_0}{\mathrm{d}h^2}\bigg|_{h=0} = \frac{1}{T_\mathrm{K}}. \tag{6.31}$$

The next sections present the results for the flow in the case of a finite magnetic field.

6.7 Numerical Results of the Flow in Finite Magnetic Field

6.7.1 Residual Off-Diagonality

When a magnetic field is applied, the starting values remain the same as in Eq. (6.3) but with the additional term

$$t^{\sigma}_{nm} = -\sigma h \gamma_n \gamma_m \tag{6.32}$$

which stems from the substitution (6.24). The term (6.32) explicitly breaks the spin symmetry as well as the particle-hole symmetry.

Fig. 6.4 depicts the residual off-diagonality for a finite magnetic field $\frac{h}{D} = 10^{-5}$.

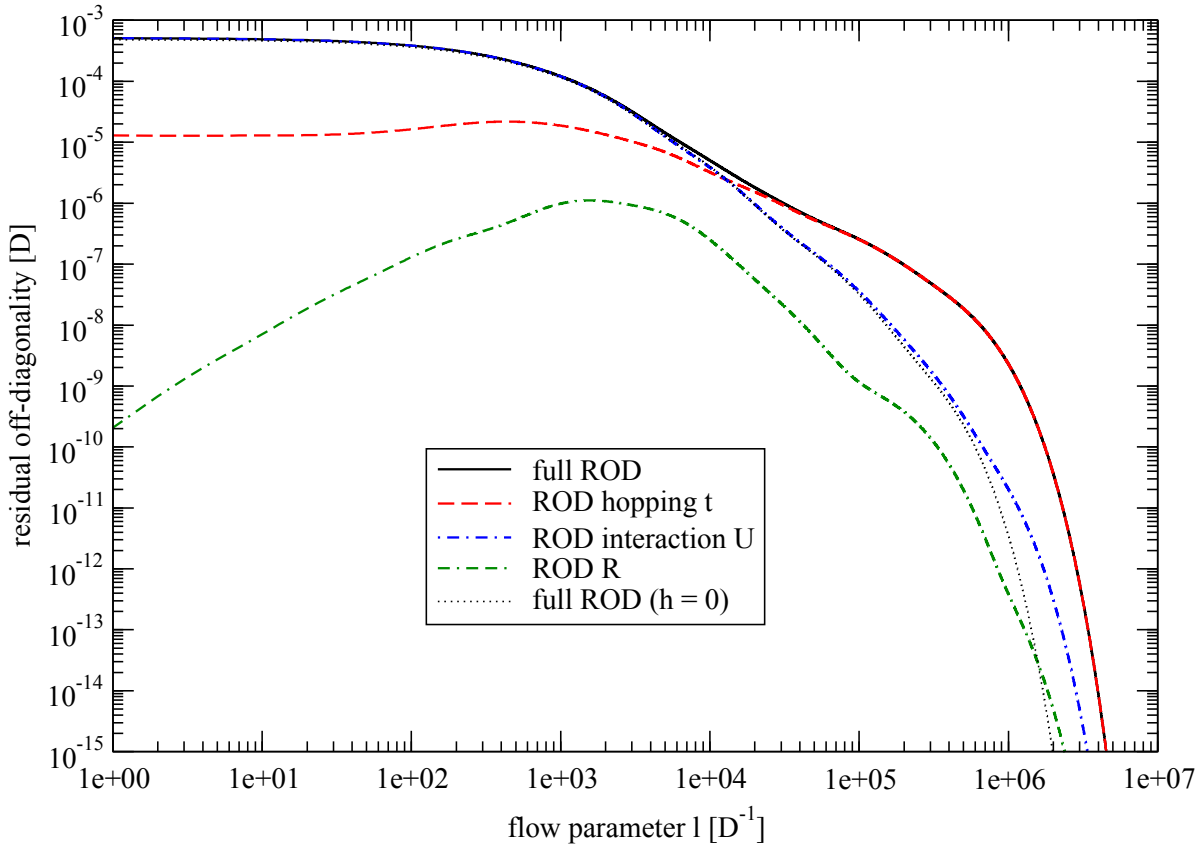

Figure 6.4: Residual off-diagonality for the Anderson model with $N = 16$, $\Lambda = 6$, $\frac{V}{D} = 0.01414$, $\frac{U}{D} = 10^{-3}$ and a magnetic field $\frac{h}{D} = 10^{-5}$. In contrast to Fig. 6.1 (where $h = 0$), the bilinear terms are non-zero for $l = 0$. In the early flow, the interaction terms $U_{n_1 n_2 n_3 n_4}$ dominate while the bilinear terms take over at larger l. The DEQ converges for finite magnetic fields and yields an effective model with the Fermi sea as the ground state.

In contrast to the residual off-diagonality for $h = 0$ (cf. Fig. 6.1), bilinear terms in order h are already present for $l = 0$ (cf. Eq. (6.3)). For $h = 0$, the interaction term dominates the residual off-diagonality throughout the whole flow while for $h \neq 0$ the hopping will become the most dominant part for large l. The differential equations (6.8*a*)-(6.8*d*), (6.11*a*), (6.11*b*), (6.12*a*) and (6.12*b*) still yield an effective model for $h > 0$.

6.7.2 Ground-State Energy and Susceptibility

For now we are interested in the constant E_0 which converges to the ground-state energy of the effective Hamiltonian.

Fig. 6.5 shows the flow of E_0 for different magnetic fields h. The influence of the magnetic field is very small so that we need to look at the inset of Fig. 6.5 in order to see its influence. As expected, the ground-state energy is reduced by the magnetic field h.

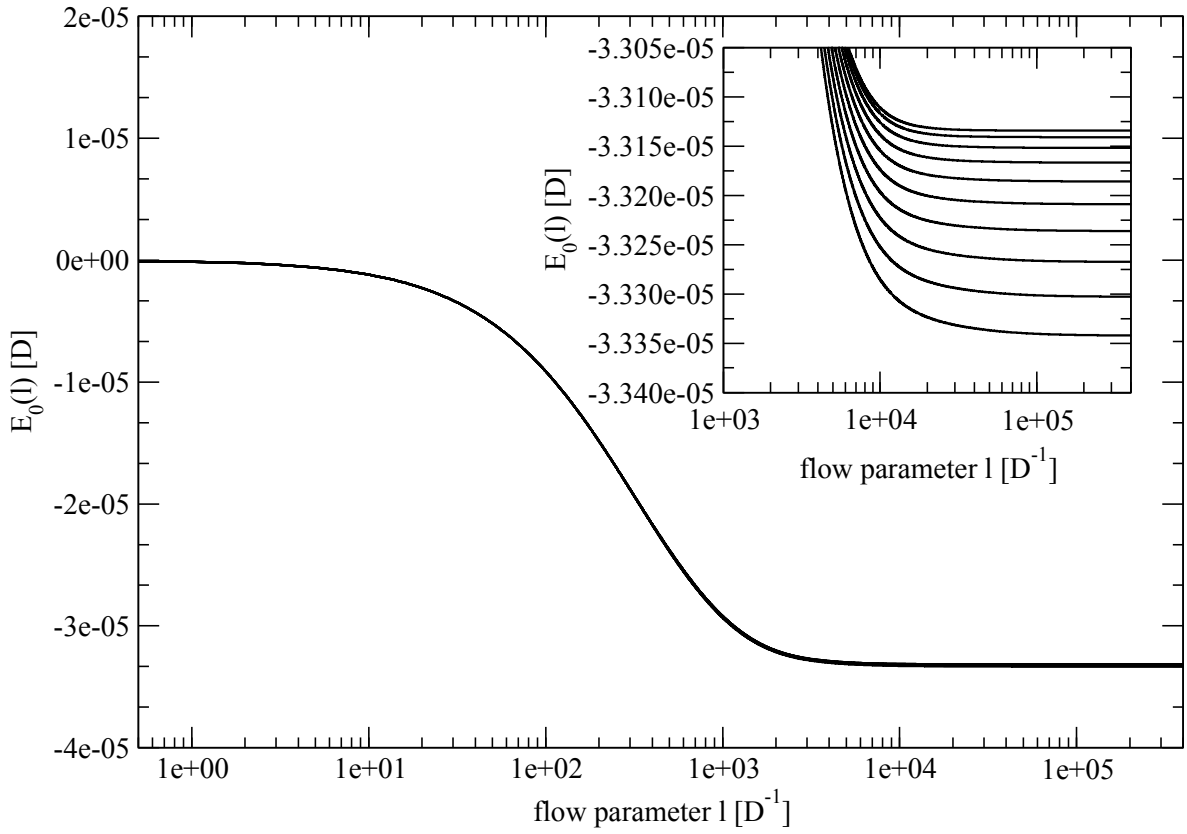

Figure 6.5: Flow of the constant E_0 from Eq. (6.2) for the Anderson model with $N = 16$, $\Lambda = 6$, $\frac{V}{D} = 0.01414$, $\frac{U}{D} = 10^{-3}$ and from top to bottom $10^6 \frac{h}{D} = 1, 2, ..., 9, 10$. The inset shows the flow for large l with a higher resolution in order to see the very small influence of the magnetic field. As we expect from second-order perturbation theory, the ground-state energy is reduced by the magnetic field.

The inset shows the numerical difference ratio of the effective model

$$\frac{\Delta E_0(h)}{\Delta h} = \frac{E_0(h+\Delta h) - E_0(h)}{\Delta h}. \tag{6.33}$$

If we assume the form

$$E_0(h) = \alpha + \beta h + \gamma h^2 \tag{6.34}$$

for the ground-state energy, we find for the numerical difference ratio (6.33)

$$\frac{\Delta E_0(h)}{\Delta h} = \beta + \gamma \Delta h + 2\gamma h \tag{6.35}$$

where the coefficients are given by

$$\alpha = E_0(h=0), \quad \beta = -\frac{2m(0)}{g_e \mu_B}, \quad \gamma = -\frac{4\chi_d}{g_e^2 \mu_B^2}. \tag{6.36}$$

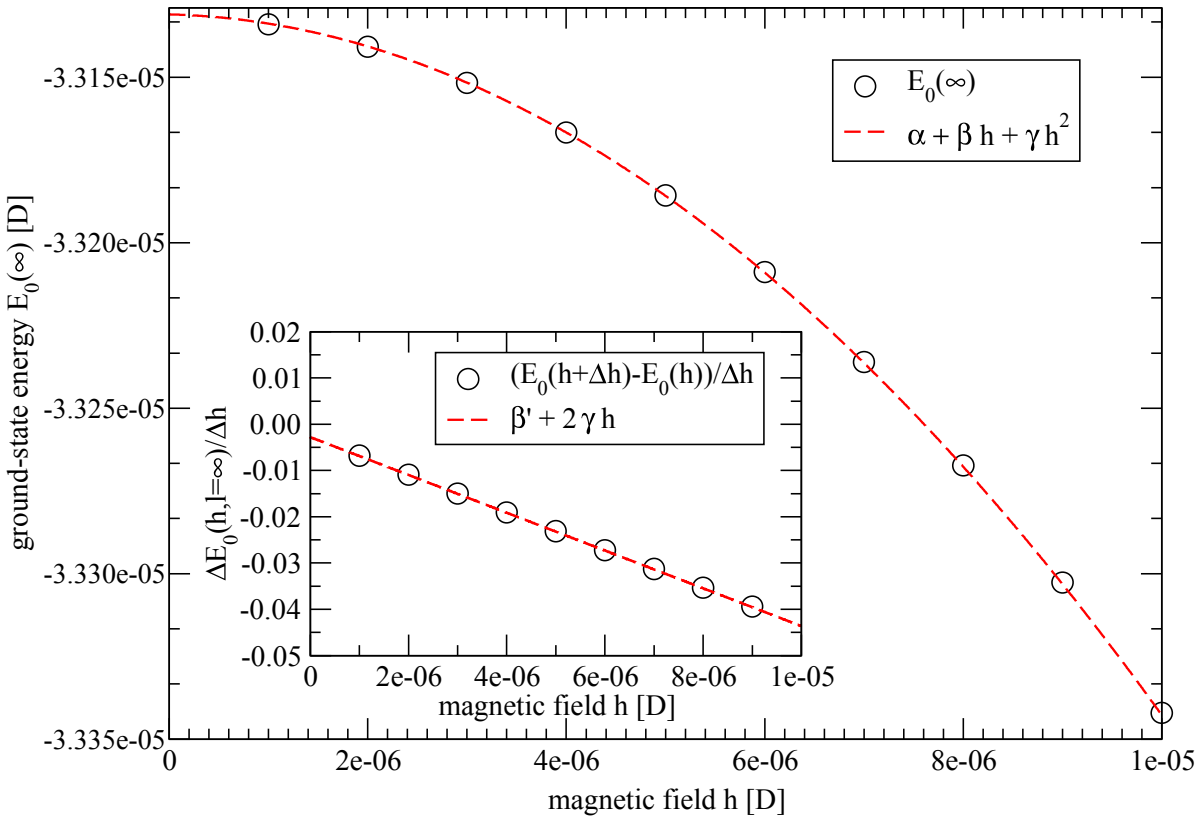

Figure 6.6: Ground-state energy $E_0(\infty)$ of the effective model for $l \to \infty$ for the Anderson model with $N = 16$, $\Lambda = 6$, $\frac{V}{D} = 0.01414$, $\frac{U}{D} = 10^{-3}$ and $\frac{\Delta h}{D} = 10^{-6}$. The ground-state energy is reduced with increasing magnetic field h. It is well approximated by $E_0(h) = \alpha + \beta h + \gamma h^2$ with $\beta \approx -0.0007585$ and $\gamma \approx -2042 D^{-1}$. The inset shows the difference ratio (6.33). We see that the approximation (6.34) is quite accurate for the chosen values of h and Δh. $\beta' = \beta + \gamma \Delta h \approx -0.0028$ is also in agreement with Eq. (6.37). Thus, we can indeed determine the susceptibility by Eq. (6.30) using the numerical results.

As long as Δh is small enough so that Eq. (6.34) is appropriate, we can derive the susceptibility from the slope of the numerical difference ratio (6.33) with respect to the magnetic field (cf. Fig. 6.6).

Fig. 6.6 depicts the ground-state energy E_0 in dependence of the magnetic field. A discretization error in order Δh influences the linear contribution β in Eq. (6.34) according to

$$\beta' = \beta + \gamma \Delta h \tag{6.37}$$

which, however, is not of interest when calculating the susceptibility χ_d as the susceptibility is only determined by the second-order contribution γ. Thus, Fig. 6.6 shows that Eq. (6.34) is a good approximation for the chosen values of h and Δh in order to calculate the susceptibility χ_d which can be determined by Eq. (6.30) as the slope of the difference ratio (6.33).

So far the numerical results show the expected behavior for the ground-state energy $E_0(\infty)$. Thus, we can study how far the strong-coupling physics of the Anderson model is captured by the differential equations (6.8*a*)-(6.8*d*), (6.11*a*), (6.11*b*), (6.12*a*) and (6.12*b*).

In Fig. 6.7 we calculate the ground-state energy for different values of h with $\frac{\Delta h}{D} = 10^{-6}$ and derive the susceptibility χ_d from Eq. (6.30) for various values of U and V.

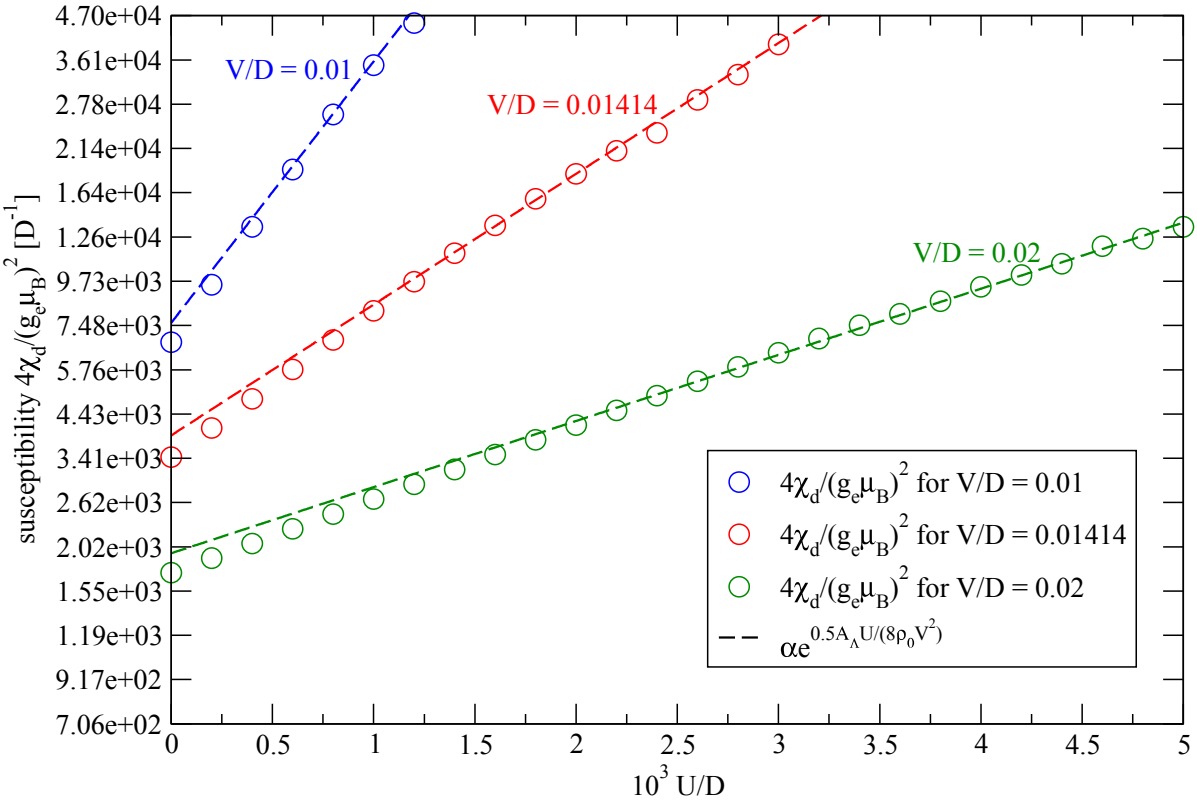

Figure 6.7: Logarithmic representation of the impurity contribution to the susceptibility χ_d derived from the second derivative of the ground-state energy $E_0(\infty)$ with respect to the magnetic field (6.30), numerically evaluated by the difference ratio (6.33) for finite $\frac{\Delta h}{D} = 10^{-6}$ for the Anderson model with $N = 16$, $\Lambda = 6$ and from top to bottom $\frac{V}{D} = 0.01$ (blue), 0.01414 (red) and 0.02 (green). There is a clear tendency towards an exponential increase of the susceptibility which is in agreement with the expected behavior (6.23). The exponential behavior is one of the benchmarks whether a method is able to capture the strong-coupling behavior. However, the exponent differs by a factor $\frac{1}{2}$ from the expected exponent while the factor A_Λ from Eq. (6.39) is an expected discretization effect.

We find an exponential increase for the curvature of the ground-state energy $E_0(\infty)$ with increasing U and thus an exponentially increasing susceptibility

$$\chi_d = \alpha e^{-\frac{1}{2} A_\Lambda \frac{U}{8\rho_0 V^2}} \tag{6.38}$$

which is in agreement with the expected qualitative behavior (6.23) but differs by a factor $\frac{1}{2}$ in the exponent. The factor

$$A_\Lambda = \frac{1}{2}\frac{\Lambda+1}{\Lambda-1}\ln\Lambda \tag{6.39}$$

included in Eq. (6.38) is an expected discretization effect [8].

In conclusion, we can state that it is a promising observation that the CUT approach is able to capture the exponential dependence on the interaction U as this is a good benchmark for the successful description of the strong-coupling behavior of the Anderson model. However, the exponent differs by a factor $\frac{1}{2}$ from the expected exponent and the results become worse for larger values of U.

Further investigations are required to identify the origin of the missing factor of two. An obvious possible source is the truncation scheme. By applying deepCUT we intended to use a systematic way of deciding which terms to neglect. But, of course, we still might miss some important contributions. We used various variations of the truncation scheme, e.g., either by completely neglecting the R-terms or by taking them fully into account. Such variations have only a minor influence on the susceptibility and do *not* affect the exponent. Including the Γ-terms with six operators is not realistic as the calculation effort is already very large when only including quartic terms.

It could also be necessary to modify the generator in order to eliminate more terms. To this end, one could study the sign-generator

$$s^U_{n_1 n_2 n_3 n_4} = \operatorname{sgn}\left(\varepsilon^{\uparrow}_{n_1} + \varepsilon^{\downarrow}_{n_2} - \varepsilon^{\downarrow}_{n_3} - \varepsilon^{\uparrow}_{n_4}\right). \tag{6.40}$$

Because of the huge calculation effort of this approach, we want to reduce the system of differential equations by introducing a scaling expansion which is presented in the next sections.

6.8 Scaling Approach to the Flow Equation

In the previous sections we were able to derive an exponential increase with respect to the interaction U for the susceptibility χ_{d} over some parameter regime. Therefore, it is interesting to investigate the differential equations (6.8*a*)-(6.8*d*), (6.11*a*), (6.11*b*), (6.12*a*) and (6.12*b*) further. In the present section we do not justify the truncation scheme in orders of a small parameter, which so far was U, but use scaling arguments instead.

The scaling approach results in a small system of differential equations which can be solved easily. The aim of the following sections is to introduce a new kind of systematic expansion in the scaling parameter λ and examine if this generates an appropriate approximation scheme.

All calculations in this chapter, the numerical treatment of the last sections as well as the scaling approach of the following sections, are new and have not been reported so far.

6.8.1 Scaling Dimension

We introduce a new quantity, the so-called scaling dimension d, by studying a simple example of a diagonal Hamiltonian

$$H_{\mathrm{D}} = \sum_{\sigma} \int_{-D}^{D} x : c^{\dagger}_{x\sigma} c_{x\sigma} : \mathrm{d}x. \tag{6.41}$$

In the spirit of the scaling approach from Chap. 3, we focus on smaller energy scales and look at a model with a reduced bandwidth

$$H^{\lambda}_{\mathrm{D}} = \sum_{\sigma} \int_{-\lambda D}^{\lambda D} x : c^{\dagger}_{x\sigma} c_{x\sigma} : \mathrm{d}x \tag{6.42}$$

with $\lambda \in [0,1]$. We can now rescale the Hamiltonian with the substitution $u = \frac{x}{\lambda}$ in Eq. (6.42) which leads to

$$\tilde{H}^{\lambda}_{\mathrm{D}} = \sum_{\sigma} \int_{-D}^{D} u : \tilde{c}^{\dagger}_{u\sigma} \tilde{c}_{u\sigma} : \mathrm{d}u \tag{6.43}$$

with

$$\tilde{H}_{\mathrm{D}}^{\lambda} = \frac{H_{\mathrm{D}}^{\lambda}}{\lambda}, \quad \tilde{c}_{u\sigma}^{\dagger} = \sqrt{\lambda} c_{\lambda u\sigma}^{\dagger}. \tag{6.44}$$

The new operators $\tilde{c}_{x\sigma}^{\dagger}$ fulfill standard fermionic anticommutator relations. We also rescale the Hamiltonian so that the diagonal part has scaling dimension zero

$$\tilde{H}_{\mathrm{D}}^{\lambda} = \lambda^0 \tilde{H}_{\mathrm{D}}. \tag{6.45}$$

$\tilde{H}_{\mathrm{D}}$ denotes a Hamiltonian of the form (6.41) but with the rescaled operators (6.44). Next, we analyze the scaling dimension of an operator of the general structure

$$H_{2N} = \sum_{\{\sigma_i\}} \int ... \int_{-D}^{D} \left[\prod_{i=1}^{2N} \rho\left(x_i\right) \right]^{\frac{1}{2}} \Gamma_{\vec{\sigma}}\left(x_1, ..., x_{2N}\right) : \prod_{i=1}^{N} c_{x_i\sigma_i}^{\dagger} \prod_{i=N+1}^{2N} c_{x_i\sigma_i} : \mathrm{d}x_1 ... \mathrm{d}x_{2N}. \tag{6.46}$$

Following the scaling steps (6.41) - (6.43) leads to

$$\tilde{H}_{2N}^{\lambda} = \lambda^{N-1} \sum_{\{\sigma_i\}} \int ... \int_{-D}^{D} \left[\prod_{i=1}^{2N} \rho\left(\lambda u_i\right) \right]^{\frac{1}{2}} \Gamma_{\vec{\sigma}}\left(\lambda \vec{u}\right) : \prod_{i=1}^{N} \tilde{c}_{u_i\sigma_i}^{\dagger} \prod_{i=N+1}^{2N} \tilde{c}_{u_i\sigma_i} : \mathrm{d}u_1 ... \mathrm{d}u_{2N} \tag{6.47}$$

from which we can see that an operator of the form (6.46) has scaling dimension $d = N - 1$ as

$$\tilde{H}_{2N}^{\lambda} = \lambda^{N-1} \tilde{H}_{2N} \tag{6.48}$$

when focusing only on the leading order of the coefficients in Eq. (6.47)

$$\Gamma_{\vec{\sigma}}\left(x_1, ..., x_{2N}\right) \quad \leftrightarrow \quad \Gamma_{\vec{\sigma}}\left(\varepsilon_{\mathrm{F}}, ..., \varepsilon_{\mathrm{F}}\right) = \tilde{\Gamma}_{\vec{\sigma}}. \tag{6.49}$$

Thus, the major finding is that the more operators a term contains, the faster it scales to zero and the less important it is for the low-energy physics.

In order to account for the λ-dependence of the coefficients, we use a Taylor expansion. The only contribution of the expansion that does not increase the scaling dimension is the leading order. From the result (6.48) we find the scaling dimensions for bilinear and quartic terms

$$\tilde{H}_2^{\lambda} = \lambda^0 \tilde{H}_2, \quad \tilde{H}_4^{\lambda} = \lambda^1 \tilde{H}_4. \tag{6.50}$$

The diagonal part from Eq. (6.45) has scaling dimension $d = 0$ by definition. The bilinear terms with constant Γ also have scaling dimension $d = 0$ while quartic terms scale with $d = 1$.

6.8.2 IR-Approximation and Scaling Expansion

The argument used in Eq. (6.49) gives a systematic justification for the approximation in the "poor man's scaling" from Sec. 3.2 and for the IR-approximation of the Continuous Unitary Transformation approach from Sec. 4.6, respectively.

The argument for the "poor man's scaling" approach is straightforward. The interaction term in the Kondo model is bilinear with respect to the bath operators and has thus the same scaling dimension as the diagonal part when focusing on the leading order of

$$J^{\mu}\left(x_1, x_2\right) \quad \leftrightarrow \quad J^{\mu}\left(\varepsilon_{\mathrm{F}}, \varepsilon_{\mathrm{F}}\right) = \tilde{J}^{\mu}. \tag{6.51}$$

This is precisely what is done in the "poor man's scaling" approach.

In order to understand the IR-approximation in the light of a scaling perspective, we first have to investigate generic terms stemming from Continuous Unitary Transformations

$$J^{\mu}\left(x_1,x_2\right)=\tilde{J}^{\mu}\left(x_1,x_2\right)\mathrm{e}^{-|x_1-x_2|l}. \tag{6.52}$$

When we scale the energies $x_i \to \lambda x_i$, we find

$$J^{\mu}\left(\lambda x_1,\lambda x_2\right)=\tilde{J}^{\mu}\left(\lambda x_1,\lambda x_2\right)\mathrm{e}^{-|x_1-x_2|\lambda l}. \tag{6.53}$$

We can absorb the factor λ in the exponent into the flow parameter

$$l'=\lambda l \tag{6.54}$$

which is convenient as we scale all energies with a factor λ. In this case, the exponential factor does not affect the scaling dimension and we can use

$$J^{\mu}\left(x_1,x_2\right)=\tilde{J}^{\mu}\left(\varepsilon_{\mathrm{F}},\varepsilon_{\mathrm{F}}\right)\mathrm{e}^{-|x_1-x_2|l}. \tag{6.55}$$

This is precisely the IR-approximation from Eq. (4.93).

In the next sections we set up a scaling expansion in order to justify a reduced closed system of differential equations.

6.8.3 Expansion in the Scaling Parameter λ

We want to expand the coefficients so that we can truncate in orders of λ. We will study the flow equation in first order so that we only need to track the first-order expansion of the coefficients

$$\Gamma\left(\vec{x}\right)=\Gamma\left(\vec{\varepsilon}_{\mathrm{F}}\right)+\vec{\nabla}\Gamma\left(\vec{\varepsilon}_{\mathrm{F}}\right)\cdot\left(\vec{x}-\vec{\varepsilon}_{\mathrm{F}}\right) \tag{6.56}$$

as all higher terms scale at least in second order in λ. The vector $\vec{\varepsilon}_{\mathrm{F}}$ denotes the vector where all entries correspond to the Fermi energy $\varepsilon_{\mathrm{F}}=0$. The operator structure so far is

$$H=H_{\mathrm{D}}+H_{\mathrm{t}}+H_{\mathrm{U}}+H_{\mathrm{R}}+H_{\Gamma} \tag{6.57}$$

with the contributions

$$\begin{aligned}
H_{\mathrm{D}} &= \sum_{\sigma}\int_{-D}^{D}\varepsilon:c^{\dagger}_{\varepsilon\sigma}c_{\varepsilon\sigma}:\mathrm{d}\varepsilon && (6.58)\\
H_{\mathrm{t}} &= \sum_{\sigma}\int\int_{-D}^{D}\left[\prod_{i=1}^{2}\rho\left(\varepsilon_i\right)\right]^{\frac{1}{2}}t_{\sigma}\left(\vec{\varepsilon}\right):c^{\dagger}_{\varepsilon_1\sigma}c_{\varepsilon_2\sigma}:\mathrm{d}\varepsilon_1\mathrm{d}\varepsilon_2\\
H_{\mathrm{U}} &= \int\int\int\int_{-D}^{D}\left[\prod_{i=1}^{4}\rho\left(\varepsilon_i\right)\right]^{\frac{1}{2}}U\left(\vec{\varepsilon}\right):c^{\dagger}_{\varepsilon_1\uparrow}c^{\dagger}_{\varepsilon_2\downarrow}c_{\varepsilon_3\downarrow}c_{\varepsilon_4\uparrow}:\mathrm{d}\varepsilon_1\mathrm{d}\varepsilon_2\mathrm{d}\varepsilon_3\mathrm{d}\varepsilon_4\\
H_{\mathrm{R}} &= \sum_{\sigma}\int\int\int\int_{-D}^{D}\left[\prod_{i=1}^{4}\rho\left(\varepsilon_i\right)\right]^{\frac{1}{2}}R_{\sigma}\left(\vec{\varepsilon}\right):c^{\dagger}_{\varepsilon_1\sigma}c^{\dagger}_{\varepsilon_2\sigma}c_{\varepsilon_3\sigma}c_{\varepsilon_4\sigma}:\mathrm{d}\varepsilon_1\mathrm{d}\varepsilon_2\mathrm{d}\varepsilon_3\mathrm{d}\varepsilon_4\\
H_{\Gamma} &= \sum_{\sigma}\int\ldots\int_{-D}^{D}\left[\prod_{i=1}^{6}\rho\left(\varepsilon_i\right)\right]^{\frac{1}{2}}\Gamma_{\sigma}\left(\vec{\varepsilon}\right):c^{\dagger}_{\varepsilon_1\sigma}c^{\dagger}_{\varepsilon_2\bar{\sigma}}c^{\dagger}_{\varepsilon_3\bar{\sigma}}c_{\varepsilon_4\bar{\sigma}}c_{\varepsilon_5\bar{\sigma}}c_{\varepsilon_6\sigma}:\mathrm{d}\varepsilon_1\ldots\mathrm{d}\varepsilon_6.
\end{aligned}$$

In addition to these terms, only terms with at least six operators occur which have a scaling dimension higher than one so that we do not need to discuss them. Applying the scaling steps (6.41) - (6.43) leads to the scaling dimensions for the terms from Eq. (6.58)

$$\begin{aligned}
\tilde{H}_{\mathrm{D}}^{\lambda} &= \lambda^0 \sum_{\sigma} \int_{-D}^{D} \varepsilon : \tilde{c}_{\varepsilon\sigma}^{\dagger} \tilde{c}_{\varepsilon\sigma} : \mathrm{d}\varepsilon \qquad (6.59)\\
\tilde{H}_{\mathrm{t}}^{\lambda} &= \lambda^0 \sum_{\sigma} \int \int_{-D}^{D} \left[\prod_{i=1}^{2} \rho\left(\lambda\varepsilon_i\right) \right]^{\frac{1}{2}} t_{\sigma}\left(\lambda\vec{\varepsilon}\right) : \tilde{c}_{\varepsilon_1\sigma}^{\dagger} \tilde{c}_{\varepsilon_2\sigma} : \mathrm{d}\varepsilon_1 \mathrm{d}\varepsilon_2 \\
\tilde{H}_{\mathrm{U}}^{\lambda} &= \lambda^1 \int \int \int \int_{-D}^{D} \left[\prod_{i=1}^{4} \rho\left(\lambda\varepsilon_i\right) \right]^{\frac{1}{2}} U\left(\lambda\vec{\varepsilon}\right) : \tilde{c}_{\varepsilon_1\uparrow}^{\dagger} \tilde{c}_{\varepsilon_2\downarrow}^{\dagger} \tilde{c}_{\varepsilon_3\downarrow} \tilde{c}_{\varepsilon_4\uparrow} : \mathrm{d}\varepsilon_1 \mathrm{d}\varepsilon_2 \mathrm{d}\varepsilon_3 \mathrm{d}\varepsilon_4 \\
\tilde{H}_{\mathrm{R}}^{\lambda} &= \lambda^1 \sum_{\sigma} \int \int \int \int_{-D}^{D} \left[\prod_{i=1}^{4} \rho\left(\lambda\varepsilon_i\right) \right]^{\frac{1}{2}} R_{\sigma}\left(\lambda\vec{\varepsilon}\right) : \tilde{c}_{\varepsilon_1\sigma}^{\dagger} \tilde{c}_{\varepsilon_2\sigma}^{\dagger} \tilde{c}_{\varepsilon_3\sigma} \tilde{c}_{\varepsilon_4\sigma} : \mathrm{d}\varepsilon_1 \mathrm{d}\varepsilon_2 \mathrm{d}\varepsilon_3 \mathrm{d}\varepsilon_4 \\
\tilde{H}_{\Gamma}^{\lambda} &= \lambda^2 \sum_{\sigma} \int \ldots \int_{-D}^{D} \left[\prod_{i=1}^{6} \rho\left(\lambda\varepsilon_i\right) \right]^{\frac{1}{2}} \Gamma_{\sigma}\left(\lambda\vec{\varepsilon}\right) : \tilde{c}_{\varepsilon_1\sigma}^{\dagger} \tilde{c}_{\varepsilon_2\bar{\sigma}}^{\dagger} \tilde{c}_{\varepsilon_3\bar{\sigma}}^{\dagger} \tilde{c}_{\varepsilon_4\bar{\sigma}} \tilde{c}_{\varepsilon_5\bar{\sigma}} \tilde{c}_{\varepsilon_6\sigma} : \mathrm{d}\varepsilon_1 \ldots \mathrm{d}\varepsilon_6.
\end{aligned}$$

We see that we can neglect H_{Γ} and all contributions of the coefficients beyond the leading order for H_{U} and H_{R} while we need additionally the linear order of the coefficients of the bilinear Hamiltonian when we focus on orders up to λ.

The major difference to the truncation scheme from the last sections is that we will expand the coefficients and thus reduce the huge system of coupled differential equations to only a few coefficients while we will neglect further contributions of the right-hand side of the DEQ which scale faster to zero than the linear order in λ. In order to find these terms, we have to analyze the flow equation itself from a scaling perspective as explained in the next section.

6.8.4 Scaling Approximation to the Flow Equation

We explain how we analyze the flow equation by discussing the procedure explicitly for the DEQ (6.8*b*) and (6.8*c*), respectively.

We focus on the part which stems from the commutation of the bilinear terms (which is already the full DEQ for $U = 0$)

$$\partial_l t_{n_1 n_2}^{\sigma} = -\left|\varepsilon_{n_1} - \varepsilon_{n_2}\right| t_{n_1 n_2}^{\sigma} + \sum_{x_1 \neq n_1, n_2} \left(s_{n_1 x_1}^{\sigma} - s_{x_1 n_2}^{\sigma} \right) t_{n_1 x_1}^{\sigma} t_{x_1 n_2}^{\sigma} \qquad (6.60)$$

where we separated the part on the right-hand side that is linear in $t_{n_1 n_2}^{\sigma}$. First, we introduce the continuum limit

$$\begin{aligned}
\sum_{\substack{n_1, n_2, \sigma \\ n_1 \neq n_2}} t_{n_1 n_2}^{\sigma} : c_{n_1\sigma}^{\dagger} c_{n_2\sigma} : &= \sum_{\substack{n_1, n_2, \sigma \\ n_1 \neq n_2}} \frac{t_{n_1 n_2}^{\sigma}}{\gamma_{n_1}\gamma_{n_2}} : \frac{c_{n_1\sigma}^{\dagger}}{\gamma_{n_1}} \frac{c_{n_2\sigma}}{\gamma_{n_2}} : \gamma_{n_1}^2 \gamma_{n_2}^2 \qquad (6.61)\\
&\to \sum_{\sigma} \int \int_{-D}^{D} \sqrt{\rho\left(\varepsilon\right)\rho\left(\varepsilon'\right)}\, t_{\sigma}\left(\varepsilon, \varepsilon'\right) : c_{\varepsilon\sigma}^{\dagger} c_{\varepsilon'\sigma} : \mathrm{d}\varepsilon \mathrm{d}\varepsilon'
\end{aligned}$$

where we used

$$\varepsilon_n \to \varepsilon\,, \quad \gamma_n^2 \to \rho(\varepsilon)\,\mathrm{d}\varepsilon\,, \quad \frac{t^{\sigma}_{n_1 n_2}}{\gamma_{n_1}\gamma_{n_2}} \to t_\sigma(\varepsilon_1,\varepsilon_2)\,, \quad \frac{1}{\gamma_{n_1}} c^\dagger_{n_1\sigma} \to \frac{1}{\sqrt{\rho(\varepsilon)}} c^\dagger_{\varepsilon\sigma}. \tag{6.62}$$

The new operators $c^\dagger_{\varepsilon\sigma}$ fulfill anticommutation relations in the continuum while the factors $\rho(\varepsilon)^{-\frac{1}{2}}$ cancel with the density of states $\rho(\varepsilon)$ to the generic factor $\sqrt{\rho(\varepsilon)}$ of each integral[7] in the continuum limit (cf. Eq. (2.42)). The continuum limit (6.62) for the DEQ (6.60) results in

$$\begin{aligned} \partial_l t_\sigma(\varepsilon,\varepsilon') &= -\left|\varepsilon-\varepsilon'\right| t_\sigma(\varepsilon,\varepsilon') \\ &+ \int_{-D}^{D} \rho(z)\left[\operatorname{sgn}(\varepsilon-z)-\operatorname{sgn}(z-\varepsilon')\right] t_\sigma(\varepsilon,z)\, t_\sigma(z,\varepsilon')\,\mathrm{d}z. \end{aligned} \tag{6.63}$$

Scaling all energies with a factor λ (including the flow parameter $l' = \lambda l$) and substituting $u = \frac{z}{\lambda}$ yields

$$\begin{aligned} &\partial_{l'} t_\sigma(\lambda\varepsilon,\lambda\varepsilon')\,\frac{\partial l'}{\partial l} = -\lambda\left|\varepsilon-\varepsilon'\right| t_\sigma(\lambda\varepsilon,\lambda\varepsilon') \\ &+ \lambda\int_{-\infty}^{\infty} \rho(\lambda u)\left[\operatorname{sgn}(\lambda\varepsilon-\lambda u)-\operatorname{sgn}(\lambda u-\lambda\varepsilon')\right] t_\sigma(\lambda\varepsilon,\lambda u)\, t_\sigma(\lambda u,\lambda\varepsilon')\,\mathrm{d}u. \end{aligned} \tag{6.64}$$

The boundaries of the integrals are set to infinity because for finite l the coefficients $t_\sigma(\varepsilon,\varepsilon')$ are exponentially suppressed (cf. Eq. (6.67)) and thus the contributions beyond the bandwidth D are negligible.

We see that the scaling dimension is reduced by one due to the scaling of the flow parameter as

$$\frac{\partial l'}{\partial l} = \lambda. \tag{6.65}$$

This observation leads to

$$\begin{aligned} &\partial_{l'} t_\sigma(\lambda\varepsilon,\lambda\varepsilon') = -\lambda^0\left|\varepsilon-\varepsilon'\right| t_\sigma(\lambda\varepsilon,\lambda\varepsilon') \\ &+ \lambda^0\int_{-\infty}^{\infty} \rho(\lambda u)\left[\operatorname{sgn}(\lambda\varepsilon-\lambda u)-\operatorname{sgn}(\lambda u-\lambda\varepsilon')\right] t_\sigma(\lambda\varepsilon,\lambda u)\, t_\sigma(\lambda u,\lambda\varepsilon')\,\mathrm{d}u. \end{aligned} \tag{6.66}$$

Thus, if we want to expand in linear order in λ, we have to expand the coefficients t_σ in linear order as well. To this end, we introduce

$$t_\sigma(\varepsilon,\varepsilon') = \tilde{t}_\sigma(\varepsilon,\varepsilon')\,\mathrm{e}^{-|\varepsilon-\varepsilon'|l} \tag{6.67}$$

in order to account for the linear term in Eq. (6.63) and focus on small energies close to the Fermi level

$$|\delta\varepsilon| = |\varepsilon-\varepsilon_\mathrm{F}| \ll D \tag{6.68}$$

which yields

$$\partial_l \tilde{t}_\sigma(\delta\varepsilon,\delta\varepsilon') = -2\int_{-\infty}^{\infty} \rho(z)\operatorname{sgn}(z)\,\tilde{t}_\sigma(\delta\varepsilon,z)\,\tilde{t}_\sigma(z,\delta\varepsilon')\,\mathrm{e}^{-2|z|l}\mathrm{d}z. \tag{6.69}$$

[7] A quartic term in the continuum limit, for instance, is of the form
$\int\int\int\int_{-D}^{D} \sqrt{\prod_{i=1}^4 \rho(\varepsilon_i)}\, U(\varepsilon_1,\varepsilon_2,\varepsilon_3,\varepsilon_4) : c^\dagger_{\varepsilon_1\uparrow} c^\dagger_{\varepsilon_2\downarrow} c_{\varepsilon_3\downarrow} c_{\varepsilon_4\uparrow} : \mathrm{d}\varepsilon_1\mathrm{d}\varepsilon_2\mathrm{d}\varepsilon_3\mathrm{d}\varepsilon_4$.

Next, we expand the coefficient in linear order

$$\tilde{t}_\sigma\left(\varepsilon,\varepsilon'\right)=\tilde{t}_\sigma+\alpha_\sigma\left(\varepsilon+\varepsilon'\right). \tag{6.70}$$

The expansion takes the form (6.70) as the coefficients must fulfill $\tilde{t}_\sigma(\varepsilon,\varepsilon')=\tilde{t}_\sigma(\varepsilon',\varepsilon)$ due to hermiticity. From Eqs. (6.70) and (6.69) we obtain

$$\begin{aligned}\partial_l\left[\tilde{t}_\sigma+\alpha_\sigma\left(\delta\varepsilon+\delta\varepsilon'\right)\right]= &-2\int_{-\infty}^{\infty}\rho(z)\,\mathrm{sgn}(z)\,\mathrm{e}^{-2|z|l}\mathrm{d}z\,\tilde{t}_\sigma^2\\ &-4\int_{-\infty}^{\infty}\rho(z)\,\mathrm{sgn}(z)\,z\,\mathrm{e}^{-2|z|l}\mathrm{d}z\,\tilde{t}_\sigma\alpha_\sigma\\ &-2\int_{-\infty}^{\infty}\rho(z)\,\mathrm{sgn}(z)\,\mathrm{e}^{-2|z|l}\mathrm{d}z\,\tilde{t}_\sigma\alpha_\sigma\left(\delta\varepsilon+\delta\varepsilon'\right)\end{aligned} \tag{6.71}$$

where we dismissed all quadratic terms in $\delta\varepsilon$ and z. Comparing the coefficients in Eq. (6.71) results in the DEQs for the expansion coefficients from Eq. (6.70)

$$\begin{aligned}\partial_l\tilde{t}_\sigma &= -2\int_{-\infty}^{\infty}\rho(z)\,\mathrm{sgn}(z)\,\mathrm{e}^{-2|z|l}\mathrm{d}z\,\tilde{t}_\sigma^2-4\int_{-\infty}^{\infty}\rho(z)\,|z|\,\mathrm{e}^{-2|z|l}\mathrm{d}z\,\tilde{t}_\sigma\alpha_\sigma\\ \partial_l\alpha_\sigma &= -2\int_{-\infty}^{\infty}\rho(z)\,\mathrm{sgn}(z)\,\mathrm{e}^{-2|z|l}\mathrm{d}z\,\tilde{t}_\sigma\alpha_\sigma.\end{aligned} \tag{6.72}$$

The starting values for the differential equation are given by

$$\tilde{t}_\sigma=-\sigma h,\quad \alpha_\sigma=0. \tag{6.73}$$

If we examine Eq. (6.72) and bear in mind that $\alpha_\sigma(l=0)=0$, we find

$$\alpha_\sigma=0\ \ \forall\ l. \tag{6.74}$$

6.8.5 First-Order Expansion for the Non-Interacting Model

In the last section we already derived the full flow equation (6.72) for $U=0$ in a first-order scaling expansion. We now want to examine if we can obtain reasonable results from this expansion.

Introducing a continuum limit (6.62) in the differential equation (6.8*a*) - (6.8*c*) for $U=0$ yields

$$\begin{aligned}\partial_l E_0 &= \sum_\sigma\int\int_{-D}^{D}\mathrm{sgn}(z_1-z_2)\left[\theta(-z_1)-\theta(-z_2)\right]\rho(z_1)\,\rho(z_2)\,\mathrm{e}^{-2|z_1-z_2|l}\mathrm{d}z_1\mathrm{d}z_2\,\tilde{t}_\sigma^2\\ \partial_l\tilde{t}_\sigma &= -2\int_{-D}^{D}\rho(z)\,\mathrm{sgn}(z)\,\mathrm{e}^{-2|z|l}\mathrm{d}z\,\tilde{t}_\sigma^2-4\int_{-D}^{D}\rho(z)\,|z|\,\mathrm{e}^{-2|z|l}\mathrm{d}z\,\tilde{t}_\sigma\alpha_\sigma\\ \partial_l\alpha_\sigma &= -2\int_{-D}^{D}\rho(z)\,\mathrm{sgn}(z)\,\mathrm{e}^{-2|z|l}\mathrm{d}z\,\tilde{t}_\sigma\alpha_\sigma\end{aligned} \tag{6.75}$$

with the starting values

$$\tilde{t}_\sigma=-\sigma h,\quad \alpha_\sigma=0,\quad E_0=0. \tag{6.76}$$

Using $\rho(z) = \rho(-z)$ and the substitution $z \leftrightarrow -z$ results in

$$\begin{aligned} \partial_l E_0 &= -2\sum_\sigma \int_0^D \int_0^D \rho(z_1)\rho(z_2) \mathrm{e}^{-2(z_1+z_2)l} \mathrm{d}z_1 \mathrm{d}z_2 \tilde{t}_\sigma^2 \\ \partial_l \tilde{t}_\sigma &= 0 \\ \partial_l \alpha_\sigma &= 0 \end{aligned} \tag{6.77}$$

where we used Eq. (6.74) which holds true because of the starting values (6.76). The remaining integral in the derivative of $\tilde{t}_\sigma$ in Eq. (6.75) yields zero and thus $\tilde{t}_\sigma$ is not renormalized during the flow. We replace $\tilde{t}_\sigma$ by its starting value (6.76) in the differential equation for E_0 from Eq. (6.77). If we additionally use the Lorentzian density of states (2.60), we find

$$\partial_l E_0 = -\frac{2}{\pi^2} h^2 \sum_\sigma \int_0^{\frac{D}{\Delta}} \int_0^{\frac{D}{\Delta}} \frac{\mathrm{e}^{-2(u_1+u_2)\Delta \cdot l}}{\left(1+u_1^2\right)\left(1+u_2^2\right)} \mathrm{d}u_1 \mathrm{d}u_2 \tag{6.78}$$

where we substituted $u_i = \frac{z_i}{\Delta}$. As the bandwidth D is the largest energy scale in the system and

$$\Delta = \frac{\pi V^2}{2D} \tag{6.79}$$

is very small, we can set the upper boundary of the integrals to infinity. Additionally, we integrate E_0 and send $l \to \infty$

$$E_0(\infty) = -\frac{2h^2}{\pi^2 \Delta} \int_0^\infty \int_0^\infty \frac{1}{(u_1+u_2)\left(1+u_1^2\right)\left(1+u_2^2\right)} \mathrm{d}u_1 \mathrm{d}u_2. \tag{6.80}$$

The only approximation so far is to set the boundaries of the integral to infinity which is well-justified. The integral can be calculated analytically

$$\int_0^\infty \int_0^\infty \frac{1}{(u_1+u_2)\left(1+u_1^2\right)\left(1+u_2^2\right)} \mathrm{d}u_1 \mathrm{d}u_2 = \frac{\pi}{2} \tag{6.81}$$

which leads to a simple expression for the ground-state energy

$$E_0(\infty, h) = -\frac{h^2}{\pi\Delta}. \tag{6.82}$$

This, of course, is not the correct formula for the ground-state energy as it would lead to a linear dependence of the magnetization. However, we do not expect to find the full magnetization from our approach because we only focused on small energies. We calculate the susceptibility from Eq. (6.30) as the second derivative of the ground-state energy (6.82) and find

$$\chi_\mathrm{d} = \frac{g_\mathrm{e}^2 \mu_\mathrm{B}^2}{2\pi\Delta} \tag{6.83}$$

which is in perfect agreement with the analytical formula for $U = 0$ [1].

This is an important result as we can obtain it from an analytic calculation with a systematic truncation criterion in orders of the scaling parameter λ. In the next section we analyze if we are able to capture interaction effects on the susceptibility χ_d when including the interaction U.

6.8.6 First-Order Expansion for the Interacting Model

In this section we analyze the differential equations (6.8*a*)-(6.8*d*), (6.11*a*), (6.11*b*), (6.12*a*) and (6.12*b*) from a scaling perspective in linear order including the interaction U.

We use the continuum limit (cf. Eq. (6.62)) and the procedure outlined in Sec. 6.8.4. Thus, we rescale $x_i \leftrightarrow \lambda x_i$ and $l' = \lambda l$ and analyze the DEQ using the expansion (6.56). We can immediately identify terms that can be neglected. Each integral contributes $+1$ (cf. Eq. (6.47)) to the scaling dimension and the rescaling of the flow parameter reduces it by one (cf. Eq. (6.64)). Thus, the lowest scaling dimension of a contribution on the right-hand side of the DEQ is

$$d_{\min} = N - 1 \tag{6.84}$$

where N denotes the number of integrals. When we focus on terms up to linear order, we can dismiss all contributions that have three integrals or more because such contributions scale at least in order λ^2. We can additionally dismiss further contributions as we already know that we need U- and R-terms only in zeroth order because their leading order already scales linearly due to the quartic bath operator structure. Hence, for these terms we can additionally dismiss all terms with at least two integrals (cf. Eq. (6.84)). This renders R-terms negligible in linear order as they emerge due to terms including two integrals (cf. Eq. (6.11*a*)). U-terms, on the other hand, will affect the results and must be taken into consideration. The difference between the R- and U-terms (and with it their asymmetric treatment) stems from the fact that U-terms are already present in the initial Hamiltonian while R-terms have to emerge first.

We expand the coefficients

$$\tilde{t}_\sigma\left(\varepsilon,\varepsilon'\right) = \tilde{t}_\sigma + \alpha_\sigma\left(\varepsilon+\varepsilon'\right), \quad \tilde{U}\left(\varepsilon_1,\varepsilon_2,\varepsilon_3,\varepsilon_4\right) = \tilde{U} \tag{6.85}$$

with

$$\begin{aligned} t_\sigma\left(\varepsilon,\varepsilon'\right) &= \tilde{t}_\sigma\left(\varepsilon,\varepsilon'\right)\mathrm{e}^{-|\varepsilon-\varepsilon'|l} \\ U\left(\varepsilon_1,\varepsilon_2,\varepsilon_3,\varepsilon_4\right) &= \tilde{U}\left(\varepsilon_1,\varepsilon_2,\varepsilon_3,\varepsilon_4\right)\mathrm{e}^{-|\varepsilon_1+\varepsilon_2-\varepsilon_3-\varepsilon_4|l}. \end{aligned} \tag{6.86}$$

We use the sign-function

$$s^U\left(\varepsilon_1,\varepsilon_2,\varepsilon_3,\varepsilon_4\right) = \mathrm{sgn}\left(\varepsilon_1+\varepsilon_2-\varepsilon_3-\varepsilon_4\right) \tag{6.87}$$

for the generator and analyze the flow equations (6.8*a*)-(6.8*d*) in a first-order scaling expansion as outlined in Sec. 6.8.4 which yields after a comparison of the coefficients

$$\begin{aligned} \partial_l E_0 &= \sum_\sigma \int\int_{-D}^{D} \mathrm{sgn}\left(z_1-z_2\right)\left[\theta\left(-z_1\right)-\theta\left(-z_2\right)\right]\rho\left(z_1\right)\rho\left(z_2\right)\mathrm{e}^{-2|z_1-z_2|l}\mathrm{d}z_1\mathrm{d}z_2\,\tilde{t}_\sigma^2 \\ \partial_l \tilde{t}_\sigma &= 2\int\int_{-D}^{D} \rho\left(z_1\right)\rho\left(z_2\right)\mathrm{sgn}\left(z_1-z_2\right)\left[\theta\left(-z_1\right)-\theta\left(-z_2\right)\right]\mathrm{e}^{-2|z_1-z_2|l}\mathrm{d}z_1\mathrm{d}z_2\,\tilde{t}_{\bar{\sigma}}\tilde{U} \\ &\quad - 2\int_{-D}^{D}\rho\left(z\right)\mathrm{sgn}\left(z\right)\mathrm{e}^{-2|z|l}\mathrm{d}z\,\tilde{t}_\sigma^2 - 4\int_{-D}^{D}\rho\left(z\right)|z|\,\mathrm{e}^{-2|z|l}\mathrm{d}z\,\tilde{t}_\sigma\alpha_\sigma \\ \partial_l \alpha_\sigma &= -2\int_{-D}^{D}\rho\left(z\right)\mathrm{sgn}\left(z\right)\mathrm{e}^{-2|z|l}\mathrm{d}z\,\tilde{t}_\sigma\alpha_\sigma \\ \partial_l \tilde{U} &= -4\sum_\sigma\int_{-D}^{D}\rho\left(z\right)\mathrm{sgn}\left(z\right)\mathrm{e}^{-2|z|l}\mathrm{d}z\,\tilde{t}_\sigma\tilde{U}. \end{aligned} \tag{6.88}$$

The DEQ (6.88) can be simplified using $\rho(z) = \rho(-z)$ and substituting $z \leftrightarrow -z$

$$\begin{aligned}
\partial_l E_0 &= -2\sum_\sigma \int_0^D \int_0^D \rho(z_1)\,\rho(z_2)\,\mathrm{e}^{-2(z_1+z_2)l}\mathrm{d}z_1\mathrm{d}z_2\,\tilde{t}_\sigma^2 \\
\partial_l \tilde{t}_\sigma &= -4\int_0^D \int_0^D \rho(z_1)\,\rho(z_2)\,\mathrm{e}^{-2(z_1+z_2)l}\mathrm{d}z_1\mathrm{d}z_2\,\tilde{t}_{\bar{\sigma}}\tilde{U} \\
\partial_l \alpha_\sigma &= 0 \\
\partial_l \tilde{U} &= 0.
\end{aligned} \tag{6.89}$$

The flow of α_σ is zero because $\alpha_\sigma(0) = 0$ which results in

$$\alpha_\sigma(l) = 0 \quad \forall\ l. \tag{6.90}$$

Additionally, as the derivative of $\tilde{U}$ is zero, we can simply replace it by its starting value

$$\tilde{U}(l) = U \tag{6.91}$$

and use the symmetry

$$\tilde{t}_{\bar{\sigma}} = -\tilde{t}_\sigma \tag{6.92}$$

which holds true during the whole flow. The differential equation for the renormalized coupling $\tilde{t}_\sigma$ then becomes

$$\partial_l \tilde{t}_\sigma = 4U\int_0^D \int_0^D \rho(z_1)\,\rho(z_2)\,\mathrm{e}^{-2(z_1+z_2)l}\mathrm{d}z_1\mathrm{d}z_2\,\tilde{t}_\sigma. \tag{6.93}$$

Using the Lorentzian density of states (2.52) and substituting $u = \frac{z}{\Delta}$ while using the limit $\frac{D}{\Delta} \to \infty$ for the upper boundaries of the integral (cf. Sec. 6.8.5) and integrating $\tilde{t}_\sigma$ yields

$$\ln\left(\frac{\tilde{t}_\sigma}{\tilde{t}_\sigma^{(0)}}\right) = \frac{2U}{\pi^2\Delta}\int_0^\infty \int_0^\infty \frac{1-\mathrm{e}^{-2(u_1+u_2)\Delta\cdot l}}{(u_1+u_2)\left(1+u_1^2\right)\left(1+u_2^2\right)}\mathrm{d}u_1\mathrm{d}u_2. \tag{6.94}$$

For $l \to \infty$, we find the renormalized coupling

$$\tilde{t}_\sigma = -\sigma h\mathrm{e}^{\frac{U}{\pi\Delta}} \tag{6.95}$$

where the integral was calculated using Eq. (6.81). We again used no approximation apart from $\frac{D}{\Delta} \to \infty$ for the integral boundaries.

Now we want to calculate the ground-state energy $E_0(\infty)$. If we take a closer look at Eq. (6.89), we find

$$\partial_l E_0 = -\frac{1}{2U}\sum_\sigma \tilde{t}_\sigma \partial_l \tilde{t}_\sigma \tag{6.96}$$

which can be written in the form

$$\partial_l E_0 = -\frac{1}{4U}\sum_\sigma \partial_l \tilde{t}_\sigma^2. \tag{6.97}$$

Integrating Eq. (6.97) yields

$$E_0(\infty) - E_0(0) = -\frac{1}{4U} \sum_\sigma \left(\tilde{t}_\sigma^2(\infty) - \tilde{t}_\sigma^2(0) \right). \tag{6.98}$$

Using the starting values (6.76) and the final result for $\tilde{t}_\sigma$ from Eq. (6.95), we find

$$E_0(\infty, h) = \frac{h^2}{2U} \left(1 - \mathrm{e}^{\frac{2U}{\pi\Delta}} \right). \tag{6.99}$$

The susceptibility is calculated from Eq. (6.30) as

$$\chi_\mathrm{d} = \frac{g_\mathrm{e}^2 \mu_\mathrm{B}^2}{4U} \left(\mathrm{e}^{\frac{16}{\pi^2} \frac{U}{8\rho_0 V^2}} - 1 \right). \tag{6.100}$$

For $U \to 0$, we find

$$\lim_{U \to 0} \chi_\mathrm{d} = \frac{g_\mathrm{e}^2 \mu_\mathrm{B}^2}{2\pi\Delta} \tag{6.101}$$

which is in agreement with Eq. (6.83). For large enough values of $\frac{U}{\pi\Delta}$, we find an exponential increase of the susceptibility in the interaction U. This is in accordance with the correct result. The exponent, however, does not perfectly agree with the correct exponent $\frac{U}{8\rho_0 V^2}$. Our result differs by a factor $\frac{16}{\pi^2} \approx 1.62$ from the correct exponent.

In summary, we can state that the scaling expansion yields the correct result for χ_d in the non-interacting case which is not trivial as we use a scaling approximation, i.e., we only focus on low energies. Additionally, we are able to capture the exponential strong-coupling behavior of the susceptibility while the exponent differs by a factor of $\frac{16}{\pi^2} \approx 1.62$ but depends on the correct ratio $\frac{U}{\pi\Delta}$. The coefficient $C(U,V)$ of the Kondo temperature

$$T_\mathrm{K} \propto C(U,V)\, \mathrm{e}^{-\frac{U}{8\rho_0 V^2}} \tag{6.102}$$

is not in perfect agreement with the correct result which is $C(U,V) = C = \text{const.}$ in leading order in J and given by

$$C(U,V) \propto \sqrt{4\rho_0 V^2 U} \tag{6.103}$$

when including the first-order corrections in J (cf. App. 9.3). In contrast, we find a coefficient $C(U,V) \propto U$. Nevertheless, the scaling expansion is able to derive the exponential dependence of the susceptibility analytically by a systematic approach which does not rely on any a priori knowledge.

Further investigations are required in order to understand the origin of the factor $\frac{16}{\pi^2}$ in the exponent. Investigating higher order expansions in λ might improve the result.

However, it might be more interesting to better understand the flow for $h = 0$ and to include the renormalization of $\tilde{U}$ induced by the commutation of U-terms with themselves which is neglected in the approach so far. This renormalization might influence the exponent and thus might improve the results.

7 Truncation in Orders of the Hybridization Element V

7.1 Parametrization and Local Operator Basis

In this chapter we deal with a third parametrization of the Anderson model. We use the discretization with respect to the flat DOS (2.51) and choose the ground state of

$$H_{\mathrm{D}} = \sum_{n,\sigma} \varepsilon_n c^\dagger_{n\sigma} c_{n\sigma} + \varepsilon_{\mathrm{d}} \sum_{\sigma} n_{\mathrm{d},\sigma} + U n_{\mathrm{d},\uparrow} n_{\mathrm{d},\downarrow} \tag{7.1}$$

as the reference state where $n_{\mathrm{d},\sigma}$ is the particle-counting operator

$$n_{\mathrm{d},\sigma} = d^\dagger_\sigma d_\sigma. \tag{7.2}$$

The singly occupied impurity state is the lowest-lying eigenstate of the Hamiltonian (7.1) and thus the reference state is degenerate with a spin degree of freedom on the impurity. Because of this spin degree of freedom, we have to use a reference ensemble for the impurity operators and thus the normal-ordering scheme is defined as

$$\langle\uparrow|:\hat{A}:|\uparrow\rangle + \langle\downarrow|:\hat{A}:|\downarrow\rangle = 0. \tag{7.3}$$

An operator basis which is normal-ordered with respect to the reference ensemble (7.3) has already been applied successfully, e.g., to the Hubbard model [81, 103]. The chosen operator basis is shown in Tab. 7.1.

bosonic operators	fermionic operators
$\mathbb{1}$	$F_{1,\uparrow} = \left(1 - n_{\mathrm{d},\downarrow}\right) d_\uparrow$
$n_z = n_{\mathrm{d},\uparrow} - n_{\mathrm{d},\downarrow}$	$F_{1,\downarrow} = \left(1 - n_{\mathrm{d},\uparrow}\right) d_\downarrow$
$d^\dagger_\uparrow d_\downarrow$	$F_{2,\uparrow} = n_{\mathrm{d},\downarrow} d_\uparrow$
$d^\dagger_\downarrow d_\uparrow$	$F_{2,\downarrow} = n_{\mathrm{d},\uparrow} d_\downarrow$
$d_\downarrow d_\uparrow$	$F^\dagger_{2,\uparrow} = n_{\mathrm{d},\downarrow} d^\dagger_\uparrow$
$d^\dagger_\uparrow d^\dagger_\downarrow$	$F^\dagger_{2,\downarrow} = n_{\mathrm{d},\uparrow} d^\dagger_\downarrow$
$\bar{n} = n_{\mathrm{d},\uparrow} + n_{\mathrm{d},\downarrow} - \mathbb{1}$	$F^\dagger_{1,\uparrow} = \left(1 - n_{\mathrm{d},\downarrow}\right) d^\dagger_\uparrow$
$\hat{D} = 2 n_{\mathrm{d},\uparrow} n_{\mathrm{d},\downarrow} - \bar{n}$	$F^\dagger_{1,\downarrow} = \left(1 - n_{\mathrm{d},\uparrow}\right) d^\dagger_\downarrow$

Table 7.1: Impurity operator basis with $n_{\mathrm{d},\sigma} = d^\dagger_\sigma d_\sigma$.

The reason for this choice of the fermionic operators becomes evident upon inspecting the local impurity configurations which are connected by these operators. As the energy difference between the empty and the singly occupied state is different from the singly to the doubly occupied state, we have no unique energy change which we can attribute to the operator $d^\dagger_\sigma$.

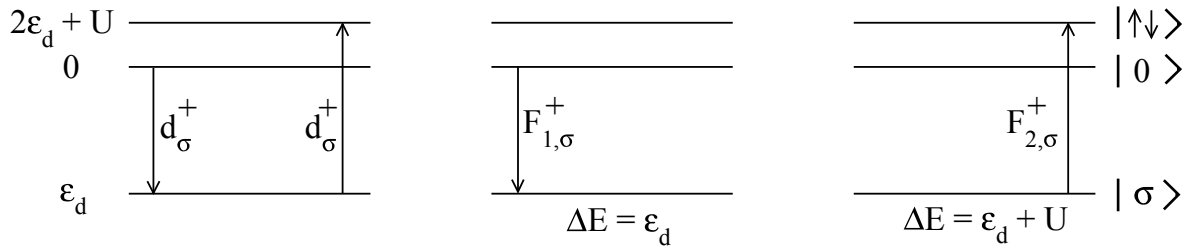

Figure 7.1: Impurity configurations connected by the superposed operators $F^\dagger_{1,\sigma}$ and $F^\dagger_{2,\sigma}$. In contrast to the operator $d^\dagger_\sigma$, the operators $F^\dagger_{1,\sigma}$ and $F^\dagger_{2,\sigma}$ can be attributed to a unique energy change.

The $d^\dagger_\sigma$-operator connects the empty to the singly occupied state and the singly occupied to the doubly occupied state. The superposed operator $F^\dagger_{1,\sigma} = (1-n_{\bar\sigma})\,d^\dagger_\sigma$ only connects the empty with the singly occupied state while the superposed operator $F^\dagger_{2,\sigma} = n_{\bar\sigma} d^\dagger_\sigma$ only connects the singly occupied with the doubly occupied state. Thus, we can attribute a unique energy difference to both superposed operators which are given by

$$\begin{aligned} \Delta E_1 &= \varepsilon_\mathrm{d} = \tilde\varepsilon_\mathrm{d} - \tilde U \\ \Delta E_2 &= \varepsilon_\mathrm{d} + U = \tilde\varepsilon_\mathrm{d} + \tilde U \end{aligned} \tag{7.4}$$

where the coefficients $\tilde U$ and $\tilde\varepsilon_\mathrm{d}$ are the coefficients of the Anderson Hamiltonian (2.51) expressed in the new operator basis from Tab. 7.1

$$H = H_\mathrm{D} + H_\mathrm{R} \tag{7.5}$$

with the diagonal Hamiltonian H_D and the hybridization part H_R

$$\begin{aligned} H_\mathrm{D} &= \sum_{n,\sigma} \varepsilon_n : c^\dagger_{n\sigma} c_{n\sigma} : + \tilde\varepsilon_\mathrm{d}\,\bar n + \tilde U \hat D \\ H_\mathrm{R} &= \sum_{n,\sigma} V_n \left(F^\dagger_{1,\sigma} c_{n\sigma} + c^\dagger_{n\sigma} F_{1,\sigma} \right) + \sum_{n,\sigma} \Gamma_n \left(F^\dagger_{2,\sigma} c_{n\sigma} + c^\dagger_{n\sigma} F_{2,\sigma} \right). \end{aligned} \tag{7.6}$$

The coefficients in the new operator basis are given by

$$V_n = V\gamma_n\,, \quad \Gamma_n = V\gamma_n\,, \quad \tilde\varepsilon_\mathrm{d} = \varepsilon_\mathrm{d} + \frac{U}{2}\,, \quad \tilde U = \frac{U}{2} \tag{7.7}$$

with the parameters ε_n and γ_n from Eq. (2.50). The bath operators are still normal-ordered with respect to the Fermi sea. If the reader is interested in performing own calculations, App. 9.9 provides useful local commutators and products for this operator basis.

7.2 The Schrieffer-Wolff Transformation Revisited

In order to become familiar with the new operator basis and the basic differential equations of this approach, we will start by reproducing the Schrieffer-Wolff transformation (cf. Sec. 2.4) with different generators.

This has already been accomplished in a slightly different approach [22] using a very specific generator only constructed for this problem which is similar to the original generator of the Schrieffer-Wolff transformation (2.26).

The procedure outlined in this section is reminiscent of the Fröhlich transformation [120] which reveals an attractive interaction between two electrons induced by an electron-phonon interaction. The Fröhlich transformation is a one-step transformation which can also be constructed from Continuous Unitary Transformations [73, 74] with a less singular result. Reproducing the Schrieffer-Wolff transformation with Continuous Unitary Transformations also results in a less singular spin-spin exchange interaction than from the one-step transformation itself. We want to study the influence of the choice of the generator on the effective spin-spin exchange interaction J_{nm} and we will simplify the transformation using deepCUT ideas so that we are able to calculate the resulting J_{nm} analytically in a simpler manner than it is done in the original work [22]. From the approach in Ref. [22] one finds for the effective spin-spin exchange coupling

$$J_{nm} = V_n V_m U \frac{(\varepsilon_\mathrm{d} - \varepsilon_n)(\varepsilon_\mathrm{d} - \varepsilon_n + U) + (\varepsilon_\mathrm{d} - \varepsilon_m)(\varepsilon_\mathrm{d} - \varepsilon_m + U)}{(\varepsilon_\mathrm{d} - \varepsilon_n)^2 (\varepsilon_\mathrm{d} - \varepsilon_n + U)^2 + (\varepsilon_\mathrm{d} - \varepsilon_m)^2 (\varepsilon_\mathrm{d} - \varepsilon_m + U)^2}. \tag{7.8}$$

The parameters ε_d and U in Eq. (7.8) differ from the initial parameters as their flow is also taken into account. Nevertheless, one can use the initial parameters (7.7) in order to compare them to the results obtained with our approach.

In principle, one can argue from deepCUT ideas (cf. the argument that leads from Eq. (7.14) to Eq. (7.18)) that the flow of the parameters ε_n, ε_d and U can and even should be neglected when targeting the lowest order of the spin-spin interaction. In this case, the initial parameters should indeed be used in this formula. Otherwise, the final result for the coupling $J_{n_\mathrm{F} n_\mathrm{F}}$ at the Fermi level $\varepsilon_{n_\mathrm{F}}$ differs in order V^4 from the result obtained by the one-step Schrieffer-Wolff transformation.

Using the symmetric Anderson model $\varepsilon_\mathrm{d} = -\frac{U}{2}$ and focusing on the couplings $J_{n n_\mathrm{F}}$ – where n_F denotes the index corresponding to the Fermi level $\varepsilon_{n_\mathrm{F}} = 0$ – and further using $V_n = V\gamma_n$, one finds

$$\frac{J_{n n_\mathrm{F}}}{\gamma_n \gamma_{n_\mathrm{F}}} = V^2 U \frac{\varepsilon_n^2 - \frac{U^2}{2}}{\left(\varepsilon_n^2 - \frac{U^2}{4}\right)^2 + \frac{U^4}{16}}. \tag{7.9}$$

In contrast to the result from the one-step Schrieffer-Wolff transformation (2.34), one can see that the coupling exhibits no divergences. Nevertheless, one should mention that there are still divergences in some couplings on the U-energy scale, e.g., in the diagonal couplings J_{nn} for an index n which corresponds to an energy $\varepsilon_n = \frac{U}{2}$. The most interesting coupling is the one at the Fermi level

$$\frac{J_{n_\mathrm{F} n_\mathrm{F}}}{\gamma_{n_\mathrm{F}}^2} = -\frac{4V^2}{U} \tag{7.10}$$

which coincides with the result from the Schrieffer-Wolff transformation (2.36). It should be mentioned that the original paper [22] stays in k-space and uses the operator basis from Eq. (2.14) instead of the one from Tab. 7.1. Here the results from Ref. [22] are presented in a slightly different manner in order to reach a better comparability to results obtained with our approach.

In the next section we will revisit the Schrieffer-Wolff transformation for different generators in order to further pursue our goal of finding an adequate description for the Kondo regime within the CUT approach.

7.2.1 Flow Equation

We want to eliminate the hybridization elements and analyze the thereby induced spin-spin interaction and thus we choose the generator

$$\eta = \sum_{n,\sigma} \eta_n^V \left(F_{1,\sigma}^\dagger c_{n\sigma} - c_{n\sigma}^\dagger F_{1,\sigma} \right) + \sum_{n,\sigma} \eta_n^\Gamma \left(F_{2,\sigma}^\dagger c_{n\sigma} - c_{n\sigma}^\dagger F_{2,\sigma} \right) + \sum_{n,m,\sigma} \eta_{nm}^t : c_{n\sigma}^\dagger c_{m\sigma} : . \quad (7.11)$$

In order to find the flow equation (4.4), we have to commute the generator (7.11) and the Hamiltonian (7.5). By calculating the commutators we find that new terms emerge during the flow which are of the form

$$\begin{aligned} H_\mathrm{t} &= \sum_{n,m,\sigma} t_{nm} : c_{n\sigma}^\dagger c_{m\sigma} : \quad (7.12) \\ H_\mathrm{J} &= \sum_{n,m,\sigma} J_{nm}^{\uparrow\downarrow} d_\sigma^\dagger d_{\bar\sigma} c_{n\bar\sigma}^\dagger c_{m\sigma} + \sum_{n,m,\sigma} J_{nm,\sigma}^{n_z} n_z : c_{n\sigma}^\dagger c_{m\sigma} : \\ &+ \sum_{n,m,\sigma} J_{nm}^{\bar n} \bar n : c_{n\sigma}^\dagger c_{m\sigma} : + \sum_{n,m} J_{nm}^{\pm} \left(d_\uparrow^\dagger d_\downarrow^\dagger c_{n\downarrow} c_{m\uparrow} + c_{m\uparrow}^\dagger c_{n\downarrow}^\dagger d_\downarrow d_\uparrow \right). \end{aligned}$$

All newly emerging terms are of order V^2 and coincide with the newly emerging terms in the Schrieffer-Wolff transformation (2.30) which contain the effective spin-spin interaction, albeit with a different sign. Through the additional sign a positive coupling corresponds to an antiferromagnetic coupling.

We target the couplings $J_{nm}^{(i)}$ from Eq. (7.12) in order V^2. To this end, we have to calculate the commutators

$$[\eta_\mathrm{R}, H_\mathrm{D} + H_\mathrm{R}] \quad \text{and} \quad [\eta_\mathrm{t}, H_\mathrm{D}] \quad (7.13)$$

as all other commutations are of order V^3 or higher.

By comparing the commutators from Eq. (7.13) to the derivatives of the Hamiltonians (7.5) and (7.12) we deduce the flow equation (4.4) for the parameters

$$\begin{aligned} \partial_l E_0 &= \sum_{n,\sigma} \left((1-\theta_n)\, \eta_n^V V_n - \theta_n \eta_n^\Gamma \Gamma_n \right) \quad (7.14) \\ \partial_l \varepsilon_\mathrm{d} &= \sum_{n,\sigma} \left(\eta_n^V V_n \theta_n + (1-\theta_n)\, \eta_n^\Gamma \Gamma_n \right) \\ \partial_l U &= \sum_{n,\sigma} \left(\eta_n^\Gamma \Gamma_n - \eta_n^V V_n \right) \\ \partial_l V_n &= \eta_n^V \left(\varepsilon_n - \tilde\varepsilon_\mathrm{d} + \tilde U \right) \\ \partial_l \Gamma_n &= \eta_n^\Gamma \left(\varepsilon_n - \tilde\varepsilon_\mathrm{d} - \tilde U \right) \\ \partial_l t_{nm} &= \eta_{nm}^t (\varepsilon_m - \varepsilon_n) - \frac{1}{2} \left(\eta_n^V V_m + \eta_m^V V_n + \eta_n^\Gamma \Gamma_m + \eta_m^\Gamma \Gamma_n \right) \\ \partial_l J_{nm}^{\bar n} &= \frac{1}{2} \left(\eta_n^V V_m + \eta_m^V V_n - \eta_n^\Gamma \Gamma_m - \eta_m^\Gamma \Gamma_n \right) \\ \partial_l J_{nm,\sigma}^{n_z} &= \frac{1}{2} \sigma \left(\eta_n^\Gamma \Gamma_m + \eta_m^\Gamma \Gamma_n - \eta_n^V V_m - \eta_m^V V_n \right) \end{aligned}$$

$$\begin{aligned}\partial_l J^{\uparrow\downarrow}_{nm} &= \eta^\Gamma_n \Gamma_m + \eta^\Gamma_m \Gamma_n - \eta^V_n V_m - \eta^V_m V_n \\ \partial_l J^{\pm}_{nm} &= \eta^\Gamma_n V_m + \eta^\Gamma_m V_n - \eta^V_n \Gamma_m - \eta^V_m \Gamma_n\end{aligned}$$

where θ_n is the occupation number with respect to the Fermi sea

$$\theta_n = \langle c^\dagger_{n\sigma} c_{n\sigma} \rangle \tag{7.15}$$

which stems from the normal-ordering of the bath electrons. The coefficients $J^{n_z}_{nm,\sigma}$ and $J^{\uparrow\downarrow}_{nm}$ fulfill the spin-rotation symmetry

$$\sigma J^{n_z}_{nm,\sigma} = \frac{1}{2} J^{\uparrow\downarrow}_{nm} \tag{7.16}$$

and $J^{\bar{n}}_{nm}$ can be deduced from $J^{n_z}_{nm,\sigma}$ as long as no further terms are added to the generator

$$\sigma J^{n_z}_{nm,\sigma} = -\frac{1}{2} J^{\bar{n}}_{nm}. \tag{7.17}$$

The symmetries (7.16) and (7.17) are conserved during the whole flow as one can see from the flow equation (7.14). The coefficients V_n and Γ_n coincide for $l = 0$ but as soon as l increases they deviate from each other. This is why we introduced them as two independent parameters. The coefficients in the generator (7.11) are still arbitrary.

We want to analyze the influence of two standard generators, namely Wegner's and the sign-generator (cf. Sec. 4.2), which have not been used so far in order to reproduce the Schrieffer-Wolff transformation. However, before we choose special generators we want to simplify the DEQ (7.14) using deepCUT ideas from Sec. 4.3.4. We target H_J from Eq. (7.12) in order V^2 and neglect all terms which act in order V^3 on H_J. In this case, we can neglect the flow of H_D and the newly emerging hopping terms t_{nm} as their corrections to H_J are of order V^3. The differential equation simplifies to

$$\begin{aligned}\partial_l V_n &= \eta^V_n \left(\varepsilon_n - \tilde{\varepsilon}_\mathrm{d} + \tilde{U}\right) \\ \partial_l \Gamma_n &= \eta^\Gamma_n \left(\varepsilon_n - \tilde{\varepsilon}_\mathrm{d} - \tilde{U}\right) \\ \partial_l J^{\uparrow\downarrow}_{nm} &= \eta^\Gamma_n \Gamma_m + \eta^\Gamma_m \Gamma_n - \eta^V_n V_m - \eta^V_m V_n \\ \partial_l J^{\pm}_{nm} &= \eta^\Gamma_n V_m + \eta^\Gamma_m V_n - \eta^V_n \Gamma_m - \eta^V_m \Gamma_n\end{aligned} \tag{7.18}$$

where we only need to calculate $J^{\uparrow\downarrow}_{nm}$ because of the symmetries (7.16) and (7.17). At first sight, this approximation might seem a bit crude and perhaps one wants to analyze the full differential equation (7.14) in order to obtain the full Hamiltonian in order V^2. However, it is an experience from deepCUT calculations that the minimal system of differential equations, which is correct up to a given order for a targeted quantity, yields the best results [110, 111]. Furthermore, the DEQ (7.18) is still correct up to order V^2 for the targeted quantity H_J. The simplification (7.18) renders it much easier to calculate the coupling $J^{\uparrow\downarrow}_{nm}$ and also leads to a coupling at the Fermi level which is in perfect agreement with the result from the Schrieffer-Wolff transformation.

7.2.2 Generators

Wegner's generator (cf. Sec. 4.2.1) is given by

$$\begin{aligned}\eta_{\text{Wegner}} &= [H_{\text{D}}, H_{\text{R}}] \\ &= \sum_{n,\sigma} \left[-\left(\varepsilon_n - \tilde{\varepsilon}_{\text{d}} + \tilde{U}\right) V_n\right] \left(F^{\dagger}_{1,\sigma} c_{n\sigma} - c^{\dagger}_{n\sigma} F_{1,\sigma}\right) \\ &+ \sum_{n,\sigma} \left[-\left(\varepsilon_n - \tilde{\varepsilon}_{\text{d}} - \tilde{U}\right) \Gamma_n\right] \left(F^{\dagger}_{2,\sigma} c_{n\sigma} - c^{\dagger}_{n\sigma} F_{2,\sigma}\right)\end{aligned} \tag{7.19}$$

while the sign-generator (cf. Eq. (7.22) and Sec. 4.2.3) uses the sign of the energy difference between the states that are connected by the operator. The operator $F^{\dagger}_{1,\sigma}$ connects the empty impurity state to the singly occupied one (cf. Eq. (7.4)) while annihilating a particle with energy ε_n in the bath (cf. Eq. (7.6)) which leads to an energy difference

$$\Delta E_{1,n} = \tilde{\varepsilon}_{\text{d}} - \tilde{U} - \varepsilon_n. \tag{7.20}$$

The operator $F^{\dagger}_{2,\sigma}$ connects the singly occupied to the doubly occupied impurity level (cf. Eq. (7.4)) and annihilates a particle with energy ε_n in the bath which leads to an energy difference

$$\Delta E_{2,n} = \tilde{\varepsilon}_{\text{d}} + \tilde{U} - \varepsilon_n. \tag{7.21}$$

Thus, the sign-generator is of the form

$$\begin{aligned}\eta_{\text{sign}} &= \sum_{n,\sigma} \left[-\text{sgn}\left(\varepsilon_n - \tilde{\varepsilon}_{\text{d}} + \tilde{U}\right) V_n\right] \left(F^{\dagger}_{1,\sigma} c_{n\sigma} - c^{\dagger}_{n\sigma} F_{1,\sigma}\right) \\ &+ \sum_{n,\sigma} \left[-\text{sgn}\left(\varepsilon_n - \tilde{\varepsilon}_{\text{d}} - \tilde{U}\right) \Gamma_n\right] \left(F^{\dagger}_{2,\sigma} c_{n\sigma} - c^{\dagger}_{n\sigma} F_{2,\sigma}\right).\end{aligned} \tag{7.22}$$

Since both generators have a very similar structure, it is useful to define the generator in the form

$$\eta^V_n = -f^+_n V_n\,, \quad \eta^{\Gamma}_n = -f^-_n \Gamma_n \tag{7.23}$$

with

$$f^{\pm}_n = \begin{cases} \varepsilon_n - \tilde{\varepsilon}_{\text{d}} \pm \tilde{U} & \text{Wegner's generator} \\ \text{sgn}\left(\varepsilon_n - \tilde{\varepsilon}_{\text{d}} \pm \tilde{U}\right) & \text{sign-generator} \end{cases}. \tag{7.24}$$

In the next section we will solve the DEQ (7.18) and analyze the induced spin-spin interaction.

7.2.3 The Induced Spin-Spin Interaction

As the flow of H_{D} (and hence the flow of the parameters ε_n, $\tilde{\varepsilon}_{\text{d}}$ and $\tilde{U}$) has been neglected, the prefactors $f^{\pm}_n$ remain constant during the flow and from the DEQ (7.18) we find

$$V_n = V\gamma_n \text{e}^{-f^+_n\left(\varepsilon_n - \tilde{\varepsilon}_{\text{d}} + \tilde{U}\right) l}\,, \quad \Gamma_n = V\gamma_n \text{e}^{-f^-_n\left(\varepsilon_n - \tilde{\varepsilon}_{\text{d}} - \tilde{U}\right) l}. \tag{7.25}$$

We can further calculate the effective spin-spin exchange interaction from the DEQ (7.18) by using Eq. (7.25)

$$\begin{aligned}\partial_l J^{\uparrow\downarrow}_{nm} &= \left[f^+_n + f^+_m\right] V^2 \mathrm{e}^{-\left[f^+_n\left(\varepsilon_n-\tilde{\varepsilon}_\mathrm{d}+\tilde{U}\right)+f^+_m\left(\varepsilon_m-\tilde{\varepsilon}_\mathrm{d}+\tilde{U}\right)\right]l}\gamma_n\gamma_m \\ &- \left[f^-_n + f^-_m\right] V^2 \mathrm{e}^{-\left[f^-_n\left(\varepsilon_n-\tilde{\varepsilon}_\mathrm{d}-\tilde{U}\right)+f^-_m\left(\varepsilon_m-\tilde{\varepsilon}_\mathrm{d}-\tilde{U}\right)\right]l}\gamma_n\gamma_m.\end{aligned} \tag{7.26}$$

Integrating Eq. (7.26) yields for Wegner's generator

$$J^{\uparrow\downarrow}_{nm,\mathrm{Wegner}}(\infty) = \sum_{\sigma=\pm1} \sigma \frac{\varepsilon_n+\varepsilon_m-2\tilde{\varepsilon}_\mathrm{d}+2\sigma\tilde{U}}{\left(\varepsilon_n-\tilde{\varepsilon}_\mathrm{d}+\sigma\tilde{U}\right)^2+\left(\varepsilon_m-\tilde{\varepsilon}_\mathrm{d}+\sigma\tilde{U}\right)^2} V^2\gamma_n\gamma_m \tag{7.27}$$

and for the sign-generator

$$J^{\uparrow\downarrow}_{nm,\mathrm{sign}}(\infty) = \sum_{\sigma=\pm1} \sigma \frac{\mathrm{sgn}\left(\varepsilon_n-\tilde{\varepsilon}_\mathrm{d}+\sigma\tilde{U}\right)+\mathrm{sgn}\left(\varepsilon_m-\tilde{\varepsilon}_\mathrm{d}+\sigma\tilde{U}\right)}{\left|\varepsilon_n-\tilde{\varepsilon}_\mathrm{d}+\sigma\tilde{U}\right|+\left|\varepsilon_m-\tilde{\varepsilon}_\mathrm{d}+\sigma\tilde{U}\right|} V^2\gamma_n\gamma_m. \tag{7.28}$$

Focusing on the couplings with $m = n_\mathrm{F}$ and $\varepsilon_{n_\mathrm{F}} = 0$ in the particle-hole symmetric case ($\tilde{\varepsilon}_\mathrm{d} = 0$) with $\tilde{U} = \frac{U}{2}$ yields the couplings (including those already derived in literature)

$$\begin{aligned}\tilde{J}_{nn_\mathrm{F},\mathrm{SW}} &= \frac{1}{4}\left[\frac{1}{x_n-1}-\frac{1}{x_n+1}-2\right] \\ \tilde{J}_{nn_\mathrm{F},\mathrm{Kehrein}} &= \frac{x_n^2-2}{\left(x_n^2-1\right)^2+1} \\ -\tilde{J}^{\uparrow\downarrow}_{nn_\mathrm{F},\mathrm{Wegner}}(\infty) &= -\frac{1}{2}\left[\frac{x_n+2}{\left(x_n+1\right)^2+1}-\frac{x_n-2}{\left(x_n-1\right)^2+1}\right] \\ -\tilde{J}^{\uparrow\downarrow}_{nn_\mathrm{F},\mathrm{sign}}(\infty) &= -\frac{1}{2}\left[\frac{\mathrm{sgn}\left(x_n+1\right)+1}{\left|x_n+1\right|+1}-\frac{\mathrm{sgn}\left(x_n-1\right)-1}{\left|x_n-1\right|+1}\right]\end{aligned} \tag{7.29}$$

with the parameters

$$x_n = \frac{2\varepsilon_n}{U}, \quad \tilde{J}_{nm} = \frac{J_{nm}}{J_0\gamma_n\gamma_m}, \quad J_0 = \frac{4V^2}{U} \tag{7.30}$$

which were introduced in order to obtain simple expressions. $\tilde{J}_{nn_\mathrm{F},\mathrm{SW}}$ denotes the result of the Schrieffer-Wolff transformation (2.34) while $\tilde{J}_{nn_\mathrm{F},\mathrm{Kehrein}}$ denotes the coupling (7.9) derived by Kehrein and Mielke [22]. The additional sign in Wegner's and the sign-generator is due to a different definition of the sign of the induced spin-spin interaction (cf. Sec. 7.2.1). On small energy scales, close to the Fermi level $\varepsilon_\mathrm{F} = 0$, all approaches coincide and yield the famous Schrieffer-Wolff result

$$\tilde{J}_{n_\mathrm{F}n_\mathrm{F}} = -1 \quad \Leftrightarrow \quad \frac{J_{n_\mathrm{F}n_\mathrm{F}}}{\gamma^2_{n_\mathrm{F}}} = -\frac{4V^2}{U}. \tag{7.31}$$

As this coupling describes an on-shell process at the Fermi level, all approaches have to coincide while away from the Fermi level the couplings describe virtual processes which can differ when using different transformations. The results for all four transformations presented in this section are compared in Fig. 7.2

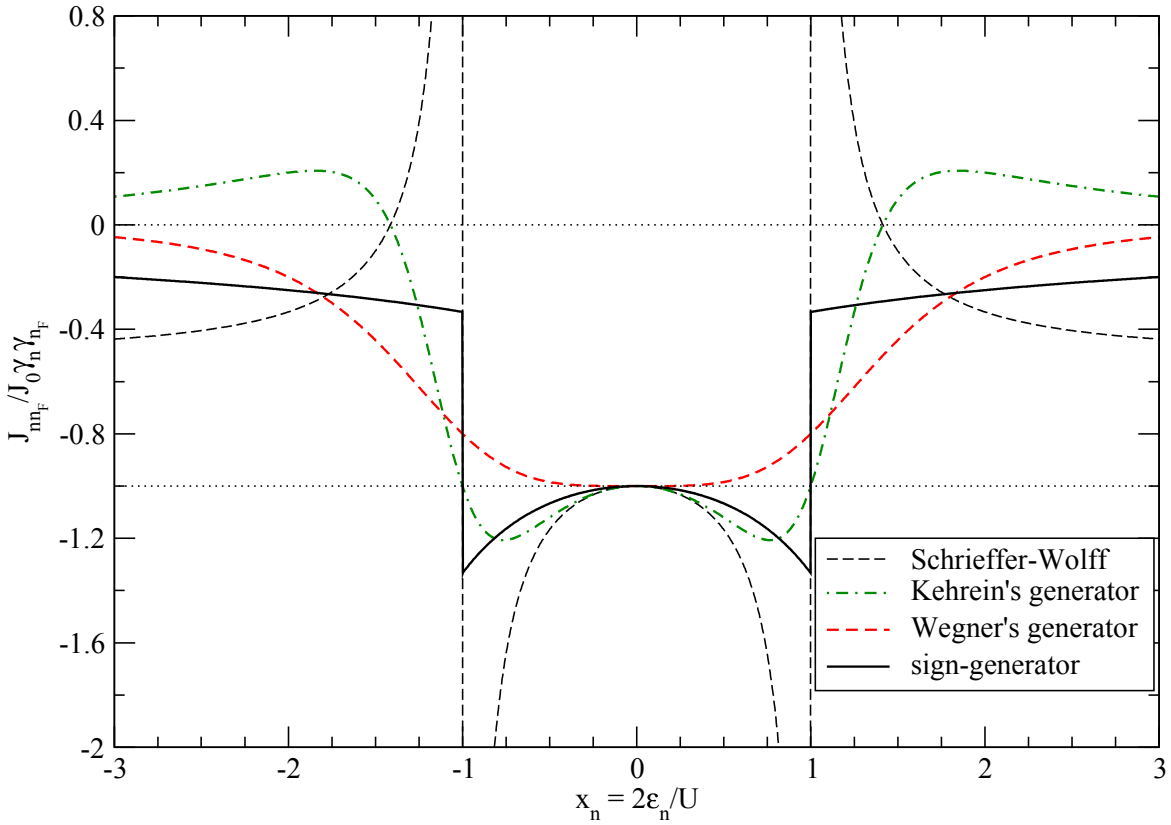

Figure 7.2: Comparison of the induced spin-spin interaction for Wegner's and the sign-generator, the generator used by Kehrein and Mielke [22] as well as the result obtained by the original Schrieffer-Wolff transformation from Eq. (7.29). The coupling $\tilde{J}_{nn_F} = \frac{J_{nn_F}}{J_0\gamma_n\gamma_{n_F}}$ with $J_0 = \frac{4V^2}{U}$ is plotted vs. $x_n = \frac{2\varepsilon_n}{U}$. Close to the Fermi level $x_{n_F} = 0$ all approaches coincide and yield $\tilde{J}_{n_F n_F} = -1$ which is equivalent to $\frac{J_{n_F n_F}}{\gamma_{n_F}^2} = -\frac{4V^2}{U}$. The results obtained by CUT are less singular than those from the Schrieffer-Wolff transformation. Wegner's and the sign-generator yield results which are antiferromagnetic over the full energy spectrum in contrast to the one-step Schrieffer-Wolff transformation and the approach used by Kehrein and Mielke [22]. This represents no disagreement as different transformations are used.

All results obtained by CUT are less singular than the result obtained by the one-step Schrieffer-Wolff transformation. Nevertheless, the CUT result still exhibits some divergences, e.g., on the U-energy scale in the diagonal couplings J_{nn} for n corresponding to an energy $\varepsilon_n = \frac{U}{2}$. The result for J_{nn_F} obtained from Wegner's and the sign-generator are antiferromagnetic over the full energy spectrum in contrast to the one-step Schrieffer-Wolff transformation and the approach used by Kehrein and Mielke. This is no disagreement as the respective couplings describe virtual processes. The coupling at the Fermi level, on the other hand, describes a real process and thus all approaches have to coincide at this point, which they do.

Fig. 7.3 depicts a case with broken particle-hole symmetry in the limit $U \to \infty$. The dimensionless parameters

$$y_n = \frac{\varepsilon_n}{\varepsilon_d}, \quad \tilde{J}_{nm} = \frac{\varepsilon_d J_{nm}}{V^2\gamma_n\gamma_m} \tag{7.32}$$

are chosen because again all results become simple functions of these parameters.

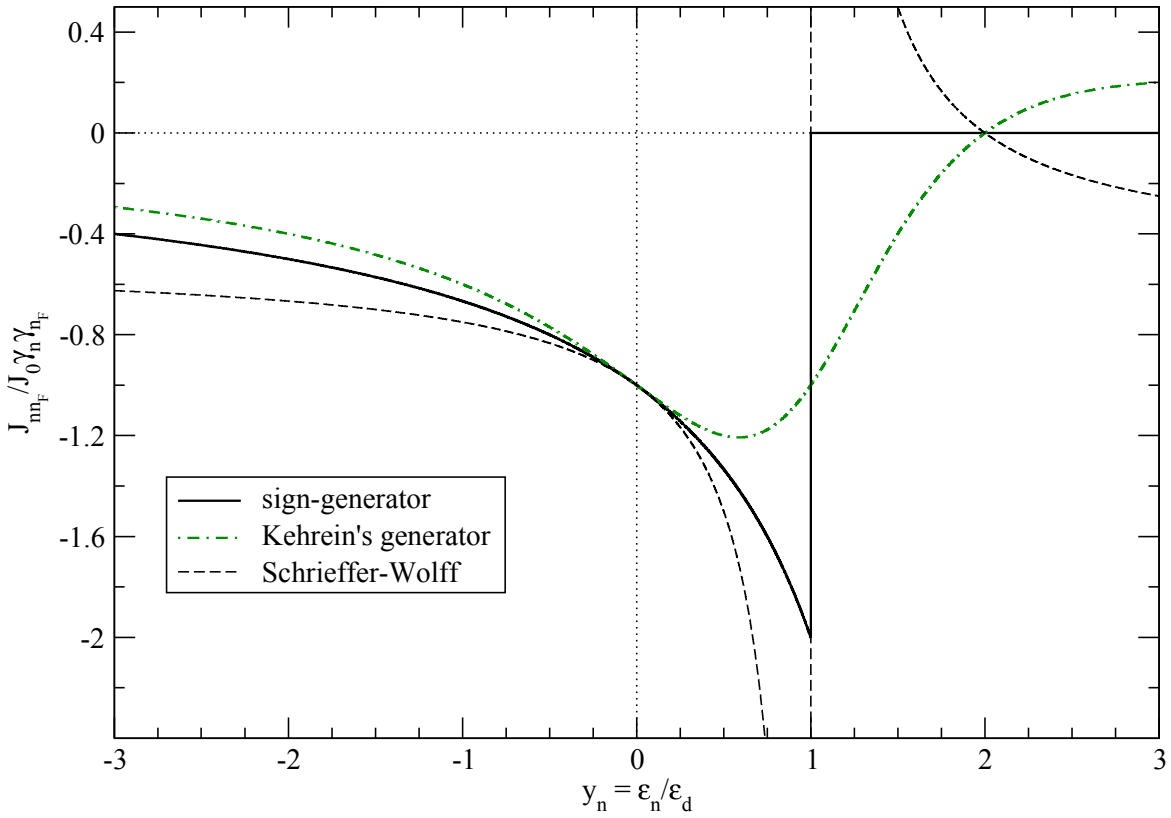

Figure 7.3: Comparison of the induced spin-spin interaction for Wegner's and the sign-generator, the generator used by Kehrein and Mielke [22] as well as the original Schrieffer-Wolff transformation from Eq. (7.33). The coupling $\tilde{J}_{nn_F} = \frac{J_{nn_F}}{J_0\gamma_n\gamma_{n_F}}$ with $J_0 = \frac{V^2}{\varepsilon_d}$ is plotted vs. $y_n = \frac{\varepsilon_n}{\varepsilon_d}$ in the limit $U \to \infty$ with $\varepsilon_d < 0$. Kehrein and Mielke's approach coincides in this special case with the result obtained by Wegner's generator. The sign-generator yields exactly zero for $\varepsilon < \varepsilon_d$. Again, the results obtained by CUT are less singular.

The couplings with the parameters from Eq. (7.32) become

$$\begin{aligned} -\tilde{J}_{nn_F,\mathrm{SW}} &= \frac{1}{2}\left[\frac{1}{y_n - 1} - 1\right] \\ -\tilde{J}_{nn_F,\mathrm{Kehrein}} &= -\frac{2 - y_n}{(1-y_n)^2 + 1} \\ \tilde{J}_{nn_F,\mathrm{Wegner}} &= -\frac{2 - y_n}{(1-y_n)^2 + 1} \\ \tilde{J}_{nn_F,\mathrm{sign}} &= -\frac{\mathrm{sgn}\,(1-y_n) + 1}{|1-y_n| + 1}. \end{aligned} \tag{7.33}$$

The signs in Eq. (7.33) are chosen differently than in Eq. (7.29) because an additional sign is introduced in the coupling (7.32) due to the fact that $\varepsilon_d < 0$. Thus, a negative coupling in Fig. 7.3 still corresponds to an antiferromagnetic one. We find a divergence of the couplings obtained from the one-step transformation at $\varepsilon = \varepsilon_d$. The result obtained by Wegner's generator and the one used by Kehrein and Mielke coincide in this special case. The sign-generator yields a result that exhibits no ferromagnetic coupling and which is exactly zero beyond ε_d.

7.3 Diagonalization of the Spin-Spin Interaction

So far we succeeded in mapping the Anderson Hamiltonian to an effective Kondo model.

Next, we try to diagonalize the induced spin-spin interaction at the same time as it is built up due to the elimination of the hybridization elements which has not been done for the Anderson model so far.

We add new terms to the generator

$$\begin{aligned}\eta_{\mathrm{J}} &= \sum_{n,m,\sigma} \eta^{\uparrow\downarrow}_{nm} d^{\dagger}_{\sigma} d_{\bar{\sigma}} c^{\dagger}_{n\bar{\sigma}} c_{m\sigma} + \sum_{n,m,\sigma} \eta^{n_z}_{nm,\sigma} n_z : c^{\dagger}_{n\sigma} c_{m\sigma} : \\ &+ \sum_{n,m,\sigma} \eta^{\bar{n}}_{nm} \bar{n} : c^{\dagger}_{n\sigma} c_{m\sigma} : + \sum_{n,m} \eta^{\pm}_{nm} \left(d^{\dagger}_{\uparrow} d^{\dagger}_{\downarrow} c_{n\downarrow} c_{m\uparrow} - c^{\dagger}_{m\uparrow} c^{\dagger}_{n\downarrow} d_{\downarrow} d_{\uparrow} \right).\end{aligned} \tag{7.34}$$

In the following, we use the sign-generator which is given by

$$\begin{aligned}\eta^{\uparrow\downarrow}_{nm} &= \mathrm{sgn}\left(\varepsilon_n - \varepsilon_m\right) J^{\uparrow\downarrow}_{nm} \\ \eta^{n_z}_{nm,\sigma} &= \mathrm{sgn}\left(\varepsilon_n - \varepsilon_m\right) J^{n_z}_{nm,\sigma} \\ \eta^{\bar{n}}_{nm} &= \mathrm{sgn}\left(\varepsilon_n - \varepsilon_m\right) J^{\bar{n}}_{nm} \\ \eta^{\pm}_{nm} &= -\mathrm{sgn}\left(\varepsilon_n + \varepsilon_m\right) J^{\pm}_{nm}.\end{aligned} \tag{7.35}$$

We only include terms that act in lowest order J^2 on the spin-spin interaction and thus we have to calculate the commutators

$$\left[\eta_{\mathrm{J}}, H_{\mathrm{D}} + H_{\mathrm{J}}\right] \tag{7.36}$$

from which we only include terms that act on H_{J}. All further terms are neglected as their feedback on the spin-spin interaction is at least of order J^3.

Calculating the commutators and comparing the coefficients in the flow equation (4.4) yields additional terms to the differential equation (7.18)

$$\begin{aligned}\partial_l J^{n_z}_{nm,\sigma} &= \left(\varepsilon_m - \varepsilon_n\right) \eta^{n_z}_{nm,\sigma} - \frac{1}{2} \sum_x \sigma \left(\eta^{\uparrow\downarrow}_{nx} J^{\uparrow\downarrow}_{xm} - \eta^{\uparrow\downarrow}_{xm} J^{\uparrow\downarrow}_{nx} \right) (1 - 2\theta_x) \\ \partial_l J^{\uparrow\downarrow}_{nm} &= \left(\varepsilon_m - \varepsilon_n\right) \eta^{\uparrow\downarrow}_{nm} + \sum_x \sigma \left(\eta^{n_z}_{xm,\sigma} J^{\uparrow\downarrow}_{nx} - \eta^{n_z}_{nx,\sigma} J^{\uparrow\downarrow}_{xm} + \eta^{\uparrow\downarrow}_{xm} J^{n_z}_{nx,\sigma} - \eta^{\uparrow\downarrow}_{nx} J^{n_z}_{xm,\sigma} \right) (1 - 2\theta_x) \\ \partial_l J^{\bar{n}}_{nm} &= \left(\varepsilon_m - \varepsilon_n\right) \eta^{\bar{n}}_{nm} - \frac{1}{2} \sum_x \left(\eta^{\pm}_{xn} J^{\pm}_{xm} + \eta^{\pm}_{xm} J^{\pm}_{xn} \right) (1 - 2\theta_x) \\ \partial_l J^{\pm}_{nm} &= \left(\varepsilon_n + \varepsilon_m\right) \eta^{\pm}_{nm} + \sum_x \left(\eta^{\bar{n}}_{xm} J^{\pm}_{nx} + \eta^{\bar{n}}_{xn} J^{\pm}_{xm} - \eta^{\pm}_{nx} J^{\bar{n}}_{xm} - \eta^{\pm}_{xm} J^{\bar{n}}_{xn} \right) (1 - 2\theta_x)\end{aligned} \tag{7.37}$$

where σ as an index labels the spin while it has the value $\sigma = \pm 1$ as a coefficient. The occupation number

$$\theta_x = \langle c^{\dagger}_{x\sigma} c_{x\sigma} \rangle \tag{7.38}$$

is calculated with respect to the Fermi sea and stems from the normal-ordering of the bath operators. Note that the σ-dependence in the derivative of $J^{\uparrow\downarrow}_{nm}$ in Eq. (7.37) cancels due to the spin-rotation symmetry (7.39) (cf. Eq. (7.40)).

Taking a closer look at the differential equation (7.37) reveals that J^{n_z} and $J^{\uparrow\downarrow}$ interact only with each other and do not couple to $J^{\pm}$ or $J^{\bar{n}}$ which also only interact with each other. The spin-rotation symmetry

$$\sigma J^{n_z}_{nm,\sigma} = \frac{1}{2} J^{\uparrow\downarrow}_{nm} \tag{7.39}$$

still holds true during the whole flow which simplifies the differential equation for $J^{\uparrow\downarrow}_{nm}$ to

$$\partial_l J^{\uparrow\downarrow}_{nm} = (\varepsilon_m - \varepsilon_n)\, \eta^{\uparrow\downarrow}_{nm} - \sum_x \left(\eta^{\uparrow\downarrow}_{nx} J^{\uparrow\downarrow}_{xm} - \eta^{\uparrow\downarrow}_{xm} J^{\uparrow\downarrow}_{nx} \right) (1 - 2\theta_x)\,. \tag{7.40}$$

This differential equation is the same as Eq. (4.89) with an isotropic coupling

$$J^{\mu}_{nm} = J^{\uparrow\downarrow}_{nm} \tag{7.41}$$

which is the flow equation for the diagonalization of the spin-spin interactions of the Kondo model.

In the last sections this differential equation was only analyzed at small energies very close to the Fermi level $\varepsilon_F = 0$ by introducing the IR-approximation

$$J^{\uparrow\downarrow}_{nm} = \tilde{J} \mathrm{e}^{-|\varepsilon_n - \varepsilon_m| l} \gamma_n \gamma_m \tag{7.42}$$

which leads to the flow (cf. Sec. 4.6.2) for the coupling at the Fermi level

$$\partial_l \tilde{J} \;=\; \frac{2\rho_0 \tilde{J}^2}{l}. \tag{7.43}$$

This coincides with the scaling equation from the "poor man's scaling" (3.35) with $l^{-1} = D_{\mathrm{eff}}$ which diverges on the Kondo energy scale $l^{-1} = T_K$ (cf. Sec. 4.6.2).

Analyzing the full differential equation (7.40) numerically not only confirms the results obtained by the IR-approximation but additionally reveals the Kondo energy scale as a crossover between diverging and non-diverging couplings, i.e., diagonal couplings J_{nn} with an index n that corresponds to an energy $|\varepsilon_n| > T_K$ converge while those with $|\varepsilon_n| < T_K$ diverge. This insight has not been reported so far and is missed when focusing only on energies at the Fermi level.

In contrast to the potential scattering model (cf. Sec. 4.6.1), where the divergence is a result of the IR-approximation, the divergence in the case of the Kondo model is also present in the full numerical solution of the differential equation (7.40).

In the following, we want to analyze the Kondo model first before we turn to the Anderson model. At first, we solve the differential equation (7.40) numerically by a 4th-order Runge-Kutta algorithm with the starting values

$$J^{\uparrow\downarrow}_{nm}(0) = J \gamma_n \gamma_m \tag{7.44}$$

which corresponds to diagonalizing the spin-spin interaction of the Kondo model.

Fig. 7.4 shows the residual off-diagonality for different interaction strengths J.

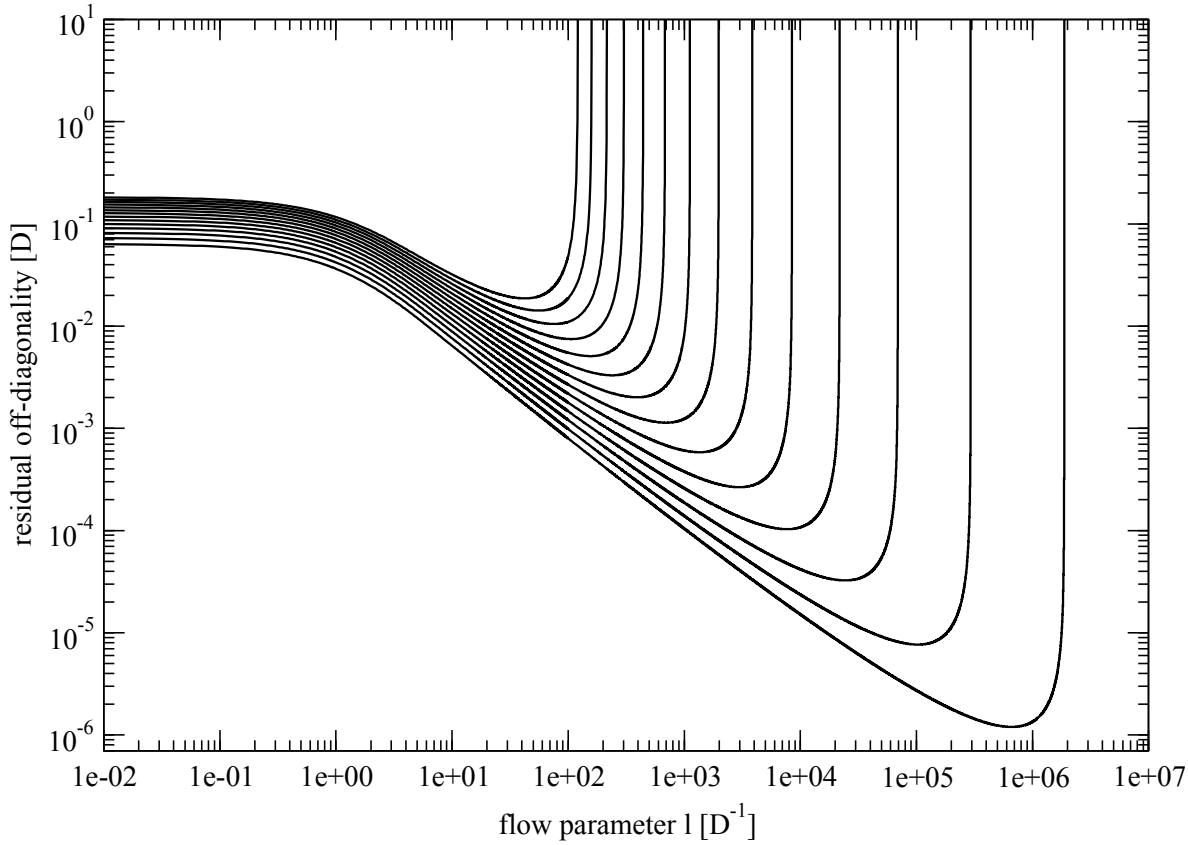

Figure 7.4: Residual off-diagonality ROD $= \sqrt{\sum_{n\neq m} |J_{nm}|^2}$ for the **Kondo model**. The DEQ (7.40) with the starting values (7.44) is solved for $N = 80$, $\Lambda = 2$ and from left to right: $2\rho_0 J = 0.2$, 0.19, 0.18, ... 0.09, 0.08, 0.07. The residual off-diagonality decreases first until the energy scales come close to the Kondo temperature T_K where the ROD quickly increases until it finally diverges on the Kondo energy scale.

First, the residual off-diagonality decreases as a result of the linear term in Eq. (7.40). As soon as the energy scale comes close to the Kondo temperature T_K, the quadratic term in Eq. (7.40) starts to dominate and leads to divergence.

Fig. 7.5 shows the energy scale on which the coupling $J^{\uparrow\downarrow}_{n_\mathrm{F} n_\mathrm{F}}$ diverges. We see that the divergence indeed occurs on the Kondo energy scale

$$T_\mathrm{K} \propto \mathrm{e}^{-\frac{A_\Lambda}{2\rho_0 J}} \tag{7.45}$$

where A_Λ is a known effect of the discretization [8] and is given by Eq. (6.39). Fig. 7.5 also verifies that the value of A_Λ coincides with Eq. (6.39) by varying the discretization parameter Λ. When Λ is reduced, A_Λ converges to one.

The IR-approximation is a very useful approach in order to gain insights into the behavior of the differential equation at the Fermi level. On the other hand, one misses another interesting and for our further purposes very important point. The IR-approximation only reveals that the coupling diverges at the Fermi level $\varepsilon_\mathrm{F} = 0$. A remaining question is how the couplings behave on other energy scales. Solving the DEQ (7.40) numerically can answer this question.

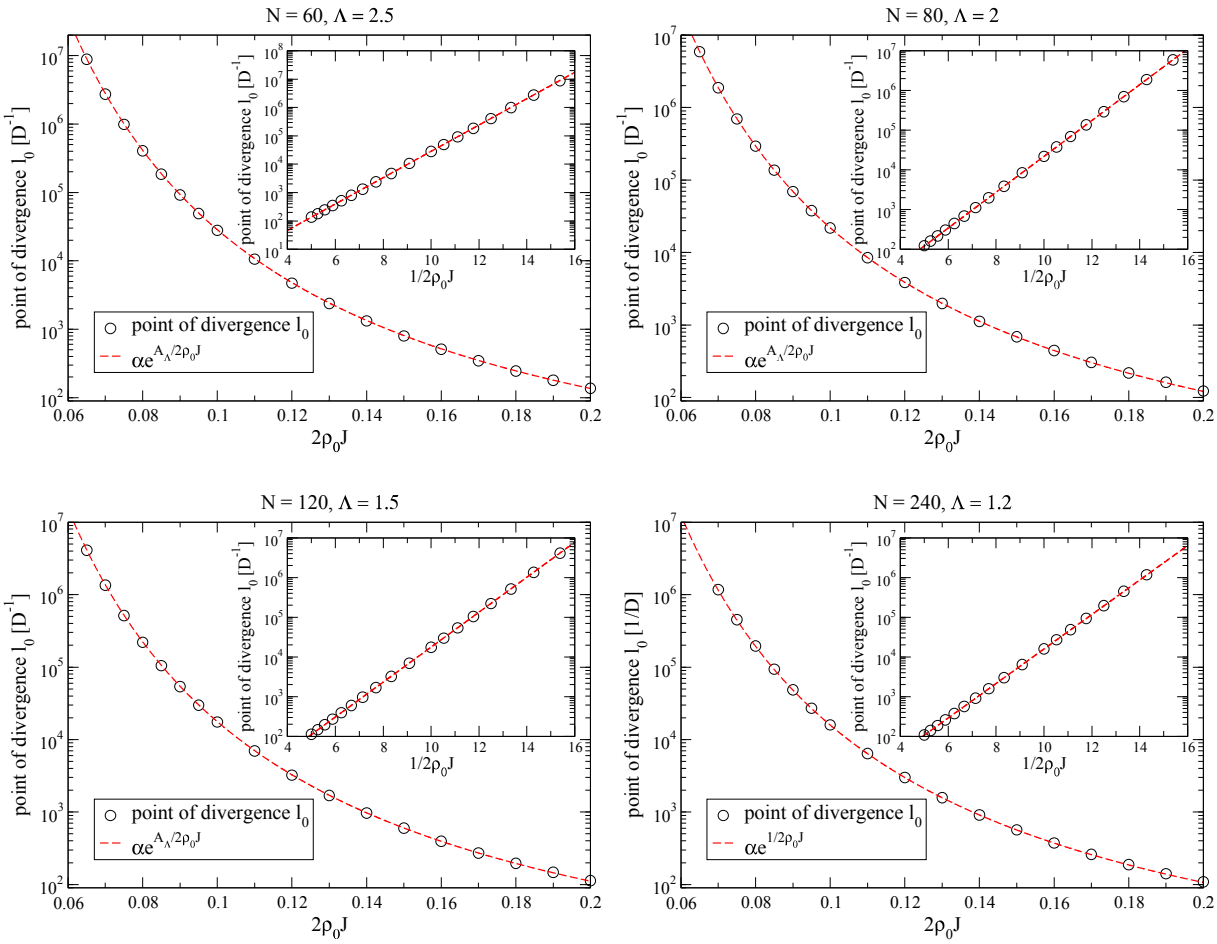

Figure 7.5: Point of divergence l_0 vs. the Kondo coupling J for the **Kondo model**. The inverse of l_0 coincides with the Kondo energy scale $l_0^{-1} = T_K$. We investigate different discretization parameters Λ (left top: $N = 60$, $\Lambda = 2.5$, right top: $N = 80$, $\Lambda = 2$, left bottom: $N = 120$, $\Lambda = 1.5$, right bottom: $N = 240$, $\Lambda = 1.2$) in order to verify that the discretization effect on the Kondo energy scale coincides with Eq. (6.39). The modification of the exponent of T_K is in perfect agreement with the known influence of the discretization (6.39) [8].

Fig. 7.6 shows the flow of the couplings $\frac{J_{nn}}{|\gamma_n|^2}$ for different n. Only couplings J_{nn} with an index n for which $|\varepsilon_n| < T_K$ diverge in contrast to those corresponding to $|\varepsilon_n| > T_K$ which converge towards a finite value.

We see this effect even clearer if we analyze the derivative of the couplings J_{nn} with respect to the flow parameter l shown in Fig. 7.7. The derivative diverges for $|\varepsilon_n| < T_K$ and tends to zero for $|\varepsilon_n| > T_K$.

This observation is very interesting as it shows that the spin-flip contributions will only play a dominant role below the Kondo energy scale and ensures that the Kondo singlet will form below the Kondo temperature T_K. We will return to this point when we discuss our new approach in Sec. 7.5.

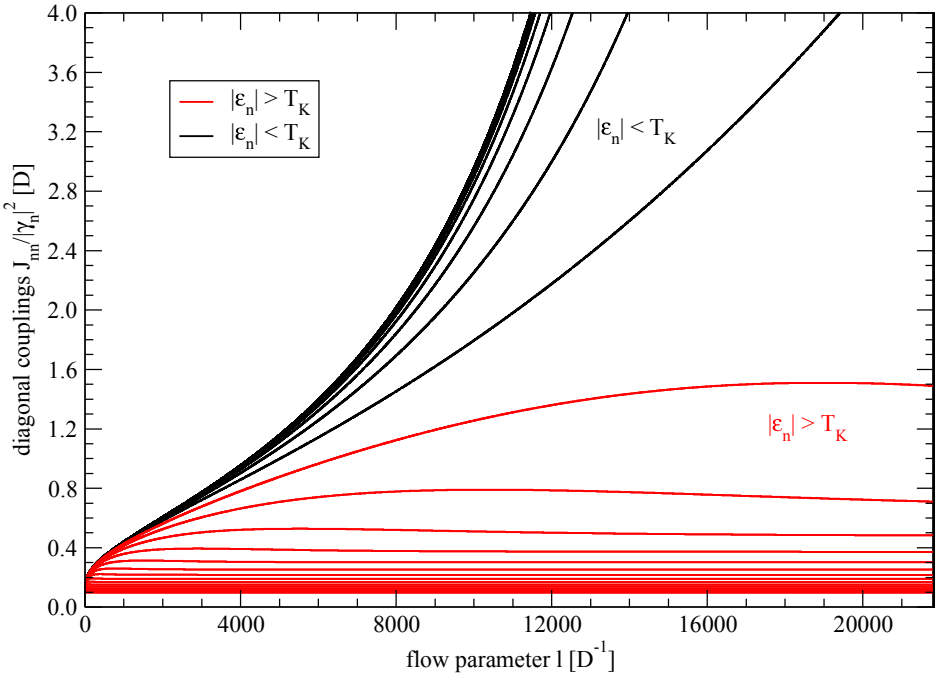

Figure 7.6: Flow of the diagonal couplings $J_{nn}/|\gamma_n|^2$ of the **Kondo model** for $N = 80$, $\Lambda = 2$ and $2\rho_0 J = 0.1$. The point of divergence for these parameters is $l_0 \approx 21825D^{-1}$ which corresponds to the Kondo energy scale $T_K \approx 4.85 \cdot 10^{-5} D$. The black lines show the couplings with an index n for which $|\varepsilon_n| < T_K$ while the red lines show the couplings with an index n for which $|\varepsilon_n| > T_K$. We can see that only couplings with $|\varepsilon_n| < T_K$ diverge while those corresponding to $|\varepsilon_n| > T_K$ converge towards a constant value.

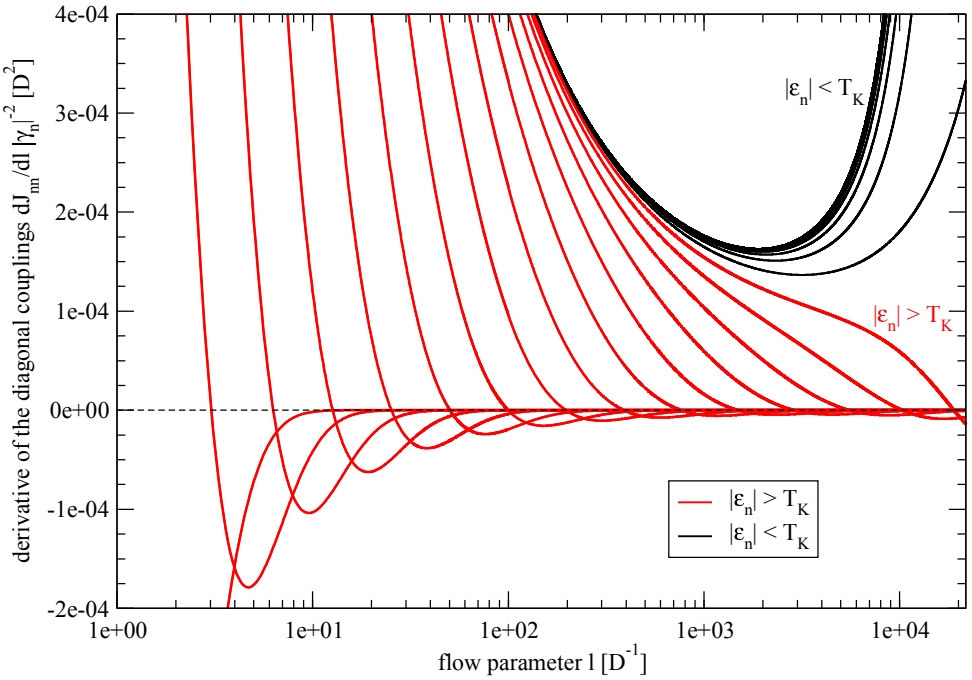

Figure 7.7: Flow of the derivative of the diagonal couplings $\frac{dJ_{nn}}{dl}/|\gamma_n|^2$ of the **Kondo model** for $N = 80$, $\Lambda = 2$ and $2\rho_0 J = 0.1$. The point of divergence for these parameters is $l_0 \approx 21825D^{-1}$ which corresponds to the Kondo temperature $T_K \approx 4.85 \cdot 10^{-5} D$. The black lines show the derivative of the couplings with an index n for which $|\varepsilon_n| < T_K$ while the red lines show the derivative of the couplings with an index n for which $|\varepsilon_n| > T_K$. We can see that only couplings with $|\varepsilon_n| < T_K$ diverge while those corresponding to $|\varepsilon_n| > T_K$ converge towards a finite value.

We started this section with the Anderson model and derived a differential equation for the induced spin-spin interaction which we already knew from the diagonalization of the spin-spin interaction of the Kondo model. This led us to analyze the flow for the Kondo model first.

Next, we want to analyze if we can directly start from the Anderson model and still find the Kondo energy scale T_K as the inverse flow parameter on which the differential equations diverge. This has not been studied so far. We want to eliminate the charge fluctuations induced by the hybridization V_{nm} and diagonalize the induced spin-spin interaction J_{nm} at the same time. Note that this is not in one-to-one correspondence with applying a Schrieffer-Wolff transformation first and then diagonalizing the effective Kondo Hamiltonian as we perform both transformations simultaneously.

Fig. 7.8 shows the point of divergence l_0 vs. the interaction U.

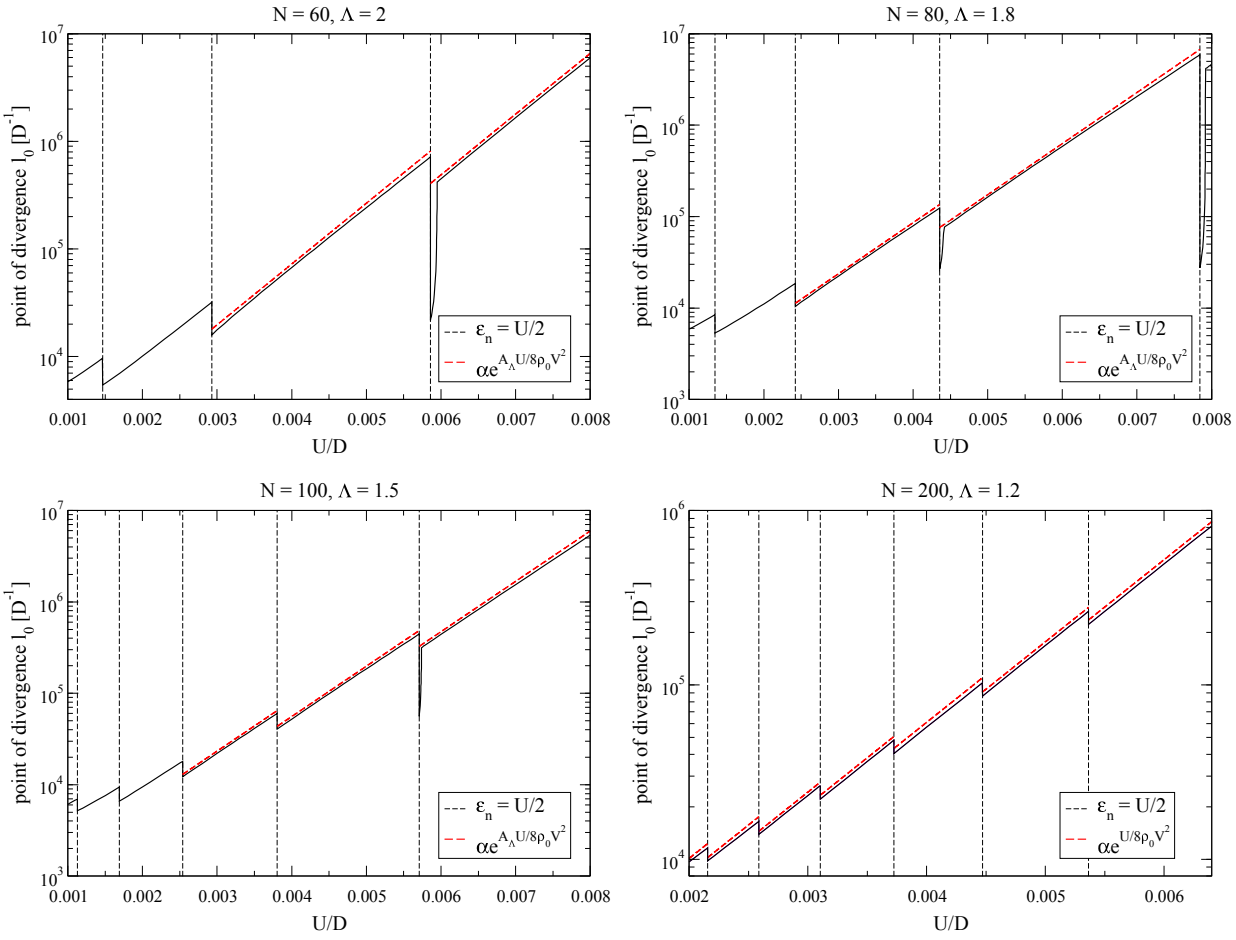

Figure 7.8: Point of divergence l_0 for the **Anderson model** vs. the Coulomb interaction U for $\frac{V}{D} = 0.01414$. The inverse of l_0 coincides with the Kondo energy scale $l_0^{-1} = T_K$. We look at different discretization parameters Λ (left top: $N = 60$, $\Lambda = 2$, right top: $N = 80$, $\Lambda = 1.8$, left bottom: $N = 100$, $\Lambda = 1.5$, right bottom: $N = 200$, $\Lambda = 1.2$) in order to see the discretization effect on the Kondo temperature T_K. The dotted vertical lines show the interaction strengths U for which $\frac{U}{2} = \varepsilon_n$. The exponent of the energy scale is influenced by the discretization precisely by A_Λ from (6.39) which is the well-known discretization effect on the Kondo temperature [8]. Additionally, discontinuities occur each time $\frac{U}{2}$ crosses an energy level ε_n which is also a discretization effect. For smaller values of Λ, there are more discontinuities as more ε_n lie in the considered interval. The discontinuities, however, become smaller for decreasing Λ.

In order to find the Kondo energy scale of the Anderson Hamiltonian with Continuous Unitary Transformations, we combine Eq. (7.18), which eliminates the hybridization elements, and Eq. (7.37) which is supposed to diagonalize the induced spin-spin interaction. This DEQ also leads to divergence on an energy scale that depends on the parameters U and V. There are certain values of U for which discontinuities occur. In the intervals between the discontinuities we find the correct exponential behavior of the Kondo temperature $T_k^{-1} \propto \exp\left(A_\Lambda \frac{U}{8\rho_0 V^2}\right)$ where A_Λ is the discretization influence on the Kondo temperature from Eq. (6.39). The origin of the discontinuities is the discretization. Each time the interaction $\frac{U}{2}$ crosses an energy level ε_n, one sign in the generator is changed discontinuously

$$\eta = -\sum_{n,\sigma}\left[\operatorname{sgn}\left(\varepsilon_n + \frac{U}{2}\right) V_n F^\dagger_{1,\sigma} c_{n\sigma} + \operatorname{sgn}\left(\varepsilon_n - \frac{U}{2}\right)\Gamma_n F^\dagger_{2,\sigma} c_{n\sigma}\right] - \text{h.c.}. \tag{7.46}$$

In Fig. 7.8 the dashed vertical lines show the different interactions with $\frac{U}{2} = \varepsilon_n$. We can see that the discontinuities indeed occur exactly each time $\frac{U}{2}$ crosses an energy level ε_n. If the discretization parameter Λ is decreased, more energy levels lie in the considered interval and thus we see more discontinuities. On the other hand, the weight $|\gamma_n|^2$ carried by the respective energy level decreases which results in smaller discontinuities.

We succeeded in turning away the hybridization elements of the Anderson model while also including the induced spin-spin interaction into the generator which results in a divergence on the Kondo energy scale T_K. This has so far only been accomplished for the Kondo model but not for the Anderson model. We can check that the exponent is also correct for different hybridizations V.

Fig. 7.9 shows the point of divergence l_0 for varying U and different hybridizations V. The exponent changes according to

$$T_\mathrm{K} = l_0^{-1} = C(U,V)\,\mathrm{e}^{-A_\Lambda \frac{U}{8\rho_0 V^2}} \tag{7.47}$$

where $C(U,V)$ describes the discontinuous behavior observed in Fig. 7.8 due to the generator (7.46) and is constant in each respective interval between two discontinuities.

Finally, we use a fixed U and vary the hybridization V. Our main goal is to find out whether discontinuities occur when varying V. As the signs in the generator (7.46) do not depend on the hybridization V, we do not expect to see such discontinuities. Fig. 7.10 shows the results for different fixed U. Indeed, no discontinuities occur which supports our explanation for the origin of the discontinuities. We again find the correct behavior of the exponent $T_\mathrm{K}^{-1} \propto \exp\left(A_\Lambda \frac{U}{8\rho_0 V^2}\right)$ with A_Λ from Eq. (6.39).

The fact that the flow equations diverge shows that the approach is not able to diagonalize important parts of the Hamiltonian. The aim of the second part of this chapter is to search for a solution of this challenging problem and to provide an advanced approach that is able to produce non-diverging parameters for energies arbitrarily close to the Fermi level $\varepsilon_\mathrm{F} = 0$. We suppose that the main problem and the reason for the divergence is the choice of the reference state. It might be suited for the local-moment regime (cf. Sec. 2.7) but obviously not for the strong-coupling regime where the spin of the impurity becomes completely screened. This screening cannot be achieved by the current reference state. Our new approach will focus on the change of the reference state during the flow which will lead to converging differential equations and an effective Hamiltonian without divergences at small energies.

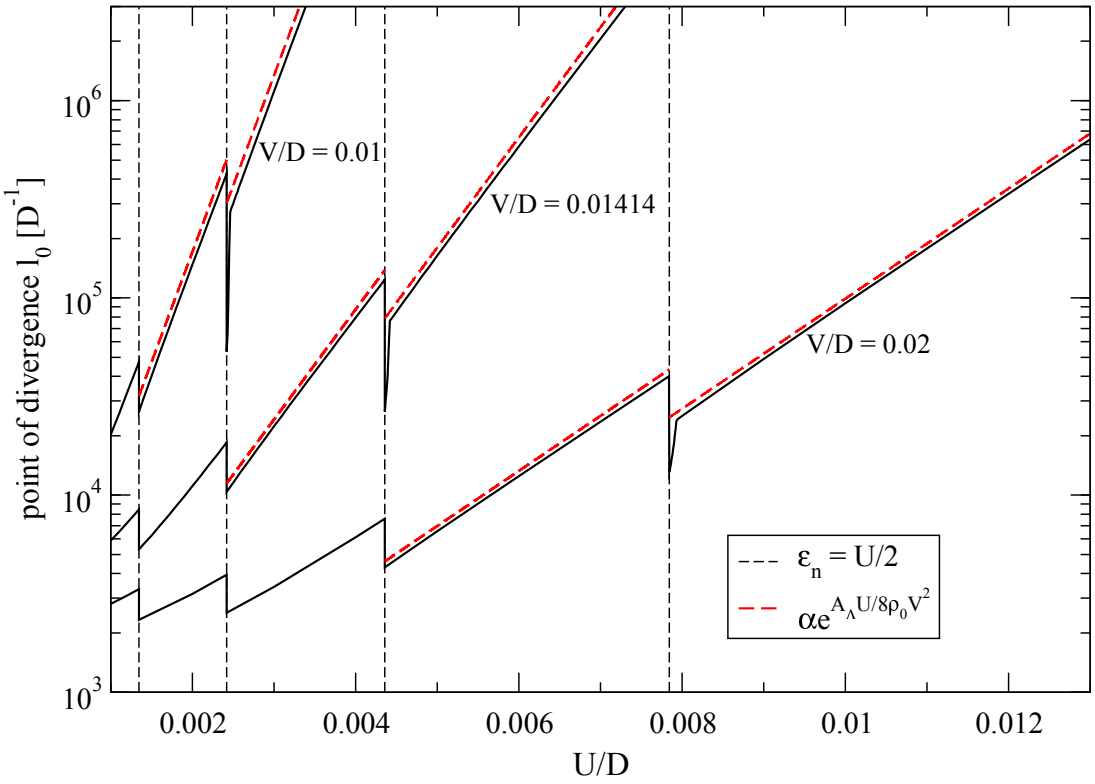

Figure 7.9: Point of divergence l_0 vs. the Coulomb interaction U of the **Anderson model** with $N = 80$, $\Lambda = 1.8$ and from top to bottom: $\frac{V}{D} = 0.01$, 0.01414 and 0.02. The inverse of l_0 coincides with the Kondo energy scale $l_0^{-1} = T_K$ with $T_K^{-1} \propto \exp\left(A_\Lambda \frac{U}{8\rho_0 V^2}\right)$ well inside the region between two discontinuities where the modification A_Λ from Eq. (6.39) is an effect due to the discretization.

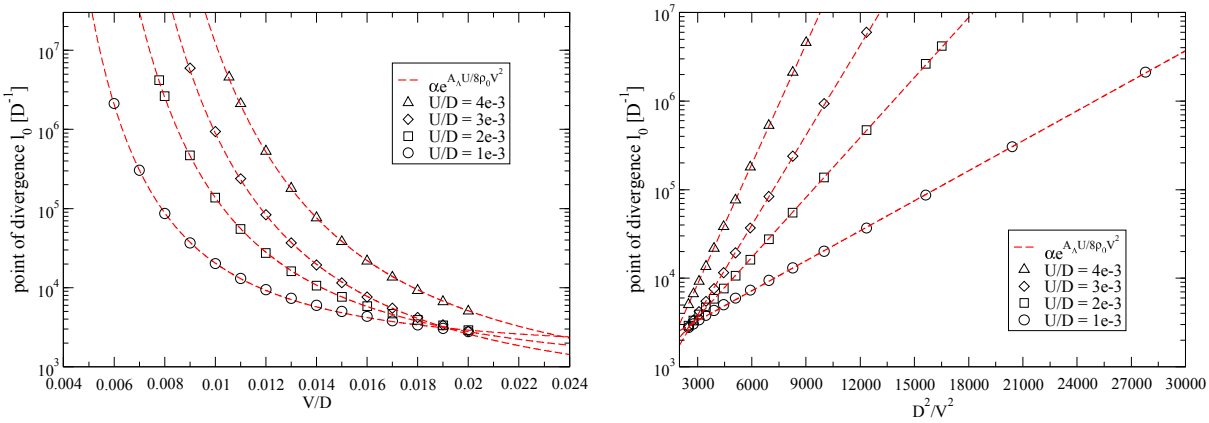

Figure 7.10: Point of divergence l_0 vs. the hybridization V (left panel) and vs. D^2/V^2 (right panel) for the **Anderson model** with $N = 60$, $\Lambda = 2$ and from top to bottom: $10^3 \frac{U}{D} = 4$, 3, 2 and 1. The inverse of l_0 coincides with the Kondo energy scale $l_0^{-1} = T_K$. The Kondo temperature scales correctly as $T_K \propto \exp\left(-A_\Lambda \frac{U}{8\rho_0 V^2}\right)$ with A_Λ from Eq. (6.39). No discontinuities occur because the hybridization has no influence on the sign in the generator (7.46) in contrast to the Coulomb interaction U. This result is in agreement with the expected behavior.

7.4 Adapted Reference State for the Kondo Model Coupled to an Auxiliary Spin

The approach of the last sections does not allow to construct an effective model as the induced spin-spin interactions J_{nn} with $|\varepsilon_n| < T_\mathrm{K}$ diverge on the Kondo energy scale. In this section we want to identify the source of this divergence and find a way to avoid it. One obvious approximation we used is the truncation of operators. However, including higher interaction terms will not solve the problem of the divergence but will only result in a better estimate of the energy scale on which the differential equation diverges [16], i.e., we find higher-order corrections to the Kondo temperature T_K.

We assume that the source of the problem is rather the chosen reference state which is convenient for the weak-coupling but not for the strong-coupling regime. As we cross from the weak- to the strong-coupling regime, diagonal spin-flip contributions become important and lead to a singlet which screens the impurity. The reference state so far is not able to account for this screening of the impurity so that the increase of the spin-spin interactions is not prevented and leads to the divergence. We want to establish an approach that does not rely on an a priori understanding of the problem and for this reason we do not simply assume a singlet reference state but modify the procedure so that it yields this behavior as a result.

We modify the diagonal part of the Hamiltonian H_D by adding the emerging diagonal spin-spin interactions and derive the adapted reference state as the ground state of the modified diagonal part of the Hamiltonian H_D. In the Kondo problem the spin-spin couplings become larger during the flow which has a significant impact on the reference state. The additional terms contributing to the diagonal Hamiltonian of the Anderson model are

$$H_{\mathrm{J}_\mathrm{diag}}^{\mathrm{Anderson}} = \sum_{n,\sigma} J_{nn}^{\uparrow\downarrow} \left(d_\sigma^\dagger d_{\bar{\sigma}} c_{n\bar{\sigma}}^\dagger c_{n\sigma} + \frac{1}{2} \sigma n_z : c_{n\sigma}^\dagger c_{n\sigma} : \right) \tag{7.48}$$

and for the Kondo model

$$H_{\mathrm{J}_\mathrm{diag}}^{\mathrm{Kondo}} = \sum_{\mu \in x,y,z} \sum_{n,\alpha,\beta} J_{nn} \sigma_{\alpha\beta}^\mu \tau^\mu : c_{n\alpha}^\dagger c_{n\beta} : . \tag{7.49}$$

If we assume that the impurity is only singly occupied and that the energy scales are small enough so that charge fluctuations are negligible, then $H_{\mathrm{J}_\mathrm{diag}}^{\mathrm{Anderson}}$ and $H_{\mathrm{J}_\mathrm{diag}}^{\mathrm{Kondo}}$ are equivalent.

In order to find an adapted approach that avoids the divergence of the differential equations, we first study a different model in which the question of the choice of the adapted reference state is much simpler.

7.4.1 Kondo Model Coupled to an Auxiliary Spin

In this section we add an auxiliary spin $S = \frac{1}{2}$ to the Kondo model which is coupled to the impurity via an isotropic spin-spin exchange coupling K. In this system it is easy to decide which modified reference state to choose and thus we can study if changing the reference state prevents the divergence found in the last sections. Additionally, we find patterns which we will recognize when dealing with the Kondo Hamiltonian. The Kondo model coupled to the auxiliary spin is of the form

$$H = \sum_{n,\sigma} \varepsilon_n : c_{n\sigma}^\dagger c_{n\sigma} : + \sum_{\mu \in x,y,z} \sum_{n,m} \sum_{\alpha,\beta} J_{nm} \sigma_{\alpha\beta}^\mu \tau^\mu : c_{n\alpha}^\dagger c_{m\beta} : + K \vec{\tau} \cdot \vec{S}_K . \tag{7.50}$$

At first sight, this seems to complicate the problem even further as we include an additional coupling and thus also new physics. However, we are only interested in an adapted operator basis and a suitable reference state in order to construct converging flow equations. This can be achieved much easier for this model because we only need to understand the physics of the isolated additional site coupled to the impurity which boils down to the coupling of two spins $S = \frac{1}{2}$ with the eigenstates

$$\begin{aligned} |0\rangle &= |s\rangle = \frac{1}{\sqrt{2}}(|\uparrow\downarrow\rangle - |\downarrow\uparrow\rangle) \\ |1\rangle &= |t_1\rangle = |\uparrow\uparrow\rangle \\ |2\rangle &= |t_2\rangle = \frac{1}{\sqrt{2}}(|\uparrow\downarrow\rangle + |\downarrow\uparrow\rangle) \\ |3\rangle &= |t_3\rangle = |\downarrow\downarrow\rangle \end{aligned} \tag{7.51}$$

where the first spin is associated to the impurity while the second one is the auxiliary spin. The corresponding energy levels are given by

$$E_{t_1,t_2,t_3} = \frac{K}{4}, \quad E_s = -\frac{3K}{4}. \tag{7.52}$$

The singlet state is the ground state and thus we introduce the normal-ordering scheme

$$|k\rangle\langle q| = |k\rangle\langle q|_{\text{non-normal-ordered}} - \mathbb{1}\delta_{ks}\delta_{qs} \tag{7.53}$$

where the states $|k\rangle$ and $|q\rangle$ denote the states from Eq. (7.51) and the index s corresponds to the singlet state. In the next step we expand τ^μ in this operator basis

$$\tau^\mu = \sum_{k,q} \alpha^\mu_{kq} |k\rangle\langle q| \quad \text{with} \quad \alpha^\mu_{kq} = \langle k|\tau^\mu|q\rangle \tag{7.54}$$

where the indices k and q again denote the states from Eq. (7.51). The expansion coefficients can be written in matrix form and are given by

$$\begin{aligned} \alpha^x &= \frac{1}{2\sqrt{2}} \begin{pmatrix} 0 & -1 & 0 & 1 \\ -1 & 0 & 1 & 0 \\ 0 & 1 & 0 & 1 \\ 1 & 0 & 1 & 0 \end{pmatrix} \\ \alpha^y &= \frac{1}{2\sqrt{2}i} \begin{pmatrix} 0 & 1 & 0 & 1 \\ -1 & 0 & 1 & 0 \\ 0 & -1 & 0 & 1 \\ -1 & 0 & -1 & 0 \end{pmatrix} \\ \alpha^z &= \frac{1}{2} \begin{pmatrix} 0 & 0 & 1 & 0 \\ 0 & 1 & 0 & 0 \\ 1 & 0 & 0 & 0 \\ 0 & 0 & 0 & -1 \end{pmatrix}. \end{aligned} \tag{7.55}$$

We find that the matrices α^μ fulfill properties very similar to the Pauli matrices

$$\alpha^\mu \alpha^\nu = \frac{\delta_{\mu\nu}}{4}\mathbb{1} + \frac{i}{2}\sum_r \varepsilon_{\mu\nu r}\alpha^r. \tag{7.56}$$

The Hamiltonian in the adapted operator basis is of the form

$$H = \sum_{n,\sigma} \varepsilon_n : c^\dagger_{n\sigma} c_{n\sigma} : + \sum_k E_k |k\rangle\langle k| + \sum_{\substack{n,m \\ k,q,\alpha,\beta}} J^{kq\alpha\beta}_{nm} |k\rangle\langle q| : c^\dagger_{n\alpha} c_{m\beta} : \tag{7.57}$$

with the energy levels

$$E_{1,2,3} = \frac{K}{4}, \quad E_0 = -\frac{3K}{4}. \tag{7.58}$$

In principle, the normal-ordering (7.53) would additionally produce hopping terms but because $J^{ss\alpha\alpha}_{nm}(0) = 0$, hopping terms are not present in the initial Hamiltonian. Moreover, a constant due to the normal-ordering of the bath operators was dismissed. The starting values of the coefficients $J^{kq\alpha\beta}_{nm}$ are given by

$$J^{kq\alpha\beta}_{nm} = \sum_{\mu \in x,y,z} J_{nm} \alpha^\mu_{kq} \sigma^\mu_{\alpha\beta}. \tag{7.59}$$

Their explicit values can be found in App. 9.10.1. The idea is to modify the diagonal part of H_D by using

$$H_\mathrm{D} = \sum_{n,\sigma} \varepsilon_n : c^\dagger_{n\sigma} c_{n\sigma} : + \sum_k E_k |k\rangle\langle k| \tag{7.60}$$

and to choose the ground state of the Hamiltonian (7.60) as the reference state which is given by

$$|\mathrm{ref}\rangle = |\mathrm{FS}\rangle |\mathrm{singlet}\rangle. \tag{7.61}$$

Note that Wick's theorem can only be applied to the bath operators but not to the singlet state formed by the impurity and the auxiliary spin because it is not a Slater determinant.

7.4.2 Generator and Flow Equation

With the previous reference state, which was the Fermi sea, states of different spin are energetically degenerate while applying a spin-flip to the new reference state, which is the singlet state, requires the energy K.

In order to transform the Hamiltonian, we choose the generator

$$\eta = \sum_{\substack{n,m \\ k,q,\alpha,\beta}} \eta^{kq\alpha\beta}_{nm} |k\rangle\langle q| : c^\dagger_{n\alpha} c_{m\beta} : . \tag{7.62}$$

The most obvious choice for the coefficients would be

$$\eta^{kq\alpha\beta}_{nm} = \mathrm{sgn}\left(E_k - E_q + \varepsilon_n - \varepsilon_m\right) J^{kq\alpha\beta}_{nm}. \tag{7.63}$$

We will see, however, that this choice leads to problems because including states that couple two triplet states leads to divergence. Luckily enough, we do not necessarily need to turn these terms away as we only want to eliminate terms that couple to the ground state of H_D. Thus, we

only eliminate terms that couple triplet states to the singlet. The generator in this case is of the form

$$\eta_{nm}^{kq\alpha\beta} = f_{kq}\mathrm{sgn}\left(E_k - E_q + \varepsilon_n - \varepsilon_m\right) J_{nm}^{kq\alpha\beta} \tag{7.64}$$

where the coefficient

$$f_{kq} = \begin{cases} 1 & \text{if } E_k - E_q \neq 0 \\ 1 & \text{if } k,q = 0 \\ 0 & \text{otherwise} \end{cases} \tag{7.65}$$

includes all terms that couple to the singlet state. In order to construct the flow equation (4.4), we calculate the commutators between η from Eq. (7.62) and H from Eq. (7.57). We truncate terms that are quartic with respect to the bath operators and further neglect the normal-ordering (7.53) of the adapted operator basis because it only affects the order J^3 of E_k. Additional terms which can occur in order J^2 within this approximation are of the form

$$H_\mathrm{V} = \sum_{k,q} V_{kq} |k\rangle\langle q|. \tag{7.66}$$

Comparing the coefficients to the derivative of H leads to the flow equation (4.4)

$$\begin{aligned} \partial_l J_{nm}^{kq\alpha\beta} &= \left(E_q - E_k + \varepsilon_m - \varepsilon_n\right) \eta_{nm}^{kq\alpha\beta} \\ &+ \sum_{\gamma,p}\sum_{x} \left(\eta_{nx}^{pq\alpha\gamma} J_{xm}^{kp\gamma\beta} - \eta_{xm}^{kp\gamma\beta} J_{nx}^{pq\alpha\gamma}\right) \theta_x \\ &+ \sum_{\gamma,p}\sum_{x} \left(\eta_{nx}^{kp\alpha\gamma} J_{xm}^{pq\gamma\beta} - \eta_{xm}^{pq\gamma\beta} J_{nx}^{kp\alpha\gamma}\right) (1-\theta_x) \\ \partial_l V_{kq} &= \sum_{\substack{n,m \\ p,\alpha,\beta}} \left(\eta_{nm}^{kp\alpha\beta} J_{mn}^{pq\beta\alpha} - \eta_{mn}^{pq\beta\alpha} J_{nm}^{kp\alpha\beta}\right) (1-\theta_m)\,\theta_n \end{aligned} \tag{7.67}$$

with $\theta_n = \langle c_{n\sigma}^\dagger c_{n\sigma}\rangle$ which stems from the normal-ordering of the bath operators with respect to the Fermi sea.

Flow of E_k and V_{kq}

A nice feature of Eq. (7.67) is that no terms V_{kq} occur for $k \neq q$. The reason for this is that at least one coefficient on the right-hand side of the differential equation for V_{kq} is forbidden by spin conservation or the right-hand side cancels due to symmetry as long as $k \neq q$. For $k = q$, on the contrary, the change of E_k (given by the change of V_{kk}) is finite. The energies of the triplet states $E_{1,2,3}$ remain degenerate during the whole flow which holds true for all parameters. This fact allows us to define an effective coupling $K(l) = E_i(l) - E_0(l)$ with $i = 1,2,3$.

Fig. 7.11 shows the flow of the diagonal elements E_k.

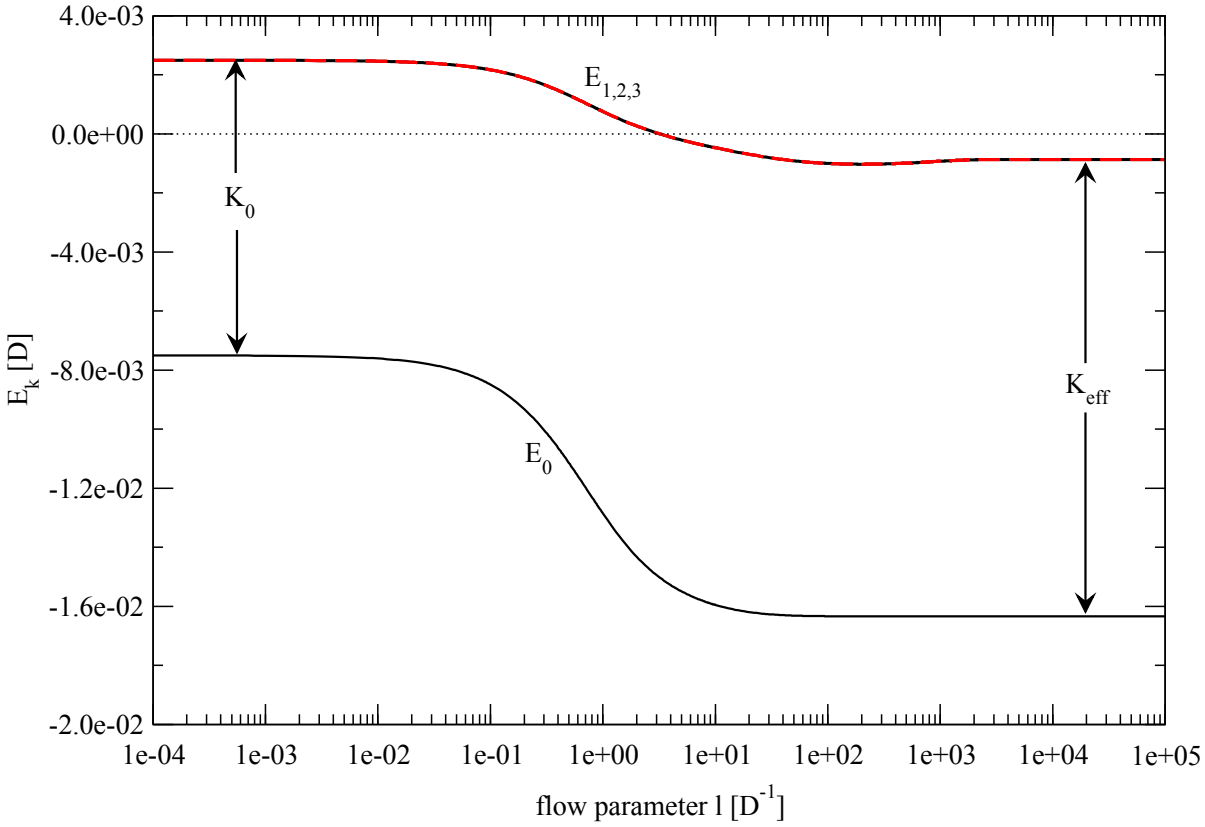

Figure 7.11: Flow of the energy levels E_k from the DEQ (7.67) for the Kondo model coupled to an auxiliary spin where $\partial_l E_k = \partial_l V_{kk}$ with $N = 40$, $\Lambda = 2$, $2\rho_0 J = 0.12$ and $2\rho_0 K(0) = 0.01$. The energy levels of the triplet states $E_{1,2,3}$ remain degenerate during the flow which allows the definition of a flowing coupling $K(l)$ that increases during the flow.

7.4.3 Vanishing Coupling and Kondo Energy Scale

In order to verify whether the DEQ (7.67) is correct and to understand how the truncation schemes for the adapted and the conventional operator basis are related to each other, we study the case $K = 0$.

When we neglect the flow of the coefficients $J_{nm}^{kk\alpha\alpha}$ and set

$$J_{nm}^{kq\alpha\beta} = J_{nm} \sum_{\mu} \alpha_{kq}^{\mu} \sigma_{\alpha\beta}^{\mu}, \quad \eta_{nm}^{kq\alpha\beta} = \eta_{nm} \sum_{\mu} \alpha_{kq}^{\mu} \sigma_{\alpha\beta}^{\mu}, \tag{7.68}$$

which is in agreement with the starting value (7.59), we find

$$\left[\partial_l J_{nm} + (\varepsilon_n - \varepsilon_m)\,\eta_{nm} + \sum_x (\eta_{nx} J_{xm} - \eta_{xm} J_{nx})\,(1 - 2\theta_x)\right] \sum_{\mu} \alpha_{kq}^{\mu} \sigma_{\alpha\beta}^{\mu} = 0. \tag{7.69}$$

This shows that Eq. (7.68) holds true during the whole flow and that the differential equation for J_{nm} coincides with the initial DEQ for the Kondo model without the auxiliary spin (7.40). When taking $J_{nm}^{kk\alpha\alpha}$ into account and using

$$J_{nm}^{kq\alpha\beta} = J_{nm} \sum_{\mu} \alpha_{kq}^{\mu} \sigma_{\alpha\beta}^{\mu} + t_{nm} \delta_{kq} \delta_{\alpha\beta}, \quad \eta_{nm}^{kq\alpha\beta} = \eta_{nm}^{J} \sum_{\mu} \alpha_{kq}^{\mu} \sigma_{\alpha\beta}^{\mu} + \eta_{nm}^{t} \delta_{kq} \delta_{\alpha\beta}, \tag{7.70}$$

we find the differential equation for the coefficients

$$\begin{aligned}\partial_l J_{nm} &= \sum_x \left(\eta^J_{nx} t_{xm} - \eta^J_{xm} t_{nx} + \eta^t_{nx} J_{xm} - \eta^t_{xm} J_{nx}\right) \\ &- \sum_x \left[\eta^J_{nx} J_{xm} - \eta^J_{xm} J_{nx}\right](1-2\theta_x) \\ \partial_l t_{nm} &= \sum_x \left(\eta^t_{nx} t_{xm} - \eta^t_{xm} t_{nx}\right) + \frac{3}{4}\sum_x \left(\eta^J_{nx} J_{xm} - \eta^J_{xm} J_{nx}\right).\end{aligned} \tag{7.71}$$

This coincides with the DEQ (4.87) in the conventional operator basis when taking hopping terms into consideration. The truncation scheme we use in the following sections is the one where the terms $J^{kk\alpha\alpha}_{nm}$ are taken into account.

Note that this is, however, not the main difference to the approach before. For $K > 0$, we find an IR-cutoff due to the coupling K and thus converging differential equations independent of the question if we take the couplings $J^{kk\alpha\alpha}_{nm}$ (which are only a small fraction of all couplings $J^{kq\alpha\beta}_{nm}$) into account.

7.4.4 IR-Approximation

Before analyzing the full differential equation (7.67) numerically it is useful to study the behavior at low energies close to the Fermi level $\varepsilon_\mathrm{F} = 0$. We use the continuum limit (cf. Sec. 6.8.4)

$$\varepsilon_n \to \varepsilon\ , \quad \gamma_n \to \rho_0 \mathrm{d}x\ , \quad \frac{J^{kq\alpha\beta}_{nm}}{\gamma_n \gamma_m} \to J^{kq\alpha\beta}\left(\varepsilon, \varepsilon'\right) \tag{7.72}$$

of the DEQ (7.67) which leads to

$$\begin{aligned}\partial_l J^{kq\alpha\beta}_{\varepsilon\varepsilon'} &= \left(E_q - E_k + \varepsilon' - \varepsilon\right)\eta^{kq\alpha\beta}_{\varepsilon\varepsilon'} \\ &+ \sum_{\gamma,p}\rho_0 \int_{-D}^{D}\left(\eta^{pq\alpha\gamma}_{\varepsilon z} J^{kp\gamma\beta}_{z\varepsilon'} - \eta^{kp\gamma\beta}_{z\varepsilon'} J^{pq\alpha\gamma}_{\varepsilon z}\right)\theta_z \,\mathrm{d}z \\ &+ \sum_{\gamma,p}\rho_0 \int_{-D}^{D}\left(\eta^{kp\alpha\gamma}_{\varepsilon z} J^{pq\gamma\beta}_{z\varepsilon'} - \eta^{pq\gamma\beta}_{z\varepsilon'} J^{kp\alpha\gamma}_{\varepsilon z}\right)(1-\theta_z)\,\mathrm{d}z\end{aligned} \tag{7.73}$$

and apply the IR-approximation in the form

$$J^{kq\alpha\beta}_{\varepsilon\varepsilon'} = \tilde{J}^{kq\alpha\beta}_{\varepsilon_\mathrm{F}\varepsilon_\mathrm{F}} \mathrm{e}^{-f_{kq}\left|E_k - E_q + \varepsilon - \varepsilon'\right| l}. \tag{7.74}$$

Using Eq. (7.74) in Eq. (7.73) for $\varepsilon = \varepsilon' = \varepsilon_\mathrm{F}$ yields

$$\begin{aligned}&\partial_l J^{kq\alpha\beta}_{\varepsilon_\mathrm{F}\varepsilon_\mathrm{F}} = -f_{kq}\left|E_q - E_k\right| J^{kq\alpha\beta}_{\varepsilon_\mathrm{F}\varepsilon_\mathrm{F}} \\ &+ \sum_{\gamma,p}\rho_0 \int_0^D f_{pq}\,\mathrm{sgn}\left(\Delta E_{pq} + z\right)\mathrm{e}^{-\left(f_{pq}\left|\Delta E_{pq}+z\right| + f_{kp}\left|\Delta E_{kp}-z\right|\right)l}\mathrm{d}z\left(\tilde{J}^{pq\alpha\gamma}_{\varepsilon_\mathrm{F}\varepsilon_\mathrm{F}}\tilde{J}^{kp\gamma\beta}_{\varepsilon_\mathrm{F}\varepsilon_\mathrm{F}} - \tilde{J}^{kp\alpha\gamma}_{\varepsilon_\mathrm{F}\varepsilon_\mathrm{F}}\tilde{J}^{pq\gamma\beta}_{\varepsilon_\mathrm{F}\varepsilon_\mathrm{F}}\right) \\ &- \sum_{\gamma,p}\rho_0 \int_0^D f_{kp}\,\mathrm{sgn}\left(\Delta E_{kp} - z\right)\mathrm{e}^{-\left(f_{pq}\left|\Delta E_{pq}+z\right| + f_{kp}\left|\Delta E_{kp}-z\right|\right)l}\mathrm{d}z\left(\tilde{J}^{pq\alpha\gamma}_{\varepsilon_\mathrm{F}\varepsilon_\mathrm{F}}\tilde{J}^{kp\gamma\beta}_{\varepsilon_\mathrm{F}\varepsilon_\mathrm{F}} - \tilde{J}^{kp\alpha\gamma}_{\varepsilon_\mathrm{F}\varepsilon_\mathrm{F}}\tilde{J}^{pq\gamma\beta}_{\varepsilon_\mathrm{F}\varepsilon_\mathrm{F}}\right)\end{aligned} \tag{7.75}$$

where

$$\Delta E_{kq} = E_k - E_q. \tag{7.76}$$

The factor f_{kq} equals one for all k and q when using the full generator (7.63) and is given by Eq. (7.65) when using the generator (7.64) which only includes terms that couple to the singlet state. We can calculate the integrals for $K \geq 0$ using the symmetries from Eq. (9.64), cf. App. 9.10.2, and by exploiting the following properties of the coefficients

$$\begin{aligned} f_{0i} &= f_{0j} \quad \text{for all } i,j>0 \\ f_{0i} &= f_{i0} \quad \text{for all } i>0 \\ f_{ij} &= f_{i'j'} \quad \text{for all } i,j,i',j'>0 \end{aligned} \tag{7.77}$$

which hold true for both the generators given by Eq. (7.63) and Eq. (7.64), respectively. Thus, the DEQ (7.75) simplifies to

$$\begin{aligned} \partial_l J^{01\uparrow\downarrow}_{\varepsilon_\mathrm{F}\varepsilon_\mathrm{F}} &= -|K| J^{01\uparrow\downarrow}_{\varepsilon_\mathrm{F}\varepsilon_\mathrm{F}} + \frac{4\rho_0}{l}\left[1-\mathrm{e}^{-(1+f_{11})Dl}\right]\mathrm{e}^{-Kl}\tilde{J}^{01\uparrow\downarrow}_{\varepsilon_\mathrm{F}\varepsilon_\mathrm{F}}\tilde{J}^{11\uparrow\uparrow}_{\varepsilon_\mathrm{F}\varepsilon_\mathrm{F}} \\ \partial_l \tilde{J}^{11\uparrow\uparrow}_{\varepsilon_\mathrm{F}\varepsilon_\mathrm{F}} &= -\frac{\rho_0}{l}\left[\mathrm{e}^{-2(D-K)l}-\mathrm{e}^{-2Kl}\right]\left(\tilde{J}^{01\uparrow\downarrow}_{\varepsilon_\mathrm{F}\varepsilon_\mathrm{F}}\right)^2 + \frac{2f_{11}\rho_0}{l}\left[1-\mathrm{e}^{-2Dl}\right]\left(\tilde{J}^{11\uparrow\uparrow}_{\varepsilon_\mathrm{F}\varepsilon_\mathrm{F}}\right)^2. \end{aligned} \tag{7.78}$$

For a more detailed calculation, see App. 9.10.4. As we performed the calculation for both generators, the one from Eq. (7.63) as well as the one from Eq. (7.64), we can now study the difference between them. If we use the full generator (7.63), all $f_{kq} = 1$. In this case, a term is present that is not exponentially suppressed by a factor e^{-Kl} (the second term in $\partial_l J^{11\uparrow\uparrow}_{\varepsilon_\mathrm{F}\varepsilon_\mathrm{F}}$), i.e., the differential equation diverges due to an integral over l^{-1}.

If we use the generator (7.64) which does not include terms that connect different triplet states, the factor f_{11} is zero. Consequently, the term that is not exponentially suppressed vanishes and thus we expect convergence. This result is convenient as only terms which couple non-degenerate states will eventually converge. When using the adapted reference state, the excitation from the singlet to a triplet state requires an energy K and thus leads to a term e^{-Kl}. The triplet states are degenerate and thus no factor occurs that could lead to convergence as the exponent is zero.

Using the generator (7.64) that only includes terms that couple to the singlet state yields the final DEQ

$$\begin{aligned} \partial_l J^{01\uparrow\downarrow}_{\varepsilon_\mathrm{F}\varepsilon_\mathrm{F}} &= -|K| J^{01\uparrow\downarrow}_{\varepsilon_\mathrm{F}\varepsilon_\mathrm{F}} + \frac{4\rho_0}{l}\left[1-\mathrm{e}^{-Dl}\right]\mathrm{e}^{-Kl}\tilde{J}^{01\uparrow\downarrow}_{\varepsilon_\mathrm{F}\varepsilon_\mathrm{F}}\tilde{J}^{11\uparrow\uparrow}_{\varepsilon_\mathrm{F}\varepsilon_\mathrm{F}} \\ \partial_l \tilde{J}^{11\uparrow\uparrow}_{\varepsilon_\mathrm{F}\varepsilon_\mathrm{F}} &= -\frac{\rho_0}{l}\left[\mathrm{e}^{-2(D-K)l}-\mathrm{e}^{-2Kl}\right]\left(\tilde{J}^{01\uparrow\downarrow}_{\varepsilon_\mathrm{F}\varepsilon_\mathrm{F}}\right)^2 \end{aligned} \tag{7.79}$$

where all terms are suppressed by a factor e^{-Kl}. This factor suppresses the integrals over l^{-1} exponentially and thus implies convergence.

Kondo Energy Scale

We can verify that Eq. (7.78) for $K = 0$ and the full generator (7.63), where all $f_{kq} = 1$, yields the same results as the approach without the auxiliary spin. Eq. (7.78) then becomes

$$\begin{aligned} \partial_l J^{01\uparrow\downarrow}_{\varepsilon_\mathrm{F}\varepsilon_\mathrm{F}} &= \frac{4\rho_0}{l}\left[1-\mathrm{e}^{-2Dl}\right]J^{01\uparrow\downarrow}_{\varepsilon_\mathrm{F}\varepsilon_\mathrm{F}}J^{11\uparrow\uparrow}_{\varepsilon_\mathrm{F}\varepsilon_\mathrm{F}} \\ \partial_l J^{11\uparrow\uparrow}_{\varepsilon_\mathrm{F}\varepsilon_\mathrm{F}} &= \frac{\rho_0}{l}\left[1-\mathrm{e}^{-2Dl}\right]\left(\left(J^{01\uparrow\downarrow}_{\varepsilon_\mathrm{F}\varepsilon_\mathrm{F}}\right)^2 + 2\left(J^{11\uparrow\uparrow}_{\varepsilon_\mathrm{F}\varepsilon_\mathrm{F}}\right)^2\right). \end{aligned} \tag{7.80}$$

Multiplying the first equation with $-\frac{1}{\sqrt{2}}$ and adding the two equations yields

$$\partial_l \tilde{J} \;=\; \frac{2\rho_0}{l}\left[1-\mathrm{e}^{-2Dl}\right]\tilde{J}^2 \tag{7.81}$$

with

$$\tilde{J} \;=\; J^{11\uparrow\uparrow}_{\varepsilon_\mathrm{F}\varepsilon_\mathrm{F}} - \frac{1}{\sqrt{2}} J^{01\uparrow\downarrow}_{\varepsilon_\mathrm{F}\varepsilon_\mathrm{F}}. \tag{7.82}$$

From the starting values (7.59) (cf. App. 9.10.1) we find that the starting value for $\tilde{J}$ coincides with the initial J of the conventional Kondo model. Thus Eq. (7.81) is the well-known scaling equation (4.96) of the Kondo model with an isotropic coupling, i.e., the new DEQ (7.67) diverges on the Kondo energy scale for $K = 0$, just as expected.

7.4.5 Numerical Residual Off-Diagonality

The IR-approximation of the last section predicts that the DEQ (7.67) converges. In order to verify this prediction, we additionally solve the full DEQ (7.67) without the IR-approximation numerically and examine the residual off-diagonality.

Fig. 7.12 shows the residual off-diagonality of Eq. (7.67) for the generator (7.64).

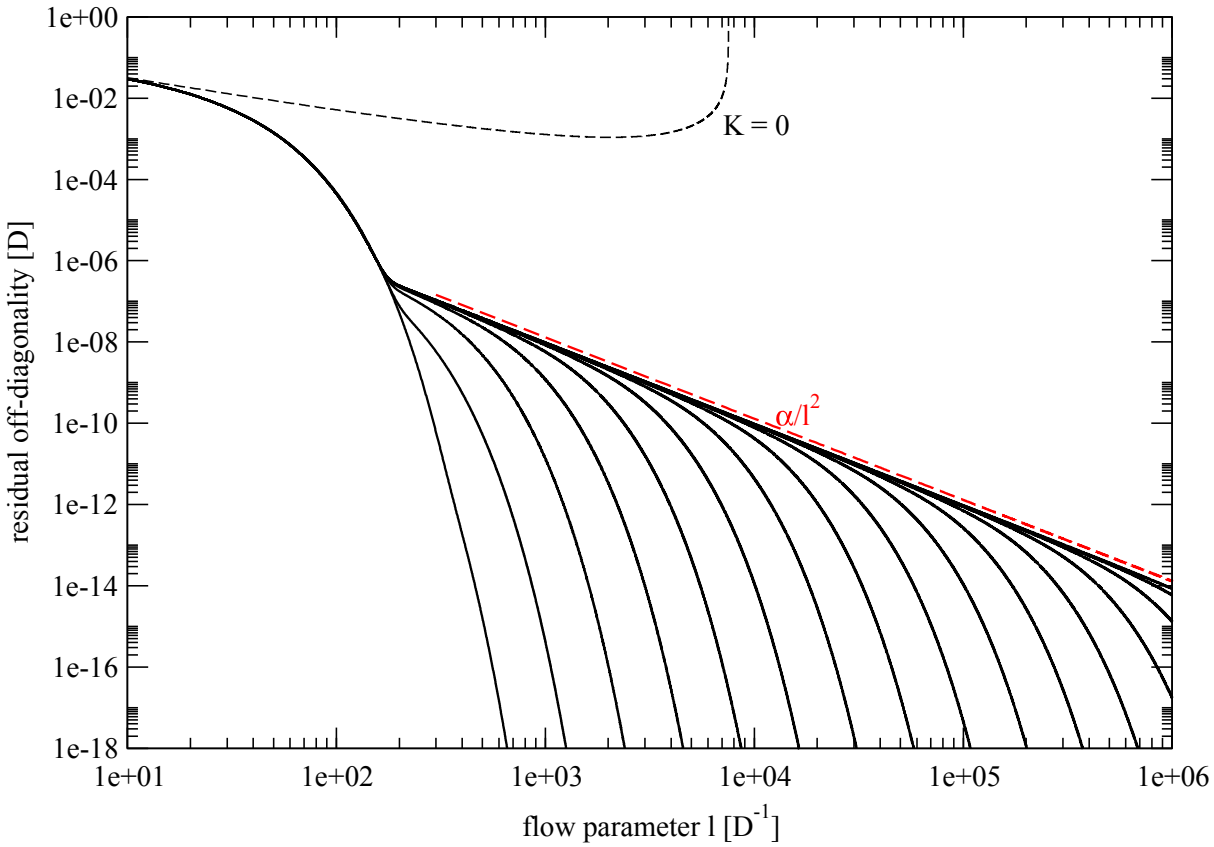

Figure 7.12: Residual off-diagonality for the Kondo model coupled to an auxiliary spin for $\Lambda = 2$, $2\rho_0 J = 0.12$, $2\rho_0 K = 1$ and from left to right: number of energy levels $N = 10, 12, 14, ..., 38, 40$. The differential equation (7.67) converges for $K > 0$ while it diverges for $K = 0$ (dashed line). For intermediate l, the residual off-diagonality is described by a power law αl^{-2}. For large l (beyond the inverse of the lowest energy scale in the system $E_N \propto \Lambda^{-\frac{N}{2}}$), the ROD decreases exponentially.

We find a power law ROD $\propto l^{-2}$ for the residual off-diagonality for intermediate l. At some point beyond the lowest energy scale in the system the residual off-diagonality decreases exponentially. The point beyond which the large l-limit behavior occurs increases exponentially as $\Lambda^{\frac{N}{2}}$ where N denotes the number of energy levels included. The lowest energy scale decreases proportional to $\Lambda^{-\frac{N}{2}}$ and thus the point for which we find the large l-limit behavior is proportional to the lowest energy scale in the system. The dashed line in Fig. 7.12 shows the residual off-diagonality for $K = 0$ which diverges. This result confirms that the new reference state leads to converging differential equations for $K > 0$.

7.5 Adapted Reference State for the Kondo and Anderson Model

In the last sections we introduced new terms to the diagonal part of the Hamiltonian H_{D} from which we derived the reference state as the ground state. The main difference compared to the previous Hamiltonian is that flipping a spin on the impurity requires an energy K which enabled us to find converging differential equations. We achieved this, however, by introducing an auxiliary spin which forces the impurity into a singlet ground state. This made it easy to modify H_{D} but does still not solve the Kondo or Anderson model. The question of the following sections is how to use the knowledge gained in the last sections in order to construct converging differential equations for the Kondo and Anderson model, respectively.

In order to construct converging flow equations, we include diagonal spin-spin interactions in the diagonal Hamiltonian

$$H_{\mathrm{D}} = \sum_{n,\sigma} \varepsilon_n : c^\dagger_{n\sigma} c_{n\sigma} : + \sum_{n,\sigma} J_{nn} \sigma^\mu_{\alpha\beta} \tau^\mu : c^\dagger_{n\alpha} c_{n\beta} : . \tag{7.83}$$

We will choose the ground state of the Hamiltonian (7.83) as the reference state. Thus, we have to understand how the ground state of H_{D} is affected by the local spin-spin interactions J_{nn}. In principle, we have to solve a many-body problem again that is itself almost as difficult as the original Hamiltonian.

Fortunately, we can find the ground state by a much simpler consideration. If the couplings J_{nn} are small enough (like in the early flow), the ground state is the Fermi sea. The reason for this is that the spin-flip contributions have no effect on the Fermi sea as all sites are either empty or doubly occupied. Thus, in order for the spin-flip contributions to affect the reference state, their action must account for the energy loss from removing a particle from the Fermi sea. This can only happen if the couplings J_{nn} are large enough. The couplings J_{nn} increase during the flow until it becomes energetically favorable at one specific site to remove a particle from the Fermi sea so that the spin-flip contribution can act. This happens on one specific site first while the residual part still forms a Fermi sea and is unaffected by the spin-flip contributions.

In order to understand how the ground state will change, we only have to focus on the impurity and the specific site where it becomes energetically favorable to remove a particle. However, we need to include three sites to our analysis because if the negative level $\varepsilon_{\bar{r}} = -\varepsilon_r$ is a level where it is energetically favored to remove a particle from the Fermi sea, then the positive level ε_r yields the same energy when adding a particle to the Fermi sea due to particle-hole symmetry.

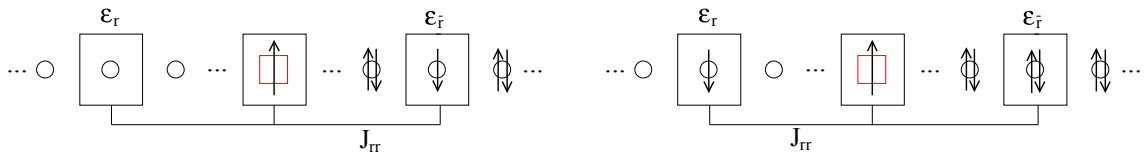

Figure 7.13: Part of the Hamiltonian H_r which consists of the sites on which it first becomes energetically favorable to remove a particle from the Fermi sea so that the spin-flip term can act on the respective site. Because of the particle-hole symmetry, removing a particle from a negative level results in the same energy loss as adding a particle to the corresponding positive level.

Thus, we only need to focus on

$$H_\mathrm{r} = \sum_\sigma \varepsilon_r \left(c^\dagger_{r\sigma} c_{r\sigma} - c^\dagger_{\bar{r}\sigma} c_{\bar{r}\sigma} \right) + J_{rr} \sum_\mu \sum_{\alpha,\beta} \sigma^\mu_{\alpha\beta} \tau^\mu \left(c^\dagger_{r\alpha} c_{r\beta} + c^\dagger_{\bar{r}\alpha} c_{\bar{r}\beta} \right) \tag{7.84}$$

where $\bar{r}$ labels operators acting on the site with energy $\varepsilon_{\bar{r}} = -\varepsilon_r$. This is a problem that can be solved by exact diagonalization and we find 32 eigenstates[8] which are given in App. 9.11.1.

In order to test the adapted approach and in order to keep the numerical calculation effort tractable, we will neglect some of these eigenstates. The states that are *not* neglected are:

1. The ones which describe the spin-spin coupling, namely the singlet state $|s^\pm\rangle$ and the triplet states $|t_i^\pm\rangle$.

2. The Fermi sea $|\mathrm{FS},\sigma\rangle$ because the reference state is changed when the singlet and the Fermi sea have the same energy, i.e., these states compete to become the ground state.

3. The state $|\tilde{\sigma}\rangle$ (cf. Eq. (7.86)) because it has also the potential to become the ground state.

These are 12 (cf. Eqs. (7.85) and (7.86)) out of the 32 eigenstates of the Hamiltonian (7.84). We neglect the remaining 20 eigenstates in order to keep the numerical calculation effort tractable. The method does not rely on this approximation but expanding in the full adapted operator basis would be less transparent (e.g. finding all symmetries) and the computational effort would increase significantly. This approximation is very useful in order to understand the approach and to verify if it works. Nevertheless, it would be an interesting task for following works to implement the flow equations without this approximation in order to study its influence or to study if one can neglect even more states.

App. 9.11.1 shows all eigenstates of the Hamiltonian (7.84) and also the ones that are discarded. We neglect all states with an energy that is higher-lying than the energies of the triplet states. The remaining states are

$$\begin{aligned}
|0\rangle = |s^-\rangle &= \frac{1}{\sqrt{2}}\left(|0,\uparrow,\downarrow\rangle - |0,\downarrow,\uparrow\rangle\right) & |4\rangle = |s^+\rangle &= \frac{1}{\sqrt{2}}\left(|\downarrow,\uparrow,\uparrow\downarrow\rangle - |\uparrow,\downarrow,\uparrow\downarrow\rangle\right) \\
|1\rangle = |t_1^-\rangle &= |0,\uparrow,\uparrow\rangle & |5\rangle = |t_1^+\rangle &= |\uparrow,\uparrow,\uparrow\downarrow\rangle \\
|2\rangle = |t_2^-\rangle &= \frac{1}{\sqrt{2}}\left(|0,\uparrow,\downarrow\rangle + |0,\downarrow,\uparrow\rangle\right) & |6\rangle = |t_2^+\rangle &= \frac{1}{\sqrt{2}}\left(|\downarrow,\uparrow,\uparrow\downarrow\rangle + |\uparrow,\downarrow,\uparrow\downarrow\rangle\right) \\
|3\rangle = |t_3^-\rangle &= |0,\downarrow,\downarrow\rangle & |7\rangle = |t_3^+\rangle &= |\downarrow,\downarrow,\uparrow\downarrow\rangle.
\end{aligned} \tag{7.85}$$

[8] Following the same procedure for the Anderson model would, in principle, lead to 64 eigenstates but as we project on a singly occupied impurity state before changing the reference state, we also find 32 eigenstates.

and further

$$
\begin{aligned}
|8\rangle &= |\mathrm{FS},\uparrow\rangle = |0,\uparrow,\uparrow\downarrow\rangle \\
|9\rangle &= |\mathrm{FS},\downarrow\rangle = |0,\downarrow,\uparrow\downarrow\rangle \\
|10\rangle &= |\tilde{\uparrow}\rangle = \frac{1}{\sqrt{6}}\left[|\uparrow,\uparrow,\downarrow\rangle - 2|\uparrow,\downarrow,\uparrow\rangle + |\downarrow,\uparrow,\uparrow\rangle\right] \\
|11\rangle &= |\tilde{\downarrow}\rangle = \frac{1}{\sqrt{6}}\left[|\downarrow,\downarrow,\uparrow\rangle - 2|\downarrow,\uparrow,\downarrow\rangle + |\uparrow,\downarrow,\downarrow\rangle\right].
\end{aligned} \tag{7.86}
$$

The notation refers to the following levels

$$
|\text{positive level } \varepsilon_r, \text{impurity level } \varepsilon_\mathrm{d}, \text{negative level } \varepsilon_{\bar{r}}\rangle \tag{7.87}
$$

with $\varepsilon_r > 0$ and $\varepsilon_{\bar{r}} = -\varepsilon_r$. The eigenvalues of these states are given by

$$
\begin{aligned}
E_{s^\pm} = -\frac{3J_{rr}}{2} - \varepsilon_r \quad , \qquad E_{t_i^\pm} = \frac{J_{rr}}{2} - \varepsilon_r \quad (i = 1,2,3) \\
E_{\mathrm{FS},\sigma} = -2\varepsilon_r \quad , \qquad E_{\tilde{\sigma}} = -2J_{rr}
\end{aligned} \tag{7.88}
$$

and thus out of the eigenstates (7.85) and (7.86) possible ground states are

$$
\begin{aligned}
|\mathrm{FS},\sigma\rangle &= |0,\sigma,\uparrow\downarrow\rangle\,, \quad E_{\mathrm{FS},\sigma} = -2\varepsilon_r \\
|s^-\rangle &= \frac{1}{\sqrt{2}}\left(|0,\uparrow,\downarrow\rangle - |0,\downarrow,\uparrow\rangle\right), \quad E_{s^-} = -\frac{3J_{rr}}{2} - \varepsilon_r \\
|s^+\rangle &= \frac{1}{\sqrt{2}}\left(|\downarrow,\uparrow,\uparrow\downarrow\rangle - |\uparrow,\downarrow,\uparrow\downarrow\rangle\right), \quad E_{s^+} = -\frac{3J_{rr}}{2} - \varepsilon_r \\
|\tilde{\sigma}\rangle &= \frac{1}{\sqrt{6}}\left[|\sigma,\sigma,\bar{\sigma}\rangle - 2|\sigma,\bar{\sigma},\sigma\rangle + |\bar{\sigma},\sigma,\sigma\rangle\right], \quad E_{\tilde{\sigma}} = -2J_{rr}.
\end{aligned} \tag{7.89}
$$

The Fermi sea $|\mathrm{FS},\sigma\rangle$ is the lowest-lying state in the early flow while the singlet state $|s^\pm\rangle$ – formed by the impurity and the positive level ε_r or the negative level $\varepsilon_{\bar{r}}$, respectively – decreases during the ongoing flow until it will eventually become smaller than the Fermi sea. The state $|\tilde{\sigma}\rangle$ becomes the ground state for larger values of J_{rr} and, in contrast to the singlet state, it is a spin carrying state, i.e., the impurity spin is not screened. It is important to note that the singlet state becomes the ground state before the state $|\tilde{\sigma}\rangle$ does when we continuously increase J_{rr}. If this was not the case, the physics would be completely different as the spin of the impurity would not be screened and an effectively ferromagnetic coupling to the remaining bath would arise. But this is not the physics of the Kondo model as in this case the singlet state forms first. The parameter regimes with their respective ground states are given by

- $J_{rr} < \frac{2\varepsilon_r}{3}$: ground state: $|\mathrm{FS},\sigma\rangle$
- $\frac{2\varepsilon_r}{3} < J_{rr} < 2\varepsilon_r$: ground state: $|s^\pm\rangle$
- $J_{rr} > 2\varepsilon_r$: ground state: $|\tilde{\sigma}\rangle$.

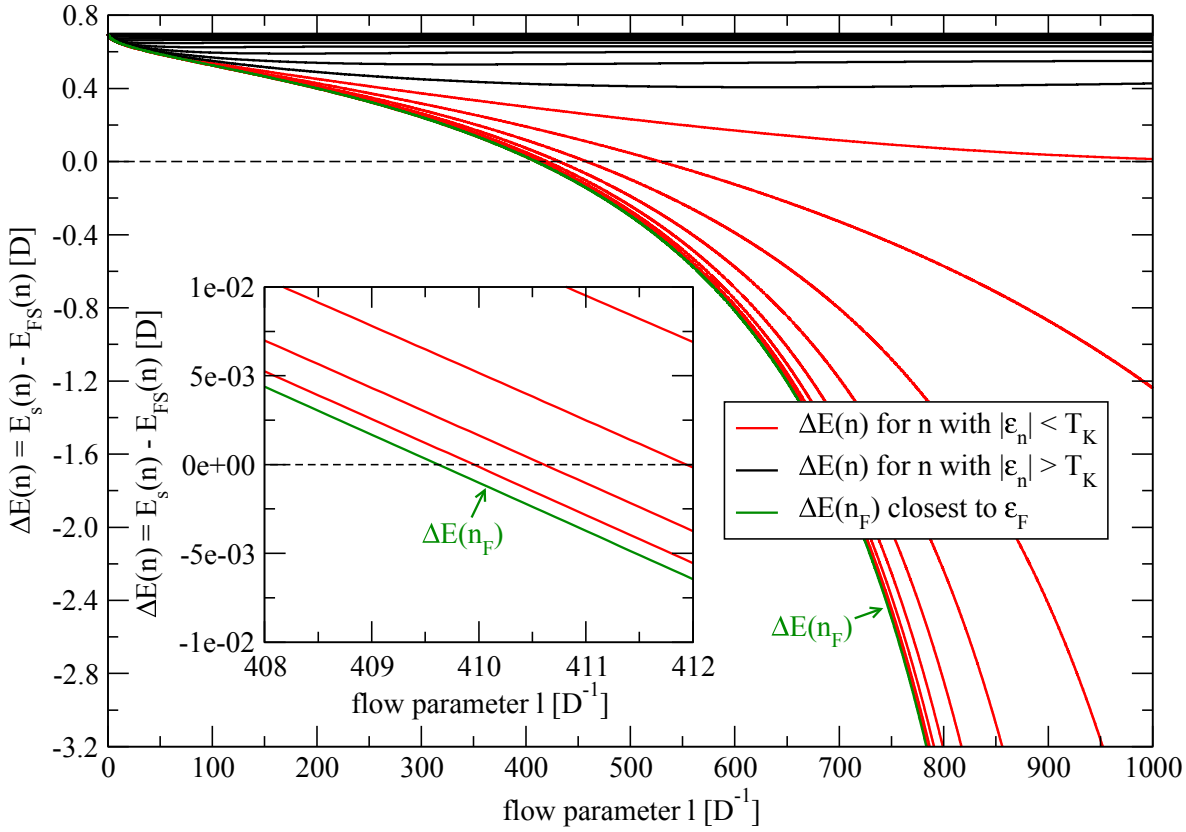

Figure 7.14: Energy difference between the singlet state and the Fermi sea $\Delta E\,(n) = E_s\,(n) - E_{\mathrm{FS}}\,(n)$ from Eq. (7.89) for the **Kondo model** with $N = 40$, $\Lambda = 2$ and $2\rho_0 J = 0.14$. The sites n belong to the negative energy levels and the absolute values of the energies are decreasing from top to bottom. The flow parameter at which the DEQ diverges if the reference state is not changed is given by $l_0 \approx 1127 D^{-1}$ which corresponds to a Kondo temperature $\frac{T_\mathrm{K}}{D} \approx 8.873 \cdot 10^{-4}$. The black lines mark the flow of $\Delta E\,(n)$ at a site n for which $|\varepsilon_n| > T_\mathrm{K}$ while the red lines mark the flow of $\Delta E\,(n)$ at a site n for which $|\varepsilon_n| < T_\mathrm{K}$. At the point where one $\Delta E\,(n)$ crosses zero, the reference state is changed and the singlet state forms at the site n. The green line shows $\Delta E\,(n_\mathrm{F})$ at the site closest to the Fermi level. The inset shows that the site that is closest to the Fermi level forms the singlet first. Because of the particle-hole symmetry, the singlet can be formed equally with both the positive as well as the negative energy level.

As soon as we reach the point where

$$J_{rr}\,(l_0) = \frac{2\varepsilon_r}{3}, \tag{7.90}$$

the singlet state $|s^{\pm}\rangle$ will become the ground state. The singlet state cannot be expressed as a product state and thus Wick's theorem cannot be applied to the respective sites involved in the formation of the singlet. The remaining bath, of course, can still be normal-ordered as before. At the point where the singlet state becomes energetically favorable, we choose the singlet state as the reference state and use the states from Eqs. (7.85) and (7.86) as a new basis. We solve the DEQ (7.40) in the initial operator basis with the Fermi sea as the reference state using the starting values (7.44) which belong to the Kondo model.

We follow the ratio $\frac{J_{nn}}{\varepsilon_n}$ at each site and as soon as the ratio becomes $\frac{J_{nn}}{\varepsilon_n} = \frac{2}{3}$ (cf. Eq. (7.90)) at one energy level ε_r, we change the reference state. The procedure is further explained in Sec. 7.5.4.

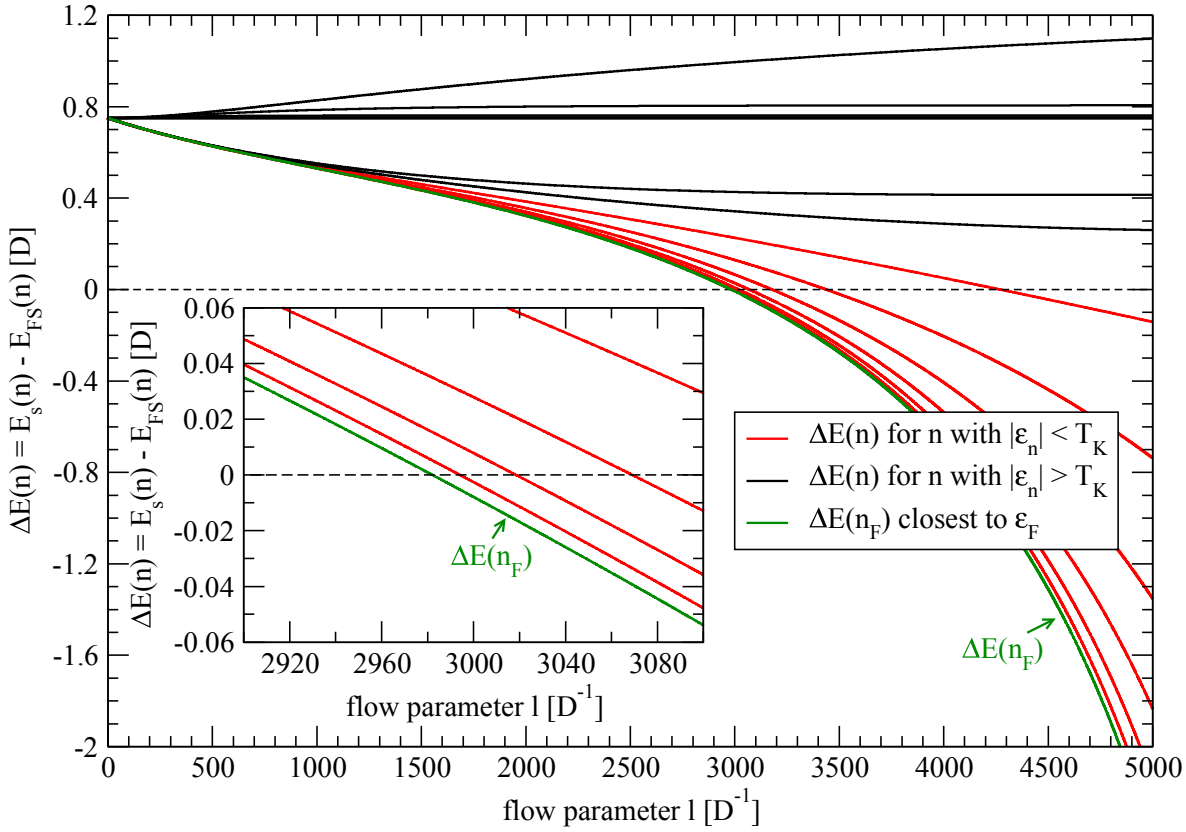

Figure 7.15: Energy difference between the singlet state and the Fermi sea $\Delta E\,(n) = E_s\,(n) - E_{\mathrm{FS}}\,(n)$ from Eq. (7.89) for the **Anderson model** with $N = 40$, $\Lambda = 2$, $\frac{U}{D} = 1.2\mathrm{e}-3$ and $\frac{V}{D} = 0.01414$. The sites n belong to the negative energy levels and the absolute values of the energies are decreasing from top to bottom. The value of the flow parameter at which the DEQ diverges if the reference state is not changed is given by $l_0 \approx 7201 D^{-1}$ which corresponds to a Kondo temperature $\frac{T_{\mathrm{K}}}{D} \approx 1.389 \cdot 10^{-4}$. The black lines mark the flow of $\Delta E\,(n)$ at a site n for which $|\varepsilon_n| > T_{\mathrm{K}}$ while the red lines mark the flow of $\Delta E\,(n)$ at a site n for which $|\varepsilon_n| < T_{\mathrm{K}}$. At the point where one $\Delta E\,(n)$ crosses zero, the reference state is changed and the singlet state forms at the site n. The green line shows $\Delta E\,(n_{\mathrm{F}})$ at the site closest to the Fermi level. The inset shows that the site that is closest to the Fermi level forms the singlet first. Because of the particle-hole symmetry, the singlet can be formed equally with both the positive as well as the negative energy level.

Fig. 7.14 depicts the energy difference between the singlet state and the Fermi sea for the Kondo model. At the point where this difference crosses zero at one site, the reference state is changed. The couplings J_{nn} only diverge for indices n with $|\varepsilon_n| < T_{\mathrm{K}}$ (cf. Sec. 7.3), i.e., only couplings below the Kondo energy scale become large enough to account for the energy loss from removing a particle from the Fermi sea by forming a singlet state. Thus, the approach ensures intrinsically that the singlet will form below the Kondo energy scale. We already know from the results of Fig. 7.6 that the smaller the energy ε_n the faster the ratio $\frac{J_{nn}}{\varepsilon_n}$ increases. Thus, the singlet forms at the lowest energy scale in the system. In a continuum this would be directly at the Fermi level ε_{F}.

Note that the site at which the singlet is formed might change during the subsequent flow. However, this possibility is neglected in the following due to practical reasons. If the site at which the singlet forms changed during the subsequent flow, we would have to change the basis again for the new site while the old site is still expressed in the adapted operator basis. This

would lead to very cumbersome basis changes. Nevertheless, it is a very interesting question at which energy scale the singlet will finally form. For now, however, we are only interested in the question if the approach works at all and not in possible optimizations. Hence, the possible shift of the site which forms the singlet ground state is neglected and we use the site that forms the singlet first throughout the whole flow.

Fig. 7.15 depicts the energy difference between the singlet state and the Fermi sea for the Anderson model. In principle, the procedure is the same as for the Kondo model except that we have to eliminate the hybridization elements additionally. We solve the DEQ (7.18) in order to eliminate the hybridization elements and thereby build up the induced spin-spin interaction which is diagonalized by the DEQ (7.40) at the same time. The further procedure coincides with that of the Kondo model (the procedure is further explained in Sec. 7.5.4).

The spin-spin couplings again increase below the Kondo energy scale until at some point the formation of a singlet state becomes energetically favorable. The singlet always forms at the site closest to the Fermi level because the ratio $\frac{J_{nn}}{\varepsilon_n}$ increases faster at smaller energies $\varepsilon_n \approx 0$.

7.5.1 Hamiltonian in the Adapted Operator Basis

In the next step we determine the effective Hamiltonian and the adapted flow equation after the reference state is changed. We denote the site which is part of the adapted operator basis by r and the flow parameter at which the reference state is changed by l_0. If the flow parameter reaches the point l_0, the effective Hamiltonian is of the form

$$H(l_0) = \sum_{n,\sigma} \varepsilon_n : c^\dagger_{n\sigma} c_{n\sigma} : + \sum_{\mu} \sum_{n,m} \sum_{\alpha,\beta} J_{nm}(l_0)\, \sigma^\mu_{\alpha\beta} \tau^\mu : c^\dagger_{n\alpha} c_{m\beta} : . \tag{7.91}$$

We separate the sites denoted by r and $\bar{r}$ (with $\varepsilon_{\bar{r}} = -\varepsilon_r$) which form the singlet state

$$\begin{aligned}
H(l_0) \;=\; & \sum_{n\neq\pm r,\sigma} \varepsilon_n : c^\dagger_{n\sigma} c_{n\sigma} : + \varepsilon_r \left(: c^\dagger_{r\sigma} c_{r\sigma} : - : c^\dagger_{\bar{r}\sigma} c_{\bar{r}\sigma} : \right) \\
& + \sum_{\mu} \sum_{\alpha,\beta} \left[J_{rr}(l_0)\, \sigma^\mu_{\alpha\beta} \tau^\mu : c^\dagger_{r\alpha} c_{r\beta} : + J_{\bar{r}\bar{r}}(l_0)\, \sigma^\mu_{\alpha\beta} \tau^\mu : c^\dagger_{\bar{r}\alpha} c_{\bar{r}\beta} : \right] \\
& + \sum_{\mu} \sum_{\alpha,\beta} \left[J_{\bar{r}r}(l_0)\, \sigma^\mu_{\alpha\beta} \tau^\mu : c^\dagger_{\bar{r}\alpha} c_{r\beta} : + J_{r\bar{r}}(l_0)\, \sigma^\mu_{\alpha\beta} \tau^\mu : c^\dagger_{r\alpha} c_{\bar{r}\beta} : \right] \\
& + \sum_{\mu} \sum_{\alpha,\beta} \sum_{n,m\neq\pm r} J_{nm}(l_0)\, \sigma^\mu_{\alpha\beta} \tau^\mu : c^\dagger_{n\alpha} c_{m\beta} : \\
& + \sum_{\mu} \sum_{\alpha,\beta} \sum_{n\neq\pm r} \left[J_{nr}(l_0)\, \sigma^\mu_{\alpha\beta} \tau^\mu : c^\dagger_{n\alpha} c_{r\beta} : + J_{rn}(l_0)\, \sigma^\mu_{\alpha\beta} \tau^\mu : c^\dagger_{r\alpha} c_{n\beta} : \right] \\
& + \sum_{\mu} \sum_{\alpha,\beta} \sum_{n\neq\pm r} \left[J_{nr}(l_0)\, \sigma^\mu_{\alpha\beta} \tau^\mu : c^\dagger_{n\alpha} c_{\bar{r}\beta} : + J_{rn}(l_0)\, \sigma^\mu_{\alpha\beta} \tau^\mu : c^\dagger_{\bar{r}\alpha} c_{n\beta} : \right] .
\end{aligned} \tag{7.92}$$

Next, we introduce the adapted operator basis

$$|k\rangle\langle q| = |k\rangle\langle q|_{\text{non-normal-ordered}} - \mathbb{1} \left(\delta_{ks^-} \delta_{qs^-} + \delta_{ks^+} \delta_{qs^+} \right) \tag{7.93}$$

where k and q denote the basis states from Eqs. (7.85) and (7.86). We expand all respective operators in this operator basis which yields

$$\begin{aligned} H(l_0) &= \sum_{n\neq\pm r,\sigma} \varepsilon_n : c^\dagger_{n\sigma} c_{n\sigma} : + \sum_k E_k |k\rangle\langle k| + \sum_{k,q:\, k\neq q} E_{kq} |k\rangle\langle q| \\ &+ \sum_{k,q} \sum_{n,m\neq\pm r} \sum_{\alpha,\beta} J^{kq\alpha\beta}_{nm} |k\rangle\langle q| : c^\dagger_{n\alpha} c_{m\beta} : \\ &+ \sum_{k,q,\sigma} \sum_{n\neq\pm r} \Gamma^{kq\sigma}_n \left(|k\rangle\langle q| c_{n\sigma} + c^\dagger_{n\sigma} |q\rangle\langle k| \right). \end{aligned} \tag{7.94}$$

As we have chosen the basis states so that terms which act only on the site r or only on the site $\bar{r}$ are diagonal, we already know that the E_k are given by the eigenvalues (7.88) where $J_{rr} = J_{rr}(l_0)$ while the starting values for the other coefficients have to be determined from

$$\begin{aligned} J^{kq\alpha\beta}_{nm}(l_0) &= J_{nm}(l_0) \sum_\mu \sigma^\mu_{\alpha\beta} \langle k|\tau^\mu|q\rangle \\ \Gamma^{kq\sigma}_n(l_0) &= J_{nr}(l_0) \sum_{\mu,\alpha} \sigma^\mu_{\alpha\sigma} \langle k|\tau^\mu c^\dagger_{r\alpha}|q\rangle + J_{n\bar{r}}(l_0) \sum_{\mu,\alpha} \sigma^\mu_{\alpha\sigma} \langle k|\tau^\mu c^\dagger_{\bar{r}\alpha}|q\rangle \\ E_{kq}(l_0) &= \sum_\mu \sum_{\alpha,\beta} J_{r\bar{r}} \left(\sigma^\mu_{\alpha\beta} \langle k|\tau^\mu c^\dagger_{\bar{r}\alpha} c_{r\beta}|q\rangle + \left(\sigma^\mu_{\alpha\beta} \langle q|\tau^\mu c^\dagger_{\bar{r}\alpha} c_{r\beta}|k\rangle \right)^* \right). \end{aligned} \tag{7.95}$$

The starting values for terms that couple the triplet and singlet states $s^\pm$ and $t^\pm$ from Eq. (7.85) are identical to the starting values for the Kondo model coupled to an auxiliary spin

$$J^{kq\alpha\beta}_{nm}(l_0) = \sum_\mu J_{nm}(l_0)\, \alpha^\mu_{kq} \sigma^\mu_{\alpha\beta} \quad \text{for} \quad k,q \in s^\pm, t^\pm_i \tag{7.96}$$

where α^μ is given by Eq. (7.55). Only states with the same number of particles couple via $J^{kq\alpha\beta}_{nm}(l_0)$, i.e., t^-_i with s^- and t^+_i with s^+, respectively. The terms that couple the Fermi sea states with different spins are given by

$$J^{kq\alpha\beta}_{nm}(l_0) = \frac{1}{2} \sum_\mu J_{nm}(l_0)\, \sigma^\mu_{\sigma_k\sigma_q} \sigma^\mu_{\alpha\beta} \quad \text{for} \quad k,q \in \mathrm{FS}, \sigma \tag{7.97}$$

where σ_k and σ_q denote the spin of the states k and q. Additionally, there is a coupling between the three-particle states $|\tilde{\sigma}\rangle$ where both the positive as well as the negative level are singly occupied

$$J^{kq\alpha\beta}_{nm}(l_0) = \frac{1}{6} \sum_\mu J_{nm}(l_0)\, s^\mu \sigma^\mu_{\sigma_k\sigma_q} \sigma^\mu_{\alpha\beta} \quad \text{for} \quad k,q \in \tilde{\sigma} \tag{7.98}$$

with $s^x = s^y = 1$ and $s^z = -1$. No further terms are allowed by spin conservation for the couplings $J^{kq\alpha\beta}_{nm}$. The explicit starting values of all non-zero couplings $J^{kq\alpha\beta}_{nm}(l_0)$ are given in App. 9.11.2. Because there is a term in the Hamiltonian (7.92) that couples the sites r and $\bar{r}$ before the reference state is changed, there is a term that couples the Fermi sea to the $|\tilde{\sigma}\rangle$-states from Eq. (7.86). Thus, the only non-zero starting values for E_{kq} are given by

$$E_{8,10} = E_{10,8} = \frac{3}{\sqrt{6}} J_{r\bar{r}}(l_0)\,, \quad E_{9,11} = E_{11,9} = -\frac{3}{\sqrt{6}} J_{r\bar{r}}(l_0)\,. \tag{7.99}$$

The starting values for the $\Gamma^{kq\sigma}_n$-terms cannot be written in a compact way and thus are only given in App. 9.11.2.

7.5.2 Generator and Reference State

The general structure of the generator is chosen to be

$$\begin{aligned}\eta &= \sum_{k,q}\eta^E_{kq}|k\rangle\langle q| + \sum_{k,q}\sum_{\alpha,\beta}\sum_{n,m\neq\pm r}\eta^{kq\alpha\beta}_{nm,J}|k\rangle\langle q| : c^\dagger_{n\alpha}c_{m\beta} : \\ &+ \sum_{k,q,\sigma}\sum_{n\neq\pm r}\eta^{kq\sigma}_{n,\Gamma}\left(|k\rangle\langle q|c_{n\sigma} - c^\dagger_{n\sigma}|q\rangle\langle k|\right).\end{aligned} \tag{7.100}$$

We want to eliminate all terms that couple to the reference state. In contrast to the Kondo model coupled to an auxiliary spin, we have to use a reference ensemble instead of a single reference state because the states $|s^-\rangle$ and $|s^+\rangle$ are degenerate due to the particle-hole symmetry

$$\langle\hat{O}\rangle = \frac{1}{2}\left(\langle\mathrm{FS}|\langle s^-|\hat{O}|s^-\rangle|\mathrm{FS}\rangle + \langle\mathrm{FS}|\langle s^+|\hat{O}|s^+\rangle|\mathrm{FS}\rangle\right). \tag{7.101}$$

The operator basis (7.93) is normal-ordered with respect to the reference ensemble (7.101). In order to eliminate all terms that couple to states of the reference ensemble, we choose the coefficients of the generator to be of the form

$$\begin{aligned}\eta^E_{kq} &= \begin{cases}\mathrm{sgn}\left(E_k - E_q\right)E_{kq} & \text{if } k \text{ or } q \in s^\pm \\ 0 & \text{otherwise}\end{cases} \\ \eta^{kq\alpha\beta}_{nm,J} &= \begin{cases}\mathrm{sgn}\left(E_k - E_q + \varepsilon_n - \varepsilon_m\right)J^{kq\alpha\beta}_{nm} & \text{if } k \text{ or } q \in s^\pm \\ \mathrm{sgn}\left(\varepsilon_n - \varepsilon_m\right)J^{kq\alpha\beta}_{nm} & \text{if } k = q \in s^\pm \\ 0 & \text{otherwise}\end{cases} \\ \eta^{kq\sigma}_{n,\Gamma} &= \begin{cases}\mathrm{sgn}\left(E_k - E_q - \varepsilon_n\right)\Gamma^{kq\sigma}_n & \text{if } k \text{ or } q \in s^\pm \\ 0 & \text{otherwise}\end{cases}.\end{aligned} \tag{7.102}$$

7.5.3 Flow Equation

In order to obtain the adapted flow equation (4.4), we have to commute the generator (7.100) with the Hamiltonian (7.94). We truncate terms with a quartic bath-operator structure. The flow equation is of the form

$$\begin{aligned}\partial_l E_{kq} &= \left(E_{qq} - E_{kk}\right)\eta^E_{kq} + \sum_{p\neq q}\eta^E_{kp}E_{pq} - \sum_{p\neq k}\eta^E_{pq}E_{kp} \\ &+ \sum_{p}\sum_{\alpha,\beta}\sum_{n,m\neq\pm r}\left(\eta^{kp\alpha\beta}_{nm,J}J^{pq\beta\alpha}_{mn} - \eta^{pq\alpha\beta}_{mn,J}J^{kp\beta\alpha}_{nm}\right)\theta_n\left(1-\theta_m\right) \\ &- \sum_{n\neq\pm r}\sum_{p,\gamma}\left(\eta^{pk\gamma}_{n,\Gamma}\Gamma^{pq\gamma}_n + \eta^{pq\gamma}_{n,\Gamma}\Gamma^{pk\gamma}_n\right)\theta_n \\ &+ \sum_{n\neq\pm r}\sum_{p,\gamma}\left(\eta^{kp\gamma}_{n,\Gamma}\Gamma^{qp\gamma}_n + \eta^{qp\gamma}_{n,\Gamma}\Gamma^{kp\gamma}_n\right)\left(1-\theta_n\right)\end{aligned} \tag{7.103a}$$

$$
\begin{aligned}
\partial_l \Gamma_n^{kq\sigma} &= \left(\varepsilon_n + E_{qq} - E_{kk}\right) \eta_{n,\Gamma}^{kq\sigma} \\
&+ \sum_{p\neq q} \left(\eta_{n,\Gamma}^{kp\sigma} E_{pq} - \eta_{pq}^{E} \Gamma_n^{kp\sigma} \right) \\
&- \sum_{p\neq k} \left(\eta_{n,\Gamma}^{pq\sigma} E_{kp} - \eta_{kp}^{E} \Gamma_n^{pq\sigma} \right) \\
&+ \sum_{p} \sum_{x\neq \pm r,\gamma} \left(\eta_{x,\Gamma}^{pq\gamma} J_{xn}^{kp\gamma\sigma} - \eta_{xn,J}^{kp\gamma\sigma} \Gamma_x^{pq\gamma} \right) \theta_x \\
&+ \sum_{p} \sum_{x\neq \pm r,\gamma} \left(\eta_{x,\Gamma}^{kp\gamma} J_{xn}^{pq\gamma\sigma} - \eta_{xn,J}^{pq\gamma\sigma} \Gamma_x^{kp\gamma} \right) (1-\theta_x)
\end{aligned}
\tag{7.103b}
$$

$$
\begin{aligned}
\partial_l J_{nm}^{kq\alpha\beta} &= \left(\varepsilon_m - \varepsilon_n + E_{qq} - E_{kk}\right) \eta_{nm,J}^{kq\alpha\beta} \\
&+ \sum_{p\neq q} \left(\eta_{nm,J}^{kp\alpha\beta} E_{pq} - \eta_{pq}^{E} J_{nm}^{kp\alpha\beta} \right) \\
&- \sum_{p\neq k} \left(\eta_{nm,J}^{pq\alpha\beta} E_{kp} - \eta_{kp}^{E} J_{nm}^{pq\alpha\beta} \right) \\
&+ \sum_{x\neq \pm r,\gamma,p} \left(\eta_{nx,J}^{pq\alpha\gamma} J_{xm}^{kp\gamma\beta} - \eta_{xm,J}^{kp\gamma\beta} J_{nx}^{pq\alpha\gamma} \right) \theta_x \\
&+ \sum_{x\neq \pm r,\gamma,p} \left(\eta_{nx,J}^{kp\alpha\gamma} J_{xm}^{pq\gamma\beta} - \eta_{xm,J}^{pq\gamma\beta} J_{nx}^{kp\alpha\gamma} \right) (1-\theta_x) \\
&- \sum_{p} \left(\eta_{n,\Gamma}^{pk\alpha} \Gamma_m^{pq\beta} + \eta_{m,\Gamma}^{pq\beta} \Gamma_n^{pk\alpha} + \eta_{n,\Gamma}^{qp\alpha} \Gamma_m^{kp\beta} + \eta_{m,\Gamma}^{kp\beta} \Gamma_n^{qp\alpha} \right).
\end{aligned}
\tag{7.103c}
$$

Note that parts of the flow equation for $J_{nm}^{kq\alpha\beta}$ are of the same structure as for the Kondo model coupled to an auxiliary spin (cf. Eq. (7.67)). In principle, due to the normal-ordering (7.93) hopping terms would emerge which would induce a flow of the on-site energies. The normal-ordering scheme is chosen such that terms emerging in this way always couple to $J_{nm}^{ss\alpha\alpha}$. As $J_{nm}^{ss\alpha\alpha}$ is not present in the initial Hamiltonian at l_0, it is of order J^2. The feedback of such terms on E_k are of order J^3. Thus, we neglect the normal-ordering (7.93) as well.

The number of indices is very large and one should optimize the differential equation by exploiting symmetries. A lot of combinations of the k and q indices, for example, are forbidden by spin conservation which can be used to reduce the numerical calculation effort. The symmetries are given in App. 9.11.3.

7.5.4 Residual Off-Diagonality

In the following sections the results obtained with the adapted approach are presented.

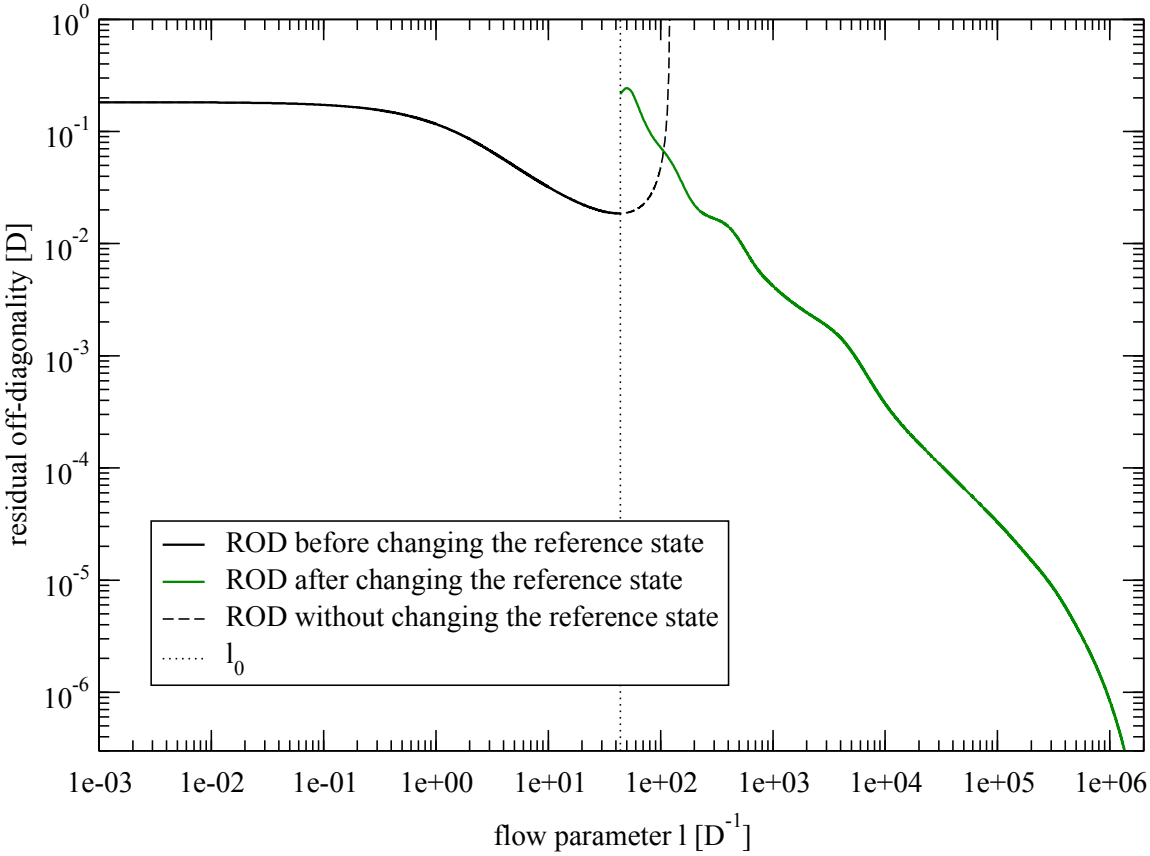

Figure 7.16: Residual off-diagonality for the **Kondo model** with $N = 40$, $\Lambda = 2$ and $2\rho_0 J = 0.2$ where the reference state is changed during the flow. At first, the Fermi sea is chosen to be the reference state and the DEQ (7.40) is solved with the starting values (7.44). The couplings below the Kondo temperature are increasing during the flow which leads to a new reference state at l_0. After changing the reference state, the new differential equations (7.103*a*) - (7.103*c*) are solved which converge in contrast to the initial DEQ (7.40). The ROD for the DEQ (7.40) without changing the reference state is denoted by the dashed line.

Fig. 7.16 depicts the residual off-diagonality of the Kondo model with the adapted approach in order to check if the differential equations (7.103*a*) - (7.103*c*) converge. We start from the Kondo Hamiltonian and solve the differential equation (7.40) with the starting values (7.44) and the Fermi sea as the reference state while following the spin-spin couplings J_{nn} numerically at each site.

For small values of l, the ratio $\frac{J_{nn}}{\varepsilon_n}$ is significantly smaller than $\frac{2}{3}$ (cf. Eq. (7.90)). At some energy scale l_0 the spin-spin coupling J_{nn} becomes large enough so that $\frac{J_{nn}}{\varepsilon_n} = \frac{2}{3}$ is fulfilled. As soon as this happens, we change the reference state and rewrite the Hamiltonian to the form (7.94) in the adapted operator basis (7.85) and (7.86). Additionally, we use the adapted differential equations (7.103*a*) - (7.103*c*) and continue with the flow starting at l_0. The differential equations are solved by a 4th-order Runge-Kutta algorithm.

For small values of l, the residual off-diagonality is the same as for the previous DEQ (7.40) because the reference state is not changed yet. When we switch to the adapted reference state, the residual off-diagonality changes discontinuously because the generator is changed and thus different types of terms are included in the residual off-diagonality.

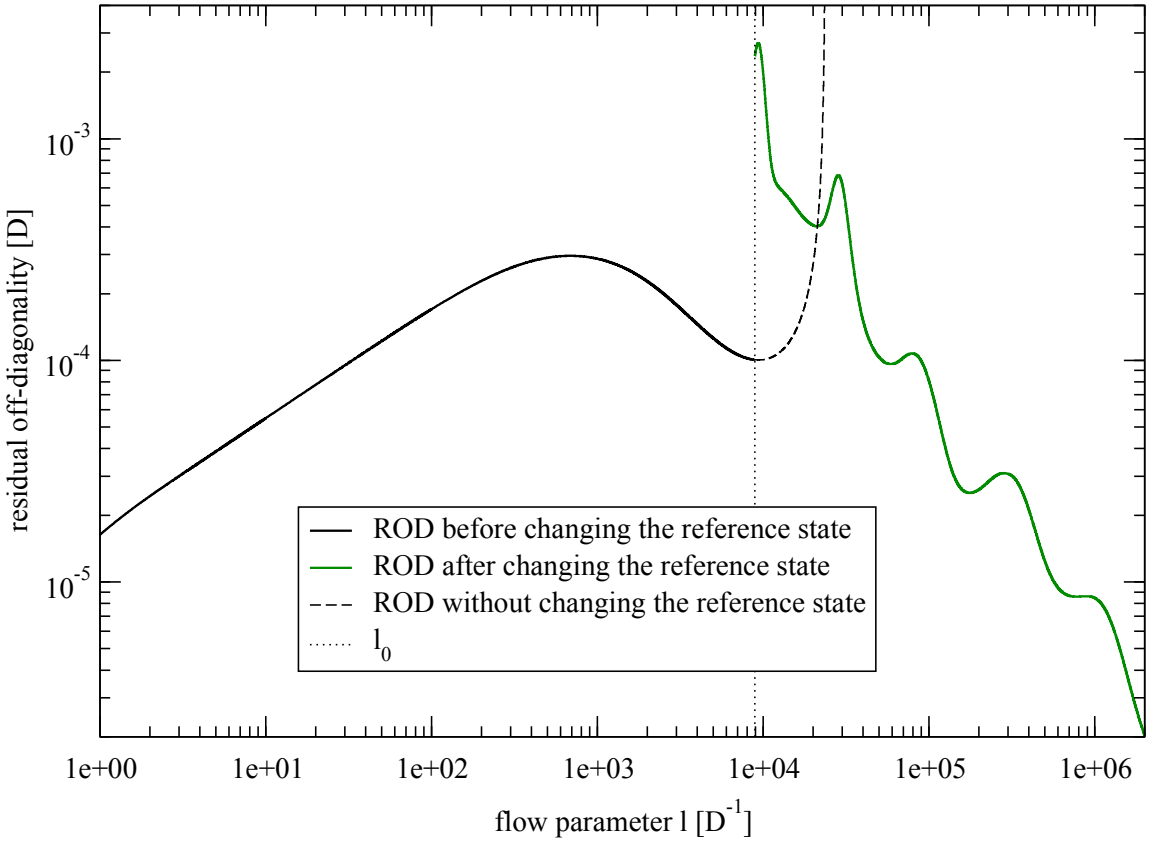

Figure 7.17: Residual off-diagonality for the **Anderson model** with $N = 52$, $\Lambda = 2$, $\frac{U}{D} = 3.2\text{e}-3$ and $\frac{V}{D} = 0.01414$. The first part of the flow only shows the ROD of the DEQ (7.40) for the induced spin-spin interaction $J^{\uparrow\downarrow}_{nm}$ from Eq. (7.12). At first, the ROD is increasing because the spin-spin interaction is zero for $l = 0$ and builds up when turning away the hybridization. The diagonalization of the induced spin-spin interaction leads to divergence (dashed black line). The couplings below the Kondo temperature T_K are increasing during the flow which leads to a change of the reference state at some flow parameter l_0. Subsequently, we solve the DEQs (7.103*a*) - (7.103*c*) which converge in contrast to the initial DEQ (7.40). The adapted approach leads to converging differential equations.

One might wonder why the residual off-diagonality increases after changing the reference state as we turn away less terms than before (we only turn away terms that couple to the singlet state). But one must also bear in mind that we include completely different types of terms into the generator.

Especially, new terms appear in the ROD after changing the reference state which are diagonal in the bath operators. We illustrate this for terms of the form

$$J^{t_i^\pm s^\pm \alpha\beta}_{nn} |t_i^\pm\rangle\langle s^\pm| : c^\dagger_{n\alpha} c_{n\beta} : \tag{7.104}$$

which have starting values at l_0 that are proportional to $J_{nn}(l_0)$. These terms were not turned away by the Continuous Unitary Transformation in the previous operator basis. Thus, these terms are large compared to the terms in the generator before the reference state is changed which are suppressed by a factor $\text{e}^{-|\varepsilon_n - \varepsilon_m| l}$. After the reference state is changed, terms that include diagonal elements in the bath operators are included in the residual off-diagonality.

Thus, the residual off-diagonality increases abruptly when changing the reference state and using the adapted generator.

The dashed line shows the behavior of the residual off-diagonality when the reference state is not changed. In this case, the residual off-diagonality diverges on the Kondo temperature T_K. The adapted flow equations (7.103*a*) - (7.103*c*) are able to prevent this divergence and lead to an effective Hamiltonian with small finite couplings at the Fermi level $\varepsilon_\mathrm{F} = 0$.

Fig. 7.17 shows the residual off-diagonality of the Anderson impurity model obtained with the adapted approach. We start from the Anderson Hamiltonian in the form (7.5) and eliminate the hybridization elements and diagonalize the thereby induced spin-spin interaction H_J from Eq. (7.12) simultaneously by using the differential equations (7.18) and (7.40).

We only plot the ROD of the spin-spin couplings $J_{nm}^{\uparrow\downarrow}$ from Eq. (7.40) because the hybridization elements – which would in principle also contribute to the ROD – are given analytically by Eq. (7.25). For small values of l, the residual off-diagonality increases as the spin-spin couplings $J_{nm}^{\uparrow\downarrow}$ are generated due to the elimination of the hybridization elements which are given by Eq. (7.25). At some point during the flow, the hybridization elements become negligible. The action of the induced spin-spin interaction on itself from Eq. (7.40) is now the driving part of the flow equation which leads to diverging couplings (dashed black line).

When the formation of a singlet state becomes energetically favorable, we first project the Anderson Hamiltonian to a singly occupied impurity state. This can be done because l_0 is far beyond the U-energy scale and thus the charge fluctuations of the impurity will not play a significant role in the subsequent flow.

The couplings $J_{nm}^{\pm}$ and $J_{nm}^{\bar{n}}$ vanish due to this projection. Using the spin-rotation symmetry (7.39) for $J_{nm,\sigma}^{n_z}$ and $J_{nm}^{\uparrow\downarrow}$ leads to an effective Kondo Hamiltonian with the couplings $J_{nm} = J_{nm}^{\uparrow\downarrow}$. Subsequently, we can follow the same procedure as used for the Kondo model. Again, the adapted approach is able to construct an effective low-energy model for the single impurity Anderson model without infrared divergences as shown in Fig. 7.17.

To conclude, so far we achieved our goal of finding a way how to construct converging DEQs within the CUT approach when truncating in orders of the hybridization V and the spin-spin interaction J, respectively. Diagonalizing important contributions of the spin-spin interaction in this way and still providing an effective model with small finite parameters arbitrarily close to the Fermi level has not been achieved so far. There are *no* previous works in the case of the Anderson model which diagonalize the induced spin-spin interaction and in the case of the Kondo model previous works resulted either in diverging DEQs [16] or still exhibit IR-divergent parameters [17] or rely on bosonization before applying the CUT [18–20].

7.5.5 Kondo Energy Scale in the Effective Model

We succeeded to provide a method that yields an effective Hamiltonian with (small) finite parameters for $\varepsilon \to \varepsilon_\mathrm{F}$. The major question is, however, if our effective Hamiltonian is able to describe the important strong-coupling physics. With the previous approach we found the Kondo temperature T_K only as the energy scale at which the differential equation diverges.

In order to study whether we capture the strong-coupling physics or not, we analyze two interesting energy scales of the flow:

1. The flow parameter l_0 at which the reference state is changed.

2. The binding energy of the singlet state.

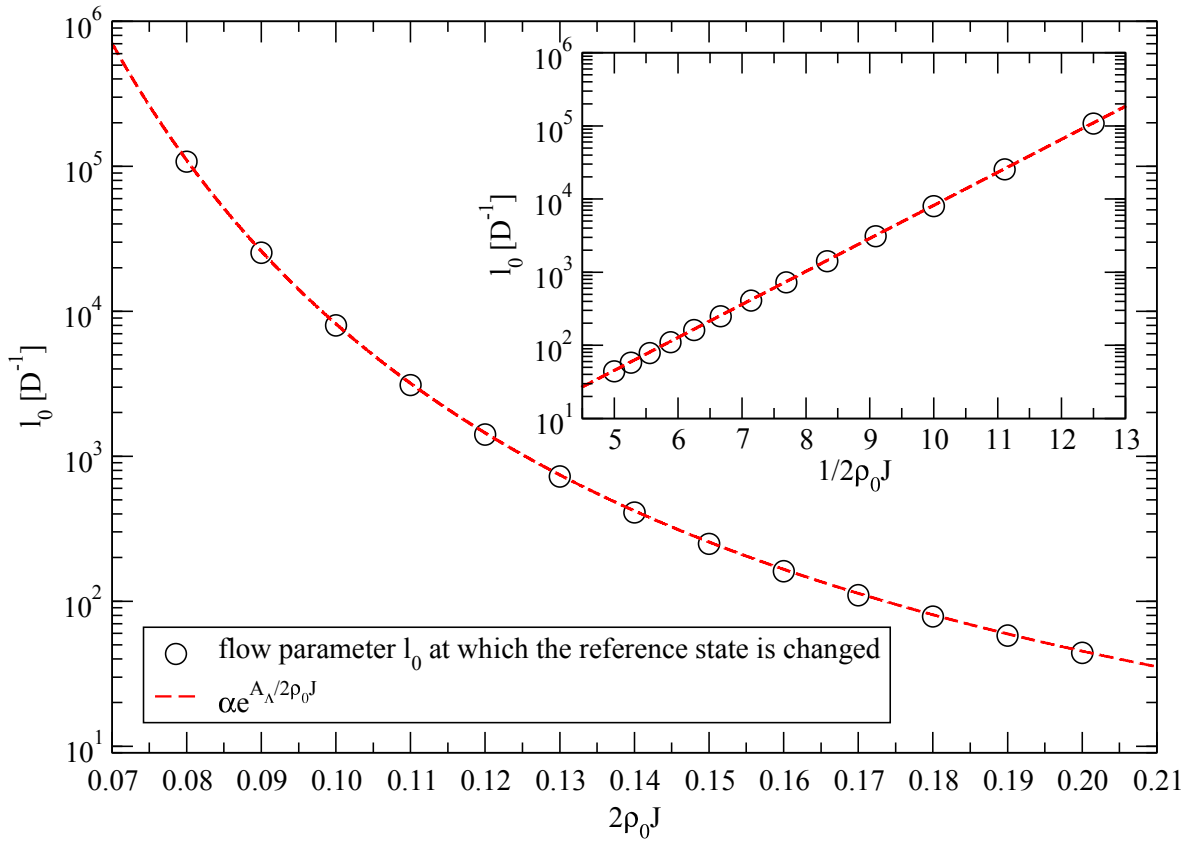

Figure 7.18: Flow parameter l_0 at which the reference state is changed for the **Kondo model** with $\Lambda = 2$ and $N = 52$. The inverse energy scale l_0 is increasing proportional to the inverse of the Kondo temperature T_K^{-1}. The factor A_Λ from Eq. (6.39) is an effect of the discretization.

Fig. 7.18 depicts the flow parameter l_0 at which the reference state is changed for the Kondo model. From the numerical data presented in Fig. 7.18 we find that the energy scale at which the reference state is changed shows an exponential behavior in the form

$$l_0^{-1} \propto \mathrm{e}^{-\frac{A_\Lambda}{2\rho_0 J}} \tag{7.105}$$

where the factor A_Λ in the exponent is an effect of the discretization and is given by Eq. (6.39). It is manifest in the discretized Kondo model regardless of the applied method [8]. Thus, we find that the energy scale at which the reference state is changed is proportional to the Kondo temperature T_K.

Following the procedure outlined in the last sections, we can also analyze the energy scale l_0^{-1} at which the new reference state is formed for the Anderson model. We again find discontinuities that we already found in Fig. 7.8. The explanation is the same as before.

Every time $\frac{U}{2}$ crosses an energy level ε_n, one sign in the generator changes discontinuously (cf. Eq. (7.46)). However, for decreasing Λ the discontinuities become smaller (cf. Fig. 7.8).

Between the discontinuities, we find (at least for large enough values of U) the exponential behavior

$$l_0^{-1} \propto \mathrm{e}^{-A_\Lambda \frac{U}{8\rho_0 V^2}}. \tag{7.106}$$

Fig. 7.19 shows the flow parameter l_0 at which the reference state is changed for the Anderson model.

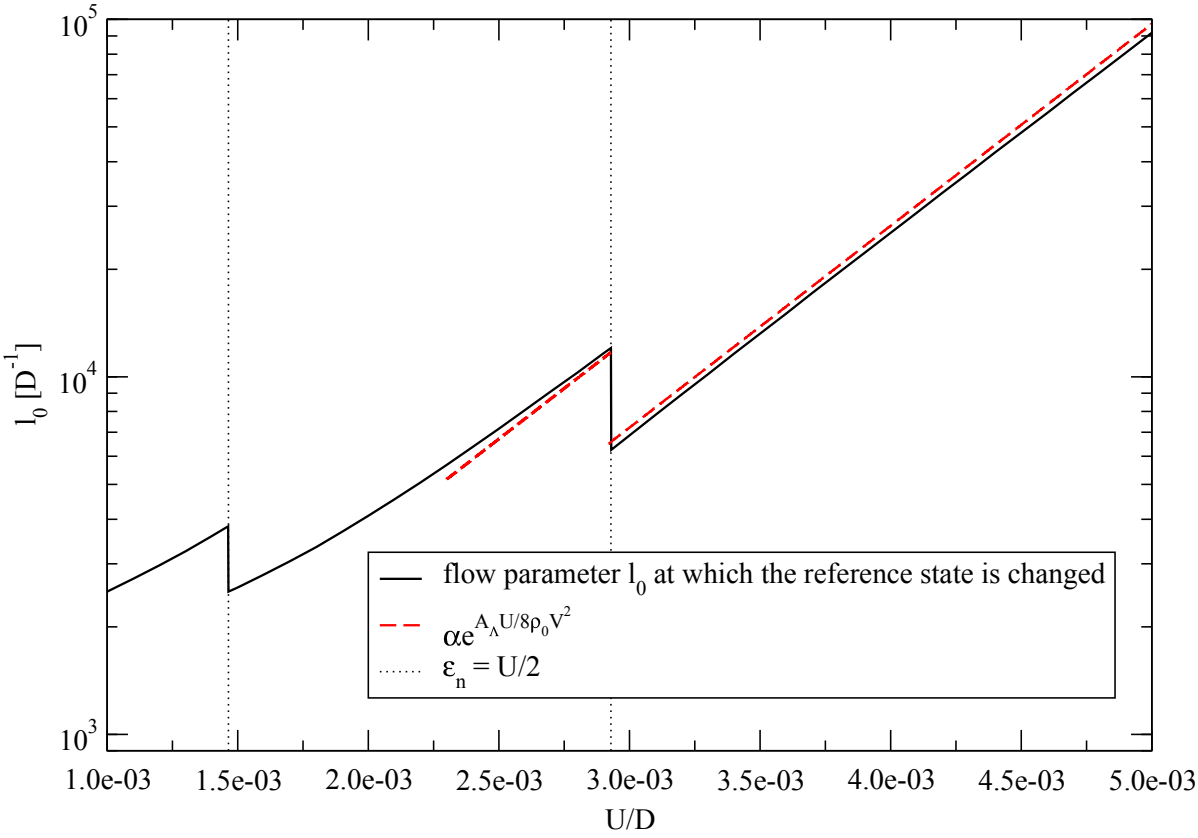

Figure 7.19: Inverse energy scale l_0 at which the reference state is changed for the **Anderson model** with $N = 52$, $\Lambda = 2$ and $\frac{V}{D} = 0.01414$. The inverse energy scale l_0 is increasing proportional to the inverse of the Kondo temperature T_{K}^{-1} for large enough values of U. The factor A_Λ from Eq. (6.39) as well as the discontinuities at $\varepsilon_n = \frac{U}{2}$ (cf. Fig. 7.8) are effects of the discretization.

The second energy scale we want to study is the binding energy of the singlet. It is an advantage of our approach that we can identify this quantity easily as the energy difference of the two lowest energies E_s and E_- from the diagonal part E_k from Eq. (7.109) of the Hamiltonian (7.108) (cf. Eq. (7.88)) for $l \to \infty$

$$\Delta_s = E_- - E_s. \tag{7.107}$$

If we forget about the interaction part for a moment and consider the form of the effective Hamiltonian

$$\begin{aligned} H_{\mathrm{eff}} &= \sum_{n,\sigma} \varepsilon_n : c^\dagger_{n\sigma} c_{n\sigma} : + \sum_{r=\pm} E_{s^r} |s^r\rangle\langle s^r| + \sum_{r=\pm} \sum_i E_{t_i^r} |t_i^r\rangle\langle t_i^r| \\ &+ \sum_\sigma E_{\mathrm{FS},\sigma} |\mathrm{FS},\sigma\rangle\langle \mathrm{FS},\sigma| + \sum_\sigma E_{\tilde{\sigma}} |\tilde{\sigma}\rangle\langle\tilde{\sigma}| + g \sum_\sigma \left(|\mathrm{FS},\sigma\rangle\langle\tilde{\sigma}| + |\tilde{\sigma}\rangle\langle \mathrm{FS},\sigma| \right), \end{aligned} \tag{7.108}$$

we can identify the binding energy of the singlet state as the energy difference between the two lowest energy levels of E_k where we have to diagonalize the E_{kq} first (cf. Eq. (7.94)). Note that Δ_s from Eq. (7.107) can only be interpreted as the binding energy for $l \to \infty$ because the singlet is the ground state of the effective model only in this limit.

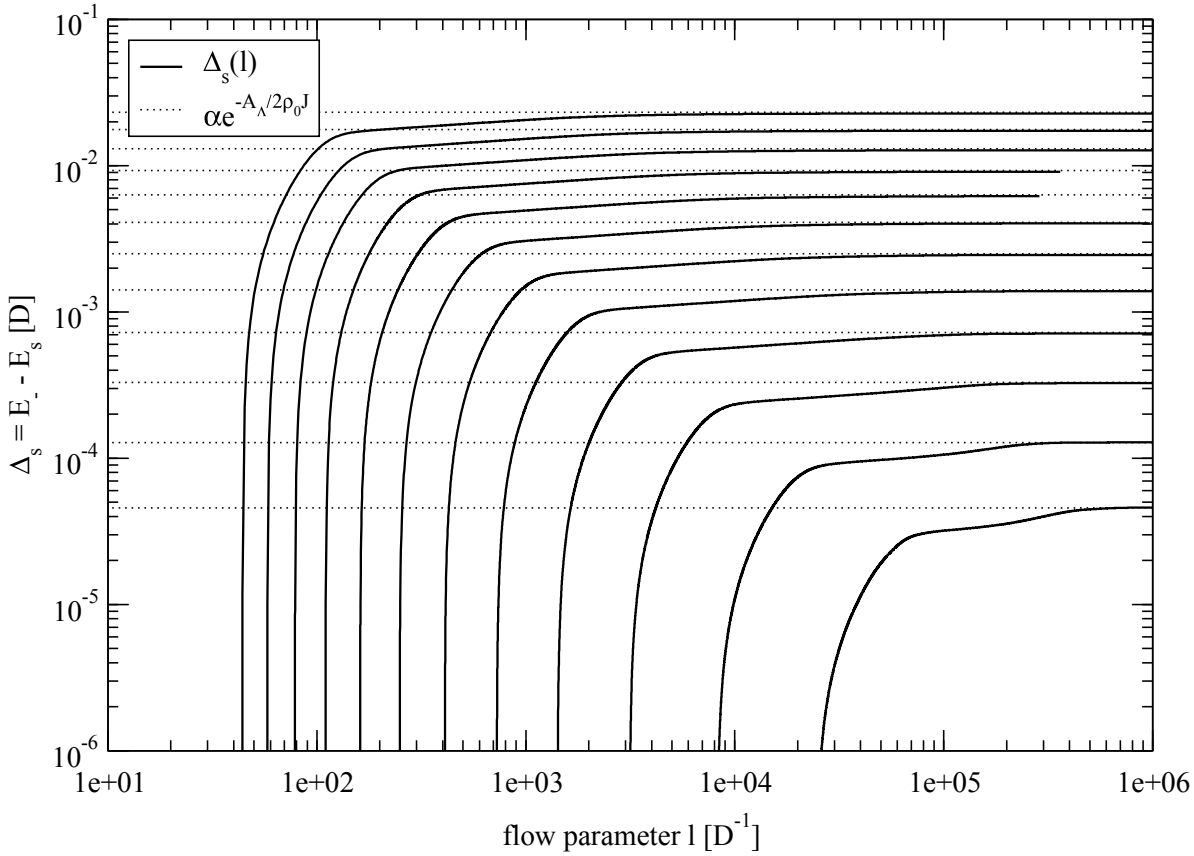

Figure 7.20: Flow of $\Delta_s(l) = E_-(l) - E_s(l)$ for the **Kondo model** with $N = 40$, $\Lambda = 2$ and from top to bottom $2\rho_0 J = 0.2, 0.19, 0.18, ..., 0.11, 0.1, 0.091$ where E_s is the energy of the singlet state and E_- is the first excitation above the singlet state (cf. Eqs. (7.109) and (7.88)). The lines for $2\rho_0 J = 0.17$ and 0.16 end before the other lines for numerical reasons. For these parameters a smaller stepsize is needed which increases the calculation effort. The binding energy for $l \to \infty$ decreases as $\Delta_s(\infty) \propto \exp\left(-\frac{A_\Lambda}{2\rho_0 J}\right)$ (dotted black lines) where A_Λ is a discretization effect and is given by Eq. (6.39). The adapted approach leads to an effective model where the Kondo temperature T_K is already manifest in the diagonal part described by the energies E_k.

For smaller values of l, there are still interaction terms present that act on the singlet state which vanish for $l \to \infty$. Diagonalizing the terms $|k\rangle\langle q|$ yields the eigenvalues

$$E_{s^\pm}, \quad E_{t^\pm_{1,2,3}}, \quad E_\pm = \frac{1}{2}\left[E_{\mathrm{FS},\sigma} + E_{\tilde{\sigma}} \pm \sqrt{\left(E_{\mathrm{FS},\sigma} - E_{\tilde{\sigma}}\right)^2 + 4g^2}\right] \tag{7.109}$$

where the lowest-lying level is the energy of the singlet E_s and the second lowest-lying is the energy level E_- which belongs to a linear combination of the Fermi sea and the $|\tilde{\sigma}\rangle$-states (cf. Eq. (7.88)). Fig. 7.20 depicts the flow of the resulting $\Delta_s(l)$ from Eq. (7.107).

The energy needed to break up the singlet ground state is given by the final difference

$$\Delta_s(\infty) = E_-(\infty) - E_s(\infty) \tag{7.110}$$

where E_s is the singlet's energy (which is the lowest lying) and E_- is given by Eq. (7.109).

For increasing l, we find a rapid increase of $\Delta_s(l)$ until it converges towards the binding energy of the singlet state $\Delta_s(\infty)$. The binding energy is analyzed in Fig. 7.22.

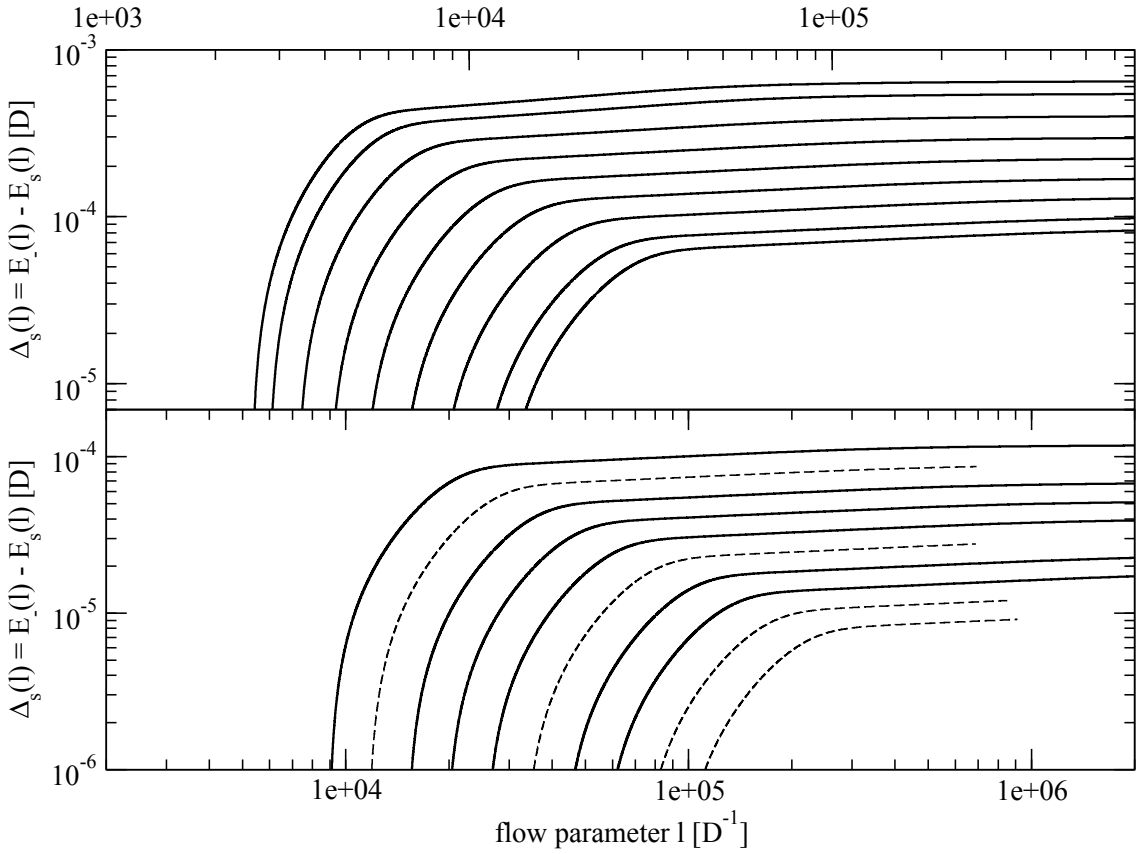

Figure 7.21: Flow of $\Delta_s(l) = E_-(l) - E_s(l)$ for the **Anderson model** with $N = 52$, $\Lambda = 2$, $\frac{V}{D} = 0.01414$ and in the top plot $\frac{U}{D}10^3 = 1.463$, 1.6, 1.8, 2, 2.2, 2.4, 2.6, 2.8, 2.93 (values of $\frac{U}{2}$ are lying between ε_9 and ε_{10}) and in the bottom plot $\frac{U}{D}10^3 = 3.2$, 3.4, 3.6, 3.8, 4, 4.2, 4.4, 4.6, 4.8, 5 (values of $\frac{U}{2}$ are lying between ε_8 and ε_9) where E_s is the energy of the singlet state and E_- the first excitation above the singlet state (cf. Eqs. (7.109) and (7.88)). The binding energy $\Delta_s(\infty)$ is further analyzed in Fig. 7.23. The dashed lines end before the others for numerical reasons. For these parameters a smaller stepsize is needed which increases the calculation effort.

In Fig. 7.21 we also analyze the flow of Δ_s for the Anderson model. Here we have to bear in mind that we find discontinuities when an energy level ε_n crosses $\frac{U}{2}$. For reasons of clarity, the regions between two ε_n are depicted separately in Fig. 7.21.

For $l \to \infty$, we find an exponential decrease of the form

$$\Delta_s(\infty) \propto \mathrm{e}^{-\frac{A_\Lambda}{2\rho_0 J}} \tag{7.111}$$

for the Kondo model and an exponential decrease of the form

$$\Delta_s(\infty) \propto \mathrm{e}^{-A_\Lambda \frac{U}{8\rho_0 V^2}} \tag{7.112}$$

for the Anderson model.

In Figs. 7.22 and 7.23 the exponential behavior (7.111) and (7.112) of the binding energy $\Delta_s(\infty)$ is shown.

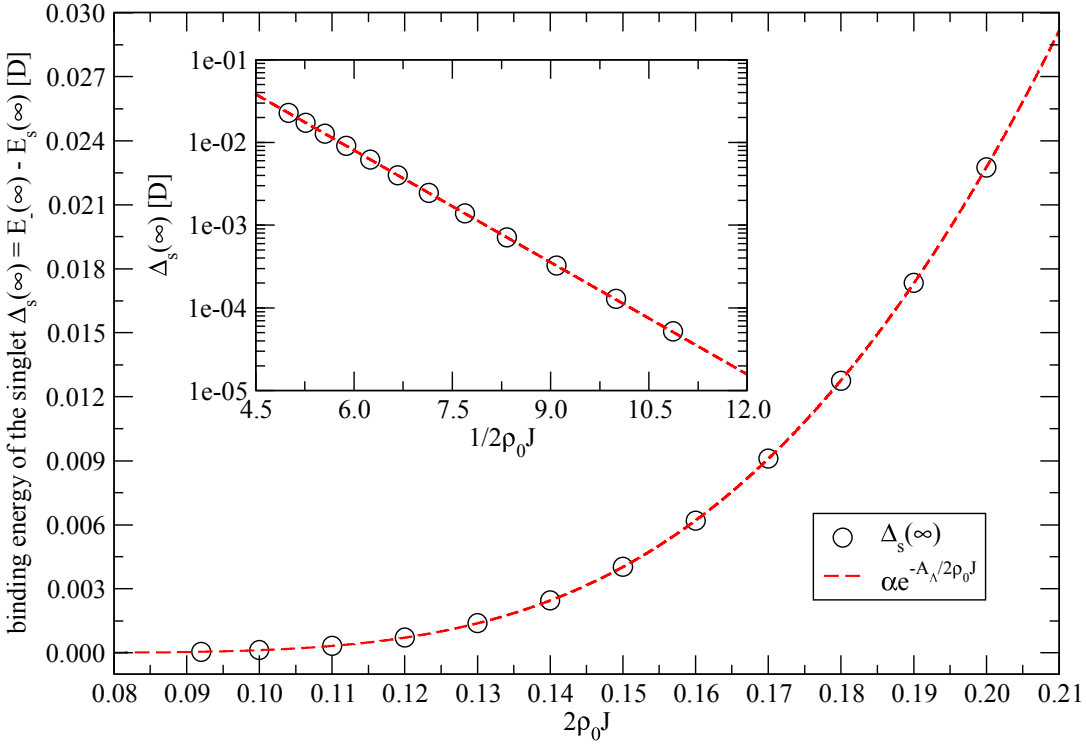

Figure 7.22: Binding energy of the singlet state $\Delta_s(\infty) = E_-(\infty) - E_s(\infty)$ for the **Kondo model** with $N = 40$ and $\Lambda = 2$ where E_s is the energy of the singlet state and E_- is the first excitation above the singlet state (7.109).

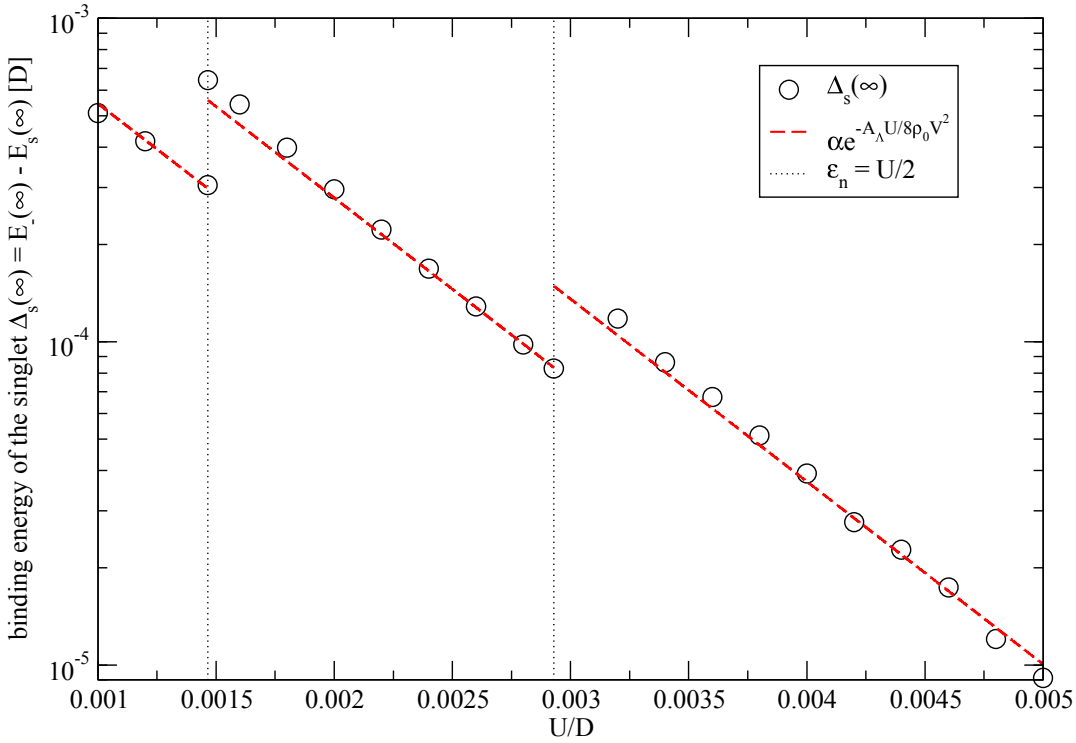

Figure 7.23: Binding energy of the singlet state $\Delta_s(\infty) = E_-(\infty) - E_s(\infty)$ for the **Anderson model** with $N = 52$, $\Lambda = 2$ and $\frac{V}{D} = 0.01414$ where E_s is the energy of the singlet state and E_- is the first excitation above the singlet state (7.109).

To conclude, it is fair to state that the adapted approach not only yields a finite, well-defined effective Hamiltonian but also results in a model where the Kondo energy scale is already manifest in the diagonal part. It is no longer hidden in the interplay between kinetic energy and interaction. If we forget about the remaining interactions, which do not couple the singlet state to other states anymore, the effective model is of a very simple structure. The physics of a screened impurity spin due to the formation of a singlet with a binding energy given by the Kondo temperature T_K is evident and confirms the results obtained with other methods, e.g., NRG [1, 8].

In the calculations presented in this chapter we used the site which forms the singlet first – which is the site closest to the Fermi level – throughout the whole flow. For test purposes, we also fixed the singlet at another site n with $|\varepsilon_n| \approx T_\mathrm{K}$ which has only a minor influence on the results presented in this chapter. Especially the binding energy of the singlet is almost independent of the site at which the singlet forms.

7.5.6 Specific Heat of the Effective Model

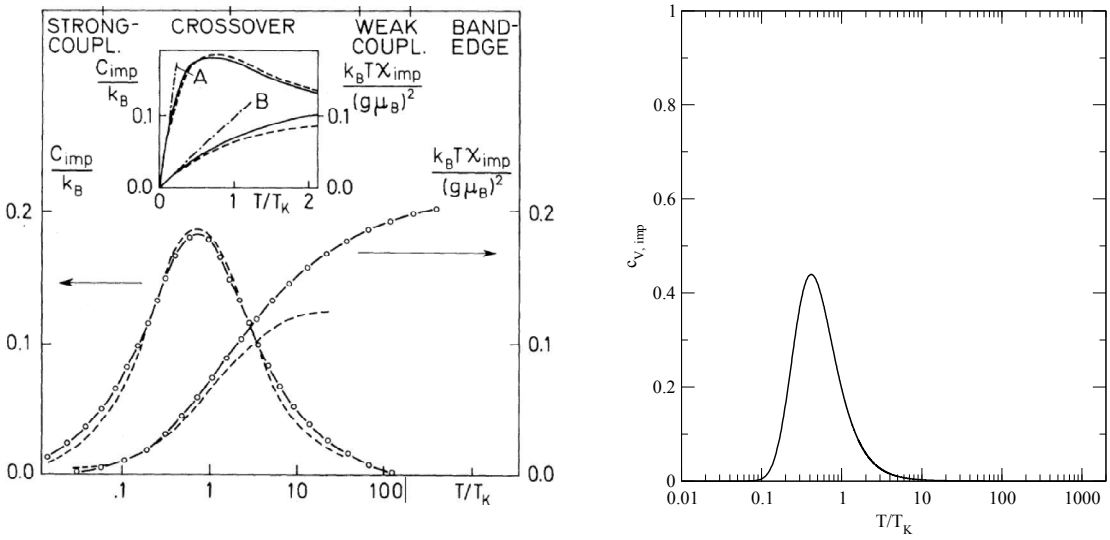

Figure 7.24: Comparison of the specific heat of the Kondo model taken from Ref. [121] (left panel) and the specific heat from Eq. (7.116) (right panel) where a low-temperature approximation was used and the influence of the bath electrons was not taken into consideration. Thus, we do not expect to find the correct high-temperature behavior or the linear behavior for $T \to 0$. The only information used is the result from Fig. 7.22, namely that the binding energy of the singlet is given by the Kondo temperature T_K. This is already enough information to find the maximum close below the Kondo temperature T_K.

In this section we want to analyze the specific heat of the effective Hamiltonian and compare it to the specific heat of the Kondo model. We use a very simple calculation in which we only want to use the information from Fig. 7.22, namely that the binding energy of the singlet is given by the Kondo temperature T_K.

We calculate the expectation value of H

$$\langle H\rangle - \langle H_0\rangle = \frac{E_s \mathrm{e}^{-\beta E_s} + E_- \mathrm{e}^{-\beta E_-}}{\mathrm{e}^{-\beta E_s} + \mathrm{e}^{-\beta E_-}} \tag{7.113}$$

where H_0 denotes the Hamiltonian for $J = 0$. We only used the two lowest energy levels E_k from Eq. (7.109) and neglected the higher-lying ones. From the numerical results we know that

$$E_- - E_s = T_\mathrm{K} \tag{7.114}$$

which we use in the next step

$$\langle H\rangle - \langle H_0\rangle = \frac{E_s + (E_s + T_\mathrm{K})\,\mathrm{e}^{-\beta T_\mathrm{K}}}{1 + \mathrm{e}^{-\beta T_\mathrm{K}}}. \tag{7.115}$$

Hence, the impurity contribution to the specific heat is given by

$$c_{V,\mathrm{imp}} = \frac{\mathrm{d}}{\mathrm{d}T}\left(\langle H\rangle - \langle H_0\rangle\right) = \frac{T_\mathrm{K}^2}{T^2} \frac{\mathrm{e}^{-\frac{T_\mathrm{K}}{T}}}{\left(1 + \mathrm{e}^{-\frac{T_\mathrm{K}}{T}}\right)^2}. \tag{7.116}$$

We notice that this is a universal function depending only on $\frac{T}{T_\mathrm{K}}$.

Fig. 7.24 compares the specific heat (7.116) (right panel) with the specific heat of the Kondo model [121] (left panel). With our straightforward calculation we already find the maximum close below the Kondo temperature. As we used a low-temperature approximation, we are not expecting to find the correct high-temperature behavior. The specific heat (7.116) decreases much faster than the correct specific heat for higher temperatures. We also miss the linear behavior $c_{V,\mathrm{imp}} \propto \frac{T}{T_\mathrm{K}}$ for $T \to 0$ which is not surprising as we neglected the influence of the bath electrons which is ultimately the reason for the linear behavior for $T \to 0$. One could try to capture this effect treating the remaining interaction terms in the effective model perturbatively or taking the flow of the ε_n into account.

8 Conclusion and Outlook

In this thesis we applied the method of Continuous Unitary Transformations to the single impurity Anderson and the Kondo model. Our aim was to study if the Continuous Unitary Transformation approach is able to deal with the challenges of the Kondo problem and to construct effective models describing the Kondo effect. We investigated three different approaches.

Chapter 5 Conclusion: Chap. 5 describes our first approach to the Anderson impurity model. We map the Hamiltonian to a semi-infinite chain representation and separate particle and hole states by applying two separate Lanczos tridiagonalizations. This is important as in this case $p^\dagger$ and $h^\dagger$ both create excitations. We wrote a CUT program that was developed in order to set up the flow equations which are solved by a 4th-order Runge-Kutta algorithm.

We truncate terms with more than six operators and additionally all terms with an interaction-range further than nearest-neighbors ($d = 1$). We compare the single-particle energies of the effective model to the lowest non-zero many-particle flow (total charge $Q = 1$ and total spin $S = 0$) derived from NRG calculations (cf. Ref. [10]) and further to the single-particle energies obtained from effective fixed-point Hamiltonians describing the respective energy regimes.

We try to identify the different energy regimes of the Anderson impurity model and find very good agreement for larger values of U in the free-orbital and the local-moment regime. We also find the crossover between these two regimes in the expected regions. For smaller values of U, the crossover is less distinct than expected and occurs a bit beyond the expected energy regime. Increasing the interaction-range d beyond nearest-neighbor interactions improves the results. For $d = 7$, the results for $\frac{U}{D} = 10^{-3}$ are also in very good agreement with NRG calculations.

However, the most interesting crossover to the strong-coupling regime is not covered with this approach. Thus, we focus on two other approaches in order to capture the strong-coupling regime as well.

Chapter 6 Conclusion: In Chap. 6 we investigate an approach which starts from a parametrization in which the Hamiltonian is diagonal for $U = 0$ and consequently the initial interaction Hamiltonian becomes completely non-local due to the diagonalization of the hybridization term.

We are able to derive the flow equations analytically by truncating emerging operators in orders of the interaction U. We solve the differential equations numerically and find converging differential equations and an effective model with small finite parameters on all energy scales.

We analyze the flow of the low-energy interaction vertex $U_{n_\mathrm{F} n_\mathrm{F} n_\mathrm{F} n_\mathrm{F}}$ and the constant E_0 which converges to the ground-state energy. The low-energy interaction vertex of the effective model becomes attractive over some parameter regime.

In order to study if we are able to describe the low-energy strong-coupling behavior, we calculate the impurity contribution to the susceptibility χ_d. We apply a magnetic field to the impurity level and calculate the ground-state energy $E_0(h)$ in dependence of the magnetic field h. We calculate the susceptibility by the second derivative of the ground-state energy with respect to the magnetic field.

At first, we calculate the susceptibility numerically by solving the full differential equation

where the ground-state energy is derived in second order U^2. We find an exponential increase of the susceptibility

$$\chi_{\mathrm{d}} = \alpha \mathrm{e}^{\frac{1}{2} A_\Lambda \frac{U}{8\rho V^2}} \tag{8.1}$$

where A_Λ is an expected discretization effect and is given by Eq. (6.39). The exponential behavior is a good benchmark whether the strong-coupling physics is captured or not. However, our result differs by a factor $\frac{1}{2}$ in the exponent.

In the second part of Chap. 6 we apply a scaling expansion to the flow equation. We expand in a scaling parameter λ and discard terms that scale faster to zero than a chosen order in λ when lowering energies. A systematic low-order expansion in first order in λ is investigated which leads to a system of differential equations that can be solved analytically. The susceptibility χ_{d} calculated from the scaling expansion is in perfect agreement with the exact result for $U = 0$ which is not trivial as the scaling expansion is an approximation, even for the non-interacting case. By including the interaction and expanding in linear order in λ, we are already able to derive the exponential behavior of the susceptibility analytically without approximations

$$\chi_{\mathrm{d}} = \frac{g_{\mathrm{e}}^2 \mu_{\mathrm{B}}^2}{4U} \left(\mathrm{e}^{\frac{16}{\pi^2} \frac{U}{8\rho_0 V^2}} - 1 \right). \tag{8.2}$$

The exponent differs from the expected exponent by a factor $\frac{16}{\pi^2} \approx 1.62$ but exhibits the correct ratio $\frac{U}{\pi\Delta}$.

Chapter 6 Outlook: The promising results from the scaling expansion suggest further investigations.

An obvious open task would be to include higher orders in the scaling parameter λ and to study if the results thereby improve. This is an entirely realistic aim as we can still neglect terms with six operators when targeting the ground-state energy in second order in λ.

However, it might also be interesting to better understand the flow for $h = 0$ and to include the renormalization of $\tilde{U}$ induced by the commutation of U-terms with themselves. This renormalization might influence the exponent and thus might improve the results.

Another interesting question would be if the calculation of further observables (e.g. the specific heat or the density of states) yields reasonable results in the framework of a scaling expansion.

As the scaling expansion is not entirely developed for the Kondo problem, it would be an interesting question to study if it can be applied to further problems as well.

Chapter 7 Conclusion: Chap. 7 describes our third approach to the Anderson and Kondo model. This time we truncate in orders of the hybridization element V and in orders of the spin-spin interaction J, respectively. An approach using a similar parametrization was already used in the context of the Kondo model [16]. With this approach the conventional scaling results were reproduced, i.e., differential equations were derived which, however, diverge on the Kondo energy scale T_{K}. This approach fails to solve the Kondo problem due to diverging spin-spin couplings just as found in the "poor man's scaling". Our aim in Chap. 7 is to modify this approach in a way that enables us to derive an effective model without infrared divergences.

In the first part of Chap. 7 we reproduce the Schrieffer-Wolff transformation by using the sign- as well as Wegner's generator in order to have a starting point to develop our improved approach.

We compare the resulting spin-spin interaction to the one-step Schrieffer-Wolff transformation and the CUT approach already used by Kehrein and Mielke [22]. We use deepCUT ideas in order to justify a truncation scheme which enables us to derive the induced spin-spin interaction J_{nm} analytically without approximations. The results from Continuous Unitary Transformations are less singular than those from the one-step transformation. The induced spin-spin couplings J_{nn_F} from the sign- as well as from Wegner's generator are antiferromagnetic over the full energy spectrum while the couplings from the Schrieffer-Wolff Transformation as well as from the generator used by Kehrein and Mielke are not. This is no disagreement as long as the couplings coincide at the Fermi level because different transformations are considered.

In the next step we aim at diagonalizing the induced spin-spin interaction. By exploiting the spin-rotation symmetry we are able to find a differential equation for the induced spin-spin interaction of the Anderson model which coincides with the one already known for the Kondo model. Trying to diagonalize the induced spin-spin interaction results in diverging differential equations where the energy scale on which the DEQ diverges is the Kondo temperature T_K. We analyze if we can simultaneously eliminate the hybridization V and the induced spin-spin interaction J in the Anderson model. We find the exponential behavior in the Coulomb interaction U of the Kondo temperature T_K given by the energy scale on which the flow equation diverges.

Our main goal of this chapter, however, is to find a way to construct effective models without infrared divergences. We identify the origin of the divergence and modify the approach so that the divergence is prevented. In order to achieve this goal, we first study the Kondo model coupled to an auxiliary spin $S = \frac{1}{2}$ via an isotropic spin-spin coupling K. The impurity and the auxiliary spin form a singlet ground state with triplets as excitations. We choose the operators $|k\rangle\langle q|$, where $|k\rangle$ and $|q\rangle$ denote the singlet and triplet states, as a new operator basis and include the thereby diagonalized spin-spin interaction between the impurity and the auxiliary spin to the diagonal part of the Hamiltonian H_D from which the reference state is deduced. The main difference in the adapted approach is that flipping a spin on the impurity requires the energy K while it requires no energy in the conventional approach. This leads to an IR-cutoff and finally to convergence. We derived the flow equation for the improved approach and found converging differential equations from a numerical treatment. Additionally, we applied the IR-approximation to the flow equation in order to verify the numerical result analytically. For $K = 0$, the IR-approximation yields diverging integrals over l^{-1} which become exponentially suppressed by a factor $\mathrm{e}^{-|K|l}$ for $K > 0$ and thus converge.

In the next step we apply this improved approach to the Anderson and the Kondo model. The main idea is to include the emerging diagonal spin-spin interactions J_{nn} to the diagonal part of the Hamiltonian H_D from which the reference state is determined. We follow the diagonal spin-spin interactions J_{nn} and change the reference state as soon as they become large enough so that the singlet state, instead of the Fermi sea, becomes the ground state of H_D. When the energy scale connected to the flow parameter l approaches the Kondo temperature T_K, a singlet state forms below the Kondo temperature. We use the same procedure as for the Kondo model coupled to the auxiliary spin and expand all respective operators in the basis operators of H_D. In the case of the Kondo model, there are further charge fluctuations in the bath (in contrast to the auxiliary spin which was by construction a fixed local moment) so that besides the singlet and triplets more states, e.g. the Fermi sea, are present in the operator basis of H_D which renders the problem more difficult.

Nevertheless, the adapted operator basis is transparent and intuitively accessible as the singlet state is directly labeled which can be seen as an advantage of our approach. In the course of the

flow the singlet state becomes the lowest-lying state and thus one can define the energy difference between this state and the first excitation above it as the binding energy of the singlet. This exemplifies how easily the parameters can be interpreted in this representation. The reference state is changed just when the singlet state becomes the lowest-lying state. Thus, the difference between the singlet's energy and the state that was the lowest-lying before is zero at this point. The energy difference increases throughout the subsequent flow and finally converges to the Kondo temperature T_K. We find perfect agreement, at least in leading order in J (cf. App. 9.3), to the Kondo temperature $T_\mathrm{K} \propto \mathrm{e}^{-A_\Lambda/2\rho_0 J}$ for the Kondo model and $T_\mathrm{K} \propto \mathrm{e}^{-A_\Lambda U/8\rho_0 V^2}$ for the Anderson model.

Finally, we calculate the impurity contribution to the specific heat only using the binding energy of the Kondo singlet derived from the numerical results. The specific heat is a universal function of the ratio $\frac{T}{T_\mathrm{K}}$ and we can already identify the maximum close below the Kondo temperature T_K.

Chapter 7 Outlook: A very interesting project would be to apply the scaling expansion (from Chap. 6) to the adapted flow equations. The main question in this context would be if the exponential strong-coupling behavior is also captured in a low-order scaling expansion. Once the scaling expansion is applied, the numerical calculation effort becomes very small because the remaining coupled coefficients would be of the order of ~ 40 coefficients.

Another remaining question is the final energy scale of the bath electrons which form the singlet with the impurity. We use the site which forms the singlet first (which is the site closest to the Fermi level) throughout the whole flow as the new reference state. It would be interesting to analyze if the singlet remains at the Fermi level or whether it becomes energetically favorable for the singlet to form on another site during the subsequent flow.

In the result for c_V we miss the linear behavior $c_{V,\mathrm{imp}} \propto \frac{T}{T_\mathrm{K}}$ for $T \to 0$ which we cannot hope to find within our approximation. This is due to the fact that we neglected the remaining interaction part of the effective model as well as the flow of the single-particle energies ε_n. It would be interesting to see if one can extract the necessary information in order to find the linear behavior, e.g., by a perturbative treatment of the remaining interaction terms in the effective model or by investigating the flow of ε_n.

To keep things as simple as possible, we discard 20 of the 32 states of the adapted operator basis. It would be interesting to use all basis states and study the influence of this approximation or to find out if one can neglect even more states.

In order to verify further that the effective model exhibits the correct low-temperature behavior, it would be an interesting task to calculate other observables.

From Ref. [16] we know that truncating the conventional approach in higher orders of J results in higher-order corrections to the Kondo temperature T_K which corresponds to the point of divergence of the flow equation. Thus, another question is if expanding the adapted flow equations in higher orders of J would also yield higher-order corrections to the Kondo temperature T_K.

9 Appendix

9.1 Abbreviations

- **DEQ**: **D**ifferential **EQ**uation
- **CUT**: **C**ontinuous **U**nitary **T**ransformation

  sCUT: **s**elf-similar CUT

  pCUT: **p**erturbative CUT

  epCUT: **e**nhanced **p**erturbative CUT

  deepCUT: **d**irectly **e**valuated **e**nhanced **p**erturbative CUT
- **NRG**: **N**umerical **R**enormalization **G**roup
- **RG**: **R**enormalization **G**roup
- **RGT**: **R**enormalization **G**roup **T**ransformation
- **ROD**: **R**esidual **O**ff-**D**iagonality
- **DOS**: **D**ensity **O**f **S**tates
- **SIAM**: **S**ingle **I**mpurity **A**nderson **M**odel
- **FO**: **F**ree **O**rbital
- **LM**: **L**ocal **M**oment
- **SC**: **S**trong **C**oupling

9.2 Units

In this thesis natural units

$$c = 1\,, \quad \hbar = 1\,, \quad k_\mathrm{B} = 1 \tag{9.1}$$

are used while all energies are expressed in units of the bandwidth D. In Chap. 6 the energy h is connected to a magnetic field B via $h = \frac{1}{2} g_\mathrm{e} \mu_\mathrm{B} B$ where g_e is the Landé g-factor while μ_B denotes the Bohr magneton. Furthermore, the Fermi energy ε_F is set to zero.

9.3 Kondo Temperature T_K

The Kondo temperature found by the "poor man's scaling" [1, 15] is given by

$$T_K = D\,\mathrm{e}^{-\frac{1}{2\rho_0 J}}. \tag{9.2}$$

Wilson derived corrections to this formula [1]. He found

$$T_K = D_{\mathrm{eff}}(J)\,\mathrm{e}^{-\Phi(2\rho_0 J)} \tag{9.3}$$

with

$$\Phi(y) = \frac{1}{y} - \frac{1}{2}\ln|y| + 1.58y + \mathcal{O}\left(y^2\right). \tag{9.4}$$

For the Anderson model, the effective bandwidth D_{eff} [1, 122] is given by

$$D_{\mathrm{eff}} = 0.182U. \tag{9.5}$$

From the Bethe ansatz [52] the Kondo temperature for the Anderson model is found to be

$$T_K = \left(\frac{U\Delta}{2}\right)^{\frac{1}{2}} \mathrm{e}^{-\pi U/8\Delta + \pi\Delta/2U}. \tag{9.6}$$

The exponent coincides with the result of Wilson (9.3) as well as with the result from the "poor man's scaling" (9.2) in leading order in J. For the Anderson model, the effective spin-spin coupling at the Fermi level is given by

$$J = \frac{4V^2}{U}. \tag{9.7}$$

When the logarithmic discretization from Sec. 2.6 is used, the Kondo temperature T_K is modified [8] by introducing the coupling J_{eff} in Eq. (9.3)

$$J_{\mathrm{eff}} = \frac{\rho_0 J}{A_\Lambda} \tag{9.8}$$

while neglecting the term proportional to y in Eq. (9.4). The factor A_Λ is given by

$$A_\Lambda = \frac{1}{2}\frac{\Lambda+1}{\Lambda-1}\ln\Lambda. \tag{9.9}$$

This results in an estimation of the Kondo temperature in leading order in J at finite Λ

$$T_K \propto \mathrm{e}^{-\frac{A_\Lambda}{2\rho_0 J}}. \tag{9.10}$$

9.4 Residual Off-Diagonality of the Non-Interacting Model

We derive the power law $\mathrm{ROD} \propto l^{-1}$ found in Sec. 5.3.2 analytically.

We consider the flow equation (5.29). In order to understand the power-law behavior, it is enough to focus on the exponential behavior of the hopping elements t_n and the single-particle energies ε_n. We use

$$t_n^0 = \alpha_\Lambda \Lambda^{-n}, \quad \varepsilon_n = \beta_\Lambda \Lambda^{-n} \tag{9.11}$$

which is true for large enough values of n (cf. Fig. 5.3). As we want to study the behavior of the ROD for intermediate and large values of l, this approximation is justified. Solving the DEQ (5.29) with these approximations we find for the hopping elements

$$t_n = t_n^0 \mathrm{e}^{-(\varepsilon_n - \varepsilon_{n+1})l} = \alpha_\Lambda \Lambda^{-n} \mathrm{e}^{-\beta_\Lambda \left(\Lambda^{-n} - \Lambda^{-n-1}\right) l}. \tag{9.12}$$

Thus, the ROD is given by

$$\mathrm{ROD}^2(l) = \sum_{n=0}^{\infty} t_n^2 = \alpha_\Lambda^2 \sum_{n=0}^{\infty} \Lambda^{-2n} \mathrm{e}^{-2\beta_\Lambda \left(\Lambda^{-n} - \Lambda^{-n-1}\right) l}. \tag{9.13}$$

In order to see that the equation follows a power law, we will rescale l with a factor Λ and look how the ROD behaves[9]. We find

$$\begin{aligned} \mathrm{ROD}^2(\Lambda l) &= \alpha_\Lambda^2 \sum_{n=0}^{\infty} \Lambda^{-2n} \mathrm{e}^{-2\beta_\Lambda \left(\Lambda^{-n} - \Lambda^{-n-1}\right) \Lambda l} \\ &= \alpha_\Lambda^2 \sum_{n=0}^{\infty} \Lambda^{-2n} \mathrm{e}^{-2\beta_\Lambda \left(\Lambda^{-n+1} - \Lambda^{-n}\right) l} \\ &= \alpha_\Lambda^2 \left(\sum_{n=0}^{\infty} \Lambda^{-2n-2} \mathrm{e}^{-2\beta_\Lambda \left(\Lambda^{-n} - \Lambda^{-n-1}\right) l} + \mathrm{e}^{-2\beta_\Lambda \left(\Lambda^{1} - 1\right) l} \right) \end{aligned} \tag{9.14}$$

where we separated the element for $n = 0$ and shifted the index of the remaining sum by one in the last step. For larger values of l, the last exponential function on the right-hand side is negligible as all differences $\Lambda^{-n} - \Lambda^{-n-1}$ in the sum are smaller than $\Lambda^1 - \Lambda^0$. This leads to

$$\mathrm{ROD}^2(\Lambda l) = \Lambda^{-2} \alpha_\Lambda^2 \sum_{n=0}^{\infty} \Lambda^{-2n} \mathrm{e}^{-2\beta_\Lambda \left(\Lambda^{-n} - \Lambda^{-n-1}\right) l} = \Lambda^{-2} \mathrm{ROD}^2(l). \tag{9.15}$$

Thus, we have found the behavior

$$\mathrm{ROD}(l) \propto l^{-1}. \tag{9.16}$$

Note that for small l the behavior differs as we cannot neglect the exponential function with the exponent $\Lambda^1 - \Lambda^0$ in Eq. (9.14). As we use an infinitely large chain, we find the power law for arbitrarily large l. For a finite chain length, this calculation only works for intermediate l while for large l the exponential function for the largest $n = N - 1$ converges slower than the residual part so that we find an exponential asymptotic behavior for large l.

[9] In order to verify this behavior for arbitrary γ, i.e., $\mathrm{ROD}^2(\gamma l) = \gamma^{-2} \mathrm{ROD}^2(l)$, the calculation is basically the same but one has to introduce $n' = \frac{n}{\log_\Lambda \gamma}$.

9.5 Flow Equation for the Kondo Model

The derivation of the flow equation for the isotropic Kondo model from Sec. 4.6.2 is given explicitly.

Useful rules for the product and the commutator of Pauli matrices used in this section are

$$\begin{aligned} \sigma^\mu \sigma^\nu &= \delta_{\mu\nu}\mathbb{1} + i\sum_{k\in x,y,z} \varepsilon_{\mu\nu k}\sigma^k \\ [\sigma^\mu, \sigma^\nu] &= 2i\sum_{k\in x,y,z} \varepsilon_{\mu\nu k}\sigma^k. \end{aligned} \tag{9.17}$$

In order to derive the flow equation (4.4), we have to commute the Hamiltonian

$$H = \sum_{n,\sigma} \varepsilon_n : c^\dagger_{n\sigma} c_{n\sigma} : + \sum_{\mu\in x,y,z} \sum_{n,m} \sum_{\alpha,\beta} J_{nm} \sigma^\mu_{\alpha\beta} \tau^\mu : c^\dagger_{n\alpha} c_{m\beta} : \tag{9.18}$$

with the generator

$$\eta = \sum_{\mu\in x,y,z} \sum_{n,m} \sum_{\alpha,\beta} \eta_{nm} \sigma^\mu_{\alpha\beta} \tau^\mu : c^\dagger_{n\alpha} c_{m\beta} : . \tag{9.19}$$

The commutation of η with the diagonal part yields

$$[\eta, H_\mathrm{D}] = \sum_{\mu} \sum_{n,m,\alpha,\beta} \left[(\varepsilon_m - \varepsilon_n)\, \eta_{nm} \right] \sigma^\mu_{\alpha\beta} \tau^\mu : c^\dagger_{n\alpha} c_{m\beta} : \tag{9.20}$$

while the commutator of the spin-spin interaction with itself can be derived by the following calculation

$$\begin{aligned} [\eta, H_\mathrm{J}] &= \sum_{\mu,\nu} \sum_{\substack{n,m,r,s \\ \alpha,\beta,\alpha',\beta'}} \eta_{nm} J_{rs} \sigma^\mu_{\alpha\beta} \sigma^\nu_{\alpha'\beta'} \left[\tau^\mu : c^\dagger_{n\alpha} c_{m\beta} :, \tau^\nu : c^\dagger_{r\alpha'} c_{s\beta'} : \right] \\ &= \sum_{\mu,\nu} \sum_{\substack{n,m,r,s \\ \alpha,\beta,\alpha',\beta'}} \eta_{nm} J_{rs} \sigma^\mu_{\alpha\beta} \sigma^\nu_{\alpha'\beta'} [\tau^\mu, \tau^\nu] : c^\dagger_{r\alpha'} c_{s\beta'} :: c^\dagger_{n\alpha} c_{m\beta} : \\ &+ \sum_{\mu,\nu} \sum_{\substack{n,m,r,s \\ \alpha,\beta,\alpha',\beta'}} \eta_{nm} J_{rs} \sigma^\mu_{\alpha\beta} \sigma^\nu_{\alpha'\beta'} \tau^\mu \tau^\nu \left[: c^\dagger_{n\alpha} c_{m\beta} :, : c^\dagger_{r\alpha'} c_{s\beta'} : \right]. \end{aligned} \tag{9.21}$$

In the second step the rules for a product of normal-ordered operators from Eq. (9.40) are used.

$$\begin{aligned} [\eta, H_\mathrm{J}] &= \sum_{\mu,\nu} \sum_{\substack{n,m,r,s \\ \alpha,\beta,\alpha',\beta'}} \eta_{nm} J_{rs} \sigma^\mu_{\alpha\beta} \sigma^\nu_{\alpha'\beta'} [\tau^\mu, \tau^\nu] : c^\dagger_{r\alpha'} c_{s\beta'} c^\dagger_{n\alpha} c_{m\beta} : \\ &+ \sum_{\mu,\nu} \sum_{\substack{n,m \\ \alpha,\beta}} \sum_x \left(\eta_{xm} J_{nx} \left[\sum_\gamma \sigma^\nu_{\alpha\gamma} \sigma^\mu_{\gamma\beta} \right] (1-\theta_x) - \eta_{nx} J_{xm} \left[\sum_\gamma \sigma^\mu_{\alpha\gamma} \sigma^\nu_{\gamma\beta} \right] \theta_x \right) [\tau^\mu, \tau^\nu] : c^\dagger_{n\alpha} c_{m\beta} : \\ &+ \sum_{\mu,\nu} \sum_{\substack{n,m \\ \alpha,\beta}} \sum_x \left(\eta_{nx} J_{xm} \left[\sum_\gamma \sigma^\mu_{\alpha\gamma} \sigma^\nu_{\gamma\beta} \right] - \eta_{xm} J_{nx} \left[\sum_\gamma \sigma^\nu_{\alpha\gamma} \sigma^\mu_{\gamma\beta} \right] \right) \tau^\mu \tau^\nu : c^\dagger_{n\alpha} c_{m\beta} : \\ &+ \sum_{\mu,\nu} \sum_{n,m} \eta_{nm} J_{mn} \left[\sum_{\alpha,\beta} \sigma^\mu_{\alpha\beta} \sigma^\nu_{\beta\alpha} \right] [\tau^\mu, \tau^\nu]\, \theta_m (1-\theta_n) \\ &+ \sum_{\mu,\nu} \sum_{n,m} \eta_{nm} J_{mn} \left[\sum_{\alpha,\beta} \sigma^\mu_{\alpha\beta} \sigma^\nu_{\beta\alpha} \right] \{\tau^\mu, \tau^\nu\}\, \theta_n. \end{aligned} \tag{9.22}$$

The definition for the expectation value

$$\langle c^\dagger_{n\sigma} c_{n\sigma} \rangle = \theta_n \tag{9.23}$$

is introduced. In the next step we discard the terms with quartic bath operators and use Eq. (9.17) as well as

$$\sum_\gamma \sigma^\mu_{\alpha\gamma}\sigma^\nu_{\gamma\beta} = [\sigma^\mu\sigma^\nu]_{\alpha\beta}\ , \quad \sum_{\mu,\nu} \varepsilon_{\mu\nu k}\varepsilon_{\mu\nu q} = 2\delta_{kq} \tag{9.24}$$

which yields

$$\begin{aligned}
[\eta, H_\mathrm{J}] &= \sum_\mu \sum_{n,m} \sum_{\alpha,\beta} \left[-\sum_x (1-2\theta_x)\left(\eta_{nx}J_{xm} - \eta_{xm}J_{nx}\right)\right] \sigma^\mu_{\alpha\beta}\tau^\mu : c^\dagger_{n\alpha} c_{m\beta} : \\
&+ \sum_{n,m,\sigma} \left[\frac{3}{4} \sum_x \left(\eta_{nx}J_{xm} - \eta_{xm}J_{nx}\right)\right] : c^\dagger_{n\sigma} c_{m\sigma} : \\
&+ i \sum_{\mu,\nu,k} \sum_{n,m} \eta_{nm}J_{mn}\varepsilon_{\mu\nu k} \left[\sum_\alpha \sigma^k_{\alpha\alpha}\right] [\tau^\mu, \tau^\nu]\, \theta_m (1-\theta_n) \\
&+ i \sum_{\mu,\nu,k} \sum_{n,m} \eta_{nm}J_{mn}\varepsilon_{\mu\nu k} \left[\sum_\alpha \sigma^k_{\alpha\alpha}\right] \{\tau^\mu, \tau^\nu\}\, \theta_n \\
&+ 3 \sum_{n,m} \eta_{nm}J_{mn}\theta_n \mathbb{1}.
\end{aligned} \tag{9.25}$$

As the trace of a Pauli matrix is zero

$$\sum_\alpha \sigma^k_{\alpha\alpha} = 0, \tag{9.26}$$

the commutator finally results in

$$\begin{aligned}
[\eta, H_\mathrm{J}] &= \sum_\mu \sum_{n,m} \sum_{\alpha,\beta} \left[-\sum_x (1-2\theta_x)\left(\eta_{nx}J_{xm} - \eta_{xm}J_{nx}\right)\right] \sigma^\mu_{\alpha\beta}\tau^\mu : c^\dagger_{n\alpha} c_{m\beta} : \\
&+ \sum_{n,m,\sigma} \left[\frac{3}{4} \sum_x \left(\eta_{nx}J_{xm} - \eta_{xm}J_{nx}\right)\right] : c^\dagger_{n\sigma} c_{m\sigma} : + 3 \sum_{n,m} \eta_{nm}J_{mn}\theta_n \mathbb{1}.
\end{aligned} \tag{9.27}$$

Constructing the flow equation by comparing the coefficients in Eq. (4.4) yields the flow equation (4.87). The remaining terms in Eq. (4.87) stem from the commutation of the spin-spin interaction and the bilinear terms as well as the commutation of the hopping terms with themselves. Both calculations only require commutations of two bilinear operators.

9.6 Energy Representation

In the following, each separate step of the calculation mentioned in Sec. 2.5 is shown explicitly.
At first, a continuum limit is introduced

$$\sum_{\mathbf{k}} \to \frac{\Omega}{8\pi^3} \int \mathrm{d}^3 k \tag{9.28}$$

where Ω is the volume of the probe. In order to maintain fermionic anticommutation relations in the continuum, new operators must be introduced

$$c^\dagger_{\mathbf{k}\sigma} \to \sqrt{\frac{8\pi^3}{\Omega}} a^\dagger_{\mathbf{k}\sigma}. \tag{9.29}$$

Next, we use spherical coordinates and exploit that the coefficients are rotation-invariant

$$\int \mathrm{d}^3 k \to 4\pi \int \mathrm{d}k\, k^2 \tag{9.30}$$

while we introduce the operator

$$a^\dagger_{\mathbf{k}\sigma} \to \frac{a^\dagger_{k\sigma}}{\sqrt{4\pi} k}. \tag{9.31}$$

In order to justify the operator substitution, one can use a spherical harmonic expansion

$$\begin{aligned} a_{\mathbf{k}\sigma} &= \frac{1}{k} \sum_{l,m} a_{klm,\sigma} Y_{lm}\left(\hat{k}\right) \\ a_{klm,\sigma} &= k \int \mathrm{d}\Omega_{\hat{k}} Y^*_{lm}\left(\hat{k}\right) a_{\mathbf{k}\sigma}. \end{aligned} \tag{9.32}$$

If the parameters $\varepsilon_{\mathbf{k}}$ and $V_{\mathbf{k}}$ are rotation-invariant, one finds that only operators with $m = l = 0$ contribute [8]. The new operators still fulfill fermionic anticommutation relations. In the next step we switch to the energy representation. We substitute

$$k \to \varepsilon(k) \tag{9.33}$$

and use

$$a^\dagger_k = \sqrt{\frac{\mathrm{d}\varepsilon_k}{\mathrm{d}k}}\, c^\dagger_{\varepsilon(k)}. \tag{9.34}$$

From the definition of the density of states

$$\rho(\varepsilon) = \sum_{\mathbf{k}} \delta(\varepsilon - \varepsilon_{\mathbf{k}}) \tag{9.35}$$

we can deduce

$$\rho(\varepsilon) = \frac{\Omega}{2\pi^2} k^2 \frac{\mathrm{d}k}{\mathrm{d}\varepsilon}. \tag{9.36}$$

This leads to the final form (2.42).

9.7 Wick's Theorem

An operator can be normal-ordered using Wick's theorem [115]

$$\begin{aligned}\hat{A}_1\hat{A}_2...\hat{A}_n &= :\hat{A}_1\hat{A}_2...\hat{A}_n: + \sum_c :\hat{A}_1...\hat{A}_i^c...\hat{A}_j^c...\hat{A}_n: \\ &+ \sum_{c,d} :\hat{A}_1...\hat{A}_i^c...\hat{A}_r^d...\hat{A}_j^c...\hat{A}_s^d...\hat{A}_n: + ...\end{aligned} \tag{9.37}$$

where the first sum runs over all single contractions and the second sum runs over all double contractions and so on. The contractions are given by the expectation value of the respective operators

$$\hat{A}_i^c\hat{A}_j^c = \langle \hat{A}_i\hat{A}_j\rangle. \tag{9.38}$$

Two contracted operators have to be brought side by side. Each time two fermionic operators are swapped, a minus sign is introduced. The normal-ordering scheme is best understood looking at a few examples

$$\begin{aligned}\hat{A}_1\hat{A}_2 &= :\hat{A}_1\hat{A}_2: + \langle\hat{A}_1\hat{A}_2\rangle \\ \hat{A}_1\hat{A}_2\hat{A}_3\hat{A}_4 &= :\hat{A}_1\hat{A}_2\hat{A}_3\hat{A}_4: + :\hat{A}_3\hat{A}_4:\langle\hat{A}_1\hat{A}_2\rangle - :\hat{A}_2\hat{A}_4:\langle\hat{A}_1\hat{A}_3\rangle + :\hat{A}_2\hat{A}_3:\langle\hat{A}_1\hat{A}_4\rangle \\ &+ :\hat{A}_1\hat{A}_4:\langle\hat{A}_2\hat{A}_3\rangle - :\hat{A}_1\hat{A}_3:\langle\hat{A}_2\hat{A}_4\rangle + :\hat{A}_1\hat{A}_2:\langle\hat{A}_3\hat{A}_4\rangle + \langle\hat{A}_1\hat{A}_2\rangle\langle\hat{A}_3\hat{A}_4\rangle \\ &- \langle\hat{A}_1\hat{A}_3\rangle\langle\hat{A}_2\hat{A}_4\rangle + \langle\hat{A}_1\hat{A}_4\rangle\langle\hat{A}_2\hat{A}_3\rangle.\end{aligned} \tag{9.39}$$

In order to calculate commutators between normal-ordered operators, one can make use of helpful rules for the products of normal-ordered operators

$$\begin{aligned}:\hat{A}_1\hat{A}_2...\hat{A}_n::\hat{B}_1\hat{B}_2...\hat{B}_m: &= :\hat{A}_1...\hat{A}_n\hat{B}_1...\hat{B}_m: + \sum_c :\hat{A}_1...A_i^c...\hat{A}_n\hat{B}_1...\hat{B}_j^c...\hat{B}_m: \\ &+ \sum_{c,d} :\hat{A}_1...A_i^c...A_r^d...\hat{A}_n\hat{B}_1...\hat{B}_j^c...\hat{B}_s^d...\hat{B}_m: + ...\end{aligned} \tag{9.40}$$

where only contractions between operators including both A and B operators are taken into account. The rule for the sign in the case of fermionic operators is the same as in Wick's theorem. Again, this rule is best explained looking at some examples. We look at the product of two bilinear normal-ordered operators

$$\begin{aligned}:\hat{A}_1\hat{A}_2::\hat{B}_1\hat{B}_2: &= :\hat{A}_1\hat{A}_2\hat{B}_1\hat{B}_2: - :\hat{A}_2\hat{B}_2:\langle\hat{A}_1\hat{B}_1\rangle + :\hat{A}_2\hat{B}_1:\langle\hat{A}_1\hat{B}_2\rangle \\ &+ :\hat{A}_1\hat{B}_2:\langle\hat{A}_2\hat{B}_1\rangle - :\hat{A}_1\hat{B}_1:\langle\hat{A}_2\hat{B}_2\rangle - \langle\hat{A}_1\hat{B}_1\rangle\langle\hat{A}_2\hat{B}_2\rangle + \langle\hat{A}_1\hat{B}_2\rangle\langle\hat{A}_2\hat{B}_1\rangle\end{aligned} \tag{9.41}$$

and at a product of a quartic and a bilinear term

$$\begin{aligned}&:\hat{A}_1\hat{A}_2\hat{A}_3\hat{A}_4::\hat{B}_1\hat{B}_2: \\ =\ &:\hat{A}_1\hat{A}_2\hat{A}_3\hat{A}_4\hat{B}_1\hat{B}_2: - :\hat{A}_2\hat{A}_3\hat{A}_4\hat{B}_2:\langle\hat{A}_1\hat{B}_1\rangle + :\hat{A}_1\hat{A}_3\hat{A}_4\hat{B}_2:\langle\hat{A}_2\hat{B}_1\rangle \\ -\ &:\hat{A}_1\hat{A}_2\hat{A}_4\hat{B}_2:\langle\hat{A}_3\hat{B}_1\rangle + :\hat{A}_1\hat{A}_2\hat{A}_3\hat{B}_2:\langle\hat{A}_4\hat{B}_1\rangle + :\hat{A}_2\hat{A}_3\hat{A}_4\hat{B}_1:\langle\hat{A}_1\hat{B}_2\rangle \\ -\ &:\hat{A}_1\hat{A}_3\hat{A}_4\hat{B}_1:\langle\hat{A}_2\hat{B}_2\rangle + :\hat{A}_1\hat{A}_2\hat{A}_4\hat{B}_1:\langle\hat{A}_3\hat{B}_2\rangle - :\hat{A}_1\hat{A}_2\hat{A}_3\hat{B}_1:\langle\hat{A}_4\hat{B}_2\rangle \\ -\ &:\hat{A}_3\hat{A}_4:\langle\hat{A}_1\hat{B}_1\rangle\langle\hat{A}_2\hat{B}_2\rangle + :\hat{A}_2\hat{A}_4:\langle\hat{A}_1\hat{B}_1\rangle\langle\hat{A}_3\hat{B}_2\rangle - :\hat{A}_2\hat{A}_3:\langle\hat{A}_1\hat{B}_1\rangle\langle\hat{A}_4\hat{B}_2\rangle \\ +\ &:\hat{A}_3\hat{A}_4:\langle\hat{A}_2\hat{B}_1\rangle\langle\hat{A}_1\hat{B}_2\rangle - :\hat{A}_1\hat{A}_4:\langle\hat{A}_2\hat{B}_1\rangle\langle\hat{A}_3\hat{B}_2\rangle + :\hat{A}_1\hat{A}_3:\langle\hat{A}_2\hat{B}_1\rangle\langle\hat{A}_4\hat{B}_2\rangle \\ -\ &:\hat{A}_2\hat{A}_4:\langle\hat{A}_3\hat{B}_1\rangle\langle\hat{A}_1\hat{B}_2\rangle + :\hat{A}_1\hat{A}_4:\langle\hat{A}_3\hat{B}_1\rangle\langle\hat{A}_2\hat{B}_2\rangle - :\hat{A}_1\hat{A}_2:\langle\hat{A}_3\hat{B}_1\rangle\langle\hat{A}_4\hat{B}_2\rangle \\ +\ &:\hat{A}_2\hat{A}_3:\langle\hat{A}_4\hat{B}_1\rangle\langle\hat{A}_1\hat{B}_2\rangle - :\hat{A}_1\hat{A}_3:\langle\hat{A}_4\hat{B}_1\rangle\langle\hat{A}_2\hat{B}_2\rangle + :\hat{A}_1\hat{A}_2:\langle\hat{A}_4\hat{B}_1\rangle\langle\hat{A}_3\hat{B}_2\rangle.\end{aligned} \tag{9.42}$$

9.8 Truncation Scheme in Orders of the Coulomb Interaction U

In this section the truncation used in Sec. 6.2 is justified systematically by an $O_{\min}/O_{\max}$ discussion as outlined in Sec. 4.3.3.

We will truncate in two parameters, namely U and h. We target the constant H_{E} from Eq. (9.44) and dismiss all terms that act on a higher order than h^2U^2 on H_{E}, i.e., we include all terms of order h^nU^m with $n,m \leq 2$. The Hamiltonian is of the form (cf. Sec. 6.1 and 6.2)

$$H = H_{\mathrm{t}} + H_{\mathrm{U}} + H_{\mathrm{R}} + H_{\Gamma} + H_{\mathrm{E}} \tag{9.43}$$

where

$$\begin{aligned}
H_{\mathrm{E}} &= E_0 \mathbb{1} && (9.44)\\
H_{\mathrm{t}} &= \sum_{n,m,\sigma} t_{nm} : c^\dagger_{n\sigma} c_{m\sigma} : \\
H_{\mathrm{U}} &= \sum_{n_1,n_2,n_3,n_4} U_{n_1 n_2 n_3 n_4} : c^\dagger_{n_1\uparrow} c^\dagger_{n_2\downarrow} c_{n_3\downarrow} c_{n_4\uparrow} : \\
H_{\mathrm{R}} &= \sum_{\substack{n_1,n_2,n_3,n_4 \\ n_2>n_1,n_4>n_3}} R^\sigma_{n_1 n_2 n_3 n_4} : c^\dagger_{n_1\sigma} c^\dagger_{n_2\sigma} c_{n_3\sigma} c_{n_4\sigma} : \\
H_{\Gamma} &= \sum_{n_1,n_6} \sum_{\substack{n_2,n_3,n_4,n_5 \\ n_3>n_2,n_5>n_4}} \Gamma^\sigma_{n_1 n_2 n_3 n_4 n_5 n_6} : c^\dagger_{n_1\sigma} c^\dagger_{n_2\bar{\sigma}} c^\dagger_{n_3\bar{\sigma}} c_{n_4\bar{\sigma}} c_{n_5\bar{\sigma}} c_{n_6\sigma} : .
\end{aligned}$$

All other emerging terms are at least of order U^3. We write the DEQ in the form

$$\partial_l H_i = \sum_{k,q} \left[\eta_k, H_q\right]_i \tag{9.45}$$

where the sum runs over the different terms from Eq. (9.44) and the index of the commutator in Eq. (9.45) denotes the contribution of the commutator with the same operator structure as the Hamiltonian H_i (where i labels the indices from Eq. (9.44)). We focus on the constant E_0 and want it to be correct up to the order h^2U^2, i.e., we include all terms that act in an order h^nU^m with $n,m \leq 2$ on E_0. The following tables show which commutations have to be taken into account.

	$O_{\min}$	included orders
H_{E}	h^2, U^2	h^nU^m with $n,m \leq 2$
H_{t}	h	h, h^2, U, U^2, hU, hU^2
H_{U}	U	h, h^2, U, U^2, hU, h^2U
H_{R}	U^2	h, h^2, U, U^2
H_{Γ}	U^2	h, U, hU
H_{residual}	$\geq U^3$	-

As H_{R} emerges in order U^2, we can drop the order h^2 because $O_{\min} > O_{\max}$. The H_{Γ}-terms are dismissed as they emerge in order U^2 and thus $O_{\min} > O_{\max}$.

Commutators acting on the constant H_{E}

Commutator	$O_{\min}$	included orders	used
$[\eta_{\mathrm{t}}, H_{\mathrm{t}}]_{\mathrm{E}}$	h^2	$h^n U^m$ with $n,m \leq 2$	✓
$[\eta_{\mathrm{U}}, H_{\mathrm{U}}]_{\mathrm{E}}$	U^2	"	✓
$[\eta_{\mathrm{R}}, H_{\mathrm{R}}]_{\mathrm{E}}$	U^4	"	✗
$[\eta_{\Gamma}, H_{\Gamma}]_{\mathrm{E}}$	U^4	"	✗

Commutators acting on H_{t}

Commutator	$O_{\min}$	included orders	used
$[\eta_{\mathrm{t}}, H_{\mathrm{t}}]_{\mathrm{t}}$	h^2	h, h^2, U, U^2, hU, hU^2	✓
$[\eta_{\mathrm{t}}, H_{\mathrm{U}}]_{\mathrm{t}} / [\eta_{\mathrm{U}}, H_{\mathrm{t}}]_{\mathrm{t}}$	hU	"	✓
$[\eta_{\mathrm{t}}, H_{\mathrm{R}}]_{\mathrm{t}} / [\eta_{\mathrm{R}}, H_{\mathrm{t}}]_{\mathrm{t}}$	hU^2	"	✓
$[\eta_{\mathrm{U}}, H_{\mathrm{U}}]_{\mathrm{t}}$	U^2	"	✓
$[\eta_{\mathrm{U}}, H_{\mathrm{R}}]_{\mathrm{t}} / [\eta_{\mathrm{R}}, H_{\mathrm{U}}]_{\mathrm{t}}$	U^3	"	✗
$[\eta_{\mathrm{U}}, H_{\Gamma}]_{\mathrm{t}} / [\eta_{\Gamma}, H_{\mathrm{U}}]_{\mathrm{t}}$	U^3	"	✗
$[\eta_{\mathrm{R}}, H_{\mathrm{R}}]_{\mathrm{t}}$	U^4	"	✗
$[\eta_{\mathrm{R}}, H_{\Gamma}]_{\mathrm{t}} / [\eta_{\mathrm{R}}, H_{\Gamma}]_{\mathrm{t}}$	U^4	"	✗
$[\eta_{\Gamma}, H_{\Gamma}]_{\mathrm{t}}$	U^4	"	✗

Commutators acting on H_{U}

Commutator	$O_{\min}$	included orders	used
$[\eta_{\mathrm{t}}, H_{\mathrm{U}}]_{\mathrm{U}} / [\eta_{\mathrm{U}}, H_{\mathrm{t}}]_{\mathrm{U}}$	hU	h, h^2, U, U^2, hU, h^2U	✓
$[\eta_{\mathrm{t}}, H_{\Gamma}]_{\mathrm{U}} / [\eta_{\Gamma}, H_{\mathrm{t}}]_{\mathrm{U}}$	hU^2	"	✗
$[\eta_{\mathrm{U}}, H_{\mathrm{U}}]_{\mathrm{U}}$	U^2	"	✓
$[\eta_{\mathrm{U}}, H_{\mathrm{R}}]_{\mathrm{U}} / [\eta_{\mathrm{R}}, H_{\mathrm{U}}]_{\mathrm{U}}$	U^3	"	✗
$[\eta_{\mathrm{U}}, H_{\Gamma}]_{\mathrm{U}} / [\eta_{\Gamma}, H_{\mathrm{U}}]_{\mathrm{U}}$	U^3	"	✗
$[\eta_{\mathrm{R}}, H_{\mathrm{R}}]_{\mathrm{U}}$	U^4	"	✗
$[\eta_{\mathrm{R}}, H_{\Gamma}]_{\mathrm{U}} / [\eta_{\Gamma}, H_{\mathrm{R}}]_{\mathrm{U}}$	U^4	"	✗
$[\eta_{\Gamma}, H_{\Gamma}]_{\mathrm{U}}$	U^4	"	✗

Commutators acting on H_{R}

Commutator	$O_{\min}$	included orders	used
$[\eta_{\mathrm{t}}, H_{\mathrm{R}}]_{\mathrm{R}} / [\eta_{\mathrm{R}}, H_{\mathrm{t}}]_{\mathrm{R}}$	hU^2	U, U^2	✗
$[\eta_{\mathrm{t}}, H_{\Gamma}]_{\mathrm{R}} / [\eta_{\Gamma}, H_{\mathrm{t}}]_{\mathrm{R}}$	hU^2	"	✗
$[\eta_{\mathrm{U}}, H_{\mathrm{U}}]_{\mathrm{R}}$	U^2	"	✓
$[\eta_{\mathrm{U}}, H_{\mathrm{R}}]_{\mathrm{R}} / [\eta_{\mathrm{R}}, H_{\mathrm{U}}]_{\mathrm{R}}$	U^3	"	✗
$[\eta_{\mathrm{U}}, H_{\Gamma}]_{\mathrm{R}} / [\eta_{\Gamma}, H_{\mathrm{U}}]_{\mathrm{R}}$	U^3	"	✗
$[\eta_{\mathrm{R}}, H_{\mathrm{R}}]_{\mathrm{R}}$	U^4	"	✗
$[\eta_{\mathrm{R}}, H_{\Gamma}]_{\mathrm{R}} / [\eta_{\Gamma}, H_{\mathrm{R}}]_{\mathrm{R}}$	U^4	"	✗
$[\eta_{\Gamma}, H_{\Gamma}]_{\mathrm{R}}$	U^4	"	✗

As we can see from the tables above, no contribution H_Γ must be taken into account. Thus, we can neglect such terms and the remaining DEQ is constructed from

$$\begin{aligned}
\partial_l H_\mathrm{E} &= [\eta_\mathrm{t}, H_\mathrm{t}]_\mathrm{E} + [\eta_\mathrm{U}, H_\mathrm{U}]_\mathrm{E} \\
\partial_l H_t &= [\eta_\mathrm{t}, H_\mathrm{t}]_\mathrm{t} + [\eta_\mathrm{t}, H_\mathrm{U}]_\mathrm{t} + [\eta_\mathrm{U}, H_\mathrm{t}]_\mathrm{t} + [\eta_\mathrm{t}, H_\mathrm{R}]_\mathrm{t} + [\eta_\mathrm{R}, H_\mathrm{t}]_\mathrm{t} + [\eta_\mathrm{U}, H_\mathrm{U}]_\mathrm{t} \\
\partial_l H_\mathrm{U} &= [\eta_\mathrm{t}, H_\mathrm{U}]_\mathrm{U} + [\eta_\mathrm{U}, H_\mathrm{t}]_\mathrm{U} + [\eta_\mathrm{U}, H_\mathrm{U}]_\mathrm{U} \\
\partial_l H_\mathrm{R} &= \left[\eta_\mathrm{R}, H_{t,\mathrm{diag}}\right]_\mathrm{R} + [\eta_\mathrm{U}, H_\mathrm{U}]_\mathrm{R} .
\end{aligned} \tag{9.46}$$

9.9 Local Commutators and Products for the Local Impurity Operator Basis

We present useful local commutators and products of the parametrization from Sec. 7.1. The operator basis is chosen to be

bosonic operators	fermionic operators
$\mathbb{1}$	$F_{1,\uparrow} = \left(1 - n_{\mathrm{d},\downarrow}\right) d_\uparrow$
$n_z = n_{\mathrm{d},\uparrow} - n_{\mathrm{d},\downarrow}$	$F_{1,\downarrow} = \left(1 - n_{\mathrm{d},\uparrow}\right) d_\downarrow$
$d_\uparrow^\dagger d_\downarrow$	$F_{2,\uparrow} = n_{\mathrm{d},\downarrow} d_\uparrow$
$d_\downarrow^\dagger d_\uparrow$	$F_{2,\downarrow} = n_{\mathrm{d},\uparrow} d_\downarrow$
$d_\downarrow d_\uparrow$	$F_{2,\uparrow}^\dagger = n_{\mathrm{d},\downarrow} d_\uparrow^\dagger$
$d_\uparrow^\dagger d_\downarrow^\dagger$	$F_{2,\downarrow}^\dagger = n_{\mathrm{d},\uparrow} d_\downarrow^\dagger$
$\bar{n} = n_{\mathrm{d},\uparrow} + n_{\mathrm{d},\downarrow} - \mathbb{1}$	$F_{1,\uparrow}^\dagger = \left(1 - n_{\mathrm{d},\downarrow}\right) d_\uparrow^\dagger$
$\hat{D} = 2 n_{\mathrm{d},\uparrow} n_{\mathrm{d},\downarrow} - \bar{n}$	$F_{1,\downarrow}^\dagger = \left(1 - n_{\mathrm{d},\uparrow}\right) d_\downarrow^\dagger$

The operators from the initial parametrization and the new one are given by

$$\begin{gathered}
d_\sigma^\dagger = F_{1,\sigma}^\dagger + F_{2,\sigma}^\dagger \\
d_\sigma^\dagger d_\sigma = \tfrac{1}{2}\left(\bar{n} + \sigma n_z + \mathbb{1}\right) \\
d_\sigma^\dagger d_\sigma d_{\bar{\sigma}}^\dagger d_{\bar{\sigma}} = \tfrac{1}{2}\left(\hat{D} + \bar{n}\right)
\end{gathered}$$

Basic commutators

$$\left[F^\dagger_{i,\sigma},\bar{n}\right] = -F^\dagger_{i,\sigma} \qquad \left[d^\dagger_\uparrow d^\dagger_\downarrow,\bar{n}\right] = -2d^\dagger_\uparrow d^\dagger_\downarrow$$
$$\left[F^\dagger_{i,\sigma},n_z\right] = -\sigma F^\dagger_{i,\sigma} \qquad \left[d^\dagger_\uparrow d^\dagger_\downarrow,n_z\right] = 0$$
$$\left[F^\dagger_{1,\sigma},\hat{D}\right] = F^\dagger_{1,\sigma} \qquad \left[d^\dagger_\uparrow d^\dagger_\downarrow,\hat{D}\right] = 0$$
$$\left[F^\dagger_{2,\sigma},\hat{D}\right] = -F^\dagger_{2,\sigma} \qquad \left[d^\dagger_\uparrow d^\dagger_\downarrow,d^\dagger_\sigma d_{\bar{\sigma}}\right] = 0$$
$$\left[F^\dagger_{i,\sigma},d^\dagger_\alpha d_{\bar{\alpha}}\right] = -F^\dagger_{i,\bar{\sigma}}\delta_{\alpha\bar{\sigma}} \qquad \left[d^\dagger_\uparrow d^\dagger_\downarrow,d_\downarrow d_\uparrow\right] = \bar{n}$$
$$\left[F^\dagger_{1,\sigma},d_\downarrow d_\uparrow\right] = -\sigma F_{2,\bar{\sigma}} \qquad \left\{F^\dagger_{1,\sigma},F_{1,\sigma}\right\} = \tfrac{1}{2}\left(\sigma n_z - \bar{n} + \mathbb{1}\right)$$
$$\left[F^\dagger_{2,\sigma},d_\downarrow d_\uparrow\right] = -\sigma F_{1,\bar{\sigma}} \qquad \left\{F^\dagger_{1,\sigma},F_{1,\bar{\sigma}}\right\} = d^\dagger_\sigma d_{\bar{\sigma}}$$
$$\left[F^\dagger_{i,\sigma},d^\dagger_\uparrow d^\dagger_\downarrow\right] = 0 \qquad \left\{F^\dagger_{2,\sigma},F_{2,\sigma}\right\} = \tfrac{1}{2}\left(\bar{n} - \sigma n_z + \mathbb{1}\right)$$
$$\left[d^\dagger_\sigma d_{\bar{\sigma}},\bar{n}\right] = 0 \qquad \left\{F^\dagger_{2,\sigma},F_{2,\bar{\sigma}}\right\} = -d^\dagger_\sigma d_{\bar{\sigma}}$$
$$\left[d^\dagger_\sigma d_{\bar{\sigma}},n_z\right] = -2\sigma d^\dagger_\sigma d_{\bar{\sigma}} \qquad \left\{F^\dagger_{2,\sigma},F_{1,\alpha}\right\} = 0$$
$$\left[d^\dagger_\sigma d_{\bar{\sigma}},\hat{D}\right] = 0 \qquad \left\{F^\dagger_{1,\sigma},F_{2,\alpha}\right\} = 0$$
$$\left[d^\dagger_\sigma d_{\bar{\sigma}},d^\dagger_\alpha d_{\bar{\alpha}}\right] = \sigma n_z \delta_{\sigma\bar{\alpha}} \qquad \left\{F^\dagger_{1,\sigma},F^\dagger_{2,\alpha}\right\} = -d^\dagger_\sigma d^\dagger_{\bar{\sigma}}\delta_{\alpha\bar{\sigma}}$$
$$\left[d^\dagger_\uparrow d^\dagger_\downarrow,n_z\right] = 0 \qquad \left\{F^\dagger_{i,\sigma},F^\dagger_{i,\alpha}\right\} = 0$$

Basic local products

$$F^\dagger_{1,\sigma}F_{1,\sigma} = \tfrac{1}{2}\left(\mathbb{1} + \sigma n_z - \hat{D}\right) \qquad F^\dagger_{2,\sigma}F_{2,\sigma} = \tfrac{1}{2}\left(\hat{D} + \bar{n}\right)$$
$$F^\dagger_{1,\sigma}F_{2,\alpha} = 0 \qquad F^\dagger_{2,\sigma}F_{1,\alpha} = 0$$
$$F^\dagger_{1,\sigma}\bar{n} = -F^\dagger_{1,\sigma} \qquad F^\dagger_{2,\sigma}\bar{n} = 0$$
$$F^\dagger_{1,\sigma}n_z = 0 \qquad F^\dagger_{2,\sigma}n_z = -\sigma F^\dagger_{2,\sigma}$$
$$F^\dagger_{1,\sigma}\hat{D} = F^\dagger_{1,\sigma} \qquad F^\dagger_{2,\sigma}\hat{D} = 0$$
$$F^\dagger_{1,\sigma}d^\dagger_\alpha d_{\bar{\alpha}} = 0 \qquad F^\dagger_{2,\sigma}d^\dagger_\alpha d_{\bar{\alpha}} = -F^\dagger_{2,\bar{\sigma}}\delta_{\sigma\bar{\alpha}}$$
$$F^\dagger_{1,\sigma}d_\downarrow d_\uparrow = -\sigma F_{2,\bar{\sigma}} \qquad F^\dagger_{2,\sigma}d_\downarrow d_\uparrow = 0$$
$$F^\dagger_{i,\sigma}d^\dagger_\uparrow d^\dagger_\downarrow = 0 \qquad d^\dagger_\uparrow d^\dagger_\downarrow d^\dagger_\sigma d_{\bar{\sigma}} = 0$$
$$\bar{n}^2 = \hat{D} \qquad \bar{n}n_z = 0$$
$$n_z^2 = \mathbb{1} - \hat{D} \qquad \bar{n}\hat{D} = \bar{n}$$
$$\hat{D}^2 = \hat{D} \qquad n_z\hat{D} = 0$$
$$d^\dagger_\sigma d_{\bar{\sigma}}\bar{n} = 0 \qquad d^\dagger_\uparrow d^\dagger_\downarrow \bar{n} = -d^\dagger_\uparrow d^\dagger_\downarrow$$
$$d^\dagger_\sigma d_{\bar{\sigma}}n_z = -\sigma d^\dagger_\sigma d_{\bar{\sigma}} \qquad d^\dagger_\uparrow d^\dagger_\downarrow n_z = 0$$
$$d^\dagger_\sigma d_{\bar{\sigma}}\hat{D} = 0 \qquad d^\dagger_\uparrow d^\dagger_\downarrow \hat{D} = d^\dagger_\uparrow d^\dagger_\downarrow$$

9.10 Kondo Model Coupled to an Auxiliary Spin

9.10.1 Starting Values

The starting values for the Kondo model coupled to an auxiliary spin (7.57) in the new operator basis from Sec. 7.4 are presented.

The starting values for the energy levels of the singlet and triplet states are given by

$E_{00} = -\frac{3K}{4}$	$E_{11} = \frac{K}{4}$	$E_{22} = \frac{K}{4}$	$E_{33} = \frac{K}{4}$

while the starting values for the couplings of the Hamiltonian (7.57) are of the form

$$J_{nm}^{kq\alpha\beta} = \sum_{\mu} J_{nm} \alpha_{kq}^{\mu} \sigma_{\alpha\beta}^{\mu} \tag{9.47}$$

where α^{μ} denotes the matrices from Eq. (7.55). The explicit values of the coefficients (9.47) are given by

$J_{nm}^{03\downarrow\uparrow}(0) = +\frac{1}{\sqrt{2}} J_{nm}(0)$	$J_{nm}^{30\uparrow\downarrow}(0) = +\frac{1}{\sqrt{2}} J_{nm}(0)$
$J_{nm}^{12\downarrow\uparrow}(0) = +\frac{1}{\sqrt{2}} J_{nm}(0)$	$J_{nm}^{21\uparrow\downarrow}(0) = +\frac{1}{\sqrt{2}} J_{nm}(0)$
$J_{nm}^{23\downarrow\uparrow}(0) = +\frac{1}{\sqrt{2}} J_{nm}(0)$	$J_{nm}^{32\uparrow\downarrow}(0) = +\frac{1}{\sqrt{2}} J_{nm}(0)$
$J_{nm}^{01\uparrow\downarrow}(0) = -\frac{1}{\sqrt{2}} J_{nm}(0)$	$J_{nm}^{10\downarrow\uparrow}(0) = -\frac{1}{\sqrt{2}} J_{nm}(0)$
$J_{nm}^{02\uparrow\uparrow}(0) = +\frac{1}{2} J_{nm}(0)$	$J_{nm}^{02\downarrow\downarrow}(0) = -\frac{1}{2} J_{nm}(0)$
$J_{nm}^{20\downarrow\downarrow}(0) = -\frac{1}{2} J_{nm}(0)$	$J_{nm}^{20\uparrow\uparrow}(0) = +\frac{1}{2} J_{nm}(0)$
$J_{nm}^{11\uparrow\uparrow}(0) = +\frac{1}{2} J_{nm}(0)$	$J_{nm}^{11\downarrow\downarrow}(0) = -\frac{1}{2} J_{nm}(0)$
$J_{nm}^{33\uparrow\uparrow}(0) = -\frac{1}{2} J_{nm}(0)$	$J_{nm}^{33\downarrow\downarrow}(0) = +\frac{1}{2} J_{nm}(0)$

The indices $k = 0$ belong to the singlet state and $k = 1,2,3$ belong to the triplet states $t_{1,2,3}$ from Eq. (7.51).

9.10.2 Symmetries of the Coefficients

The symmetries of the coefficients $J_{nm}^{kq\alpha\beta}$ from Eq. (7.57) of the Kondo model coupled to an auxiliary spin from Sec. 7.4.1 are outlined in the following.

Besides the hermiticity

$$J_{nm}^{kq\alpha\beta} = J_{mn}^{qk\beta\alpha}, \tag{9.48}$$

the coefficients also fulfill a number of symmetries. There are 64 coefficients for each index pair (n,m). However, a lot of combinations of the indices k, q, α and β are forbidden by spin conservation. By using the S_z-spin conservation only 20 coefficients remain. The coefficients allowed by spin conservation are

$J_{nm}^{01\uparrow\downarrow}$	$J_{nm}^{12\downarrow\uparrow}$	$J_{nm}^{03\downarrow\uparrow}$	$J_{nm}^{23\downarrow\uparrow}$	$J_{nm}^{02\uparrow\uparrow}$	$J_{nm}^{20\uparrow\uparrow}$	$J_{nm}^{00\uparrow\uparrow}$	$J_{nm}^{11\uparrow\uparrow}$	$J_{nm}^{22\uparrow\uparrow}$	$J_{nm}^{33\uparrow\uparrow}$
$J_{nm}^{10\downarrow\uparrow}$	$J_{nm}^{21\uparrow\downarrow}$	$J_{nm}^{30\uparrow\downarrow}$	$J_{nm}^{32\uparrow\downarrow}$	$J_{nm}^{02\downarrow\downarrow}$	$J_{nm}^{20\downarrow\downarrow}$	$J_{nm}^{00\downarrow\downarrow}$	$J_{nm}^{11\downarrow\downarrow}$	$J_{nm}^{22\downarrow\downarrow}$	$J_{nm}^{33\downarrow\downarrow}$

where the indices $k = 0$ belong to the singlet state and $k = 1,2,3$ belong to the triplet states $t_{1,2,3}$ from Eq. (7.51). All other coefficients remain zero during the whole flow. Some coefficients are connected by further symmetries

$J_{nm}^{00\uparrow\uparrow} = +J_{nm}^{00\downarrow\downarrow}$	$J_{nm}^{01\uparrow\downarrow} = -J_{nm}^{03\downarrow\uparrow}$
$J_{nm}^{22\uparrow\uparrow} = +J_{nm}^{22\downarrow\downarrow}$	$J_{nm}^{10\downarrow\uparrow} = -J_{nm}^{30\uparrow\downarrow}$
$J_{nm}^{11\uparrow\uparrow} = +J_{nm}^{33\downarrow\downarrow}$	$J_{nm}^{12\downarrow\uparrow} = +J_{nm}^{32\uparrow\downarrow}$
$J_{nm}^{33\uparrow\uparrow} = +J_{nm}^{11\downarrow\downarrow}$	$J_{nm}^{21\uparrow\downarrow} = +J_{nm}^{23\downarrow\uparrow}$
$J_{nm}^{02\uparrow\uparrow} = -J_{nm}^{02\downarrow\downarrow}$	$J_{nm}^{20\uparrow\uparrow} = -J_{nm}^{20\downarrow\downarrow}$

Finally, only **10** coefficients remain which are not connected by a symmetry.

9.10.3 Vanishing Coupling and Kondo Energy Scale

The calculation from Sec. 7.4.3 is demonstrated explicitly.

Useful rules for the products and commutators of the matrices α^μ from Eq. (7.55) used in this section are

$$\begin{aligned} \alpha^\mu \alpha^\nu &= \frac{1}{4}\delta_{\mu\nu}\mathbb{1} + \frac{i}{2}\sum_{k\in x,y,z} \varepsilon_{\mu\nu k}\alpha^k \\ [\alpha^\mu, \alpha^\nu] &= i\sum_{k\in x,y,z} \varepsilon_{\mu\nu k}\alpha^k. \end{aligned} \tag{9.49}$$

Furthermore, the calculation rule for the Levi-Civita symbol

$$\sum_{\mu,\nu} \varepsilon_{\mu\nu s}\varepsilon_{\mu\nu r} = 2\delta_{sr} \tag{9.50}$$

is used. We start from the differential equation (7.67) with $K = 0$

$$\begin{aligned} \partial_l J_{nm}^{kq\alpha\beta} &= (\varepsilon_m - \varepsilon_n)\,\eta_{nm}^{kq\alpha\beta} \\ &+ \sum_{\gamma,p}\sum_{x}\left(\eta_{nx}^{pq\alpha\gamma} J_{xm}^{kp\gamma\beta} - \eta_{xm}^{kp\gamma\beta} J_{nx}^{pq\alpha\gamma}\right)\theta_x \\ &+ \sum_{\gamma,p}\sum_{x}\left(\eta_{nx}^{kp\alpha\gamma} J_{xm}^{pq\gamma\beta} - \eta_{xm}^{pq\gamma\beta} J_{nx}^{kp\alpha\gamma}\right)(1-\theta_x). \end{aligned} \tag{9.51}$$

It is important to note that the flow of the single-particle energies ε_n is neglected in this approximation and thus we can replace ε_n by its starting value ε_n^0. We make the ansatz

$$\begin{aligned} \partial_l J_{nm}^{kq\alpha\beta} &= J_{nm}\sum_\mu \alpha_{kq}^\mu \sigma_{\alpha\beta}^\mu + \tilde{t}_{nm}\delta_{kq}\delta_{\alpha\beta} \\ \partial_l \eta_{nm}^{kq\alpha\beta} &= \eta_{nm}^J \sum_\mu \alpha_{kq}^\mu \sigma_{\alpha\beta}^\mu + \eta_{nm}^t \delta_{kq}\delta_{\alpha\beta} \end{aligned} \tag{9.52}$$

where $\tilde{t}_{nm}$ has the starting value zero. Hence, $\tilde{t}_{nn} \neq \varepsilon_n$ but $\partial_l \tilde{t}_{nn} = \partial_l \varepsilon_n$. Thus, we can define a new quantity

$$t_{nm} = \tilde{t}_{nm} + \varepsilon_n^0 \delta_{nm} \quad \Leftrightarrow \quad \partial_l t_{nm} = \partial_l \tilde{t}_{nm}. \tag{9.53}$$

This quantity now coincides with the standard hopping terms used in Eq. (4.87). Introducing

the coefficients (9.52) yields

$$\begin{aligned}
\partial_l \left(J_{nm} \sum_\mu \alpha^\mu_{kq} \sigma^\mu_{\alpha\beta} + \tilde{t}_{nm} \delta_{kq} \delta_{\alpha\beta} \right) &= \sum_x \eta^J_{nx} J_{xm} \sum_{\mu,\nu} [\alpha^\nu \alpha^\mu]_{kq} [\sigma^\mu \sigma^\nu]_{\alpha\beta} \, \theta_x \\
&- \sum_x \eta^J_{xm} J_{nx} \sum_{\mu,\nu} [\alpha^\mu \alpha^\nu]_{kq} [\sigma^\nu \sigma^\mu]_{\alpha\beta} \, \theta_x \\
&+ \sum_x \eta^J_{nx} J_{xm} \sum_{\mu,\nu} [\alpha^\mu \alpha^\nu]_{kq} [\sigma^\mu \sigma^\nu]_{\alpha\beta} \, (1-\theta_x) \\
&- \sum_x \eta^J_{xm} J_{nx} \sum_{\mu,\nu} [\alpha^\nu \alpha^\mu]_{kq} [\sigma^\nu \sigma^\mu]_{\alpha\beta} \, (1-\theta_x) \\
&+ \sum_x \left(\eta^t_{nx} J_{xm} - \eta^t_{xm} J_{nx} \right) \sum_\mu \alpha^\mu_{kq} \sigma^\mu_{\alpha\beta} \\
&+ \left[\left(\varepsilon^0_m - \varepsilon^0_n \right) \eta^J_{nm} + \sum_x \left(\eta^J_{nx} \tilde{t}_{xm} - \eta^J_{xm} \tilde{t}_{nx} \right) \right] \sum_\mu \alpha^\mu_{kq} \sigma^\mu_{\alpha\beta} \\
&+ \left[\left(\varepsilon^0_m - \varepsilon^0_n \right) \eta^t_{nm} + \sum_x \left(\eta^t_{nx} \tilde{t}_{xm} - \eta^t_{xm} \tilde{t}_{nx} \right) \right] \delta_{kq} \delta_{\alpha\beta}
\end{aligned} \tag{9.54}$$

where we used

$$\sum_\gamma \sigma^\mu_{\alpha\gamma} \sigma^\nu_{\gamma\beta} = [\sigma^\mu \sigma^\nu]_{\alpha\beta} \, , \quad \sum_p \alpha^\mu_{kp} \alpha^\nu_{pq} = [\alpha^\mu \alpha^\nu]_{kq} \, . \tag{9.55}$$

In the next step we use Eqs. (9.17), (9.49) and (9.50) which results in

$$\begin{aligned}
\partial_l J_{nm} \sum_\mu \alpha^\mu_{kq} \sigma^\mu_{\alpha\beta} &+ \partial_l t_{nm} \delta_{kq} \delta_{\alpha\beta} \\
&= \sum_x \left(\eta^t_{nx} J_{xm} - \eta^t_{xm} J_{nx} \right) \sum_\mu \alpha^\mu_{kq} \sigma^\mu_{\alpha\beta} \\
&+ \sum_x \left(\left(\tilde{t}_{xm} + \varepsilon^0_x \delta_{xm} \right) \eta^J_{nx} - \left(\tilde{t}_{nx} + \varepsilon^0_n \delta_{nx} \right) \eta^J_{xm} \right) \sum_\mu \alpha^\mu_{kq} \sigma^\mu_{\alpha\beta} \\
&- \sum_x \left(\eta^J_{nx} J_{xm} - \eta^J_{xm} J_{nx} \right) (1-2\theta_x) \sum_\mu \sigma^\mu_{\alpha\beta} \alpha^\mu_{kq} \\
&+ \sum_x \left(\left(\tilde{t}_{xm} + \varepsilon^0_x \delta_{xm} \right) \eta^t_{nx} - \left(\tilde{t}_{nx} + \varepsilon^0_n \delta_{nx} \right) \eta^t_{xm} \right) \delta_{kq} \delta_{\alpha\beta} \\
&+ \frac{3}{4} \sum_x \left(\eta^J_{nx} J_{xm} - \eta^J_{xm} J_{nx} \right) \delta_{kq} \delta_{\alpha\beta} \, .
\end{aligned} \tag{9.56}$$

Comparing the coefficients and using Eq. (9.53) yields the final differential equation

$$\begin{aligned}
\partial_l J_{nm} &= \sum_x \left(\eta^J_{nx} t_{xm} - \eta^J_{xm} t_{nx} + \eta^t_{nx} J_{xm} - \eta^t_{xm} J_{nx} \right) \\
&- \sum_x \left(\eta^J_{nx} J_{xm} - \eta^J_{xm} J_{nx} \right) (1-2\theta_x) \\
\partial_l t_{nm} &= \sum_x \left(\eta^t_{nx} t_{xm} - \eta^t_{xm} t_{nx} \right) + \frac{3}{4} \sum_x \left(\eta^J_{nx} J_{xm} - \eta^J_{xm} J_{nx} \right) .
\end{aligned} \tag{9.57}$$

This differential equation coincides with Eq. (4.87).

9.10.4 IR-Approximation

In the following, we give some intermediate steps for the calculation from Sec. 7.4.4.

We start from the continuum limit (7.73)

$$\begin{aligned}\partial_l J^{kq\alpha\beta}_{\varepsilon\varepsilon'} &= \left(E_q - E_k + \varepsilon' - \varepsilon\right)\eta^{kq\alpha\beta}_{\varepsilon\varepsilon'} \\ &+ \sum_{\gamma,p}\rho_0\int_{-D}^{D}\left(\eta^{pq\alpha\gamma}_{\varepsilon z}J^{kp\gamma\beta}_{z\varepsilon'} - \eta^{kp\gamma\beta}_{z\varepsilon'}J^{pq\alpha\gamma}_{\varepsilon z}\right)\theta_z\,\mathrm{d}z \\ &+ \sum_{\gamma,p}\rho_0\int_{-D}^{D}\left(\eta^{kp\alpha\gamma}_{\varepsilon z}J^{pq\gamma\beta}_{z\varepsilon'} - \eta^{pq\gamma\beta}_{z\varepsilon'}J^{kp\alpha\gamma}_{\varepsilon z}\right)(1-\theta_z)\,\mathrm{d}z.\end{aligned} \tag{9.58}$$

Applying the IR-approximation (7.74) to Eq. (9.58) yields

$$\begin{aligned}&\partial_l J^{kq\alpha\beta}_{\varepsilon_\mathrm{F}\varepsilon_\mathrm{F}} = -f_{kq}\left|E_q - E_k\right|J^{kq\alpha\beta}_{\varepsilon_\mathrm{F}\varepsilon_\mathrm{F}} \\ &+ \sum_{\gamma,p}\rho_0\int_0^D f_{pq}\mathrm{sgn}\left(\Delta E_{pq}+z\right)\mathrm{e}^{-\left(f_{pq}\left|\Delta E_{pq}+z\right|+f_{kp}\left|\Delta E_{kp}-z\right|\right)l}\mathrm{d}z\left(\tilde{J}^{pq\alpha\gamma}_{\varepsilon_\mathrm{F}\varepsilon_\mathrm{F}}\tilde{J}^{kp\gamma\beta}_{\varepsilon_\mathrm{F}\varepsilon_\mathrm{F}} - \tilde{J}^{kp\alpha\gamma}_{\varepsilon_\mathrm{F}\varepsilon_\mathrm{F}}\tilde{J}^{pq\gamma\beta}_{\varepsilon_\mathrm{F}\varepsilon_\mathrm{F}}\right) \\ &- \sum_{\gamma,p}\rho_0\int_0^D f_{kp}\mathrm{sgn}\left(\Delta E_{kp}-z\right)\mathrm{e}^{-\left(f_{pq}\left|\Delta E_{pq}+z\right|+f_{kp}\left|\Delta E_{kp}-z\right|\right)l}\mathrm{d}z\left(\tilde{J}^{pq\alpha\gamma}_{\varepsilon_\mathrm{F}\varepsilon_\mathrm{F}}\tilde{J}^{kp\gamma\beta}_{\varepsilon_\mathrm{F}\varepsilon_\mathrm{F}} - \tilde{J}^{kp\alpha\gamma}_{\varepsilon_\mathrm{F}\varepsilon_\mathrm{F}}\tilde{J}^{pq\gamma\beta}_{\varepsilon_\mathrm{F}\varepsilon_\mathrm{F}}\right)\end{aligned} \tag{9.59}$$

where $f_{kq}=1$ for the full generator (7.63) and a f_{kq} which is given by Eq. (7.65) for the generator that does not include operators which couple two triplet states. Note that the coefficient on the left-hand side as well as the coefficient in the linear term on the right-hand side have no tilde. Additionally,

$$\Delta E_{kq} = E_k - E_q \tag{9.60}$$

was introduced. Calculating the coefficients for $K \geq 0$, using the symmetries outlined in App. 9.10.2 yields

$$\begin{aligned}\partial_l \tilde{J}^{11\downarrow\downarrow}_{\varepsilon_\mathrm{F}\varepsilon_\mathrm{F}} &= -\partial_l \tilde{J}^{11\uparrow\uparrow}_{\varepsilon_\mathrm{F}\varepsilon_\mathrm{F}} \\ \partial_l J^{01\uparrow\downarrow}_{\varepsilon_\mathrm{F}\varepsilon_\mathrm{F}} &= -\left|K\right|J^{01\uparrow\downarrow}_{\varepsilon_\mathrm{F}\varepsilon_\mathrm{F}} + 2\left(1+f_{11}\right)\rho_0\int_0^D \mathrm{e}^{-(K+(1+f_{11})z)l}\mathrm{d}z\left(\tilde{J}^{11\uparrow\uparrow}_{\varepsilon_\mathrm{F}\varepsilon_\mathrm{F}}\tilde{J}^{01\uparrow\downarrow}_{\varepsilon_\mathrm{F}\varepsilon_\mathrm{F}} - \tilde{J}^{12\downarrow\uparrow}_{\varepsilon_\mathrm{F}\varepsilon_\mathrm{F}}\tilde{J}^{02\uparrow\uparrow}_{\varepsilon_\mathrm{F}\varepsilon_\mathrm{F}}\right) \\ \partial_l J^{02\uparrow\uparrow}_{\varepsilon_\mathrm{F}\varepsilon_\mathrm{F}} &= -\left|K\right|J^{02\uparrow\uparrow}_{\varepsilon_\mathrm{F}\varepsilon_\mathrm{F}} - 2\left(1+f_{11}\right)\rho_0\int_0^D \mathrm{e}^{-(K+(1+f_{11})z)l}\mathrm{d}z\,\tilde{J}^{01\uparrow\downarrow}_{\varepsilon_\mathrm{F}\varepsilon_\mathrm{F}}\tilde{J}^{12\downarrow\uparrow}_{\varepsilon_\mathrm{F}\varepsilon_\mathrm{F}} \\ \partial_l \tilde{J}^{11\uparrow\uparrow}_{\varepsilon_\mathrm{F}\varepsilon_\mathrm{F}} &= 2\rho_0\int_0^D \mathrm{sgn}\left(z-K\right)\mathrm{e}^{-2|z-K|l}\mathrm{d}z\left(\tilde{J}^{01\uparrow\downarrow}_{\varepsilon_\mathrm{F}\varepsilon_\mathrm{F}}\right)^2 + 2f_{11}\rho_0\int_0^D \mathrm{e}^{-2zl}\mathrm{d}z\left(\tilde{J}^{12\downarrow\uparrow}_{\varepsilon_\mathrm{F}\varepsilon_\mathrm{F}}\right)^2 \\ \partial_l \tilde{J}^{12\downarrow\uparrow}_{\varepsilon_\mathrm{F}\varepsilon_\mathrm{F}} &= 4f_{11}\rho_0\int_0^D \mathrm{e}^{-2zl}\mathrm{d}z\,\tilde{J}^{12\downarrow\uparrow}_{\varepsilon_\mathrm{F}\varepsilon_\mathrm{F}}\tilde{J}^{11\uparrow\uparrow}_{\varepsilon_\mathrm{F}\varepsilon_\mathrm{F}} - 4\rho_0\int_0^D \mathrm{sgn}\left(z-K\right)\mathrm{e}^{-2|z-K|l}\mathrm{d}z\,\tilde{J}^{02\uparrow\uparrow}_{\varepsilon_\mathrm{F}\varepsilon_\mathrm{F}}\tilde{J}^{01\uparrow\downarrow}_{\varepsilon_\mathrm{F}\varepsilon_\mathrm{F}}\end{aligned} \tag{9.61}$$

where for both generators

$$\begin{aligned}f_{0i} &= f_{0j} \quad \text{for all } i,j>0 \\ f_{0i} &= f_{i0} \quad \text{for all } i>0 \\ f_{ij} &= f_{i'j'} \quad \text{for all } i,j,i',j'>0\end{aligned} \tag{9.62}$$

as well as $f_{01} = 1$ was used. All other coefficients are either forbidden by spin conservation or can be calculated using a symmetry from App. 9.10.2. Calculating the integral finally yields

$$\begin{aligned}
\tilde{J}^{00\uparrow\uparrow}_{\varepsilon_F\varepsilon_F} &= \tilde{J}^{22\uparrow\uparrow}_{\varepsilon_F\varepsilon_F} = 0 \\
\tilde{J}^{11\downarrow\downarrow}_{\varepsilon_F\varepsilon_F} &= -\tilde{J}^{11\uparrow\uparrow}_{\varepsilon_F\varepsilon_F} \\
\partial_l J^{01\uparrow\downarrow}_{\varepsilon_F\varepsilon_F} &= -|K| J^{01\uparrow\downarrow}_{\varepsilon_F\varepsilon_F} + \frac{2\rho_0}{l}\left[1-\mathrm{e}^{-(1+f_{11})Dl}\right]\mathrm{e}^{-Kl}\left(\tilde{J}^{11\uparrow\uparrow}_{\varepsilon_F\varepsilon_F}\tilde{J}^{01\uparrow\downarrow}_{\varepsilon_F\varepsilon_F} - \tilde{J}^{12\downarrow\uparrow}_{\varepsilon_F\varepsilon_F}\tilde{J}^{02\uparrow\uparrow}_{\varepsilon_F\varepsilon_F}\right) \\
\partial_l J^{02\uparrow\uparrow}_{\varepsilon_F\varepsilon_F} &= -|K| J^{02\uparrow\uparrow}_{\varepsilon_F\varepsilon_F} - \frac{2\rho_0}{l}\left[1-\mathrm{e}^{-(1+f_{11})Dl}\right]\mathrm{e}^{-Kl}\tilde{J}^{01\uparrow\downarrow}_{\varepsilon_F\varepsilon_F}\tilde{J}^{12\downarrow\uparrow}_{\varepsilon_F\varepsilon_F} \\
\partial_l \tilde{J}^{11\uparrow\uparrow}_{\varepsilon_F\varepsilon_F} &= -\frac{\rho_0}{l}\left[\mathrm{e}^{-2(D-K)l}-\mathrm{e}^{-2Kl}\right]\left(\tilde{J}^{01\uparrow\downarrow}_{\varepsilon_F\varepsilon_F}\right)^2 + \frac{f_{11}\rho_0}{l}\left[1-\mathrm{e}^{-2Dl}\right]\left(\tilde{J}^{12\downarrow\uparrow}_{\varepsilon_F\varepsilon_F}\right)^2 \\
\partial_l \tilde{J}^{12\downarrow\uparrow}_{\varepsilon_F\varepsilon_F} &= \frac{2\rho_0}{l}\left[\mathrm{e}^{-2(D-K)l}-\mathrm{e}^{-2Kl}\right]\tilde{J}^{02\uparrow\uparrow}_{\varepsilon_F\varepsilon_F}\tilde{J}^{01\uparrow\downarrow}_{\varepsilon_F\varepsilon_F} + \frac{2f_{11}\rho_0}{l}\left[1-\mathrm{e}^{-2Dl}\right]\tilde{J}^{12\downarrow\uparrow}_{\varepsilon_F\varepsilon_F}\tilde{J}^{11\uparrow\uparrow}_{\varepsilon_F\varepsilon_F}.
\end{aligned} \tag{9.63}$$

We find the symmetries

$$J^{02\uparrow\uparrow}_{\varepsilon_F\varepsilon_F} = -\frac{1}{\sqrt{2}}J^{01\uparrow\downarrow}_{\varepsilon_F\varepsilon_F}, \quad J^{12\downarrow\uparrow}_{\varepsilon_F\varepsilon_F} = \sqrt{2}J^{11\uparrow\uparrow}_{\varepsilon_F\varepsilon_F} \tag{9.64}$$

which is consistent with the starting values. Thus, we can simplify the differential equation (9.63) further

$$\begin{aligned}
\partial_l J^{01\uparrow\downarrow}_{\varepsilon_F\varepsilon_F} &= -|K| J^{01\uparrow\downarrow}_{\varepsilon_F\varepsilon_F} + \frac{4\rho_0}{l}\left[1-\mathrm{e}^{-(1+f_{11})Dl}\right]\mathrm{e}^{-Kl}\tilde{J}^{01\uparrow\downarrow}_{\varepsilon_F\varepsilon_F}\tilde{J}^{11\uparrow\uparrow}_{\varepsilon_F\varepsilon_F} \\
\partial_l \tilde{J}^{11\uparrow\uparrow}_{\varepsilon_F\varepsilon_F} &= -\frac{\rho_0}{l}\left[\mathrm{e}^{-2(D-K)l}-\mathrm{e}^{-2Kl}\right]\left(\tilde{J}^{01\uparrow\downarrow}_{\varepsilon_F\varepsilon_F}\right)^2 + \frac{2f_{11}\rho_0}{l}\left[1-\mathrm{e}^{-2Dl}\right]\left(\tilde{J}^{11\uparrow\uparrow}_{\varepsilon_F\varepsilon_F}\right)^2
\end{aligned} \tag{9.65}$$

which coincides with Eq. (7.78).

9.11 Adapted Operator Basis for the Kondo and Anderson Model

9.11.1 Basis States for the Adapted Operator Basis

The basis states of the adapted basis from Sec. 7.5 for the sites included in the formation of a singlet reference state are chosen to be the eigenstates of

$$H_\mathrm{r} = \sum_\sigma \varepsilon_r\left(c^\dagger_{r\sigma}c_{r\sigma} - c^\dagger_{\bar{r}\sigma}c_{\bar{r}\sigma}\right) + J_{rr}\sum_\mu\sum_{\alpha,\beta}\sigma^\mu_{\alpha\beta}\tau^\mu\left(c^\dagger_{r\alpha}c_{r\beta} + c^\dagger_{\bar{r}\alpha}c_{\bar{r}\beta}\right). \tag{9.66}$$

All eigenstates of the Hamiltonian (9.66) are shown in the following tables. We truncate basis states that are higher lying then the triplet states. The eigenstates are sorted by particle number.

zero-particle subspace

k	zero-particle states	energy ε_i	$\Delta E_i = \varepsilon_i - \varepsilon_{s^-}$ $J_{rr}=\frac{2\varepsilon_r}{3}$	used
-	$\lvert a_1\rangle = \lvert 0,\uparrow,0\rangle$	$\varepsilon_{a_1} = 0$	$\Delta E_{a_1} = 2\varepsilon_r$	✗
-	$\lvert a_2\rangle = \lvert 0,\downarrow,0\rangle$	$\varepsilon_{a_2} = 0$	$\Delta E_{a_2} = 2\varepsilon_r$	✗

one-particle subspace

k	one-particle states	energy ε_i	$\Delta E_i = \varepsilon_i - \varepsilon_{s^-}$ $J_{rr}=\frac{2\varepsilon_r}{3}$	used
0	$\|s^-\rangle = \frac{1}{\sqrt{2}}(\|0,\uparrow,\downarrow\rangle - \|0,\downarrow,\uparrow\rangle)$	$\varepsilon_{s^-} = -\frac{3J_{rr}}{2} - \varepsilon_r$	$\Delta E_{s^-} = 0$	✓
1	$\|t_1^-\rangle = \|0,\uparrow,\uparrow\rangle$	$\varepsilon_{t_1^-} = \frac{J_{rr}}{2} - \varepsilon_r$	$\Delta E_{t_1^-} = \frac{4}{3}\varepsilon_r$	✓
2	$\|t_2^-\rangle = \frac{1}{\sqrt{2}}(\|0,\uparrow,\downarrow\rangle + \|0,\downarrow,\uparrow\rangle)$	$\varepsilon_{t_2^-} = \frac{J_{rr}}{2} - \varepsilon_r$	$\Delta E_{t_2^-} = \frac{4}{3}\varepsilon_r$	✓
3	$\|t_3^-\rangle = \|0,\downarrow,\downarrow\rangle$	$\varepsilon_{t_3^-} = \frac{J_{rr}}{2} - \varepsilon_r$	$\Delta E_{t_3^-} = \frac{4}{3}\varepsilon_r$	✓
-	$\|a_3\rangle = \frac{1}{\sqrt{2}}(\|\uparrow,\downarrow,0\rangle - \|\downarrow,\uparrow,0\rangle)$	$\varepsilon_{a_3} = -\frac{3J_{rr}}{2} + \varepsilon_r$	$\Delta E_{a_3} = 2\varepsilon_r$	✗
-	$\|a_4\rangle = \|\downarrow,\downarrow,0\rangle$	$\varepsilon_{a_4} = \frac{J_{rr}}{2} + \varepsilon_r$	$\Delta E_{a_4} = \frac{10}{3}\varepsilon_r$	✗
-	$\|a_5\rangle = \frac{1}{\sqrt{2}}(\|\uparrow,\downarrow,0\rangle + \|\downarrow,\uparrow,0\rangle)$	$\varepsilon_{a_5} = \frac{J_{rr}}{2} + \varepsilon_r$	$\Delta E_{a_5} = \frac{10}{3}\varepsilon_r$	✗
-	$\|a_6\rangle = \|\uparrow,\uparrow,0\rangle$	$\varepsilon_{a_6} = \frac{J_{rr}}{2} + \varepsilon_r$	$\Delta E_{a_6} = \frac{10}{3}\varepsilon_r$	✗

three-particle subspace

k	one-particle states	energy ε_i	$\Delta E_i = \varepsilon_i - \varepsilon_{s^-}$ $J_{rr}=\frac{2\varepsilon_r}{3}$	used
4	$\|s^+\rangle = \frac{1}{\sqrt{2}}(\|\downarrow,\uparrow,\uparrow\downarrow\rangle - \|\uparrow,\downarrow,\uparrow\downarrow\rangle)$	$\varepsilon_{s^+} = -\frac{3J_{rr}}{2} - \varepsilon_r$	$\Delta E_{s^+} = 0$	✓
5	$\|t_1^+\rangle = \|\uparrow,\uparrow,\uparrow\downarrow\rangle$	$\varepsilon_{t_1^+} = \frac{J_{rr}}{2} - \varepsilon_r$	$\Delta E_{t_1^+} = \frac{4}{3}\varepsilon_r$	✓
6	$\|t_2^+\rangle = \frac{1}{\sqrt{2}}(\|\downarrow,\uparrow,\uparrow\downarrow\rangle + \|\uparrow,\downarrow,\uparrow\downarrow\rangle)$	$\varepsilon_{t_2^+} = \frac{J_{rr}}{2} - \varepsilon_r$	$\Delta E_{t_2^+} = \frac{4}{3}\varepsilon_r$	✓
7	$\|t_3^+\rangle = \|\downarrow,\downarrow,\uparrow\downarrow\rangle$	$\varepsilon_{t_3^+} = \frac{J_{rr}}{2} - \varepsilon_r$	$\Delta E_{t_3^+} = \frac{4}{3}\varepsilon_r$	✓
-	$\|a_7\rangle = \frac{1}{\sqrt{2}}(\|\uparrow\downarrow,\downarrow,\uparrow\rangle - \|\uparrow\downarrow,\uparrow,\downarrow\rangle)$	$\varepsilon_{a_7} = -\frac{3J_{rr}}{2} + \varepsilon_r$	$\Delta E_{a_7} = 2\varepsilon_r$	✗
-	$\|a_8\rangle = \|\uparrow\downarrow,\uparrow,\uparrow\rangle$	$\varepsilon_{a_8} = \frac{J_{rr}}{2} + \varepsilon_r$	$\Delta E_{a_8} = \frac{10}{3}\varepsilon_r$	✗
-	$\|a_9\rangle = \|\uparrow\downarrow,\downarrow,\downarrow\rangle$	$\varepsilon_{a_9} = \frac{J_{rr}}{2} + \varepsilon_r$	$\Delta E_{a_9} = \frac{10}{3}\varepsilon_r$	✗
-	$\|a_{10}\rangle = \frac{1}{\sqrt{2}}(\|\uparrow\downarrow,\downarrow,\uparrow\rangle + \|\uparrow\downarrow,\uparrow,\downarrow\rangle)$	$\varepsilon_{a_{10}} = \frac{J_{rr}}{2} + \varepsilon_r$	$\Delta E_{a_{10}} = \frac{10}{3}\varepsilon_r$	✗

two-particle subspace

k	one-particle states	energy ε_i	$\Delta E_i = \varepsilon_i - \varepsilon_{s^-}$ $J_{rr}=\frac{2\varepsilon_r}{3}$	used
8	$\|\mathrm{FS},\uparrow\rangle = \|0,\uparrow,\uparrow\downarrow\rangle$	$\varepsilon_{\mathrm{FS},\uparrow} = -2\varepsilon_r$	$\Delta E_{\mathrm{FS},\uparrow} = 0$	✓
9	$\|\mathrm{FS},\downarrow\rangle = \|0,\downarrow,\uparrow\downarrow\rangle$	$\varepsilon_{\mathrm{FS},\downarrow} = -2\varepsilon_r$	$\Delta E_{\mathrm{FS},\downarrow} = 0$	✓
10	$\|\tilde{\uparrow}\rangle = \frac{1}{\sqrt{6}}[\|\uparrow,\uparrow,\downarrow\rangle - 2\|\uparrow,\downarrow,\uparrow\rangle + \|\downarrow,\uparrow,\uparrow\rangle]$	$\varepsilon_{\tilde{\uparrow}} = -2J_{rr}$	$\Delta E_{\tilde{\uparrow}} = \frac{2}{3}\varepsilon_r$	✓
11	$\|\tilde{\downarrow}\rangle = \frac{1}{\sqrt{6}}[\|\downarrow,\downarrow,\uparrow\rangle - 2\|\downarrow,\uparrow,\downarrow\rangle + \|\uparrow,\downarrow,\downarrow\rangle]$	$\varepsilon_{\tilde{\downarrow}} = -2J_{rr}$	$\Delta E_{\tilde{\downarrow}} = \frac{2}{3}\varepsilon_r$	✓
-	$\|a_{11}\rangle = \frac{1}{\sqrt{2}}[\|\uparrow,\uparrow,\downarrow\rangle - \|\downarrow,\uparrow,\uparrow\rangle]$	$\varepsilon_{a_{11}} = 0$	$\Delta E_{a_{11}} = 2\varepsilon_r$	✗
-	$\|a_{12}\rangle = \frac{1}{\sqrt{2}}[\|\downarrow,\downarrow,\uparrow\rangle - \|\uparrow,\downarrow,\downarrow\rangle]$	$\varepsilon_{a_{12}} = 0$	$\Delta E_{a_{12}} = 2\varepsilon_r$	✗
-	$\|a_{13}\rangle = \frac{1}{\sqrt{3}}[\|\uparrow,\uparrow,\downarrow\rangle + \|\uparrow,\downarrow,\uparrow\rangle + \|\downarrow,\uparrow,\uparrow\rangle]$	$\varepsilon_{a_{13}} = J_{rr}$	$\Delta E_{a_{13}} = \frac{8}{3}\varepsilon_r$	✗
-	$\|a_{14}\rangle = \frac{1}{\sqrt{3}}[\|\downarrow,\downarrow,\uparrow\rangle + \|\downarrow,\uparrow,\downarrow\rangle + \|\uparrow,\downarrow,\downarrow\rangle]$	$\varepsilon_{a_{14}} = J_{rr}$	$\Delta E_{a_{14}} = \frac{8}{3}\varepsilon_r$	✗
-	$\|a_{15}\rangle = \|\uparrow,\uparrow,\uparrow\rangle$	$\varepsilon_{a_{15}} = J_{rr}$	$\Delta E_{a_{15}} = \frac{8}{3}\varepsilon_r$	✗
-	$\|a_{16}\rangle = \|\downarrow,\downarrow,\downarrow\rangle$	$\varepsilon_{a_{16}} = J_{rr}$	$\Delta E_{a_{16}} = \frac{8}{3}\varepsilon_r$	✗
-	$\|a_{17}\rangle = \|\uparrow\downarrow,\uparrow,0\rangle$	$\varepsilon_{a_{17}} = 2\varepsilon_r$	$\Delta E_{a_{17}} = 4\varepsilon_r$	✗
-	$\|a_{18}\rangle = \|\uparrow\downarrow,\downarrow,0\rangle$	$\varepsilon_{a_{18}} = 2\varepsilon_r$	$\Delta E_{a_{18}} = 4\varepsilon_r$	✗

four-particle subspace

k	one-particle states	energy ε_i	$\Delta E_i = \varepsilon_i - \varepsilon_{s-}$ $_{J_{rr}=\frac{2\varepsilon_r}{3}}$	used
-	$\|4,\uparrow\rangle = \|\uparrow\downarrow,\uparrow,\uparrow\downarrow\rangle$	$\varepsilon_{4,\uparrow} = 0$	$\Delta E_{4,\uparrow} = 2\varepsilon_r$	✗
-	$\|4,\downarrow\rangle = \|\uparrow\downarrow,\downarrow,\uparrow\downarrow\rangle$	$\varepsilon_{4,\downarrow} = 0$	$\Delta E_{4,\downarrow} = 2\varepsilon_r$	✗

9.11.2 Starting Values

The starting values of the Kondo (Anderson) model in the adapted operator basis (7.94) from Sec. 7.5 are given explicitly. The indices belong to the states from Sec. 9.11.1 (row k).

$E_{0,0} = -\frac{3J_{rr}}{2} - \varepsilon_r$	$E_{1,1} = \frac{J_{rr}}{2} - \varepsilon_r$	$E_{2,2} = \frac{J_{rr}}{2} - \varepsilon_r$	$E_{3,3} = \frac{J_{rr}}{2} - \varepsilon_r$
$E_{4,4} = -\frac{3J_{rr}}{2} - \varepsilon_r$	$E_{5,5} = \frac{J_{rr}}{2} - \varepsilon_r$	$E_{6,6} = \frac{J_{rr}}{2} - \varepsilon_r$	$E_{7,7} = \frac{J_{rr}}{2} - \varepsilon_r$
$E_{8,8} = -2\varepsilon_r$	$E_{9,9} = -2\varepsilon_r$	$E_{10,10} = -2J_{rr}$	$E_{11,11} = -2J_{rr}$
$E_{10,8} = \frac{3}{\sqrt{6}} J_{r\bar{r}}$	$E_{8,10} = \frac{3}{\sqrt{6}} J_{r\bar{r}}$	$E_{11,9} = -\frac{3}{\sqrt{6}} J_{r\bar{r}}$	$E_{9,11} = -\frac{3}{\sqrt{6}} J_{r\bar{r}}$

$\Gamma_n^{10,0,\uparrow} = -\frac{3}{2\sqrt{12}} J_{nr}$	$\Gamma_n^{11,0,\downarrow} = +\frac{3}{2\sqrt{12}} J_{nr}$
$\Gamma_n^{8,0,\uparrow} = +\frac{3}{2\sqrt{2}} J_{n\bar{r}}$	$\Gamma_n^{9,0,\downarrow} = +\frac{3}{2\sqrt{2}} J_{n\bar{r}}$
$\Gamma_n^{10,2,\uparrow} = +\frac{5}{2\sqrt{12}} J_{nr}$	$\Gamma_n^{10,1,\downarrow} = -\frac{5}{2\sqrt{6}} J_{nr}$
$\Gamma_n^{8,2,\uparrow} = -\frac{1}{2\sqrt{2}} J_{n\bar{r}}$	$\Gamma_n^{8,1,\downarrow} = +\frac{1}{2} J_{n\bar{r}}$
$\Gamma_n^{11,3,\uparrow} = -\frac{5}{2\sqrt{6}} J_{nr}$	$\Gamma_n^{11,2,\downarrow} = +\frac{5}{2\sqrt{12}} J_{nr}$
$\Gamma_n^{9,3,\uparrow} = -\frac{1}{2} J_{n\bar{r}}$	$\Gamma_n^{9,2,\downarrow} = +\frac{1}{2\sqrt{2}} J_{n\bar{r}}$
$\Gamma_n^{5,8,\uparrow} = +\frac{1}{2} J_{nr}$	$\Gamma_n^{6,8,\downarrow} = +\frac{1}{2\sqrt{2}} J_{nr}$
$\Gamma_n^{6,9,\uparrow} = +\frac{1}{2\sqrt{2}} J_{nr}$	$\Gamma_n^{4,8,\downarrow} = -\frac{3}{2\sqrt{2}} J_{nr}$
$\Gamma_n^{4,9,\uparrow} = +\frac{3}{2\sqrt{2}} J_{nr}$	$\Gamma_n^{7,9,\downarrow} = +\frac{1}{2} J_{nr}$
$\Gamma_n^{5,10,\uparrow} = -\frac{5}{2\sqrt{6}} J_{n\bar{r}}$	$\Gamma_n^{6,10,\downarrow} = -\frac{5}{2\sqrt{12}} J_{n\bar{r}}$
$\Gamma_n^{6,11,\uparrow} = +\frac{5}{2\sqrt{12}} J_{n\bar{r}}$	$\Gamma_n^{4,10,\downarrow} = +\frac{3}{2\sqrt{12}} J_{n\bar{r}}$
$\Gamma_n^{4,11,\uparrow} = +\frac{3}{2\sqrt{12}} J_{n\bar{r}}$	$\Gamma_n^{7,11,\downarrow} = +\frac{5}{2\sqrt{6}} J_{n\bar{r}}$

$J_{nm}^{0,3,\downarrow\uparrow} = +\frac{1}{\sqrt{2}}J_{nm}$	$J_{nm}^{4,7,\downarrow\uparrow} = +\frac{1}{\sqrt{2}}J_{nm}$
$J_{nm}^{3,0,\uparrow\downarrow} = +\frac{1}{\sqrt{2}}J_{nm}$	$J_{nm}^{7,4,\uparrow\downarrow} = +\frac{1}{\sqrt{2}}J_{nm}$
$J_{nm}^{1,2,\downarrow\uparrow} = +\frac{1}{\sqrt{2}}J_{nm}$	$J_{nm}^{5,6,\downarrow\uparrow} = +\frac{1}{\sqrt{2}}J_{nm}$
$J_{nm}^{2,1,\uparrow\downarrow} = +\frac{1}{\sqrt{2}}J_{nm}$	$J_{nm}^{6,5,\uparrow\downarrow} = +\frac{1}{\sqrt{2}}J_{nm}$
$J_{nm}^{2,3,\downarrow\uparrow} = +\frac{1}{\sqrt{2}}J_{nm}$	$J_{nm}^{6,7,\downarrow\uparrow} = +\frac{1}{\sqrt{2}}J_{nm}$
$J_{nm}^{3,2,\uparrow\downarrow} = +\frac{1}{\sqrt{2}}J_{nm}$	$J_{nm}^{7,6,\uparrow\downarrow} = +\frac{1}{\sqrt{2}}J_{nm}$
$J_{nm}^{0,1,\uparrow\downarrow} = -\frac{1}{\sqrt{2}}J_{nm}$	$J_{nm}^{4,5,\uparrow\downarrow} = -\frac{1}{\sqrt{2}}J_{nm}$
$J_{nm}^{1,0,\downarrow\uparrow} = -\frac{1}{\sqrt{2}}J_{nm}$	$J_{nm}^{5,4,\downarrow\uparrow} = -\frac{1}{\sqrt{2}}J_{nm}$
$J_{nm}^{0,2,\uparrow\uparrow} = +\frac{1}{2}J_{nm}$	$J_{nm}^{4,6,\uparrow\uparrow} = +\frac{1}{2}J_{nm}$
$J_{nm}^{2,0,\uparrow\uparrow} = +\frac{1}{2}J_{nm}$	$J_{nm}^{6,4,\uparrow\uparrow} = +\frac{1}{2}J_{nm}$
$J_{nm}^{2,0,\downarrow\downarrow} = -\frac{1}{2}J_{nm}$	$J_{nm}^{6,4,\downarrow\downarrow} = -\frac{1}{2}J_{nm}$
$J_{nm}^{0,2,\downarrow\downarrow} = -\frac{1}{2}J_{nm}$	$J_{nm}^{4,6,\downarrow\downarrow} = -\frac{1}{2}J_{nm}$
$J_{nm}^{1,1,\uparrow\uparrow} = +\frac{1}{2}J_{nm}$	$J_{nm}^{5,5,\uparrow\uparrow} = +\frac{1}{2}J_{nm}$
$J_{nm}^{1,1,\downarrow\downarrow} = -\frac{1}{2}J_{nm}$	$J_{nm}^{5,5,\downarrow\downarrow} = -\frac{1}{2}J_{nm}$
$J_{nm}^{3,3,\uparrow\uparrow} = -\frac{1}{2}J_{nm}$	$J_{nm}^{7,7,\uparrow\uparrow} = -\frac{1}{2}J_{nm}$
$J_{nm}^{3,3,\downarrow\downarrow} = +\frac{1}{2}J_{nm}$	$J_{nm}^{7,7,\downarrow\downarrow} = +\frac{1}{2}J_{nm}$

$J_{nm}^{8,8,\uparrow\uparrow} = +\frac{1}{2}J_{nm}$	$J_{nm}^{8,8,\downarrow\downarrow} = -\frac{1}{2}J_{nm}$
$J_{nm}^{8,9,\downarrow\uparrow} = +J_{nm}$	$J_{nm}^{9,8,\uparrow\downarrow} = +J_{nm}$
$J_{nm}^{9,9,\uparrow\uparrow} = -\frac{1}{2}J_{nm}$	$J_{nm}^{9,9,\downarrow\downarrow} = +\frac{1}{2}J_{nm}$

$J_{nm}^{10,10,\uparrow\uparrow} = -\frac{1}{6}J_{nm}$	$J_{nm}^{10,10,\downarrow\downarrow} = +\frac{1}{6}J_{nm}$
$J_{nm}^{10,11,\downarrow\uparrow} = +\frac{1}{3}J_{nm}$	$J_{nm}^{11,10,\uparrow\downarrow} = +\frac{1}{3}J_{nm}$
$J_{nm}^{11,11,\uparrow\uparrow} = +\frac{1}{6}J_{nm}$	$J_{nm}^{11,11,\downarrow\downarrow} = -\frac{1}{6}J_{nm}$

9.11.3 Symmetries

Without symmetries we have $12^2 = 144$ coefficients $E_{k,q}$, $2 \cdot 12^2 = 288$ coefficients $\Gamma_n^{k,q,\sigma}$ for each index n and $4 \cdot 12^2 = 576$ coefficients $J_{nm}^{k,q,\alpha\beta}$ for each index pair (n,m). However, a lot of combinations of the indices k, q, α and β are forbidden by spin conservation. Only 20 coefficients of $E_{k,q}$, 24 coefficients of $\Gamma_n^{k,q,\sigma}$ for each index n and 64 coefficients of $J_{nm}^{k,q,\alpha\beta}$ for each index pair (n,m) remain when using S_z-spin conservation. The coefficients allowed by spin conservation are

Allowed coefficients by spin and particle conservation for $J_{nm}^{k,q,\alpha\beta}$

$J_{nm}^{0,1,\uparrow\downarrow}$	$J_{nm}^{1,2,\downarrow\uparrow}$	$J_{nm}^{0,3,\downarrow\uparrow}$	$J_{nm}^{2,3,\downarrow\uparrow}$	$J_{nm}^{0,2,\uparrow\uparrow}$	$J_{nm}^{2,0,\uparrow\uparrow}$	$J_{nm}^{0,0,\uparrow\uparrow}$	$J_{nm}^{1,1,\uparrow\uparrow}$	$J_{nm}^{2,2,\uparrow\uparrow}$	$J_{nm}^{3,3,\uparrow\uparrow}$
$J_{nm}^{1,0,\downarrow\uparrow}$	$J_{nm}^{2,1,\uparrow\downarrow}$	$J_{nm}^{3,0,\uparrow\downarrow}$	$J_{nm}^{3,2,\uparrow\downarrow}$	$J_{nm}^{0,2,\downarrow\downarrow}$	$J_{nm}^{2,0,\downarrow\downarrow}$	$J_{nm}^{0,0,\downarrow\downarrow}$	$J_{nm}^{1,1,\downarrow\downarrow}$	$J_{nm}^{2,2,\downarrow\downarrow}$	$J_{nm}^{3,3,\downarrow\downarrow}$

$J_{nm}^{4,5,\uparrow\downarrow}$	$J_{nm}^{5,6,\downarrow\uparrow}$	$J_{nm}^{4,7,\downarrow\uparrow}$	$J_{nm}^{6,7,\downarrow\uparrow}$	$J_{nm}^{4,6,\uparrow\uparrow}$	$J_{nm}^{6,4,\uparrow\uparrow}$	$J_{nm}^{4,4,\uparrow\uparrow}$	$J_{nm}^{5,5,\uparrow\uparrow}$	$J_{nm}^{6,6,\uparrow\uparrow}$	$J_{nm}^{7,7,\uparrow\uparrow}$
$J_{nm}^{5,4,\downarrow\uparrow}$	$J_{nm}^{6,5,\uparrow\downarrow}$	$J_{nm}^{7,4,\uparrow\downarrow}$	$J_{nm}^{7,6,\uparrow\downarrow}$	$J_{nm}^{4,6,\downarrow\downarrow}$	$J_{nm}^{6,4,\downarrow\downarrow}$	$J_{nm}^{4,4,\downarrow\downarrow}$	$J_{nm}^{5,5,\downarrow\downarrow}$	$J_{nm}^{6,6,\downarrow\downarrow}$	$J_{nm}^{7,7,\downarrow\downarrow}$

$J_{nm}^{8,8,\uparrow\uparrow}$	$J_{nm}^{8,9,\downarrow\uparrow}$	$J_{nm}^{9,9,\uparrow\uparrow}$	$J_{nm}^{10,10,\uparrow\uparrow}$	$J_{nm}^{10,11,\downarrow\uparrow}$	$J_{nm}^{11,11,\uparrow\uparrow}$
$J_{nm}^{8,8,\downarrow\downarrow}$	$J_{nm}^{9,8,\uparrow\downarrow}$	$J_{nm}^{9,9,\downarrow\downarrow}$	$J_{nm}^{10,10,\downarrow\downarrow}$	$J_{nm}^{11,10,\uparrow\downarrow}$	$J_{nm}^{11,11,\downarrow\downarrow}$
$J_{nm}^{8,11,\downarrow\uparrow}$	$J_{nm}^{9,10,\uparrow\downarrow}$	$J_{nm}^{8,10,\uparrow\uparrow}$	$J_{nm}^{10,8,\uparrow\uparrow}$	$J_{nm}^{9,11,\uparrow\uparrow}$	$J_{nm}^{11,9,\uparrow\uparrow}$
$J_{nm}^{11,8,\uparrow\downarrow}$	$J_{nm}^{10,9,\downarrow\uparrow}$	$J_{nm}^{8,10,\downarrow\downarrow}$	$J_{nm}^{10,8,\downarrow\downarrow}$	$J_{nm}^{9,11,\downarrow\downarrow}$	$J_{nm}^{11,9,\downarrow\downarrow}$

Allowed coefficients by spin and particle conservation for $E_{k,q}$

$E_{0,0}$	$E_{1,1}$	$E_{2,2}$	$E_{3,3}$	$E_{0,2}$	$E_{2,0}$
$E_{4,4}$	$E_{5,5}$	$E_{6,6}$	$E_{7,7}$	$E_{4,6}$	$E_{6,4}$

$E_{8,8}$	$E_{9,9}$	$E_{10,10}$	$E_{11,11}$
$E_{8,10}$	$E_{10,8}$	$E_{9,11}$	$E_{11,9}$

Allowed coefficients by spin and particle conservation for $\Gamma_n^{k,q,\sigma}$

$\Gamma_n^{8,0,\uparrow}$	$\Gamma_n^{10,0,\uparrow}$	$\Gamma_n^{8,2,\uparrow}$	$\Gamma_n^{10,2,\uparrow}$	$\Gamma_n^{9,3,\uparrow}$	$\Gamma_n^{11,3,\uparrow}$
$\Gamma_n^{9,0,\downarrow}$	$\Gamma_n^{11,0,\downarrow}$	$\Gamma_n^{8,1,\downarrow}$	$\Gamma_n^{10,1,\downarrow}$	$\Gamma_n^{9,2,\downarrow}$	$\Gamma_n^{11,2,\downarrow}$
$\Gamma_n^{5,8,\uparrow}$	$\Gamma_n^{4,9,\uparrow}$	$\Gamma_n^{6,9,\uparrow}$	$\Gamma_n^{5,10,\uparrow}$	$\Gamma_n^{4,11,\uparrow}$	$\Gamma_n^{6,11,\uparrow}$
$\Gamma_n^{4,8,\downarrow}$	$\Gamma_n^{6,8,\downarrow}$	$\Gamma_n^{7,9,\downarrow}$	$\Gamma_n^{4,10,\downarrow}$	$\Gamma_n^{6,10,\downarrow}$	$\Gamma_n^{7,11,\downarrow}$

Hermiticity

$$\begin{aligned} E_{kq} &= E_{qk} \\ J_{nm}^{kq\alpha\beta} &= J_{mn}^{qk\beta\alpha} \end{aligned} \tag{9.67}$$

Symmetries for the coefficients $J_{nm}^{k,q,\alpha\beta}$

$J_{nm}^{0,0,\uparrow\uparrow} = +J_{nm}^{0,0,\downarrow\downarrow}$	$J_{nm}^{4,4,\uparrow\uparrow} = +J_{nm}^{4,4,\downarrow\downarrow}$
$J_{nm}^{2,2,\uparrow\uparrow} = +J_{nm}^{2,2,\downarrow\downarrow}$	$J_{nm}^{6,6,\uparrow\uparrow} = +J_{nm}^{6,6,\downarrow\downarrow}$
$J_{nm}^{1,1,\uparrow\uparrow} = +J_{nm}^{3,3,\downarrow\downarrow}$	$J_{nm}^{5,5,\uparrow\uparrow} = +J_{nm}^{7,7,\downarrow\downarrow}$
$J_{nm}^{3,3,\uparrow\uparrow} = +J_{nm}^{1,1,\downarrow\downarrow}$	$J_{nm}^{7,7,\uparrow\uparrow} = +J_{nm}^{5,5,\downarrow\downarrow}$
$J_{nm}^{0,2,\uparrow\uparrow} = -J_{nm}^{0,2,\downarrow\downarrow}$	$J_{nm}^{4,6,\uparrow\uparrow} = -J_{nm}^{4,6,\downarrow\downarrow}$
$J_{nm}^{0,1,\uparrow\downarrow} = -J_{nm}^{0,3,\downarrow\uparrow}$	$J_{nm}^{4,5,\uparrow\downarrow} = -J_{nm}^{4,7,\downarrow\uparrow}$
$J_{nm}^{1,0,\downarrow\uparrow} = -J_{nm}^{3,0,\uparrow\downarrow}$	$J_{nm}^{5,4,\downarrow\uparrow} = -J_{nm}^{7,4,\uparrow\downarrow}$
$J_{nm}^{1,2,\downarrow\uparrow} = +J_{nm}^{3,2,\uparrow\downarrow}$	$J_{nm}^{5,6,\downarrow\uparrow} = +J_{nm}^{7,6,\uparrow\downarrow}$
$J_{nm}^{2,1,\uparrow\downarrow} = +J_{nm}^{2,3,\downarrow\uparrow}$	$J_{nm}^{6,5,\uparrow\downarrow} = +J_{nm}^{6,7,\downarrow\uparrow}$
$J_{nm}^{2,0,\uparrow\uparrow} = -J_{nm}^{2,0,\downarrow\downarrow}$	$J_{nm}^{6,4,\uparrow\uparrow} = -J_{nm}^{6,4,\downarrow\downarrow}$

$J_{nm}^{8,8,\uparrow\uparrow} = +J_{nm}^{9,9,\downarrow\downarrow}$	$J_{nm}^{10,8,\uparrow\uparrow} = -J_{nm}^{11,9,\downarrow\downarrow}$
$J_{nm}^{8,8,\downarrow\downarrow} = +J_{nm}^{9,9,\uparrow\uparrow}$	$J_{nm}^{10,8,\downarrow\downarrow} = -J_{nm}^{11,9,\uparrow\uparrow}$
$J_{nm}^{8,9,\downarrow\uparrow} = +J_{nm}^{9,8,\uparrow\downarrow}$	$J_{nm}^{10,9,\downarrow\uparrow} = -J_{nm}^{11,8,\uparrow\downarrow}$
$J_{nm}^{8,10,\uparrow\uparrow} = -J_{nm}^{9,11,\downarrow\downarrow}$	$J_{nm}^{10,10,\uparrow\uparrow} = +J_{nm}^{11,11,\downarrow\downarrow}$
$J_{nm}^{8,10,\downarrow\downarrow} = -J_{nm}^{9,11,\uparrow\uparrow}$	$J_{nm}^{10,10,\downarrow\downarrow} = +J_{nm}^{11,11,\uparrow\uparrow}$
$J_{nm}^{8,11,\downarrow\uparrow} = -J_{nm}^{9,10,\uparrow\downarrow}$	$J_{nm}^{10,11,\downarrow\uparrow} = +J_{nm}^{11,10,\uparrow\downarrow}$

Symmetries for the coefficients $\Gamma_n^{k,q,\sigma}$

$\Gamma_n^{4,8,\downarrow} = -\Gamma_n^{4,9,\uparrow}$	$\Gamma_n^{8,0,\uparrow} = +\Gamma_n^{9,0,\downarrow}$
$\Gamma_n^{4,10,\downarrow} = +\Gamma_n^{4,11,\uparrow}$	$\Gamma_n^{8,1,\downarrow} = -\Gamma_n^{9,3,\uparrow}$
$\Gamma_n^{6,8,\downarrow} = +\Gamma_n^{6,9,\uparrow}$	$\Gamma_n^{8,2,\uparrow} = -\Gamma_n^{9,2,\downarrow}$
$\Gamma_n^{6,10,\downarrow} = -\Gamma_n^{6,11,\uparrow}$	$\Gamma_n^{10,0,\uparrow} = -\Gamma_n^{11,0,\downarrow}$
$\Gamma_n^{5,8,\uparrow} = +\Gamma_n^{7,9,\downarrow}$	$\Gamma_n^{10,1,\downarrow} = +\Gamma_n^{11,3,\uparrow}$
$\Gamma_n^{5,10,\uparrow} = -\Gamma_n^{7,11,\downarrow}$	$\Gamma_n^{10,2,\uparrow} = +\Gamma_n^{11,2,\downarrow}$

Symmetries for the coefficients $E_{k,q}$

$E_{0,0} = E_{4,4}$
$E_{1,1} = E_{2,2} = E_{3,3} = E_{5,5} = E_{6,6} = E_{7,7}$

The number of remaining coefficients that are not forbidden by spin conservation or connected by symmetries are 10 for $E_{k,q}$, 12 for each index n of $\Gamma_n^{k,q,\sigma}$ and 28 for each index pair (n,m) of $J_{nm}^{k,q,\alpha\beta}$.

Bibliography

[1] A.C. Hewson. *The Kondo Problem to Heavy Fermions*. Cambridge University Press, Cambridge, (1993).

[2] J. Kondo. *Resistance Minimum in Dilute Magnetic Alloys*. Prog. Theor. Phys. **32**, 37-49, (1964).

[3] P.W. Anderson. *Localized Magnetic States in Metals*. Phys. Rev. **124**, 41-53, (1961).

[4] W.J. de Haas, J. de Boer, and G.J. van dën Berg. *The electrical resistance of gold, copper and lead at low temperatures*. Physica **1**, 1115-1124, (1934).

[5] J. Friedel. *On some electrical and magnetic properties of metallic solid solutions*. Can. J. Phys. **34**, 1190-1211, (1956).

[6] G.J. van dën Berg. *Chapter IV Anomalies in Dilute Metallic Solutions of Transition Elements*. Progress in Low Temperature Physics (ed C.J. Gorter, North-Holland, 1964), **IV**, 194-264, (1964).

[7] K.G. Wilson. *The renormalization group and the ϵ expansion*. Phys. Rep. **12**, 75-199, (1974).

[8] H.R. Krishna-murthy, J.W. Wilkins, and K.G. Wilson. *Renormalization-group approach to the Anderson model of dilute magnetic alloys. I. Static properties for the symmetric case*. Phys. Rev. B **21**, 1003-1043, (1980).

[9] H.R. Krishna-murthy, J.W. Wilkins, and K.G. Wilson. *Renormalization-group approach to the Anderson model of dilute magnetic alloys. II. Static properties for the asymmetric case*. Phys. Rev. B **21**, 1044-1083, (1980).

[10] R. Bulla, T.A. Cost, and T. Pruschke. *Numerical renormalization group method for quantum impurity systems*. Rev. Mod. Phys. **80**, 395-450, (2008).

[11] F. Wegner. *Flow-equations for Hamiltonians*. Ann. Physik **3**, 77-91, (1994).

[12] A. Mielke. *Flow equations for band-matrices*. Eur. Phys. J. B **5**, 605-611, (1998).

[13] C. Knetter and G.S. Uhrig. *Perturbation theory by flow equations: dimerized and frustrated $S = 1/2$ chain*. Eur. Phys. J. B **13**, 209-225, (2000).

[14] C. Knetter, K.P. Schmidt, and G.S. Uhrig. *The structure of operators in effective particle-conserving models*. J. Phys. A: Math. Gen. **36**, 7889–7907, (2003).

[15] P.W. Anderson. *A poor man's derivation of scaling laws for the Kondo problem*. J. Phys. C: Solid St. Phys. **3**, 2436-2441, (1970).

[16] S. Kehrein. *The Flow Equation Approach to Many-Particle Systems*. Springer Tracts in Modern Physics **217**, Springer, (2006).

[17] E. Vogel. *Flussgleichungen für das Kondo-Modell*. Ph.D. thesis, Heidelberg, (2005).

[18] W. Hofstetter and S. Kehrein. *Flow equation analysis of the anisotropic Kondo model*. Phys. Rev. **B** 63, 140402, (2001).

[19] D. Lobaskin and S. Kehrein. *Crossover from nonequilibrium to equilibrium behavior in the time-dependent Kondo model*. Phys. Rev. B **71**, 193303, (2005).

[20] C. Slezak, S. Kehrein, T. Pruschke, and M. Jarrell. *Semianalytical solution of the Kondo model in a magnetic field*. Phys. Rev. B **67**, 184408, (2003).

[21] S.K. Kehrein and A. Mielke. *Flow equations for the Anderson Hamiltonian*. Phys. A: Math. Gen. **27**, 4259-4279, (1994).

[22] S.K. Kehrein and A. Mielke. *Theory of the Anderson Impurity Model: The Schrieffer–Wolff Transformation Reexamined*. Ann. Phys. **252**, 1-32, (1996).

[23] T. Stauber and F. Guinea. *Assisted hopping in the Anderson impurity model: A flow equation study*. Phys. Rev. B **69**, 0353014, (2004).

[24] M. Kaveh and N. Wiser. *Electron-electron scattering in conducting materials*. Advances in physics **33**, 257-372, (1984).

[25] N. Wiser. *The Electrical Resistivity of the Simple Metals*. CONTEMP. PHYS. **25**, 211-249, (1984).

[26] F. Bloch. *Zum elektrischen Widerstandsgesetz bei tiefen Temperaturen*. Z. Physik **59**, 208-214, (1930).

[27] J. Kondo. *Anomalous Density of States in Dilute Magnetic Alloys*. Prog. Theor. Phys. **33**, 575-584, (1965).

[28] C. Zener. *Interaction Between the d Shells in the Transition Metals*. Phys. Rev. **81**, 440-444, (1951).

[29] T. Kasuya. *A Theory of Metallic Ferro- and Antiferromagnetism on Zener's Model*. Prog. Theor. Phys. **16**, 45-57, (1956).

[30] K. Yosida. *Magnetic Properties of Cu-Mn Alloys*. Phys. Rev. **106**, 893-898, (1957).

[31] B.T. Matthias, M. Peter, H.J. Williams, A.M. Clogston, E. Corenzwit, and R.C. Sherwood. *Magnetic moment of transition metal atoms in dilute solution and their effect on superconducting transition temperature*. Phys. Rev. Lett. **5**, 542-544, (1960).

[32] J.R. Schrieffer and P.A. Wolff. *Relation between the Anderson and Kondo Hamiltonians*. Phys. Rev. **149**, 491-492, (1966).

[33] P.W. Anderson and G. Yuval. *Exact Results in the Kondo Problem: Equivalence to a Classical One-Dimensional Coulomb Gas*. Phys. Rev. Lett. **23**, 89-92, (1969).

[34] G. Yuval and P. W. Anderson. *Exact Results for the Kondo Problem: One-Body Theory and Extension to Finite Temperature*. Phys. Rev. B **1**, 1522-1528, (1970).

[35] P.W. Anderson, G. Yuval, and D.R. Hamann. *Exact Results in the Kondo Problem. II. Scaling Theory, Qualitatively Correct Solution, and Some New Results on One-Dimensional Classical Statistical Models*. Phys. Rev. B **1**, 4464-4473, (1970).

[36] P.W. Anderson and G. Yuval. *Scaling theory for the Kondo and one-dimensional Ising models*. Solid St. Commun. **8**, 1033-1037, (1970).

[37] K. Yosida. *Bound State Due to the s-d Exchange Interaction*. Phys. Rev. **147**, 223-227, (1966).

[38] A. Okiji. *Bound State due to the s-d Exchange Interaction - Effect of the Higher Order Perturbation*. Prog. Theor. Phys. **36**, 712-725, (1966).

[39] K. Yosida. *Ground State Energy of Conduction Electrons Interacting with a Localized Spin*. Prog. Theor. Phys. **36**, 875-886, (1966).

[40] Y. Nagaoka and T. Matsuura. *Bound States Due to a Magnetic Impurity in a Superconductor. I.* Prog. Theor. Phys. **46**, 364-386, (1971).

[41] E. Pavarini, E. Koch, F.B. Anders, and M. Jarrell. *Correlated Electrons: From Models to Materials*. Verlag des Forschungszentrum Jülich, (2012).

[42] G.R. Stewart. *Heavy-fermion systems*. Rev. Mod. Phys. **56**, 755-787, (1984).

[43] M.J. Rozenberg, X.Y. Zhang, and G. Kotliar. *Mott-Hubbard transition in infinite dimensions*. Phys. Rev. Lett. **69**, 1236-1239, (1992).

[44] A. Georges, G. Kotliar, W. Krauth, and M.J. Rozenberg. *Dynamical mean-field theory of strongly correlated fermion systems and the limit of infinite dimensions*. Rev. Mod. Phys. **68**, 13-125, (1996).

[45] M. Grobis, I. G. Rau, R. M. Potok, and D. Goldhaber-Gordon. *Kondo Effect in Mesoscopic Quantum Dots*. Handbook of Magnetism and Advanced Magnetic Materials Vol. **5**, Wiley, (ed H. Kronmüller, S. Parkin), also available at arXiv:cond-mat/0611480, (2007).

[46] K.G. Wilson. *The renormalization group: Critical phenomena and the Kondo problem*. Rev. Mod. Phys. **47**, 773-840, (1975).

[47] N. Andrei. *Diagonalization of the Kondo Hamiltonian*. Phys. Rev. Lett. **45**, 379-382, (1980).

[48] P.B. Vigman. *Exact solution of s-d exchange model at T = 0*. JETP Letters **31**, 364-370, (1980).

[49] A.C. Hewson. *Renormalized Perturbation Expansions and Fermi Liquid Theory*. Phys. Rev. Lett. **70**, 4007-4008, (1992).

[50] A.C. Hewson. *Renormalized perturbation calculations for the single-impurity Anderson model*. J. Phys.: Condens. Matter **13**, 10011-10029, (2001).

[51] A.C. Hewson. *Spin and charge dynamics in a renormalized perturbation theory*. J. Phys.: Condens. Matter **18**, 1815-1832, (2006).

[52] K. Edwards and A.C. Hewson. *A new renormalization group approach for systems with strong electron correlation*. J. Phys.: Condens. Matter **23**, 045601, (2011).

[53] J.F. Herbst, R.E. Watson, and J.W. Wilkins. *Relativistic calculations of 4f excitation energies in the rare-earth metals: Further results*. Phys. Rev. B **17**, 3089-3098, (1978).

[54] P.W. Anderson. *Basic Notions of Condensed Matter Physics*. 6th edn, Addison-Wesley, Reading Mass, (1996).

[55] P. Morel and P.W. Anderson. *Calculation of the Superconducting State Parameters with Retarded Electron-Phonon Interaction*. Phys. Rev. **125**, 1263-1271, (1962).

[56] F.D.M. Haldane. *Scaling Theory of the Asymmetric Anderson Model*. Phys. Rev. Lett **40**, 416-419, (1978).

[57] J.H. Jefferson. *A renormalisation group approach to the mixed valence problem*. J. Phys. C: Solid State Phys. **10**, 3589-3599, (1977).

[58] D.C. Mattis. *Symmetry of Ground State in a Dilute Magnetic Metal Alloy*. Phys. Rev. Lett. **19**, 1478-1481, (1967).

[59] L.M. Brown, M. Dresden, R.S. Mills, S.S. Schweber, T.Y. Cao, and D.V. Shirkov. *Renormalization: From Lorentz to Landau (and Beyond)*. Springer-Verlag, (1993).

[60] K.G. Wilson. *Renormalization Group and Critical Phenomena. I. Renormalization Group and the Kadanoff Scaling Picture*. Phys. Rev. B **4**, 3174-3183, (1971).

[61] K.G. Wilson. *Renormalization Group and Critical Phenomena. II. Phase-Space Cell Analysis of Critical Behavior*. Phys. Rev. B **4**, 3184-3205, (1971).

[62] K.G. Wilson. *Renormalization group methods*. Adv. Math. **16**, 170-186, (1975).

[63] S.-K. MA. *Modern Theory of Critical Phenomena*. Advanced Books Classics, Westview Press, (2000).

[64] M. Salmhofer. *Renormalization: An Introduction*. Springer-Verlag, (1999).

[65] J. Cardy. *Scaling and Renormalization in Statistical Physics*. Cambridge Lecture Notes in Physics **5**, Cambridge University Press, (1996).

[66] S.D. Głazek and K.G. Wilson. *Renormalization of Hamiltonians*. Phys. Rev. D **48**, 5863-5872, (1993).

[67] S.D. Głazek and K.G. Wilson. *Perturbative renormalization group for Hamiltonians*. Phys. Rev. D **49**, 4214-4218, (1994).

[68] R.W. Brockett. *Dynamical systems that sort lists, diagonalize matrices, and solve linear programming problems*. Linear Algebra Appl.**146**, 79-91, (1991).

[69] M.T. Chu. *A list of matrix flows with applications*. Fields Institute Communications **3**, Hamiltonian and Gradients Flows, Algorithms and Control, University of Michigan, Ann Arbor, MI, Ed. Anthony Bloch, 87-97, (1994).

[70] M.T. Chu. *Scaled Toda-like flows*. Linear Algebra Appl.**215**, 261-273, (1995).

[71] T.S. Walhout. *Similarity renormalization, Hamiltonian flow equations, and Dyson's intermediate representation*. Phys. Rev. D **59**, 065009, (1999).

[72] S.D. Głazek. *Running Couplings in Hamiltonians*. Acta Phys. Polon. B **31**, 909-930, (2000).

[73] P. Lenz and F. Wegner. *Flow equations for electron-phonon interactions*. Nuc. Phys. B **482**, 693-712, (1996).

[74] M. Ragwitz and F. Wegner. *Flow equations for electron-phonon interactions: phonon damping*. Eur. Phys. J. B **8**, 9-17, (1999).

[75] S.K. Kehrein, A. Mielke, and P. Neu. *Flow equations for the spin-boson problem*. Z. Phys. B **99**, 269-280, (1996).

[76] S.K. Kehrein and A. Mielke. *On the spin-boson model with a sub-ohmic bath*. Phys. Rev. A **219**, 313-318, (1996).

[77] S.K. Kehrein and A. Mielke. *Low temperature equilibrium correlation functions in dissipative quantum systems*. Ann. Physik **6**, 90-135, (1997).

[78] S.K. Kehrein and A. Mielke. *Diagonalization of System plus Environment Hamiltonians*. J. Stat. Phys. **90**, 889-898, (1998).

[79] J. Stein. *Flow equations and the strong-coupling expansion for the Hubbard model*. J. Stat. Phys. **88**, 487-511, (1997).

[80] A. Reischl, E. Müller-Hartmann, and G.S. Uhrig. *Systematic mapping of the Hubbard model to the generalized t-J model*. Phys. Rev. B **70**, 245124, (2004).

[81] S.A. Hamerla, S. Duffe, and G.S. Uhrig. *Derivation of the t-J model for finite doping*. Phys. Rev. B **82**, 235117, (2010).

[82] H.-Y. Yang, A.M. Läuchli, F. Mila, and K.P. Schmidt. *Effective Spin Model for the Spin-Liquid Phase of the Hubbard Model on the Triangular Lattice*. Phys. Rev. Lett. **105**, 267204, (2010).

[83] C. Knetter, K.P. Schmidt, and G.S. Uhrig. *High order perturbation theory for spectral densities of multi-particle excitations: $S = \frac{1}{2}$ two-leg Heisenberg ladder*. Eur. Phys. J. B **36**, 525–544, (2003).

[84] K.P. Schmidt and G.S. Uhrig. *Excitations in One-Dimensional $S = 1/2$ Quantum Antiferromagnets*. Phys. Rev. Lett. **90**, 227204, (2003).

[85] K.P. Schmidt, H. Monien, and G.S. Uhrig. *Rung-singlet phase of the $S = 1/2$ two-leg spin-ladder with four-spin cyclic exchange*. Phys. Rev. B **67**, 184413, (2003).

[86] K.P. Schmidt, C. Knetter, and G.S. Uhrig. *Spectral properties of the dimerized and frustrated $S = 1/2$ chain*. Phys. Rev. B **69**, 104417, (2004).

[87] K.P. Schmidt and G.S. Uhrig. *Hard-core magnons in the $S = 1/2$ Heisenberg model on the square lattice*. Phys. Rev. B **73**, 172407, (2006).

[88] C.P. Heidbrink and G.S. Uhrig. *Renormalization by continuous unitary transformations: one-dimensional spinless fermions*. Eur. Phys. J. B **30**, 443-459, (2002).

[89] S. Kehrein. *Flow Equation Solution for the Weak- to Strong-Coupling Crossover in the Sine-Gordon Model*. Phys. Rev. Lett. **83**, 4914-4917, (1999).

[90] S. Kehrein. *Flow equation approach to the sine-Gordon model*. Nucl. Phys. B **592**, 512–562, (2001).

[91] A. Reischl, K.P. Schmidt, and G.S. Uhrig. *Temperature in one-dimensional bosonic Mott insulators*. Phys. Rev. A **72**, 063609, (2005).

[92] K. Meyer. *Flow equation approach to heavy fermion systems*. Eur. Phys. J. B **42**, 17–30, (2004).

[93] C.P. Heidbrink and G.S. Uhrig. *Landau's Quasiparticle Mapping: Fermi Liquid Approach and Luttinger Liquid Behavior*. Phys. Rev. Lett. **88**, 146401, (2002).

[94] M. Garst, S. Kehrein, T. Pruschke, A. Rosch, and M. Vojta. *Quantum phase transition of Ising-coupled Kondo impurities*. Phys. Rev. B **69**, 214413, (2004).

[95] S. Kehrein. *Scaling and Decoherence in the Nonequilibrium Kondo Model*. Phys. Rev. Lett. 95, 056602, (2005).

[96] F. Wegner. *Flow equations and normal ordering: a survey*. J. Phys. A: Math. Gen. **39**, 8221–8230, (2006).

[97] S. Dusuel and G.S. Uhrig. *The quartic oscillator: a non-perturbative study by continuous unitary transformations*. J. Phys. A: Math. Gen. **37**, 9275–9294, (2004).

[98] S. Sykora, A. Hübsch, and K.W. Becker. *Projector-based renormalization method (PRM) and its application to many-particle systems*. Europhys. Lett. **85**, 57003, (2009).

[99] S. Sykora, A. Hübsch, and K.W. Becker. *Coexistence of superconductivity and charge-density waves in a two-dimensional Holstein model at half-filling*. arXiv:0809.3360 [cond-mat.str-el], (2009).

[100] T. Fischer, S. Duffe, and G.S. Uhrig. *Adapted continuous unitary transformation to treat systems with quasi-particles of finite lifetime*. New Journal of Physics **12**, 033048, (2010).

[101] T. Fischer. *Description of quasiparticle decay by continuous unitary transformations*. Ph.D. thesis, Technische Universität Dortmund, (2011).

[102] S. Duffe. *Effective Hamiltonians for Undoped and Hole-Doped Antiferromagnetic Spin-$1/2$ Ladder by Self-Similar Continuous Unitary Transformations in Real Space.* Ph.D. thesis, Technische Universität Dortmund, (2010).

[103] S.A. Hamerla. *Systematic derivation of generalized t-J models from Hubbard models in one and two dimensions at and away from half-filling.* Diploma thesis, Technische Universität Dortmund, (2009).

[104] T. Fischer. *Beschreibung von Quantendimermodellen mittels kontinuierlicher unitärer Transformationen.* Diploma thesis, Technische Universität Dortmund, (2007).

[105] N.A. Drescher. *Optimierte Basiswahl und Trunkierungsfehler bei kontinuierlichen unitären Transformationen am Beispiel der dimerisierten Spin-$1/2$-Kette.* Diploma thesis, Technische Universität Dortmund, (2009).

[106] S. Duffe and G.S. Uhrig. *Hole dispersions for antiferromagnetic spin-$\frac{1}{2}$ two-leg ladders by self-similar continuous unitary transformations*. European Physical Journal B **84**(3), 475-490, (2011).

[107] T. Fischer, S. Duffe, and G.S. Uhrig. *Microscopic model for Bose-Einstein condensation and quasiparticle decay*. Europhysics Letters **96**(4), 47001, (2011).

[108] G.S. Uhrig and B. Normand. *Microscopic model for Bose-Einstein condensation and quasiparticle decay*. Phys. Rev. B **58**, R14705-R14708, (1998).

[109] K.P. Schmidt. *Spectral Properties of Quasi One-dimensional Quantum Antiferromagnets.* Ph.D. thesis, Universität zu Köln, (2004).

[110] H. Krull, N.A. Drescher, and G.S. Uhrig. *Enhanced perturbative continuous unitary transformations*. Phys. Rev. B **86**, 125113, (2011).

[111] H. Krull. *Verbesserte perturbative kontinuierliche unitäre Transformation mit direkter Auswertung: Erläutert anhand der Spin $S = 1/2$ antiferromagnetischen Heisenberg-Leiter.* Diploma thesis, Technische Universität Dortmund, (2011).

[112] H.Y. Yang and K.P. Schmidt. *Effective models for gapped phases of strongly correlated quantum lattice models*. European Physics Letters **94**, 17004, (2011).

[113] A. Reischl, E. Müller-Hartmann, and G.S. Uhrig. *Systematic mapping of the Hubbard model to the generalized t-J model.* Phys. Rev. B **70**, 245124, (2004).

[114] A. Reischl. *Derivation of Effective Models using Self-Similar Continuous Unitary Transformations in Real Space.* Ph.D. thesis, Universität zu Köln, (2006).

[115] G.C. Wick. *The Evaluation of the Collision Matrix*. Phys. Rev. **80**, 268-272, (1950).

[116] M. Gaudin. *Une démonstration simplifiée du théorème de wick en mécanique statistique*. Nuc. Phys. **15**, 89-91, (1960).

[117] C. Lanczos. *An Iteration Method for the Solution of the Eigenvalue Problem of Linear Differential and Integral Operators*. J. Res. Natl. Bur. Stand. **45**, 255-282, (1955).

[118] W.H. Press, S.A. Teukolsky, H.A. Bethe, W.T. Vetterling, and B.P. Flannery. *Numerical Recipes - The Art of Scientific Computing*. Third Edition, Cambridge University Press, (2007).

[119] A.M. Tsvelick and P.B. Wiegmann. *Exact results in the theory of magnetic alloys*. Adv. Phys. **32**, 453-713, (1983).

[120] H. Fröhlich. *Interaction of Electrons with Lattice Vibrations*. Proc. R. Soc. A **215**, 291-298, (1952).

[121] L.N. Oliveira and J.W. Wilkins. *Specific Heat of the Kondo Model*. Phys. Rev. Lett. **47**, 1553-1556, (1981).

[122] F.D.M. Haldane. *Theory of the atomic limit of the Anderson model: I. Perturbation expansions re-examined*. J. Phys. C: Solid State Phys. **11**, 5015-5O34, (1978).

Danksagung

Ganz besonderer Dank gilt Herrn Prof. Dr. Götz S. Uhrig für die spannende Themenstellung sowie seiner hervorragenden Betreuung. Seine stets einfallsreichen Anmerkungen hatten richtungsweisenden Einfluss auf die Entstehung dieser Arbeit.

Ich möchte mich auch bei Herrn Prof. Dr. Anders dafür bedanken, dass er die Aufgabe des Zweitgutachters übernommen hat.

Dr. Sebastian Schmitt will ich gebührenden Dank für hilfreiche Unterredungen während meiner Einarbeitungsphase in den Themenkomplex der Kondo-Physik sowie für die Bereitstellung von Vergleichsdaten aussprechen.

Ich will an dieser Stelle auch Dr. Sebastian Duffe dafür danken, dass er immer ein sehr angenehmer Bürokollege war sowie für seine Bereitschaft Fragen meinerseits stets zu beantworten.

Ich danke weiterhin allen Mitarbeitern des Lehrstuhls TI und TII für das angenehme Arbeitsklima. Dabei will ich besonders Dr. Sebastian Duffe, Thorben Linneweber, Dr. Stefano Pasini, Daniel Spannenkrebs, Lars Gravert, Dr. Gregor R. Foltin, Dr. Simone A. Hamerla, Nils A. Drescher, Benedikt Fauseweh, Dr. Mark Daniel Schulz und Dr. Carsten Nase hervorheben.

Freunden und Familie danke ich für die Unterstützung in jeglicher Hinsicht.

Von Herzen danke ich meiner Frau, Timea-Elisabeth Krones, und meinem Sohn, Jan-Erik Krones.